MONTAN UNIVERSITÄT
WWW.UNILEOBEN.AC.AT

Investigations on the effects of microwaves on hard rock

Dipl.-Ing. Philipp Hartlieb

Doctoral Thesis

Supervisors

Univ.Prof. Dipl.-Ing. Dr.mont. Peter Moser

em.O.Univ.Prof. Dr.phil. Friedemar Kuchar

January 2013

Chair of Mining Engineering and Mineral Economics
Department Mineral Resources and Petroleum Engineering
Montanuniversität Leoben

mining engineering
mineral economics

Declaration of authorship

I declare in lieu of oath that this thesis is entirely my own work except where otherwise indicated. The presence of quoted or paraphrased material has been clearly signaled and all sources have been referred. The thesis has not been submitted for a degree at any other institution and has not been published yet.

Philipp Hartlieb

Preface, Dedication, Acknowledgement

Many thanks go to Prof. Peter Moser and Prof. Friedemar Kuchar for coming up with the idea of this thesis. Both of them were also supporting me throughout the research activities by having an open ear to questions, providing me with useful input and being partners for profound discussion on the topic.

Nikolaus Sifferlinger, Hubert Kargl, Marin Gimpel, Uwe Restner and many other people within Sandvik supported me in every possible way. Technical assistance as well as discussion was without question perfect and supportive. A major part of the costs for infrastructure and sample material were covered by Sandvik Mining and Construction which has to be thanked particularly.

The Austrian Research Agency (FFG) has to be thanked for sponsoring the project “Non-mechanical rock cutting concepts” as part of the Bridge 2 framework program.

Many thanks go to Fritz Pichlmair and Gerhard Hebenstreit and their teams in the Sandvik rock testing and cutting laboratories for their support throughout the years. They provided a helping hand whenever necessary and guaranteed for a smooth and accurate laboratory procedure.

From the many helping hands within the University of Leoben Mario Sorger and Heinz Mali have to be highlighted for providing measurements and especially the availability of a perfect microscope for detailed investigations.

There are many people more who contributed to the successful finalization of this thesis: My colleagues in the office and at the department helped wherever necessary and together we solved all kinds of problems. A special thank goes to Finn Ouchterony for countless hours of valuable discussions Additionally Janine guided me through the shallow waters of the English language.

Last but not least I want to thank my family for supporting me throughout the years and to whom I will be thankful for the rest of my life.

Abstract

This study investigates the response of various types of hard rock to microwave irradiation. Two basic laboratory setups have been implemented and the consequences of microwave irradiation on the behaviour of rock samples have been analysed. Small-scale low-power microwave irradiation was performed with a 3.2 kW standard household microwave. Large-scale experiments were performed with a self-designed high-power microwave apparatus operating at a maximum output power of 30 kW. Irradiation times vary from a few seconds to minutes.

With the low-power apparatus only rocks with relatively good microwave absorption properties (basalt, gabbro) could be sufficiently heated and significantly damaged, represented by a reduction in sound wave velocity from 5000 to 3500 m/s after 120 s of irradiation. The influence of the sample geometry is obvious from the crack pattern. Evidence for consequences of differential heating, as proposed in various literature sources, could not be found. This can presumably only be achieved by short irradiation with higher power than applied in the present thesis. The occurrence of small amounts of water (1-2 wt.%) in porous rocks has a positive influence on the destruction of rock by building up vapour pressure leading to stresses in the rock exceeding its tensile strength.

High-power microwave irradiation with up to 30 kW leads to heating and cracking of all investigated rock types. The different rock types (fine grained strong absorbers, coarse grained strong and weak absorbers, water bearing) show completely different effects of damage. Rocks with strong microwave absorption (greenstones) heat rapidly (ΔT = 270 °C in 6 s with 25 kW) with coinciding fast generation of temperature gradients and spallation of craters at the surface. Here cracks are not aligned to grain boundaries. In weakly absorbing rocks (sandstone, granite) temperature rises are less distinctive (ΔT = 240 °C in 30 s with 25 kW for granite) radial cracks develop originating in the centre of irradiation. Cracks are largely bound to grain boundaries or cleavage planes of single minerals but are assumed not to originate in intergranular temperature stresses but in the global stresses induced by the stronger heating of the centre of the irradiated volume. Small amounts of water in the porous volume of sandstone play a major role in high power irradiation as well. Excellent microwave absorption by water leads to fast generation of vapour pressure and explosive generation of craters with up to 6 cm of depth.

An attempt was made to quantify damage induced by microwave irradiation by a linear cutting test-rig. Despite the observation of a trend towards a reduction of cutting forces after microwave irradiation the large scattering of results does not allow for a reliable conclusion.

Zusammenfassung

Die vorliegende Studie beschäftigt sich mit den Auswirkungen von Mikrowellenbestrahlung auf unterschiedliche Hartgesteinstypen. Im Zuge der Untersuchungen wurden zwei Laboraufbaue umgesetzt und die Veränderungen im Gestein hinsichtlich Festigkeit und Textur untersucht. Kleimaßstäbliche Versuche wurden in einer Haushaltsmikrowelle mit 3.2 kW durchgeführt. Für großmaßstäbliche Versuche wurde eine Mikrowellenanlage mit einer maximalen Leistung von 30 kW entwickelt und verwendet. Die Bestrahlungsdauern betrugen einige Sekunden bis Minuten.

In den kleinmaßstäblichen Versuchen konnten lediglich Gesteine mit relativ guten Absorptionseigenschaften (Basalt, Gabbro) ausreichend erhitzt und in weiterer Folge geschädigt werden, was durch die Reduktion der Schallwellengeschwindigkeit im Gestein von 5000 auf 3500 m/s nach 120 s gezeigt wird. Es zeigt sich dabei ein deutlicher Einfluss der Probengeometrie. Differenzielle Aufheizung der Gesteinskomponenten und daraus resultierende Risse entlang von Korngrenzen können, im Gegensatz zu Vorschlägen diverser Literaturquellen, nicht bestätigt werden. Dafür wären wesentlich kürzere Bestrahlungszeiten und höhere Leistungen, als in der vorliegenden Arbeit, erforderlich. Das Vorhandensein von Wasser (1-2 Gew.%) führte zu erhöhten Dampfdruck im Porenraum und somit zu Spannungen, die die Zugfestigkeit der Gesteine überschreiten.

Hochleistungsbestrahlung mit 30 KW führt in allen untersuchten Gesteinen zu Temperaturerhöhung und Rissbildung. Die unterschiedlichen Gesteinstypen (feinkörnig mit starker Absorption, grobkörnig mit starker und schwacher Absorption, wasserhaltig) weisen dabei gänzlich unterschiedliche Schädigungsmuster auf. Gesteine mit guten Absorptionsfähigkeiten (Basalt, Gabbro) erhitzen sehr rasch ($\Delta T = 270$ °C in 6 s mit 25 kW) unter rascher Ausbildung der Temperaturgradienten, was zur Abplatzung von Kratern an der Oberfläche führt. Risse sind dabei nicht and die Korngrenzen gebunden. Schwach absorbierende Gesteine (Sandstein, Granit) erhitzen weniger stark ($\Delta T = 240$ °C in 30 s mit 25 kW) und es entwickeln sich radiale Risse. Diese sind großteils an vorhandene Korngrenzen oder Spaltbarkeitsflächen einzelner Minerale gebunden. Auch bei hoher Mikrowellenleistung spielt das Vorhandensein von Wasser eine entscheidende Rolle. In feuchtem Sandstein führt Absorption durch Wasser zu hohem Dampfdruck und explosiver Zerstörung sowie zur Ausbildung von bis zu 6 cm tiefen Kratern im Gestein.

Zusätzliche Versuche wurden unternommen, um den Einfluss der Mikrowellenbestrahlung auf die mechanische Schneidleistung zu Untersuchen. Obwohl die Tendenz zu einer Reduktion der angewandten Schneidkräfte ersichtlich ist, kann auf Grund der großen Streuung der Messergebnisse keine gesicherte Aussage darüber getroffen werden.

Table of contents

1 Introduction into mechanical hard rock excavation

Mechanical hard rock excavation has a lot of advantages on drilling and blasting, e.g. more precise excavation profiles, no blasting fumes and smaller ground vibrations. Apart from that mechanical rock excavation is a continuous process which can be much easier integrated into a complex system of different mining processes.

While in tunnelling full face tunnel boring machines are frequently used, in mining operations such big types of machines can hardly be used due to their size and low flexibility concerning cross-section and curvature. In mining the typical the typical mechanical excavation machine would be a roadheader or continuous miner.

Mechanical excavation methods on the basis of roadheaders can only be used in soft or medium hard ground. Rock mass of high strength and / or high abrassivity cannot be excavated economically with today's technologies. Therefore there is a strong interest to improve roadheaders with new and alternative breaking methods.

1.1 Current excavation technologies on the basis of roadheaders

Roadheaders are used in civil engineering and mining since the 1950's. They operate based on mechanical excavation principles by cutter picks mounted on a rotating cutterhead. The picks penetrate the rock mass which disintegrates as result of the mechanical action. The loosened material is loaded and hauled to the rear end of the machine where it is deposited on a conveyor or shuttle car (Jordan et al. 2011). This working principle guarantees for a continuous working process considered as being one major asset for highly productive mining as well as tunnelling operations. Due to their high flexibility they can be applied in a wide range of operations, geological settings and excavation geometries. They can be used successfully in multi-face and step operations because of the very quick mobilization of the equipment (Restner and Reumueller 2004) especially when compared to other mechanical systems like tunnel boring machines (TBM). A further major advantage of roadheaders compared to drill and blast operations is the accuracy and smoothness of the operation. Due to the smooth cutting profile guaranteeing for only limited overcut stability problems can be excluded. This results in a significant reduction of the material and effort spent for stabilizing the tunnel. Shotcreting and bolting can be reduced increasing the economic performance of the operation. A reduction in overcut of 80 % is reported by Restner and Reumueller (2004). This study emphasises the fact that also the costs for lining and grouting are reduced significantly by the operation of a roadheader compared to drilling and blasting. Especially in the vicinity

of settlements and urban areas but also in classical mining environments a reduction of vibrations and noise is described as the third major advantage of roadheaders over other technologies. According to Plinninger (2011) this is caused by the way the energy is applied. Compared to drilling and blasting a roadheader acts punctually over a long period of time, whereas a blast applies all the energy at the same time.

Besides the numerous advantages the application of roadheaders is constrained by several operational limitations: The operation is influenced by both scheduled and unscheduled maintenance and breakdowns, electrical demand and demand for water are comparably high (Jordan et al. 2011). A major limiting factor for the application of a roadheader is the strength of the rock represented by the uniaxial compressive strength and its abrasivity. Originally roadheaders were used in soft to medium strength lithologies like coal, potash and salt (Jordan et al. 2011; Plinninger 2011). Several publications show that the performance of a roadheader which is quantified by the net cutting rate [solid m^3/net cutting hour] decreases with increasing compressive strength and abrasivity of the rock mass. The specific pick consumption [picks/solid m^3] is another cost intensive parameter influenced by the rock conditions (eg. Thuro and Plinninger 2002; Plinninger 2011; Jordan et al. 2011) and literature therein). Some of these restrictions can be overcome by increasing the size as well as power of the applied machine and equipment. However, if the rock is too strong or abrasive current technologies are facing an economical and technical limit of application. In Summary three different types of rock can be defined according to their compressive strength and abrasivity represented by the Cerchar Abrasivity Index (CAI): Rocks cuttable with current technologies (green area), rocks cuttable with improved picks and new procedures of operation (yellow and red area, Icutrock technology) and rocks not to be cut economically with the current methods and technologies (blue areas; Figure 1-1).

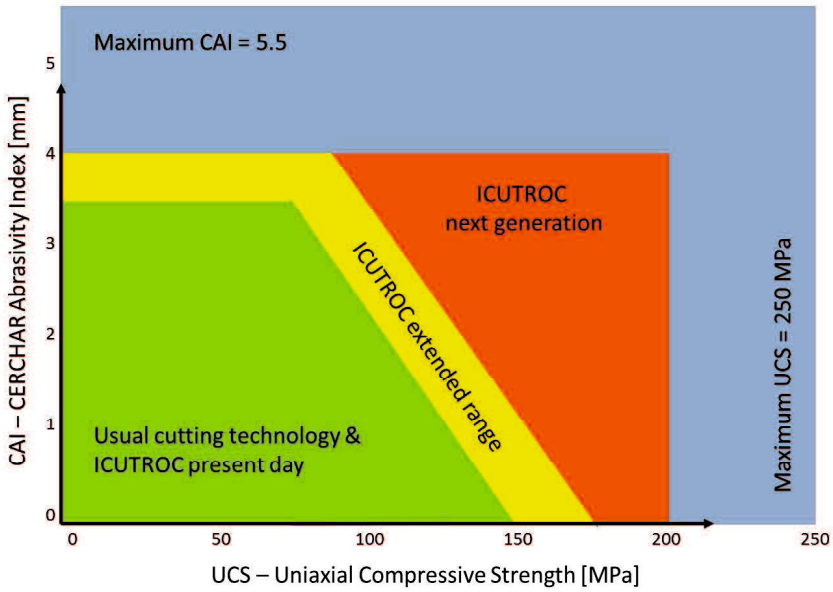

Figure 1-1: Range of UCS and CAI of natural rocks and different technologies applied to cut these rocks (Figure courtesy of Sandvik Mining and Construction).

Another influencing factor on the cuttability is the crack density of the rock mass. It has been demonstrated by several authors how the joint status of the rock mass influences the applicability of a roadheader (Bieniawski 1989; Vasek and Dlouhy 1978; Sandbak 1985). It is demonstrated in these publications that the joint spacing, the RQD-value, the fracture frequency and the RMR-value play a major role when it comes to the cuttability of a rock mass. Restner and Gehring (2002) show that the Net Cutting Rate as well as Specific Pick Consumption are strongly governed by the RMR-value (Figure 1-2). In this Figure (I) denotes the ripping zone where the rock is predominantly ripped off the face by the tool; (II) is an intermediate zone where ripping and cutting occur and (III) is the cutting zone where the majority of the rock must be cut.

Considering all influences of rock and rock mass it can be summarized that the major factors governing the cuttability and excavatability with roadheaders are the strength of the intact rock (UCS), the intensity of parting (number of joints, joint spacing) the joint conditions and the orientation of these joints (Restner and Gehring 2002).

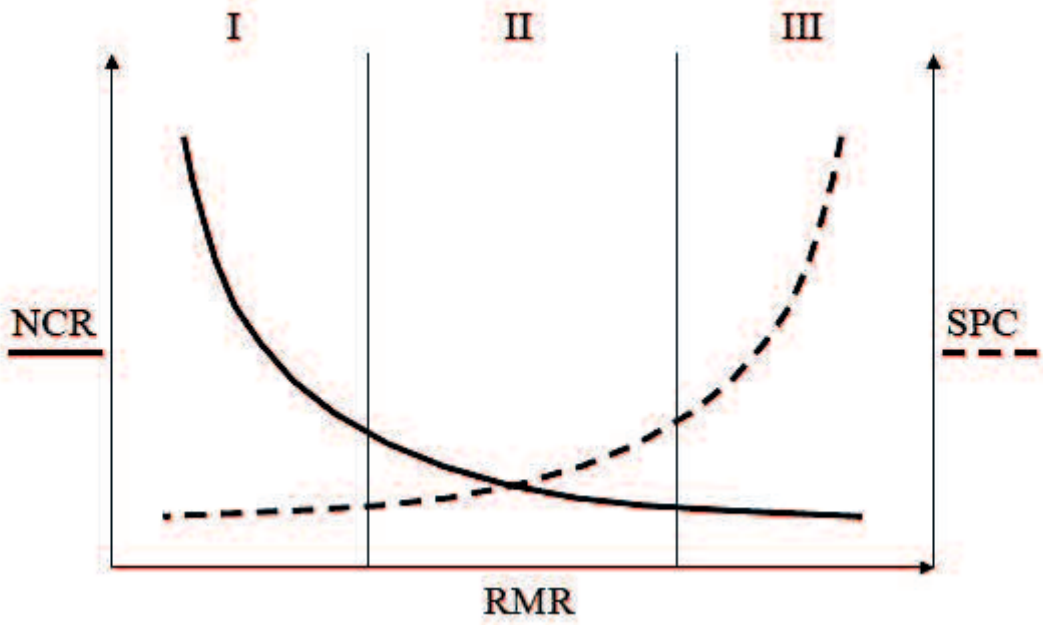

Figure 1-2: Influence of rock mass characteristics (defined by RMR) on Net Cutting Rate (NCR) and Specific Pick Consumption (SPC, Restner and Gehring 2002).

1.2 New approaches of hard rock cutting

A lot of research was performed ever since the 1930's in order to develop new and improved methods of rock fragmentation, cutting, drilling and boring. These alternative methods try to combine the positive aspects of conventional cutting like precise and flexible operations with future techniques in order to overcome the restrictions described in the previous chapter. The application of these new and alternative methods of rock cutting and disintegration shall provide the existing equipment with even greater flexibility enabling them to cutting stronger material while increasing economical results (eg.Ciccu and Grosso 2010).

The wide range of possible technologies covers the disintegration of rocks by pulsed electronic beams, hydraulic fracturing, electric sparks and high pressure water jets (Brown et al. 1976). In the 1970's several promising approaches towards alternative methods for rock disintegration have been identified. These methods can apply one of the four following principles: mechanically induced stresses, thermal spalling, fusion or chemical reactions. According to Maurer (1976) mechanical approaches include turbine drills, explosive drills, liquid explosive drills, ultrasonic and spark drills. Thermal spalling is the major idea behind the application of jet piercing drills, flame drills, electric disintegration drills, induction and microwave drills. Back in this era nuclear power was a popular source for energy and thus a nuclear drill was also proposed by the author in order to fuse holes in a rock mass. Fusion can also be achieved by electric arc drills, plasma drills, focused

electron beam and LASER drills. The high reaction potential of chemicals like fluorine can also be used to drill into sandstone, limestone and granite.

Major research has been performed ever since in the fields of water jet cutting (e.g. (Ciccu, and Grosso 2010; Cohen et al. 2005; Hagan 1992), LASER and microwave treatment of rock.

Research performed since the development of the microwave technology concentrated on increasing the knowledge about the interaction of microwaves with rocks. Over the past fifty years researchers all over the world have provided data on this topic. The focus of the entire work done lies in the broad field of disintegration, grinding and mineral processing. Santamarina (1989) is providing a good overview of the work done before the 1980s. In recent years microwaves have been strongly investigated in the field of mineral processing and comminution. The authors dealing with this topic are giving evidence that a strongly absorbing grain within a non absorbing matrix can be heated easily and that damage can be inferred by differential thermal expansion and a separation of these phases can be achieved. Detailed descriptions of these processes are provided by Walkiewicz et al. (1988), Jones et al. (2005) and Satish et al. (2006). Microwaves are also broadly used in extractive metallurgy. They can be used in several processes where oxide ores are involved like drying, calcination and sintering, reduction and smelting, slag heating and reduction and in the segregation process (Pickles 2009b). The author also points out the positive aspects of recycling of Electric Arc Furnace dust and the roasting of gold ores.

2 Framework of this thesis

The framework of the thesis was the project “Non-mechanical rock cutting concepts” sponsored by the Austrian Research Promotion Agency (FFG). This project was organized in cooperation with Sandvik Mining and Construction a major producer of mining machinery in various applications all over the world. The company shows a strong interest in developing a suitable technique to overcoming the known technological restrictions and limitations of mechanical hard rock cutting technology which have been described above. Developing a cutting machine that could be used in hard rock, based on a combination of classical and alternative rock breaking methods would be a major advantage for the application in new and future mining and tunnelling operations. Therefore Sandvik in cooperation with the Chair of Mining Engineering and Mineral Economics at the University of Leoben proposed the project “Non-mechanical rock cutting concepts” to the FFG to investigate possible alternative methods for hard rock cutting and to specially focus on a study of the application of microwaves.

The aim of the triennial FFG project “Non-mechanical rock cutting concepts” was to increase the knowledge of the behaviour of a set of hard rocks when subjected to microwave irradiation. A further goal of the project was to increasing the provided energy in order to improve the damage induced in the rock samples. The FFG-project was based on the results of a previous project where tests were performed with a standard 3.2 kW multimode microwave oven. The results were summarized in a diploma thesis (Peinsitt 2009). Therefore in course of the new FFG-project increased knowledge on the behaviour of microwave-rock interaction as well as possible damage mechanisms in rocks should be generated. Experiments were planned to be performed on both lab-scale as well as full-scale basis. For achieving the task of understanding the physics of rock fragmentation with microwaves different modes and different power levels of microwave irradiation were scheduled to be carried out. With the gathered knowledge the feasibility of the microwave-preconditioning of rocks for mechanical cutting tests should be demonstrated. For fulfilling these tasks a working strategy was developed ranging from microwave irradiation experiments to structural investigations as well as numerical modelling of microwave propagation inside a rock and resulting heating characteristics. Six work packages have been developed which are as follows:

(1) Extended rock damage tests on lab scale basis with microwaves

(2) Fundamentals of rock microwave interaction

(3) Alternatives to rock fragmentation with microwaves

(4) Set-up of microwave installation for full scale cutting tests

(5) Mechanical cutting tests

(6) Health, Safety and Environmental aspects of microwave use for rock fragmentation

WP 1 was dedicated to continue the experimental studies of the preparatory work. It was aimed at widening the series of rock types, better understanding the mechanisms of microwave rock fragmentation and to quantify the rock damage.

WP 2 was dedicated to understanding the physical principles of microwave rock interaction. Numerical models should have been developed to better understand microwave propagation in a rock mass, resulting heating characteristics and formation of stresses leading to damage of the rock.

WP 3 was aimed at investigating alternative methods of non-mechanical hard rock cutting and compare them to the microwave technology.

Within WP 4 a large-scale microwave apparatus was developed and implemented. A decision of the technical details had to be made and the testing procedure had to be designed. A large-scale irradiation apparatus can a) provide higher microwave power and b) a sample geometry and test procedure that is closer to a possible real-life application. In addition the large-scale irradiation apparatus was aimed to provide the possibility of combining irradiation tests with Sandvik's existing cutting test-rig.

During WP 5 extended studies were scheduled to investigating cracking and fragmentation of rocks on larger scale and with increased microwave energy compared to WP 1. Following WP 4 a procedure should have been developed combining microwave irradiation and subsequent rock cutting and studying the improvement of the rock cutting performance as result of microwave irradiation.

WP 6 was dedicated to analysing the HSE-issues of high power microwave irradiation in a possible future application. Information should be gathered on reflection from the surface of machinery, possible scenarios of microwave application in a mining environment and necessary shielding to guarantee for a safe working procedure.

Work Package	2009				2010				2011			
	Q1	Q2	Q3	Q4	Q1	Q2	Q3	Q4	Q1	Q2	Q3	Q4
WP1 - Extended lab-scale tests												
WP2 - Fundamentals of rock microwave interaction												
WP3 - Alternatives to rock fragmentation with microwaves												
WP4 - Set-up of full-scale installation												
WP5 - Mechanical cutting tests												
WP6 - HSE - aspects												

Table 2-1: Planned work packages and scheduled progress of activities of the project "Non-mechanical rock cutting concepts".

The procedure was scheduled in way to gather extended information on basis of lab-scale tests in the beginning (Table 2-1). From the investigations of 11 different sample localities and more than 300 samples several implications on the interaction of microwaves and rocks will be provided in this study. Detailed studies on the formation of cracks are made giving a better insight into the topic. Based on the knowledge from previous work performed by Peinsitt (2009) and results from small-scale tests performed during this project it is evident that the geometry of the sample as well as the way of microwave irradiation and application play a major role in the formation of cracks.

3 Principles of microwave irradiation and their interaction with rocks

The intention of this chapter is the discussion of the principle mechanisms behind microwave irradiation. An introduction of electromagnetic waves and their interaction with solids is provided. Subsequently the generation of heat and the concepts behind microwave treatment of rocks and ores are investigated. Understanding the nature of electromagnetic waves, how they are generated and the limitations and specific characteristics of rocks and rock constituents will help understanding the mechanisms of the investigated technique and provide the basis for future considerations in terms of microwave treatment, applied power and geometry of the set-up.

3.1.1 Electromagnetic principles

The first presentation of a complete theory of electromagnetic waves was given by James Maxwell in 1864 (see Gupta and Wong 2007). Electromagnetic energy is emitted in form of a wave travelling at the speed of light. The propagation of electromagnetic waves is governed by Maxwell's equations. As shown in Figure 3-1 electric and magnetic fields oscillate perpendicular to each other. According to Maxwell's equations a time-varying electric field generates a magnetic field and the other way round.

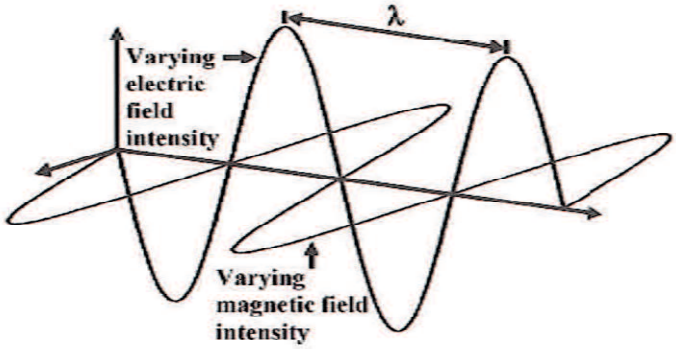

Figure 3-1: Electric and magnetic fields of a linearly polarized electromagnetic (from Gupta and Wong 2007).

Electromagnetic waves are classified according to their wavelength in gamma rays, x-rays, ultraviolet radiation, visible light, infrared radiation, microwaves and radio waves (Figure 3-2). Microwaves are in the bandwidth between a frequency of 0.3 and 300 GHz. Their spectrum is situated between radio and infrared waves. A further classification of microwaves can be made between Ultra High Frequency (UHF) microwaves ranging from 300 MHz to 3 GHz, Super High frequency (SHF) microwaves ranging from 3 GHz to 30

GHz and Extremely High Frequency (EHF) microwaves ranging from 30 GHz to 300 GHz. Most microwave operations in medical, industrial, scientific and military application use one of four standard wave bands operating at 915, 2450, 5800 or 22125 MHz.

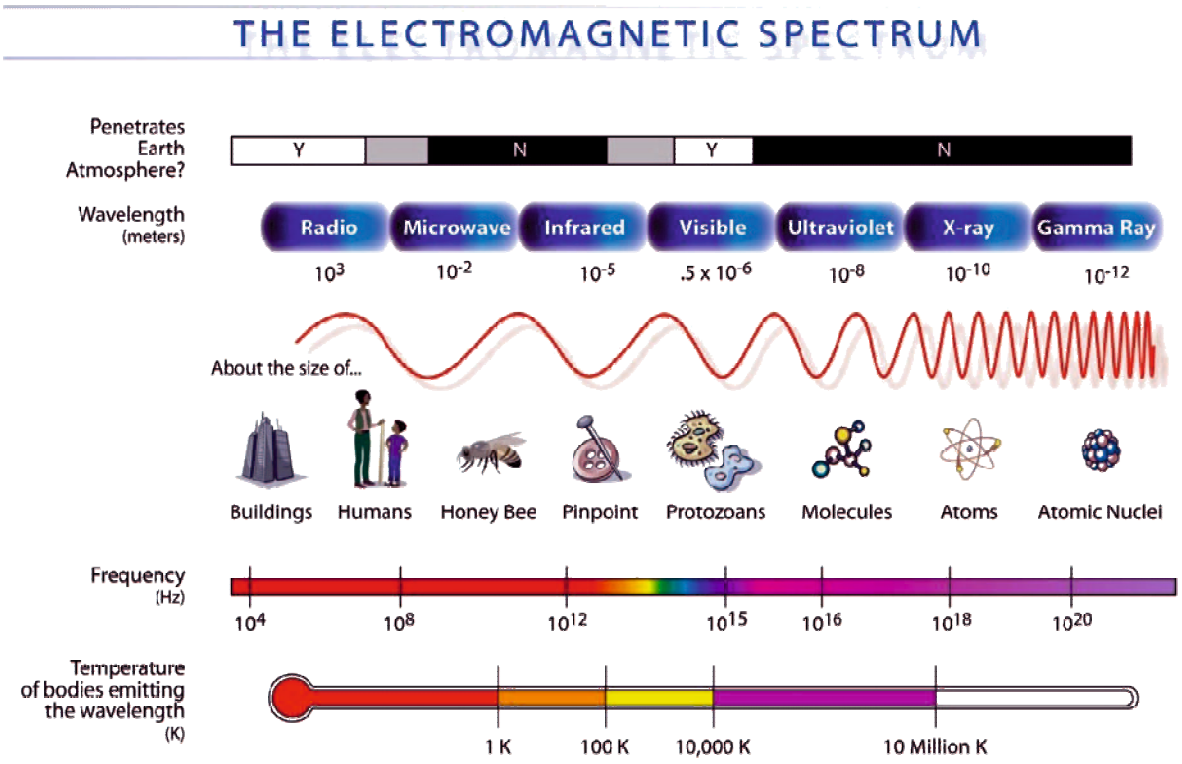

Figure 3-2: The electromagnetic spectrum (image courtesy of NASA).

The propagation of microwaves in different materials is depending on the electromagnetic properties of the medium. Dielectric and magnetic properties are characterized by the complex permittivity ε and the complex permeability μ.

They are expressed by:

$$\varepsilon = \varepsilon' - i\varepsilon'' \qquad \textbf{3-1}$$

and

$$\mu = \mu' - i\mu'' \qquad \textbf{3-2}$$

The real part of the complex permittivity ε' is also referred to as the dielectric constant, describing the response of a medium to an electromagnetic field and governing the propagation of microwaves (e.g. the velocity) in the material whereas the imaginary part ε" is also known as dielectric loss factor representing the ability of a material to absorb energy. As shown later on in chapter 4 both ε' and ε" strongly depend on the applied frequency and temperature. This effect is also described for water (Rankin 2009) and

shown in Figure 3-3. μ' is the real part of the complex magnetic permeability, describing the response of a medium to a magnetic field and μ" is the imaginary part of the complex magnetic permeability representing the magnetic loss factor under the influence of the magnetic field. The permeability is of importance in magnetic materials only.

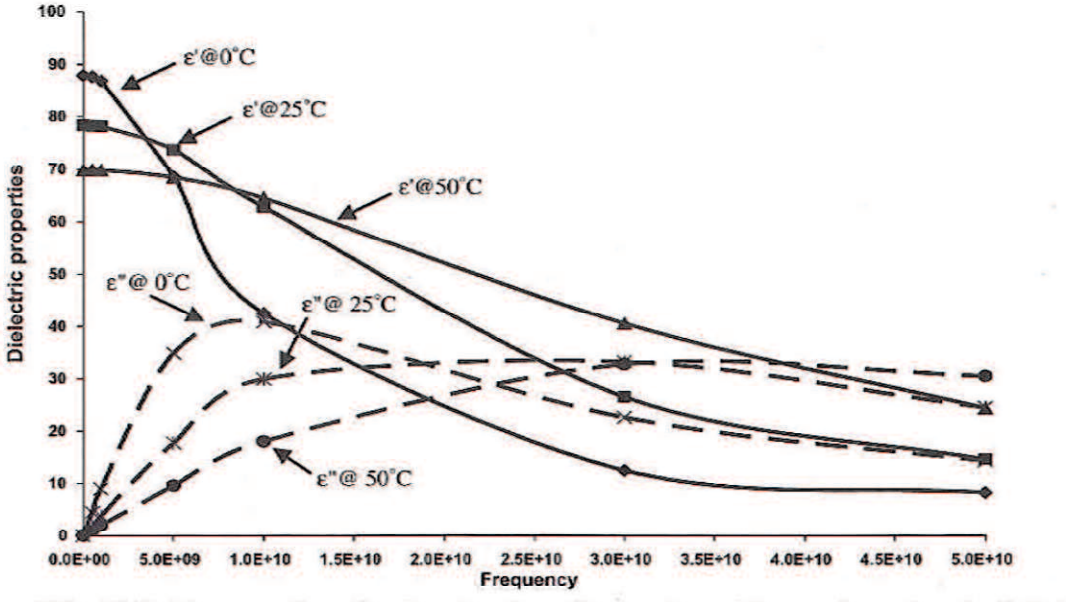

Figure 3-3: Dielectric properties of water at different temperatures as function of the frequency (from Gupta and Wong 2007).

A normalization (in S.I. units) of the complex permittivity ε with the constant permittivity of vacuum $\varepsilon_0 = 8.854*10^{-12}\ \frac{As}{Vm}$ leads to complex relative permittivity κ (equivalent for μ with μ_0) where

$$\kappa = \frac{\varepsilon}{\varepsilon_0}. \qquad \textbf{3-3}$$

The relation of ε' and ε", also expressed as tanδ, represents the ability of a material to convert absorbed electromagnetic energy into heat.

$$\tan\delta = \frac{\varepsilon''}{\varepsilon'} \qquad \textbf{3-4}$$

Materials are subdivided into high and low loss materials. High loss materials are characterized by κ"/ κ' >> 1, whereas low loss materials are represented by κ"/ κ' <<1.

The absorbed power and related heating of a medium can be denoted as

$$P = 2\pi f \varepsilon_0 \kappa'' E^2 \qquad \textbf{3-5}$$

where E is the strength of the electric field.

The depth of microwave penetration in a medium is called *penetration depth* D_p. It is defined as the distance from the surface at which the power of the electromagnetic wave has been attenuated to 1/e. the power at the surface (Santamarina 1998). It can be denoted as:

$$D_p = \frac{1}{2\omega}\left[\frac{2}{\mu'\mu_0\varepsilon_0\kappa'}\right]^{\frac{1}{2}}\left[\left(1+\left(\kappa''/\kappa'\right)^2\right)^{\frac{1}{2}}-1\right]^{-\frac{1}{2}} \quad \textbf{3-6}$$

A difference is made between low-loss and high-loss materials. The penetration depth can be simplified in this respect to

$$D_p = \frac{\lambda\kappa'^{\frac{1}{2}}}{2\pi\kappa''} \quad \textbf{3-7}$$

for low-loss materials and to

$$D_p = \frac{\lambda}{2\pi\kappa''^{\frac{1}{2}}} \quad \textbf{3-8}$$

for high-loss materials.

The given equations show that the penetration depth is inversely proportional to the wavelength of the electromagnetic field; it decreases with increasing imaginary part of the permittivity as well as increasing conductivity. A high conductivity is represented by a high imaginary part of the dielectric constant. Typical penetration depths for water, granite and basalt are provided in Table 3-1.

Component	κ'	κ''	Penetration depth [cm]
Water	76.7	12	1.4
Granite	5.0 - 5.8	0.03 - 0.2	21 - 156
Basalt	5.4 - 9.4	0.08 - 0.8	5 - 74

Table 3-1: Typical κ', κ'' and associated penetration depths for water, granite and basalt at 2450 MHz microwave frequency. After Santamarina (1998).

Another important factor governing microwave irradiation of materials is the heating rate represented by the temperature increase ΔT in a certain time Δt.

$$\frac{\Delta T}{\Delta t} = \frac{P}{\rho C} = \frac{2\pi f\varepsilon_0\kappa''E^2}{\rho C} \quad \textbf{3-9}$$

Where ρ is the density [kg/m³] and C is the specific heat capacity [J/kgK] of the material. This equation displays the dependence and positive correlation of heating on the dielectric

loss κ" and the frequency. The equation is strictly valid only for homogeneous power density and negligible heat loss (by heat conduction or radiation).

3.1.2 Dielectric heating

The complex topic of interaction of a material with electromagnetic waves leads to dielectric heating of the irradiated medium. The electric and magnetic field components of the electromagnetic wave may be reflected, transmitted or absorbed by the irradiated material (Schiffmann 1997). Four categories of materials are defined according to their behaviour in the electromagnetic field and are as follows:

Opaque materials reflect and do not allow electromagnetic waves to pass through. The electromagnetic fields decay within a very short distance (penetration depth or skin depth). Conducting materials with free electrons like metals fall into this category.

Transparent materials allow microwaves to pass through. Ideally they do not absorb radiation. In reality, however, even typical insulating materials like glass or ceramics have a low dielectric loss.

Absorbing materials lie between insulators and conductors. Their properties as high dielectric loss materials allow them to convert radiation energy into heat.

Magnetic materials interact with the magnetic component of the electromagnetic wave and get heated as well.

Although several mechanisms for dielectric heating are identified some of the phenomena associated with it are not explained sufficiently yet (Gupta and Wong 2007). Dielectric response is characterized by the redistribution of charges or a polarization when applying an electromagnetic field. The main mechanisms include electronic polarization, dipolar polarization, atomic or ionic polarization as well as interfacial polarization. An overview of the different mechanisms is provided in Figure 3-4. The energy associated with the polarization can be partly transferred into vibrational energy of the atoms or molecules in the solid, i.e. into heat. This results in a loss of radiation energy or attenuation of the wave. In contrary to dielectric loss, materials with high electrical conductivity are heated by conduction losses (e.g. metals) and magnetic materials by magnetic losses.

When applying an external E-field to a neutral atom **electronic polarization** may be observed. The electrons are shifted from equilibrium positions with respect to the positively charged nucleus resulting in an induced dipole moment. This effect can be observed with covalent bonds, e.g. in crystalline silicon, where the valence electrons are easily shifted compared to the cores resulting in large dielectric constants of covalent

crystals like silicon and also germanium with ε' = 11.9 and 16, respectively (Kasap 2000 in Gupta and Wong 2007).

Several materials like water and hydrogen-chloride are made up of permanent dipoles. These dipoles are randomly orientated in absence of an electric field. When applying a rapidly varying electric field **dipole polarization** occurs when the dipoles respond to the E-field by rotating and aligning to the field. This leads to collisions of single molecules and thus dielectric heating.

In contrary to electronic polarization where only electron charges around a nucleus are shifted **ionic** or **atomic polarization** is caused by relative displacement of ions or atoms within molecules or crystal structures. Under an applied electric field the positive and negative ions are displaced from their equilibrium positions leading to a net dipole moment. Alkali halides like KCl or KF are amongst those crystals (Gupta and Wong 2007).

Free charges at interfaces like grain boundaries or defect regions are involved in **interfacial polarization**. In absence of an electromagnetic field no separation of the equal number of positive and negative charges is given leading to a random distribution inside the material. After the application of an electric field mobile charges are moved and accumulated at grain and phase boundaries leading to interfacial polarization.

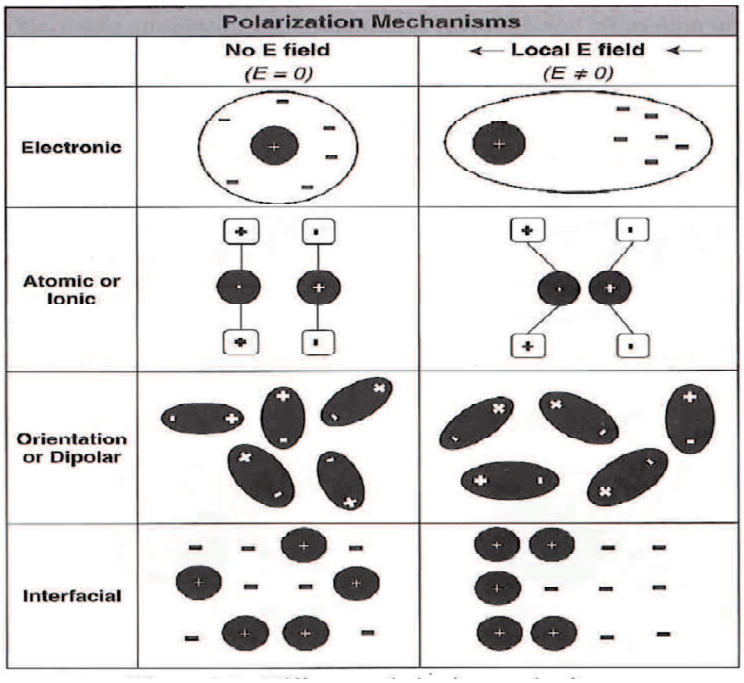

Figure 3-4: Different mechanisms of polarization (from Gupta and Wong 2007).

All these mechanisms lead to heating of the material via energy transfer from vibrations of the charged particles (electrons, ions) to mechanical vibrations of atoms or molecules in the lattice of the solid material. The energy of the latter ones is heat. How strong the

generated heat leads to an increase in temperature of the irradiated material depends on the degree of freedom of the lattice constituents, i.e. on the specific heat capacity (see equ. 3-9).

As highlighted above heating of a material with the help of microwaves is based on the absorption of electromagnetic waves by the material. Therefore microwave heating takes advantage of several unique features in comparison to conventional heating. According to Stein et al. (1994) and Gupta and Wong (2007) the main advantages are the penetrating radiation, rapid heating, controllable field distribution, selective heating of materials and self-limiting reactions. Some of the main features of the described advantages are listed as: internal heating, reverse thermal gradients, low surface temperature, very fast power response, remoteness of the applicator, high energy concentration as well as very rapid and selective heating of internal and surface constituents. However, some negative side effects and disadvantages are also coinciding with this technology: transparent materials are difficult to heat, generation of hot spots, arcing and generation of plasmas and the difficult control of the internal temperature.

One of the big advantages of microwave heating over conventional methods is the *penetrating radiation*. In this way heat can be generated inside a material as a result of the absorption and not from the outside where heating is depending on the heat transfer between applicator and material. Thus rapid volumetric heating can be achieved without overheating of the surface (Gupta and Wong 2007). The uniform radiation of several samples is a major feature exploited in the field of mineral processing with the help of microwaves (see chapter 4).

The differences in dielectric features of the constituents of an irradiated material are one of the major focuses of microwave irradiation. *Selective heating* can be achieved using the individual dielectric properties. This effect is widely used for heating of food as well as drying of wood and chemicals (Stein et al. 1994 and references therein). The effect is also used in several kinds of mineral processing, extractive metallurgy and rock breaking (e.g Pickles 2009a, 2009b).

3.1.3 Microwave sources and applicators

In principal a microwave system is made up of three major components. A microwave source generates the electromagnetic radiation, the transmission lines bring the energy from the source to the applicator where radiation is absorbed or reflected by the irradiated material (Thostenson and Chou 1999).

The **generation of microwave irradiation** is caused by the acceleration of charge. According to the desired power and frequency as well as factors like gain, noise, phase stability, size and costs several technologies are available. Amongst the currently available microwave generators are magnetrons, travelling wave tubes, klystrons and gyrotrons.

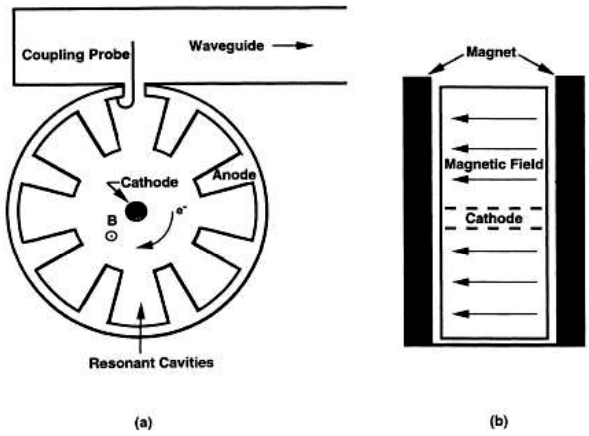

Figure 3-5: Schematic diagram of a microwave tube. (a) top view, (b) side view (Thostenson and Chou 1999).

The most common sources for industrial applications are magnetrons. They can be produced comparably cheap and in large quantities (Thostenson and Chou 1999) but are only able to emit a fixed microwave frequency. A high potential of the anode compared to the heated cathode is applied in a vacuum tube. In this way valence electrons are loosened and accelerated towards the anode by the electric field (Figure 3-5). Additional acceleration is caused by external magnets. Electrons pass the resonant cavities causing oscillations in the electron cloud. The frequency of these oscillations is controlled by the size of the resonant cavities. The energy is coupled from one of the resonant cavities to the transmission line being either a coaxial line or a waveguide launcher. The output power can be controlled by varying the current amplitude of the cathode or by adjusting the strength of the magnetic field.

A **transmission line** is essential for bringing the energy from the microwave source to the applicator. For low power operations coaxial cables are easy to apply and widely used up to about 60 GHz. Waveguides are used at higher frequencies and microwave powers. They are metallic tubes in which the electromagnetic waves propagate. In rectangular tubes the wave is linearly polarized.

The absorption of the electromagnetic wave by the load can be optimized by applying a **tuner** matching and adjusting the impedance and phase of the applied wave and the load.

Applicators are the interface between the microwave source and waveguide on the one hand and the material to be irradiated on the other hand. They are dedicated to cause controlled interaction of the electromagnetic energy and the material and provide safe, reliable, repeatable and economical conditions (Stein et al. 1994). Two basic concepts of applicators are found: multimode applicators/cavities and single mode applicators/cavities.

Multi mode applicators are relatively large compared to the wavelength of the electromagnetic field. They are commonly used for the irradiation of pieces larger than the wavelength and for bulk processing of materials or in household applications. These kinds of applicators are capable of sustaining a number of high order modes of the electromagnetic wave at the same time (Thostenson and Chou 1999). In this way they can be adapted to a wide range of applications and are less sensitive to the position of the product or the geometry. However, the number of possible resonant modes is increasing with the size of the cavity. This leads to the generation of various hotspots inside the applicator. One way of homogenization would be an increase in size of the cavity to more than 10-times the wavelength (approx. 1.2 m at 2450 MHz) or by applying wave stirrers and rotating sample holders guaranteeing for a randomly distributed electromagnetic field throughout the cavity.

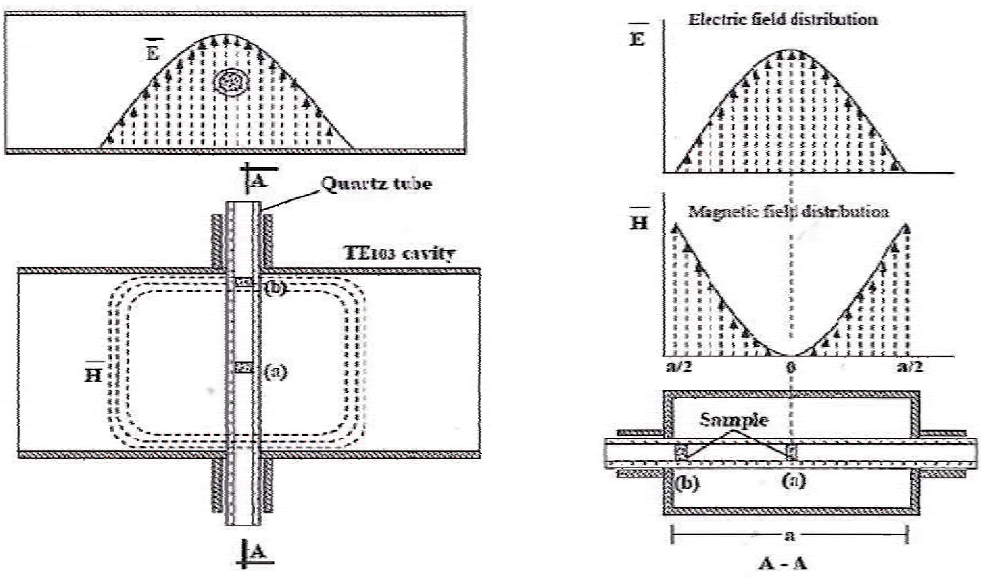

Figure 3-6: Examples of electric and magnetic field distributions in a single mode cavity (Gupta and Wong 2007).

Single mode applicators are characterized by their ability to host one hot spot where the microwave field strength is highest. This is achieved by solving Maxwell's equations in order to supporting one resonant mode inside the cavity. This normally leads to cavities sized in the order of one wavelength (approx. 12 cm for 2450 MHz). As shown in

Figure 3-6 a sample can be placed in the maximum of the electric or magnetic wave optimizing the utilization of the microwave technology. The positive features of the achievable high field strength like high efficiency and the possibility of irradiating low-loss materials as well are opposed by the limitation to specific product purposes, geometry of the load and position of the material (Stein et al. 1994; Thostenson and Chou 1999).

4 Research history of microwave treatment of minerals, ores and rocks

The following chapters will provide a short and brief overview over investigations in the wide field of microwave irradiation of rocks and rock constituents over the past decades. Most of the research was performed for mineral processing of various ores where a clear distinction between microwave absorbent grain and transparent matrix can be made. The influence of microwave irradiation on cracking, grinding and also leaching and recovery will be shown. Only few authors deal with the more complex topic of the irradiation of rocks like basalt, granite, sandstone and andesite which are not made up of components with such a distinctive difference in dielectric properties.

4.1 Microwave heating characteristics of rocks and rock constituents

The easiest way of assessing the microwave absorption of different materials is the measurement of the temperature of a sample after the irradiation. Walkiewicz et al. (1988) provide a detailed study of how different chemical compounds as well as natural materials heat up when irradiated with microwaves. The authors show that ore minerals can reach rather high temperatures. Magnetite can get as hot as 1258 °C after 2.75 minutes of irradiation with 1 kW at 2450 MHz whereas pyrite can get as hot as 1019 °C after nearly 7 minutes of irradiation. On the other hand silicates like zircon, albite and quartz only heat up to 52, 69 and 79 °C, respectively, after 7 minutes of irradiation. It is concluded that most silicates, carbonates and sulphates are transparent to microwaves whereas sulphides, arsenides, sulphosalts and sulphoarsenides show strong heating with microwave irradiation.

Santamarina (1989) provides an overview over research done before 1989. He gives a detailed overview of dielectric properties of all kinds of rock and related materials at different frequencies (Table 4-1). Typical values for most rocks range from 10^{-3} to 50 for κ' and from 2 to 10 for κ'' whereas the dielectric constant for water is much higher. According to most authors this implies that the water content is crucial to the heating behaviour of rocks. At lower frequencies (100 Hz to 1 MHz) an influence of the sample temperature on κ' can be reported for most materials. However this effect decreases with increasing temperature and the dielectric constant as well as the loss tangent approach constant values (Saint-Amant and Strangway 1970). A very detailed summary of dielectric constants of various inorganic materials is furthermore provided by Young et al. (1973). This collection provides data about dielectric constant and loss tangent for about 300

different materials as function of temperature and/or frequency. Further data about the complex dielectric constants of selected materials cover the range from 1 to 22 GHz (Nelson et al. 1989). The authors show that ε' of goethite and pyroxene is not influenced by the microwave frequency in this range. Other metal-oxides and silicates show partly strong reduction of permittivity as function of increasing frequency in this range.

Material	450 MHz		3000 MHz	
	κ'	κ''	κ'	κ''
Andesite, Hornblende	5.1	0.02	5.1	0.03
Basalt (9 Types)	5.6-9.6	0.06-0.86	5.4-9.4	0.08-0.88
Gabbro, Sytownite	7	0.14	7	0.13
Granite (7 Types)	5-6	0.02-0.15	5-5.8	0.03-0.2
Muscovite (26 °C)	5.4	0.002	5.4	0.0016
Marble (dry)	8.8	0.2	8.7	0.14
Obsedian (2 Types)	5.5-6.8	0.1-0.13	5.5-6.6	0.1-0.2
Peridotite (3 Types)	6.0-7.5	0.06-0.18	5.8-7.5	0.07-0.18
Pumice	2.5	0.02	2.5	0.03
Phyolite	3.38	0.05	3.4	0.04
Serpentinite (2 Types)	6.4-7	0.07-0.13	6.4-6.8	0.1-0.2
Syenite	8	0.4	7	0.6
Trachyte	5	0.13	5.2	0.13
Tuff (3 Types)	2.6-6.1	0.02-0.36	2.6-5.8	0.04-0.36
Volcanic Ash (3 Types)	2.7-3.4	0.08-0.23	2.7-3.2	0.06-0.15
Sandy Soil (w% = 0)	2.55	0.028	2.55	0.016
Sandy Soil (w% = 2.2)	2.5	0.063	2.5	0.075
Sandy Soil (w% = 3.9)	4.5	0.125	4.4	0.202
Sandy Soil (w% = 16.8)	20	0.3	20	2.6
Water	77.7	0.1	76.7	12.04
Water (95 °C)	52	0.384	52	0.244
Water (0.1 molal NaCl)	76	65	75.5	18.12
Water (0.5 molal NaCl)	96	290	67	41.87
Ice pure (-12 °C)	3.5	0.008	3.2	0.003

Table 4-1: Values for dielectric constants for various types of rocks at different microwave frequencies (after Santamarina 1989).

McGill et al. (1988) analysed powders of different materials at different microwave power levels (Figure 4-1). They showed, in similarity to other authors, that low loss materials like SiO_2 and $CaCO_3$ did not heat at power levels below 2000 W and that high-loss materials like PbS and Fe_3O_4 heat rapidly also with low applied power.

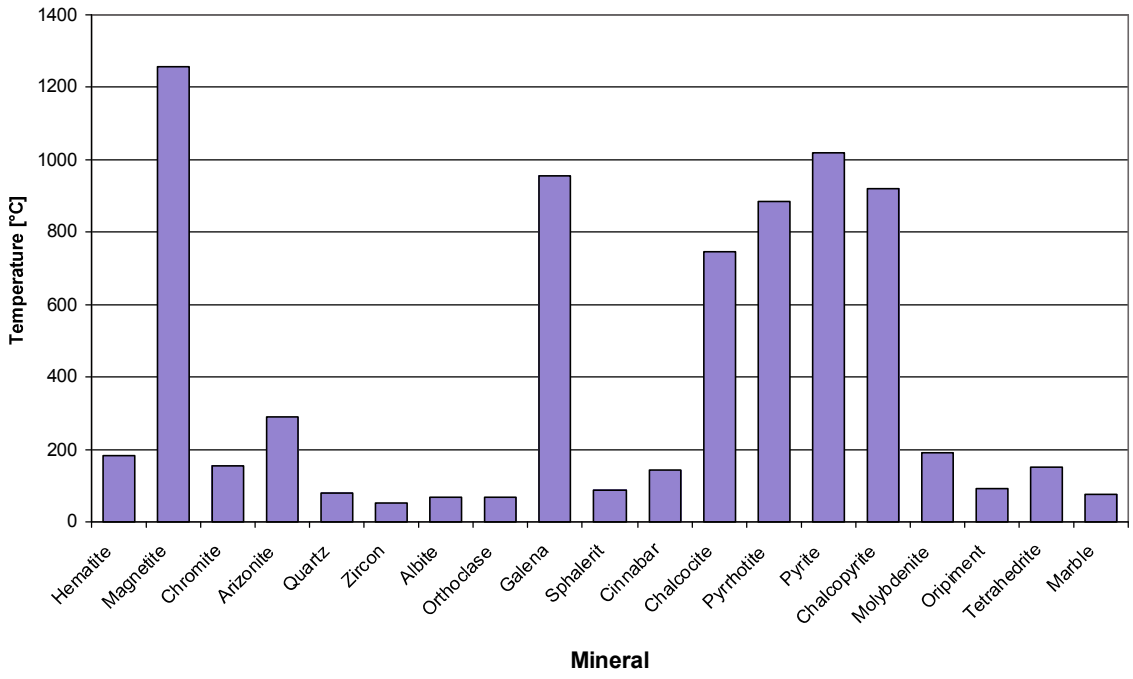

Figure 4-1: Qualitative effect of microwave irradiation on the temperature of different natural minerals (after Walkiewicz 1988).

Another summary of former publications on the topic of the heating behaviour of different rocks, minerals and as well as oxides and sulphides in the microwave field is provided by Haque (1999). He defined a classification of some constituents according to their heating capability. According to Haque a distinction can be made between hyperactive materials (UO_2, MoS_2, Fe_3O_4), active materials (NiO_2, Co_2O_3, CuO, Fe_2O_3), materials difficult to heat (Al_2O_3, PbO, MgO, ZnO, MoO_3) and inactive materials (CaO, $CaCO_3$, SiO_2). He provides a more detailed determination according to the mineralogy. Transparent mineral groups are carbonates, jarosite-type compounds, silicates, sulfates and some others (fergusonite, monazite, sphalerite and stibnite). Oxides cannot be classified that easily. Some like allanite, fergusonite and monazite do not heat whereas hematite, magnetite and pitchblende heat up readily when exposed to microwave irradiation. Most ores heat rapidly with some exceptions like nickeline, sphalerite or stibnite. ,

A more general approach for assessing the dielectric properties of rocks is the consideration of their chemical composition and a relation to geochemical measurements (Wang et al. 1999). ε' is in positive correlation to metal oxides and the water content represented by the LOI (Loss on Ignition) but in negative correlation with K_2O and SiO_2. For ε" a positive correlation to MgO, Fe_2O_3, SiO_2 and LOI could be demonstrated.

As already mentioned earlier it is well known and also backed up by experimental results (Jerby and Dikhtyar 2001; Peinsitt et al. 2010) that dielectric properties of rocks and minerals change not only with frequency but also with temperature. However, most of the data in literature is provided at room temperature only. Hutcheon et al. (1992a, 1992b, 1992c) introduce a system capable of measuring temperature dependent dielectric properties of various materials. For some ore minerals like siderite, magnesite, chalcopyrite, pyrite and galenite dramatic changes in ε' and ε" are reported at temperatures specific for each mineral (Lovás et al. 2010). Individual changes in real and imaginary part of ε are strongly linked to mineralogical changes. A similar trend is reported for andesite showing a significant rise in ε" from 0.05 to 0.9 at approximately 1100 °C. These strong changes in ε" can be linked to observed melting of the material. A significant rise in ε' and ε" with increasing temperature is also reported for hematite and nickeliferous limonitic laterite (Pickles 2004). The described change is strongly linked to phase transformations like the dehydroxylation of goethite (Pickles 2009a). Changes with increasing temperature of both ε' and ε" are also reported for sulphidic gold ores (Amankwah and Pickles 2009). The oxidation of sulphur and carbon at lower temperatures as well as the removal of sulphur and carbon at higher temperatures are believed to be of highest importance for the described behaviour.

4.2 Experimental studies on microwave heating of ores and the consequences for mineral processing

The occurrence of cracks and newly generated surfaces is of vital interest in several fields of mineral processing. After Haque (1999) 8 possible applications of microwave irradiation reaching from leaching to pretreatment of refractory gold ores, dehydration of chemical products, stripping of gold loaded carbon, regeneration of spent carbon, decontamination of soil, decomposition of smelter gas and vitrification of inorganic waste can be defined. Pickles (2009b) widens the spectrum of possible applications of microwaves in mineral processing and extractive metallurgy to drying, calcination and sintering, reduction and smelting, slag heating and reduction, segregation, treatment of Electric Arc Furnace dust as well as recovery of gold.

Didenko et al. (1997) and Sharkeev et al. (1997) report of dislocations within the subsurface layers of copper specimens after microwave irradiation with power densities between 2 and 400 kW/cm².

Kingman et al. (1999, 2000) investigated the influence of microwaves on massive ilmenite, refractory gold ore, carbonatite ore and massive sulphide ore. They demonstrated that the mineralogy of an ore has a strong influence on the absorption of microwaves and with it the grindability of the ore. According to this study ores with a consistent mineralogy that are surrounded by a transparent matrix show best effects, whereas finely disseminated ores show only little response to the irradiation. Other studies show that powders of massive sulphide ores develop strong intragranular cracking and a reduction in bond-work index of up to 70% as result of microwave irradiation with 650 W (Vorster et al. 2001).

A significant influence on the flotation recovery of copper ores after microwave irradiation with of up to 12 kW is reported by Sahyoun et al. (2005). According to the authors this increase in recovery is governed by an increase in intergranular cracks. A detailed look at the figures in the presented paper, however, gives rise to serious doubts of the conclusions drawn.

Experimental studies performed with a copper carbonatite ore at microwave powers of 10.5 kW in a single mode cavity conclude that intergranular fractures are introduced between microwave susceptible and non-susceptible minerals (Scott 2008). A better recovery of copper of up to 8 percent points compared to untreated samples could be achieved in this way.

After 5 s of irradiation with 5 kW a copper ore does not show obvious signs of breakage (Rizmanoski 2011). However, the investigated ore, made up of quartz and calcite as non-absorbers and chalcopyrite amongst others as the major absorber shows a reduction in breaking energy determined by the drop weight test.

Tests with a lead-zinc ore at microwave powers between 3 and 15 kW indicate that good damage can be achieved in only one second (Kingman et al. 2004a). According to the authors the application of a single-mode cavity will produce even stronger damage. Additionally the influence of the sample size is stressed. Smaller ore-samples show faster damage than a coarser grained feed. Reduction of required breakage energy by 30 % can be demonstrated for a carbonatite ore with the same experimental set-up (Kingman et al. 2004b).

Another process of interest is the liberation of gold. The generation of thermal stresses after 800 W microwave irradiation for 5 min was demonstrated (Amankwah et al. 2005; Amankwah and Ofori-Sarpong 2011). The alignment of cracks can be intergranular as well as transgranular. Lower rock strength and increased gold extraction after cyanidation coincides with the increased crack density.

Additionally to the grinding and breaking behaviour of ores and ore minerals some authors also investigated the grindability of coals (Lester et al. 2005; Kumar et al. 2011; Sahoo et al. 2011). It is shown that grinding characteristics of all investigated samples improved significantly as result of microwave irradiation. Kumar et al. also postulate that the increased crack density might be useful for the production of coalbed methane in inaccessible coal seams. It is shown that moisture plays a significant role in the generation of cracks at only 850 W of applied power (Samanli 2011).

4.3 Numerical investigations of heating and cracking of ores

A first numerical investigation of the behaviour of a mixture of a mineral particle in a non-absorbing host rock is provided by Salsman et al. (1996). They postulate for pyrite in a calcite matrix that the mineral will heat and that sufficiently high stresses will develop at the grain boundaries. The grain size is believed to play a major roll in this process.

The effect of microwave irradiation on 10 vol.% of pyrite particles within a transparent calcite host rock was numerically investigated by Whittles et al. (2003). They postulate that the strength of a sample after irradiation represented by the point load index and unconfined compressive strength can be decreased from 126 to 79 MPa after 30 s of irradiation with 2.6 kW. However damage is strongly depending on the power density provided. With higher power density a more significant reduction shall be achieved.

A simple calcite/pyrite system is also used by Jones et al. (2005, 2007) to identify the underlying fracture mechanisms. They postulate that the particle size is a governing factor when irradiating the sulphide. Particles of 50 µm heat up much stronger than particles of 500 µm. Fractures are caused by radial tensile stresses within the calcite matrix and by shear stresses along the grain boundaries to the pyrite particles. On the other hand the pyrite particle is not damaged because of the high compressive stress in the interior of the particles. The effect of microwave heating upon the liberation of pyrite and calcite is also demonstrated in another numerical study (Wang et al. 2008) demonstrating that cracks form along grain boundaries and stressing the fact that considerable mechanical energy can be saved by pre-treatment with microwaves.

Recent studies indicate that apart from grain size and irradiation time the power density provided is very important for commnution (Wang et al. 2008; Ali and Bradshaw 2009, 2010). In numerical simulations the dependence of crack density around a strongly absorbing grain in a non-absorbing matrix was calculated. The reports suggest that there is a minimum power density required to induce damage around grain boundaries which can not be compensated by a longer irradiation time. In this way not only the total input

energy can be reduced but the generated stresses can be concentrated around the grain boundaries of the irradiated ore. The effect of applied power density upon the generation of cracks is also stressed by Ali and Bradshaw (2011).

4.4 Experimental studies of microwave heating of hard rocks

The authors listed in the previous chapters generally focus on mineral comminution and the irradiation of small particles of a strong absorber within a transparent matrix. They demonstrate that differential absorption and heating lead to thermal stresses and the damage of the rock sample. Numerical simulations explain the mechanisms of cracking and damage. Only few papers discuss the possibilities of inducing damage in weaker absorbing rocks composed of particles with less difference in dielectric properties and thus heating rate and temperature gradients.

Santamarina (1989) summarizes experimental studies performed before the 1980ies. These works imply that a broad variety of rocks can be damaged with the help of microwaves. Granite, sandstone, slate and also porphyrite were successfully tested and destroyed.

Murova et al. (2000) demonstrate the heating of various rock types within a 900 W multimode cavity for 5 minutes. Tested rock types range from magnesite to andesite, dolomite, siderite and travertine. All tested rock types of this study show a reduction of ultrasonic wave velocity, as indicator of strength and crack density, after irradiation. A remaining strength of 37 % for magnesite is the most spectacular result reported in this study. However, it has to be noticed that sample dimensions are varying strongly throughout this study and a direct relation to the absorbed energy can thus not be drawn.

The influence of low power microwaves at 2450 MHz on basalt is demonstrated by Satish et al. (2006). They demonstrate that irradiation of basalt samples, 38 mm in diameter and 40 mm in height, can be heated to approximately 115 °C after 360 s of irradiation. Cracks were visible after 180 and 360 s going along with a decrease in compressive strength from 118 to 78 MPa and point load index from 5.62 to 3.73 MN/m² after 360 s of irradiation.

Kimberlite is another hard and abrasive kind of rock with ultrabasic magmatic origin. Investigations about the influence of 600 W microwave irradiation have been carried out in Russia (Didenko et al. 2005). It was demonstrated that samples could be heated rapidly and that subsequent dispersion appeared. More rapid damage at lower temperatures

could be realized when saturating the samples with water for 1.5 hours prior to irradiation with microwaves. With this set-up the rock burst into pieces of 2-4 mm in size. The occurrence of up to 8% of water incorporated in the pores of the host rock is believed to play a major role in the disintegration of the samples (Prokopenko 2011). However, also destruction of dry samples is reported in this publication leading to a better recovery of incorporated diamonds.

Sikong and Bunsin presented in 2009 that also granite can be damaged sufficiently by the help of low power microwaves (600 and 850 W). Dry and wet samples have been conventionally treated as well as water quenched after irradiation. Experiments show that compressive strength can decrease for 70 % when irradiated with 850 W and quenched with water afterwards. Cutting tests show a performance increase of 38%.

In 2010 Peinsitt et al. demonstrated the irradiation of a broader variety of rocks within a multimode cavity. They showed that basalt samples can be damaged significantly in only 2 minutes with 3.2 kW. Caused by the mineralogical composition granite heats up much slower but can be slightly damaged as well, whereas dry sandstone is not influenced by microwaves at all. They repeated their tests with water saturated samples. Here it could be shown that damage was hardly influenced for basalt but doubled for water saturated granite and increased four-fold for water saturated sandstone.

Drilling by localized microwave energy is another possible approach of utilizing this kind of energy (Jerby and Dikhtyar 2001; Jerby 2002). Small holes with a diameter of 2 mm can be generated in almost any material by the help of a coaxial waveguide directed on the surface of the material and utilizing a very fast thermal runaway effect to generate the hole.

As demonstrated above a lot of research was performed over the past decades dealing with the topic of microwave-rock interaction. It is also shown that only limited experimental data is available of the effects caused by microwave irradiation of different materials. Furthermore only limited knowledge was generated about the irradiation of fine grained and / or weakly absorbing rocks and rock constituents (non-ores). Although many reports suggest that microwave irradiation is a feasible and economically viable way of rock treatment for the different tasks given in comminution, breaking and leaching no successful installation of an industrial microwave apparatus in this field is reported yet.

5 Investigated rock types, methods of rock damage determination and experimental setup

5.1 Characterisation of investigated rock-types

As mentioned in chapter 2 the goal of this study is to investigate the effect of microwaves on hard and abrasive rocks with different microwave absorbing characteristics. The selection of rock samples follows these considerations as well as the availability of large and homogeneous block. Greenstones, granite and sandstone represent three major groups of rocks in terms of hardness and abrasivity on one hand and microwave absorption properties on the other hand. Whereas greenstones like basalt and diabase are relatively good absorbers and fine grained rocks, sandstone and granite have worse absorption properties and completely different mineralogical textures compared to basalt. Gabbro is a good absorber with a medium-grained texture and sulphidic copper ore is especially hard and tough and a good absorber only under very specific circumstances.

5.1.1 Basalt Weitendorf

The quarry of Weitendorf is located to the south of Graz. According to Heritsch (1963) the matrix of these rocks is made up of plagioclase, olivine, pyroxene, ilmenite and dolomite. Several porphyroblasts of olivine and plagioclase as well as hornblende can be found. A rather unfortunate feature of this rock is the occurrence of natural cracks being a result of the cooling process. These cracks are often healed and filled with calcite. The occurrence of cracks has a positive influence on the destruction of samples but complicates the interpretation of results because they are randomly distributed throughout the sample mass.

5.1.2 Basalt Klöch

Klöch is situated in Eastern Styria close to the boarder to Slovenia. Volcanic rocks in the region can be defined as nephelinbasanites. According to Heritsch (1976) the rocks are mainly composed of a matrix of clinopyroxene and lighter colored constituents like plagioclase, nepheline and analcime with inclusions of olivine and clinopyroxene. According to XRD-analyses the main phases in the investigated samples are augite, nepheline, montmorillonite, analcime and anorthite.

Samples investigated for this study have been taken from the quarry of the Klöcher Basaltwerke GmbH & Co KG in Klöch. Samples were taken from a relatively recently blasted area from the quarry. The exact weathering conditions could however not be reconstructed.

5.1.3 Diabase Oberhaag

The quarry of Oberhaag is situated in the south of Styria near the Slovenian border. The rock shows a fine-grained crystalline texture. The main mineral phases are albite, quartz, chlorite, calcite, edenite and biotite. Several joints are filled with calcite.

5.1.4 Diabase Jakomini

The Jakomini quarry near Bad Bleiberg in Carinthia provides a volcanic breccia which is sold as diabase and known to be very hard material.

5.1.5 Diabase Saalfelden

In Saalfelden two different quarries are mining for diabase. Hinterburgbruch and Tagebau21 being a newly opened quarry. The main phases of this rock are quartz, ferriwinchite, chlorite and albite. Amongst the most important accessories are graphite, galena, pyrite, markasite and others (Fischer 1978). The rock shows fine and coarse grained texture.

5.1.6 Gabbro Nerro Assoluto

According to Okrusch (2005) gabbro is the equivalent of basalt for plutonic rocks. The only significant difference between the two types of rocks is the texture. Basalt represents a dense and fine-grained variety whereas gabbro is normally composed of a medium- to coarse-grained texture of plagioclase, augit, pyroxene, olivine and others.

Santamarina (1989) reports that the dielectric properties of gabbro are similar to those of basalt ($\kappa' = 7$ and $\kappa'' = 0.13$; Table 4-1).

The origin of the investigated type of gabbro is unknown. Its trade name at the local stonemason, however, is Nerro Assoluto.

5.1.7 Copper Ore –Neves Corvo

Neves Corvo is a metal deposit in the Spanish Pyrite belt. It is comprised of different sulphides. Chalcopyrite ($CuFeS_2$) and pyrite (FeS_2) are the main components of this ore. Minor amounts of sphalerite (ZnS), galena (PbS), aresonpyrite (FeAsS) and tin bearing phases can be found as well (Pohl et al. 1992; Vorster et al. 2001).

According to the literature metal sulphides have an excellent absorption of microwaves (Santamarina 1989). Thus good heating and destruction of the samples were expected.

5.1.8 Sandstone Imberg

Metasandstone of Imberg is mainly composed of quartz, feldspar, muscovite and chlorite. It shows weak metamorphosis with newly formed chlorite. Quartz grains are subgranular and show pressure solution as well as interlocking due to recrystallisation. The sediment is fairly classified with grains sizes < 1 mm but poorly sorted with the occurrence of feldspar and coarse grained mica. Feldspar is partly alterated and sericitized (Mali 2007).

5.1.9 Granite Neuhaus

Granite of Neuhaus shows granular texture with some xenomorphic crystals. The main constituents are quartz, feldspar, biotite, muscovite and chlorite. Plagioclases are often twinned or sericitized whereas orthoclases occur as pertithe or microcline. Accessories are apatite, epidote, sphene and xenotime (Mali 2007)

5.2 Assessment of rock damage caused by of microwave irradiation

For the challenging task of identifying all possible changes of rocks properties as a consequence of microwave irradiation a broad variety of analysis-tools were used. Both, destructive and non-destructive test methods were utilized. The big advantage of non-destructive test methods such as the determination of ultrasonic wave velocities lies in the re-usability of the very same sample. In this way the changes inside the irradiated rock-samples could be analysed as a function of repeated irradiation. The occurrence of naturally incorporated water in the tested rock specimen leads to coinciding mineralogical and structural changes as result of microwave irradiation. Many of those changes could only be evaluated with non-destructive test methods.

With the broad variety of tests both qualitative and quantitative results could be obtained. Qualitative investigations help understanding the mechanisms of damage, crack propagation and heating as result of microwave irradiation. Quantitative results such as p-

wave velocity or cutting tests help measuring the influence of microwave irradiation and comparing the exploited energy to other rock cutting methods.

5.2.1 Determination of the chemical composition

The determination of the chemical composition of the samples was performed at the chair of General and Analytical Chemistry at the University of Leoben.

For the determination of Loss on Drying (Dry) and Loss on Ignition (LOI) fine grained samples where heated to 105 and 1000 °C, respectively.

X-ray fluorescence analyses (XRF) where used to gather quantitative data of the element composition of the investigated rock types. Fused discs where prepared by melting 1 g of sample powder with 8 g of lithiumtetraborate in a “Vulcan Fluxer” provided by Fluxana. The analyses of both major- and minor elements where accomplished with a wavelength-dispersive X-ray fluorescence spectrometer (WD-XRF) provided by Panalytical and an in-house developed calibration programme named GeoWSU. The calibration-method consists of more than 50 geological samples of different composition and is validated by the participation in a Proficiency Testing Programme (GeoPT organized by IAG) twice a year. Accuracy ranges in dependence of the element concentrations with varying from 2 % for SiO_2 to 20 % for concentrations below 50 mg/kg.

5.2.2 X-ray diffractrometrical (XRD) analyses

Mineralogical compositions of investigated rock types were determined with the help of x-ray diffractometry. Tests on powdered samples were performed by H. Hopfinger at the Chair of Ceramics at University of Leoben.

A Bruker AXS D8 Advance X-ray diffractometer was used applying Bragg-Brentano geometry. The range between 2° and 65° of the doubled angle of diffraction was investigated in steps of 0.05°. A LynxEye Super Speed detector detected the refracted x-ray beam. Data analysis was done with DIFFRACplus measurement centre and DIFFRACplus EVA for qualitative evaluation by comparing the measurement with the ICCD PDF4+ database.

5.2.3 Optical microscopy

Optical assessment of the influence of microwave irradiation, the mineralogy and occurring cracks was done with an Olympus BX 60 microscope. Standard and resin saturated thin sections were prepared in the laboratories of the Chair of Resource Mineralogy and of the Chair of Geology and Economic Geology at University of Leoben.

For better presentation of cracks some samples were saturated with a blue resin prior to the preparation of the thin section.

5.2.4 P-wave velocity measurements

The travelling time of sound waves through a sample can be considered as being an excellent indicator for the occurrence of cracks and disturbances. A longer travelling time of the p-wave indicates a less densely packed sample and thus the occurrence of cracks.

For the determination of the travelling time [µs] an EG-Meter model DIGI EG c3 provided by Labek was used applying a measurement frequency of 2 MHz which has been chosen in order to detect also small inhomogenities. The accuracy depends on the investigated material and geometry of the specimen. For proper coupling of rock and transmitter and detector, sample surfaces were treated with a coupling agent and a pneumatic stand was used guaranteeing for a defined contact pressure which is essential for reproducible measurements. The sound velocity [m/s] can be easily back-calculated by knowledge of the travelling distance and travelling time of the waves. .

5.2.5 Temperature measurements

Microwaves heat materials at some distance below the surface which is depending on the specific dielectric constants. The measurement of the temperature inside a sample is a complicated task. Two factors influence correct measurements to a great extent. The easiest way of measuring the temperature inside a sample is the application of a sensor inside the sample mass. This can be achieved by drilling a hole in which the sensor will be placed. However, three problems occur with this kind of measurement. (a) The drill hole will influence the electromagnetic field, the heating characteristics and also the heat flow within the sample. (b) The sensor is made of metal influencing the heating characteristics and electromagnetic field. It is working as a focus for microwave irradiation. (c) The cable of the sensor which has to be guided through the wall of the safety cavity is working as antenna and thus causes problems to the safety of the procedure. Furthermore, the application of a temperature sensor provides randomly distributed data of the vicinity of the sensor.

A first indication of microwave absorption is given by the surface temperature [°C] after a certain irradiation time. This method can be applied easily without further sample preparation.

Surface temperature of irradiated samples was measured with an Ahlborn MR721420 infrared thermometer with adjustable focus and emissivity ε, according to the specific emissivity of the rock types calibrated with a standard thermocouple.

The application of an infrared camera (IR-camera) is a more complex procedure.It gives a detailed image of the temperature distribution of the observed area and it helps overcoming the effects of the sample preparation and application of sensors on the electromagnetic field and heat flow.

For measuring the temperature inside rock samples they were cut into two pieces very thoroughly to provide very smooth faces (Figure 6-8). Whilst irradiation the cut faces have been put together again and tightened with a tape at the circumference. After irradiation a fast dispatch of the two half cylinders (< 5 s) was possible and a picture could be taken with the IR-camera (Figure 6-9). It is assumed that due to the smooth faces this procedure has only little influence on the heat flow during irradiation and can be considered as a good approach for getting a better insight into the heating effects of microwaves.

The described infrared measurements were performed with a ThermaCam SC500 thermocamera from FLIR in cooperation with Beate Oswald-Tranta and Mario Sorger at the Chair of Automation at University of Leoben. The detector is an Uncooled Focal Plane Array with a resolution of 320 x 240 pixels operating in a spectral range between 7.5 and 13 µm. The camera has a thermal solution of 0.1 °C at 30 °C and an accuracy of ± 2 % or ± 2 °C in a temperature range between -20 °C and +2000 °C.

5.2.6 Liquid penetrant inspection

Liquid penetrant inspection is a simple and effective method of examining surfaces for cracks, defects and discontinuities (Cartz 1995). After the surface has been cleaned from oil, grease or other contaminants the penetrant is applied as a spray. After some minutes when it is allowed to penetrate flaws the excess penetrant is removed from the surface and the developer is applied. It draws out the penetrant from open cracks forming visible indications of cracks.

For this study cleaner, penetrant and developer of the Diffu-Therm line of H. Klumpf KG have been used as available in the Sandvik testing laboratories.

5.2.7 Numerical simulation of microwave-rock interaction

Numerical simulation provides necessary information for better understanding of the interaction of microwaves and rocks. The results of two kinds of simulations were taken into account in the discussion of the results of this thesis. (a) Microwave propagation in a

block of rock, i.e. simulation of the propagation in the large-scale experiment. (b) Generation of temperature gradients and stresses in cylindrical samples of the small scale experiments. Expertise available at the University of Leoben was used: for (a) at the Institute of Physics (R.Meisels, F.Kuchar, Finite Difference Time Domain (FDTD) - method with FullWAVE software package by RSoft Design. for (b) Institute of Mechanics (R. Leindl, T. Antretter, Finite Element Modelling (FEM) with an ABAQUS v6.10 software package).

5.2.8 Mechanical cutting tests

Apart from macro- and microscopic investigations an assessment of the induced damage in the whole rock mass was performed. The goal was to check the feasibility of microwave induced damage in a possible large-scale application and to quantify the influence of microwave irradiation on different rock types. Samples were prepared in a way to investigate the differences between irradiated and untreated areas with the help of a cutting test-rig. An overview of the test-rig is provided in Figure 5-1. A pick is dragged over the rock sample by the help of a hydraulic piston. Side-, normal- and cutting forces acting on the tool in action are measured automatically. In this way an estimation can be given of how much energy is needed to damage / or cut a certain kind of rock under the given circumstances. The exemplaric evaluation of one single cutting line is displayed in Figure 5-2. Here the measured forces in [kN] are displayed as a function of the position of the pick on the sample. Ultimately a difference of the measured forces between irradiated and untreated sample surfaces would indicate a strong influence of microwave irradiation on the cutting resistivity of the rock samples. The analysis of the data includes a detailed examination of every single cut as well as averaging and statistical approaches over a set of data.

Figure 5-1: Linear cutting test rig prior to test. Sample placed in tray. The pick is dragged over the sample surface with defined speed and penetration depth.

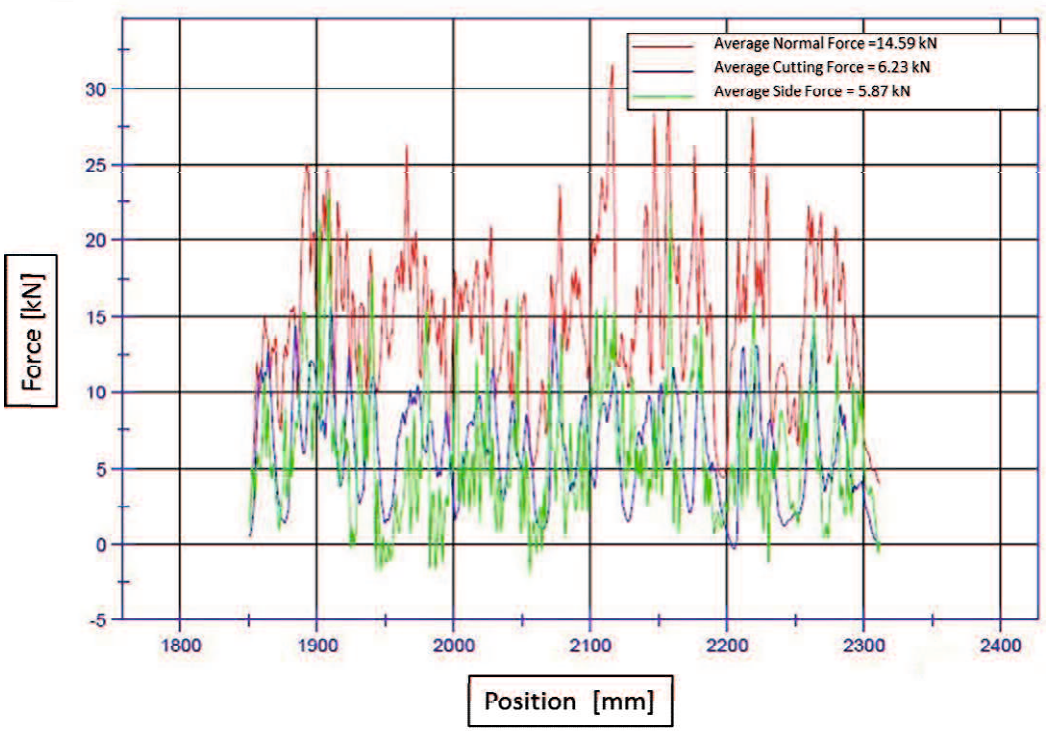

Figure 5-2: Exemplaric measurement of a single cut in the linear cutting test-rig. Side-, Normal and Cutting forces [kN] as a function of position of the pick [mm].

Figure 5-12 shows an exemplary irradiation pattern for these kinds of tests. Two larger areas of approximately 200 x 250 mm² were irradiated whereas the rest of the rock mass remains untreated. As indicated by the hatching in the Figure the pick was dragged from the right to the left side of the sample with a defined moving speed of 1.5 m/s. The depth and spacing of individual cuts is depending on the investigated rock type. A total number of 20 – 25 cuts per cutting plane could be performed in this way. In order to getting an insight into the penetration depth of microwaves and the coinciding development of damage within this depth between 3 and 5 cutting levels have been investigated. The number of different levels depended on the respective rock type.

Prior to these investigations a rough sample surface had to be established in order to provide good comparability between individual cuts and different levels of depth. This was done by cutting the surface before the first irradiation of the sample.

5.2.9 Presentation of data

Common illustrations of the measured data would concentrate on highlighting the average value and indicating the standard deviation. This kind of illustration would eliminate the extreme outliers and subsumizes them in an average value. Due to the fact that in most

cases only five samples of each population could be tested in course of this study the occurrence of outliers would have major impacts on the average values. It is also stressed by Hosteller and Tukey (1977) that the resistance of a summary to outliers is an important factor. This is demonstrated by a simple example explaining why the arithmetic mean is the prototype of a non-resistant summary. The average value of (1+2+2+3+···+23) / 101 = 9.58. Changing only one value to 1010002 instead of 2 would lead to an arithmetic mean of (1+2+101002+3+···+23) / 101 = 1009.58. So changing only 1/101st of the data would change the mean significantly. The median of the same sets of data would only change from 9 to 9.5, respectively, and represent a summary being much more resistant to large fluctuations.

However, the occurrence of outliers especially amongst the lower values of the p-wave velocity is considered as being a major indicator for the inferred damage after microwave irradiation in a sample. An outlier with a very low velocity for example would indicate excellent damage but would not be sufficiently highlighted in an average value. Thus boxplot diagrams were chosen which help identifying the broad variations in collected data and ease the identification of outliers. One can easily identify the locations of quartiles, mean, median and extreme values. The spread and variation of extreme values, the range, is quickly displayed with the help of a box and whisker plot. Amongst the other advantages of boxplots are the easy identification of skewness of data sets and the comparability of several parallel groups of data (Tukey 1977; Liu 2008). One can quickly see how data sets differ from each other and identify how changes of the mean values are influenced by extreme outliers of the data set.

In the applied calculation of the box plots used in this study 50 % of all values are higher and 50 % are lower than the Median displayed by a black horizontal line. The box covers the upper and lower Quartile lying at 75 % and 25 % of all values, respectively. Values that lie outside that range are covered by the so called whiskers which are 1.5 times the height of the box. Outliers and extreme outliers are represented as dots and stars according to their distance to the box.

5.3 Small-scale microwave irradiation

For small-scale microwave irradiation experiments and investigations a standard household microwave Panasonic NE-3240 operating at 2450 MHz with a power of 3.2 kW in a multi-mode configuration was applied (Figure 5-3). Rock samples predominantly had a diameter of 50 mm and a height of 50 mm. As shown in this figure samples were placed on top of a cylinder made of quartz glass in the centre of the microwave cavity. Quartz-glass was chosen because it is penetrated by microwaves without any absorption and

thus has no further influence on the experiment and allows for a positioning of the sample in the place with the highest field strength inside the cavity.

Figure 5-3: Experimental arrangement for small scale laboratory tests. Sample placed in centre of microwave on top of glass cylinder and infrared thermometer with data logger (left and on top of microwave door) for the investigation of surface temperature after irradiation (Foto taken by T. Peinsitt).

The energy input into the sample is directly proportional to the irradiation time. Standard experiments have been performed in a way to investigate the influence of different irradiation times, equalling different energy input. The goal of the experiments was to assess the damage inferred within a rock and the coinciding mechanisms as a function of irradiation time and thus energy input. Generally one can say, the longer a rock is irradiated with microwaves the more damage will occur. Samples were placed in the centre of the cavity and irradiated for the desired time. The door of the cavity was opened immediately after irradiation and the surface temperature of the irradiated samples was measured with an infrared thermometer.

A minimum of five samples was tested for each rock type and irradiation time.

5.3.1 Increasing power density with the help of a steel cone

The conventional microwave oven used for experiments provides a randomly distributed microwave field throughout the whole cavity. However, from tests performed with a water load instead of a rock sample we know that only 60 % of the provided energy (60 % of 3.2 kW = 1.9 kW) goes into the sample. Considering the relatively weak absorption of rocks compared to water even less energy is absorbed by the rock mass. An experimental setup was developed to increase the efficiency of this process.

Due to the nature of the electromagnetic field, microwaves concentrate at sharp edges and tips particularly of metallic bodies. We designed and manufactured a steel cone that helps concentrating microwave energy at its cone point (Figure 5-4). The cone was placed on a cylinder manufactured of pure quartz-glass to provide an upright position in the centre of the cavity. With the help of this steel cone an increase in energy in the contact zone of cone and sample can be provided.

Experiments have been performed in a similar way as “standard” experiments. Several irradiation times have been performed for each rock-type investigated.

The quantitative assessment of the damage as result of p-wave velocity measurements is rather difficult in this case. Due to the nature of the experiments a spot of molten material remains at the surface after irradiation. This molten point complicates the correct placement of the sensors which have to be positioned tightly to the plain surface. Thus samples had to be polished after irradiation in order to maintain a suitable surface for p-wave velocity measurements.

Figure 5-4: Arrangement of steel cone in microwave oven. Glass cylinder, sample and steel cone (bottom to top) inside the cavity. The steel cone is kept in position with help of a glass tube. For the glass parts non-absorbing quartz glass is used.

5.3.2 Quenching of hot samples

A very ancient approach for reducing a rocks’ strength is classical fire-setting and was performed successfully for several centuries all over Europe. After a fire was burnt inside a tunnel the heated faces where quenched with water to decrease the strength of the rocks and make them easier to treat with hammer and chisel.

This approach was tested in this study by cooling pre-heated samples with liquid nitrogen with a temperature of -190 °C In the performed experiments samples where heated in the microwave cavity as described in “standard” experiments. Irradiation times were chosen according to the specific behaviour of each investigated rock type and in order to achieve a very high temperature gradient in reasonable time. Hot samples were removed from the cavity with metal pliers and immersed into the liquid nitrogen immediately. Samples remained in the cooling liquid for 15 minutes, put out again and were allowed to slowly heat to room temperature before further testing.

5.3.3 2nd heating cycle

Some samples have gone through a second heating process which was performed with exactly the same parameters as the first treatment. Samples that were irradiated for 120 s in the first step were also irradiated for 120 s in the second step. In this way the influence of the first irradiation on the absorption and heating properties of the rock types could be tested. As will be shown in the subsequent chapters some rocks loose a certain amount of mass (most likely water) as result of microwave irradiation. The goal of these investigations was to validate the influence of this change on the heating behaviour and resulting temperature.

5.4 Large-scale microwave irradiation

The success of microwave irradiation of rocks is strongly depending on the generation of temperature gradients inside the rock mass. Fast heating of the absorbing phases in comparison to the non-absorbing constituents of the rock mass is a prerequisite. Only when heating of these constituents happens much faster than thermal conduction between them sufficiently high gradients can be achieved. Microwave irradiation of small samples in a multimode cavity at relatively low output power leads to relatively slow heating of the entire sample in tens of seconds or even minutes depending on the respective rock-type. Significant damage is occurring after inacceptable long irradiation time. Because of the more or less homogenous distribution of the electromagnetic field in the cavity only a small fraction of the provided energy goes into the rock mass.

Fast heating is not only necessary for the generation of sufficiently high stresses inside the rock mass. Furthermore cracking and damaging in short time and sort operational cycles are a prerequisite for a technical and economical application of the described technique.

In addition to these technological considerations, the application of a small multi-mode cavity does not reflect a possible real-life application of the technique in a mining environment. Here an one-sided irradiation of the area of interest is most likely.

There are two complementary approaches to increase the efficiency in terms of heating a spot or sample in the shortest possible time. First of all the applied power has to be increased significantly and secondly the coupling of rock and microwave has to be improved.

The energy absorbed by the rock sample increases as function of the applied power. Here the simple increase in output power of the microwave system will lead to an improvement.

Secondly the proper placement of the sample in front of the waveguide will lead to better coupling of microwave and rock and a further increase in the specific energy applied to the area of interest. In a conventional multi-mode microwave cavity the electromagnetic field is distributed all over the cavity. In a large technical application the applicator will most likely only be a fraction of the size of the irradiated face. This relatively small cross section (typically 43*86 mm² for a frequency of 2450 MHz) leads to a significant increase in specific power [W/m²] applied to this single spot.

It was decided to treat samples with a surface many times larger than the waveguide in order to study this specific setup and to exclude side effects incorporated by the geometry of the sample. Sample sizes where therefore either 30*30*30 cm³ or 50*50*30 cm³ (w*l*h) depending on the availability of sample material. The height of 30 cm roughly corresponds to the effective penetration depths in most investigated materials as can also be seen in Figure 10-4)

5.4.1 Large-scale microwave irradiation apparatus

An apparatus was designed and implemented in order to fulfil the described requirements. Considerations were also made according to safety as well as experimental feasibility. The following chapters will explain both the underlying problems and the applied technical solutions.

5.4.1.1 Safety considerations

Applying a high amount of microwave power requires certain precautions in the application of safety procedures and arrangements. According to Bergqvist et al. (1998) and Österreichischer Verband für Elektrotechnik Fachausschuss Elektromagnetische Verträglichkeit (2006) levels of exposure to electromagnetic fields for different frequencies and groups of persons are set. As shown in Table 5-1 the basic restrictions for the SAR

(Specific energy absorption rate) for occupational exposure are set for 2450 MHz as follows:

- Whole-body average SAR: 0.4 W/kg
- Localized SAR (head and trunk): 10 W/kg
- Localized SAR (limbs): 20 W/kg

Exposure characteristics	Frequency range	Current density for head and trunk (mAm^{-2})	Whole-body average SAR (Wkg^{-1})	Localized SAR (head and trunk) (Wkg^{-1})	Localized SAR (limbs) (Wkg^{-1})
Occupational exposure	up to 1 Hz	40	-	-	-
	1-4 Hz	40/f	-	-	-
	4 Hz - 1 kHz	10	-	-	-
	1-100 kHz	f/100	-	-	-
	100 kHz - 10 MHz	f/100	0.4	10	20
	10 MHz - 10 GHz	-	0.4	10	20
General public exposure	up to 1 Hz	8	-	-	-
	1-4 Hz	8/f	-	-	-
	4 Hz - 1 kHz	2	-	-	-
	1-100 kHz	f/500	-	-	-
	100 kHz - 10 MHz	f/500	0.08	2	4
	10 MHz - 10 GHz	-	0.08	2	4

Table 5-1: Basic restrictions for time varying electric and magentic fields for frequencies up to 10 GHz. After Bergqvist et al. (1998).

The afore mentioned values are only measurable with complicated methods. That is why reference levels are set from mathematical calculations (Table 5-2). Their measurement is much easier and meeting these levels will guarantee meeting the basic restrictions also under the most unfortunate conditions. The most important reference levels for occupational exposure are as follows:

- Electric field strength: 137 V/m
- Magnetic field strength: 0.36 A/m
- Equivalent plane wave power density: 50 W/m²

The construction of every microwave facility has to take these values into account. A cavity has to be constructed guaranteeing to meet the limits.

Frequency range	E-field strength (Vm^{-1})	H-field strength (Am^{-1})	B-field (μT)	Equivalent plane wave power density S_{eq} (Wm^{-2})
up to 1 Hz	-	1.63x105	$2x10^5$	-
1-8 Hz	20000	$1.63x10^5f^2$	$2x10^5/f^2$	-
8-25 Hz	20000	$2x10^4/f$	$2.5x10^4/f$	-
0.025-0.82 kHz	500/f	20/f	25/f	-
0.82-65 kHz	610	24.4	30.7	-
0.065-1 MHz	610	1.6/f	2.0/f	-
1-10 MHz	610/f	1.6/f	2.0/f	-
10-400 MHz	61	0.16	0.2	10
400-2000MHz	$3f^{1/2}$	$0.008f^{1/2}$	$0.01f^{1/2}$	f/40
2-300 GHz	137	0.36	0.45	50

Table 5-2: Reference levels for occupational exposure to time-varying elctric and magnetic fields (unperturbed rims values). After Bergqvist et al. (1998).

5.4.1.2 Technical specifications of large-scale microwave apparatus

The system consists of two parts. (a) the microwave generator and waveguide system (Figure 5-6) which provides microwave energy and (b) the safety cavity (Figure 5-7) guaranteeing for a safe and smooth experimental procedure. Figure 5-5 shows the final set-up of the microwave test rig.

Figure 5-5: Final assembly of microwave test-rig. Magnetron and control unit (covered with a construction of sheet metal; left side) and safety cavity (right side).

The microwave generator is supplied by Mügge Company. It can be seen in Figure 5-6. The magnetron has a maximum output power of 30 KW operating at a frequency of 2450 MHz. An automatic tuner guarantees the reduction of possible reflections as well as excellent coupling of microwaves to the irradiated samples. Additionally this tuner is capable of logging all essential parameters like actual frequency, forward and reflected

power as well as the phase of the waves. The magnetron is controlled by an electronic unit. Here the operator can set the time of operation for the desired output power. Power is tuneable from 10 % of the maximum power (=3 kW) to 100 %. In this way a pseudo-pulsed operation can be achieved as well: pulses of 30 kW can be alternated with resting times of only 3 kW.

The circulator deflects microwave reflected by the system into a water load protecting the sensitive magnetron from too high reflected power. A further safety mechanism is a photo diode placed close to the magnetron detecting lightning and electric arcs. A detected arc will lead to the shutdown of the system guaranteeing for the safety of the magnetron. A Teflon window is permeable for microwave radiation but prevents whirled up dust to travel through the waveguide

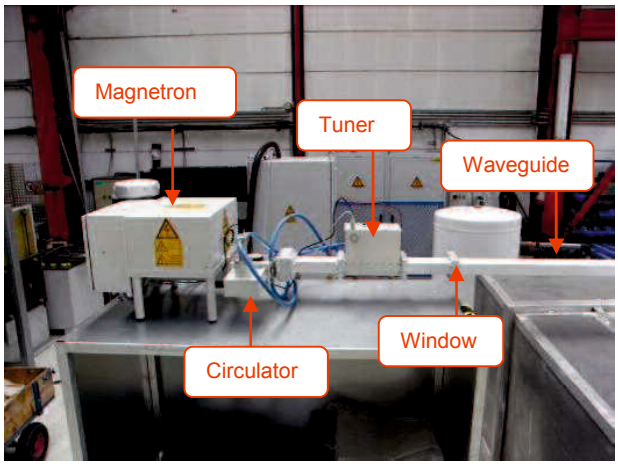

Figure 5-6: Set-up of the microwave test-rig. Magnetron, circulator, tuner and waveguide towards the cavity (left to right, highlighted by red arrows).

To meet the given standards and provide smooth operation a cavity was designed which can a) provide the safety requirements and b) guarantee easy handling of rocks and application of microwaves (Figure 5-8). This safety cavity is an essential step in the construction of the high-power laboratory equipment. It has been developed in strong cooperation with TÜV Austria, guaranteeing to meet the given safety standards under any circumstances.

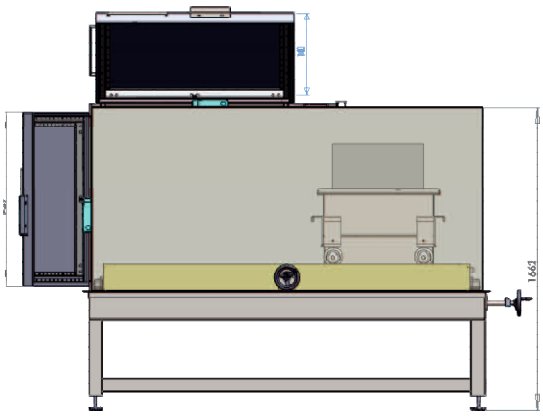

Figure 5-7: Sketch of the safety cavity. Doors in front and on top, sample in sample movable sample try, hand wheels for xy-movement of the tray.

As shown in Figure 5-8 the waveguide is inserted from above and microwave energy can be applied directly to the surface. The waveguide has dimensions of 43*86 mm².

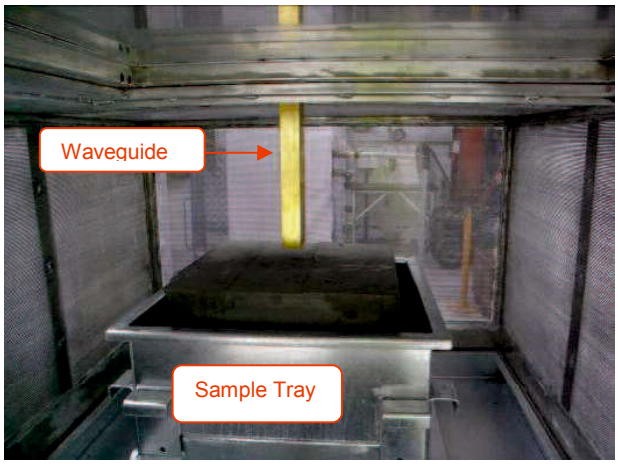

Figure 5-8: View inside the cavity with sample on xy-table, waveguide from top.

A xy-table with a tray for rock samples provides the precise manoeuvrability and handling during the testing procedure. Rock samples of a maximum size of 50*50*30 cm³ (w*l*h) can be inserted with a forklift from the front or with a crane from above. The table can be moved by two separate precision hand wheels (Figure 5-9). The design of these hand wheels is a critical point in the design of the cavity. The construction of an axle which passes through the wall of the safety cavity must lead to the generation of a small slot at the circumference of this axle. This slot, however, would be a proper pathway for the electromagnetic field and thus the axle would act as antenna on the outside when the microwave field is applied in the inside of the cavity. By designing a complicated maze of bearings and metal sheet a solution was found which seals this slot preventing the apparatus from acting as dangerous antenna. A similar system was implemented for the

door sealings and is shown in Figure 5-10. A spring sealing together with a large bearing face prevent any electromagnetic radiation from exiting the safety cavity.

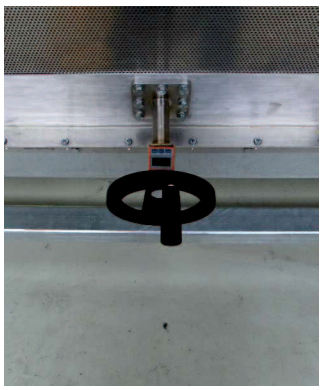

Figure 5-9: One of two hand wheel sat the outside of the cavity for precise movement of the sample tray beneath the waveguide.

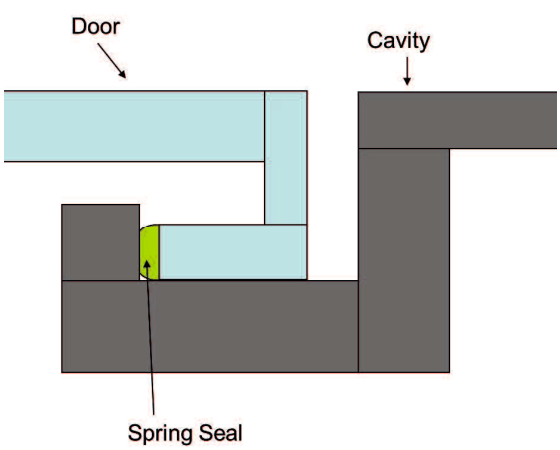

(a) (b)

Figure 5-10: Sketch of door sealings (a) and application of spring sealing in door of safety cavity (b).

Automatic door locks are installed to prevent unauthorized opening of the cavity during operation. In the case of unpredictable leakage of microwave irradiation monitors are installed in critical areas (control unit, hand wheels) shutting down the system automatically (Figure 5-11).

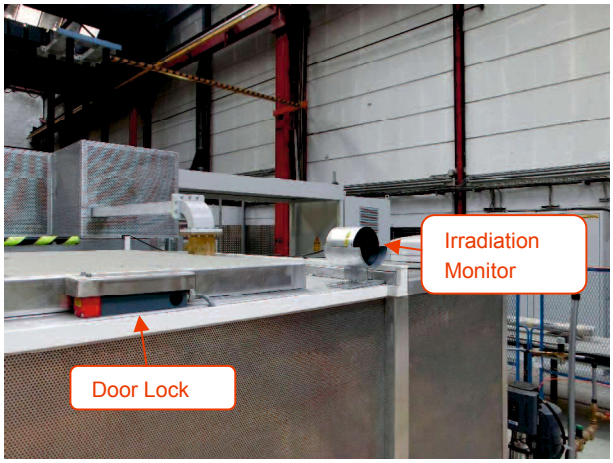

Figure 5-11: Automatic door lock and microwave irradiation monitor at the top door of the cavity.

5.4.2 Methods of large-scale microwave irradiation

Experiments were performed a) with continuous power directed at one spot; b) with continuous power whilst the waveguide was moved at constant speed over the sample and c) in pulsed mode. An overview of the performed tests is provided in Table 7-1. In this table the most important experiments, the test parameters, results and further investigations performed on the sample are listed. These three methods are considered as being best suited for investigating the influence of microwaves and their penetration depth at one hand. Secondly a near realistic scenario could be tested when moving the sample beneath the waveguide. Microwave irradiation in combination with mining machinery will have to be handled on rotating parts with changing faces.

The energy brought into the system can be controlled by the time of application for (a) and (c) and by the moving speed for (b). Time and speed are derived from knowledge of small scale tests and by empirical studies on the large scale and have been chosen in a way to provide a certain amount of damage in shortest possible time and with manageable technical side-effects such as arcing.

5.4.2.1 Continuous wave positioned at one spot

In the course of these tests relatively large samples were placed directly under the waveguide with a maximum distance of 15 mm to the sample surface. The size of the irradiated spot lies in the order of the dimensions of the waveguide (86*43 mm²).

Cubic samples for the tests where cut out of larger samples. This process lead to a very smooth and plain surface of the samples. Depending on investigated lithology and experience from former tests, samples were irradiated between 6 and 70 seconds on the same location allowing this spot to heat up (the applied power and the moving speed can

be seen in Table 7-1). The advantages of this kind of treatment lie in the controlled amount of energy and the relatively small volume of irradiated rock reducing the amount of unknown variables.

5.4.2.2 Continuous wave with moving sample

As described earlier the irradiation of a moving sample most closely resembles one of the possible practical industrial applications of this method and is capable of irradiating a larger volume of rock in a predefined range of time. Irradiation with simultaneous movement of the sample underneath the waveguide results in a stripe-like pattern which is also demonstrated in Figure 5-12. Several adjoining stripes have been combined to areas which can be clearly distinguished from untreated areas. The irradiation pattern of samples was chosen in a way to highlight the differences between treated and untreated parts of a sample in subsequent cutting tests.

The applied power as well as the moving speed for different lithologies is listed in Table 7-1.

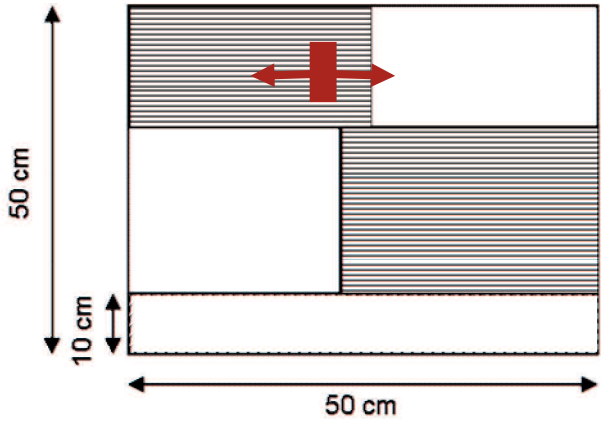

Figure 5-12: Schematic irradiation pattern for the continuous irradiation of rock samples. Dashed areas represent irradiated surfaces, blank areas untreated surfaces. Red rectangle represents cross section of waveguide, arrows indicate moving direction whilst irradiation.

As opposed to most of the tests described in Chapter 5.4.2.1 these tests were solely performed on a rough surface. The advantage of the rough surface compared to plain surfaces is the more realistic set-up and it is of importance for comparison in subsequent cutting tests. A regular rough surface was established by conditioning the rock in the linear cutting test-rig prior to irradiation. The degree of roughness depends on the individual cutting parameters which were applied for different rock types. Impressions of the roughness can be found in Figure 7-13, Figure 7-22 and Figure 7-28.

One disadvantage of this method of sample preparation is that the rough surface causes enhancement of the microwave field at sharp corners. Subsequently arcing effects occur

before the initially desired irradiation time leading to the shutdown of the microwave source. Therefore the moving speed of the sample was adapted to the arcing characteristics of samples and was often faster than initially planned.

5.4.2.3 Pulsed wave

Due to technical restrictions continuous waves were not able to be applied at the maximum possible output power of the microwave source. As seen in Table 7-1 most tests with this method were performed at 25 kW. Nevertheless it is desirable to apply a higher amount of power for shorter time in order to realize differential heating in the investigated samples. Short intervals of relaxation may assist thermal effects and increase induced damage. With the application of pulsed waves this effect can be simulated. In this study pulsed waves had a maximum power of 30 kW for 1 second and intervals of 6 kW for 2 seconds. Although the maximum power is higher the average input power is decreased significantly in this method of irradiation compared to continuous waves described in the previous chapters. Due to the fact that power is not completely turned off between the peaks this method is sometimes also referred to as “pseudo-pulsed irradiation”.

6 Small-Scale microwave irradiation tests

Overview of small-scale laboratory tests and results

Sample Location	Treatment	min Time [s]	max Time [s]	T max [°C]	USV reduction [m/s]	Effect	Remarks	Tests
Weitendorf Basalt	dry	10	120	450	2300	extensive cracking and melting after 270s	good absorber, rock with most tests	USV, UCS, Thin sections, Penspray, Thermocam, Simulation
	wet	10	60	320	2500	cracking, no difference to dry samples		USV, UCS, Thomas Peinsitt
	steel cone	10	120	-	3500	Spallation and melting at contact, extensive cracking	extreme heating at contact	UISV, Thin sections
	2nd dry	20	120	330	2300	no further effect		USV
	quenching	20	120		2300	broader variation than heated only		USV
Saalfelden Diabase - HB	dry	30	90	527	2400	cracking	good absorber	USV, Thin sections
	2nd dry	30	60	323	1200	further cracking ans shattering		
Saalfelden Diabase - TB	dry	30	120	498	2400	cracking	good absorber	USV, Thin sections
	2nd dry	30	90		1000	cracking	similiar to 1st heating, no second heating possible longer than 90s	
Jakomini Diabase	dry	20	120	409	1100	creation of small cracks after 60s, breaking after 120s	good absorber	USV, Thin sections
	2nd dry	20	120	406	-	breaking after short time		
Klöch Basalt	dry	10	30	350	1200	blasting and complete disintegration after 23s	OH groups in crystalline structure leads to extreme steam pressure	
Oberhaag Diabase	dry	60	180	421	4200	possible breaking after 160 s		USV, Thin sections
	2nd dry	60	120	221	2300	no differnce after 60s, breaking apart after short time for 180s		
Neuhaus Granite	dry	60	300	230	1000	little cracking		USV, UCS, Thomas Peinsitt
	saturated	60	300	300	1600	cracking and reduction of USV	better heating and reduction of USV than dry samples	
	steel cone	-	-	-	-	cracking and melting at contact		
Imberg Sandstone	dry	60	300	250	-	no effects		USV, UCS, Thomas Peinsitt
	saturated	10	30	130	-	destruction after 28-31s	steam pressuer leads to bursting and destruction	
	steel cone	-	-	-	-	cracking and melting at contact		
Somincor - Copper Sulphide	dry	10	360	385	1400	strong heating at bottom, generation of sulphuric acid?	short penetration depth	USV
	steel cone	-	-	-	-	slittle damage, generation of carbon black and sulphuric acid		
Gabbro	dry	30	140	490	1200	cracking and melting after max. 140 s, reduction in USV		USV, Penspray, Thin sections

Table 6-1: Overview of small-scale laboratory tests. Rocks, treatment methods, results, effects and further tests are highlighted. "USV reduction" - Reduction of Ultrasonic Velocity compared to initial state; "Dry" - dried for 48 h at 110°C; "saturated" – saturated in water for 48 h; "2nd dry" – second heating with the same parameters; "quenching" – quenching of hot samples in water and liquid nitrogen; "steel cone" – additional tests with a steel cone (See also chapter 6.5).

A detailed description of the behaviour of different strong and medium absorbing rocks

exposed to microwave irradiation will be given in the following chapters. An overview over tested rocks, the parameters, major results and effects and further testing methods is provided in Table 6-1.

6.1 Irradiation of Basalt

As shown in chapter 4 basalt has good dielectric properties considering penetration depth and absorption. They range from 0.08 – 0.8 for κ' and from 5.4 – 9.4 for κ" representing good heating and a penetration depth between 0.05 and 0.74 m (after Santamarina 1988). It was shown by Peinsitt (2009) and Peinsitt et al. (2010) that sufficient heating of basalt can be achieved to generate a certain amount of cracks leading to a decrease in rock strength. Sufficient heating of basalt can be achieved by irradiating a sample for a certain period of time (10 – 120 s) with 3.2 kW at 2450 MHz.

Several different kinds of basalt and other greenstones like diabase having similar dielectric properties have been irradiated and investigated.

6.1.1 Basalt Weitendorf

Microwave heating of basalt from the Weitendorf quarry appeared to be successful in terms of heating and creation of cracks.

Generally, samples simply get hotter the more energy they absorb which is equivalent to the irradiation time. An untreated sample is shown in Figure 6-1 where no obvious cracks can be seen. After a while one can observe the formation of tiny cracks visible at the circumference of 50 x 50 mm² samples. Many samples show macroscopical evidence of damage after irradiation for 40 s. Cracks widen and different supplementary effects can be observed the longer a sample is irradiated. After 120 s of irradiation, cracks widen significantly (Figure 6-2). In some samples even more damage can be observed. Here sections of the sample surface spall off. This effect is demonstrated in Figure 6-3.

When a sample of Weitendorf basalt is irradiated for approximately 4 ½ minutes the centre of the sample is heated up to approx. 1000 °C. This leads to the formation of molten material and subsequently fracturing of the sample. In Figure 6-4 one can see the centre of such a sample after it has cooled down to room temperature.

Figure 6-1: Untreated sample of Weitendorf basalt. No cracking visible.

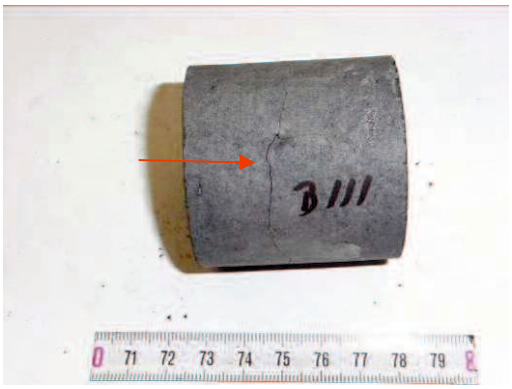

Figure 6-2: Sample B111 of Weitendorf basalt after 120 s of irradiation. Axial and radial cracks macroscopically visible (highlighted with red arrow).

Figure 6-3: Surface part of sample B121 of Weitendorf basalt spalls off after 120 s of irradiation.

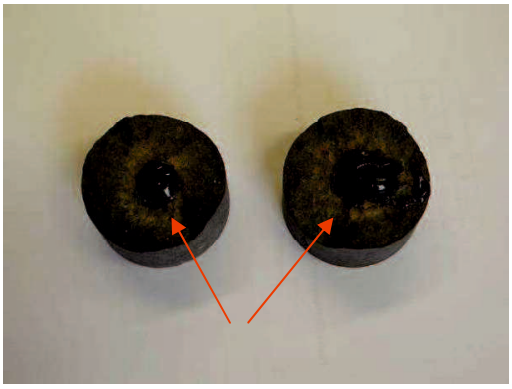

Figure 6-4: Centre of sample irradiated for 240 s. Centre of sample melts and is broken due to irradiation (spots marked with red arrows).

6.1.1.1 Chemistry and Mineralogy

XRD analyses show the composition of Weitendorf basalt (Figure 6-5). In this Figure Ba0 (black) is an untreated sample whereas Ba24 (red) was irradiated for 120 s. The main phases for the untreated sample are anorthite, sanidine, montmorillonite, augite and nepheline.

The X-ray diffractogramm (XRD, Figure 6-5) shows a clear change after 120 s of irradiation. Whereas the water-bearing clay mineral montmorillonite $(Na,Ca)_{0.3}(Al,Mg)2Si_4O_{10}(OH)_2xH_2O$ positioned at 6° at the 2-Theta scale is a strongly represented phase in the untreated sample (Ba0) it is vanished in the irradiated sample Ba24 and illite $K_{0.65}Al_2(Al_{0.65}Si_{3.35}O_{10})(OH)_2$ is formed instead (9° at 2-Theta scale).

These observations are supported by the data in Table 6-2. It represents the distribution of major elements in the same samples. They are composed of 52.84 and 53.46 wt.% SiO2, 16.27 and 16.53 wt.% Al_2O_3 and 6.17 and 6.14 wt.% Fe_2O_3, respectively. A strong change between the untreated and the irradiated sample can be reported for the LOI which changes from 1.59 wt.% in the initial state down to 0.84 wt.% when irradiated for 120 s.

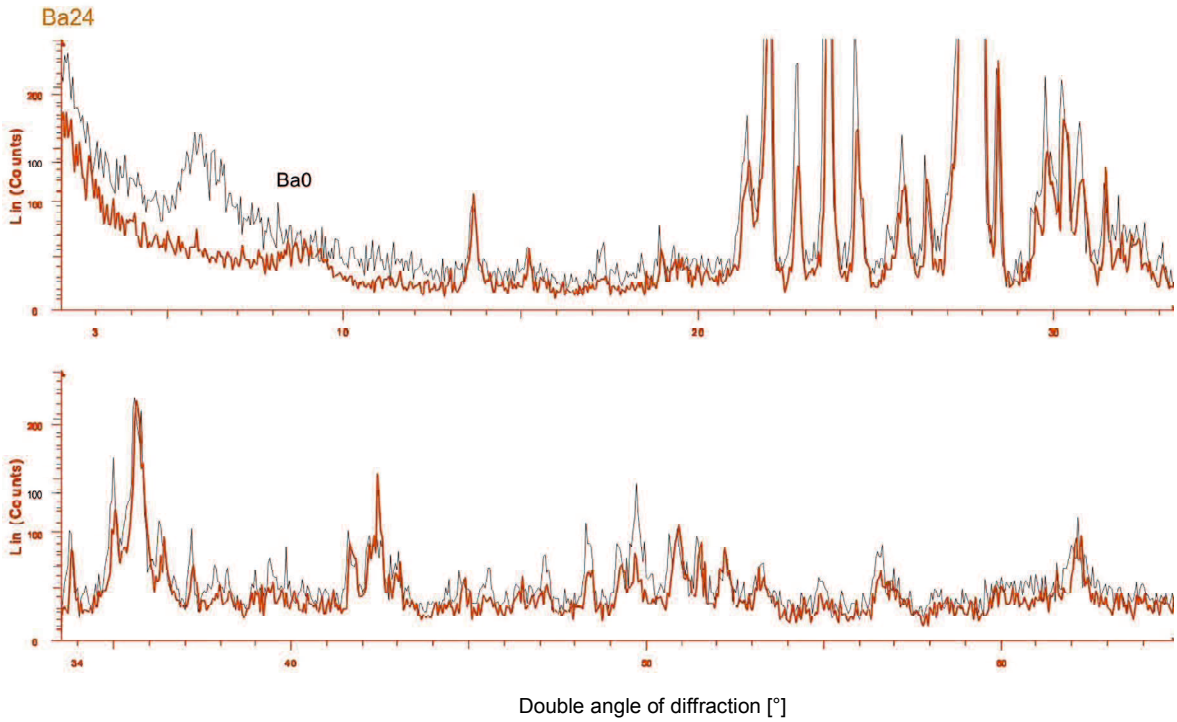

Figure 6-5: XRD - analyses of samples Ba0 (without microwave irradiation, black line) and Ba24 (after 120 s of irradiation, red line). Montmorillonite at 6° not present in irradiated sample, whereas illite at 9° appears.

Sample / Oxide	Ba0	Ba24
SiO_2	52.84	53.46
Al_2O_3	16.27	16.53
Fe_2O_3	6.17	6.14
MnO	0.11	0.11
MgO	5.89	6.05
CaO	7.75	7.62
Na_2O	2.90	2.94
K_2O	2.61	2.66
TiO_2	0.80	0.82
P_2O_5	0.46	0.47
LOI	1.59	0.84
Dry	1.22	0.28
SUM	98.61	97.92

Table 6-2: Major elements [wt. %] of a Weitendorf basalt sample before (Ba0) and after irradiation for 120 s with 3.2 kW (Ba24).

6.1.1.2 Temperature and Sound velocity

Figure 6-6 shows the increase in surface temperature of Weitendorf basalt samples as function of irradiation time. One can see that the initial temperature of 20 °C increases to

approximately 70 °C after 10 s of irradiation, 150 °C after 40 s and 450 °C after 120 s of irradiation.

This strong increase in surface temperature coincides with a significant decrease in ultrasound velocity. Untreated samples have a vp of approximately 5600 m/s (Figure 6-7). This value decreases with increasing irradiation time to 4000 m/s after 40 s and is as low as 3300 m/s after 120 s of irradiation with 3.2 kW. One will notice that the variation of p-wave velocity increases with irradiation time. Samples irradiated for 10 s have only little variation from 5626 – 5693 m/s whereas samples irradiated for 120 s vary from 3034 – 3840 m/s.

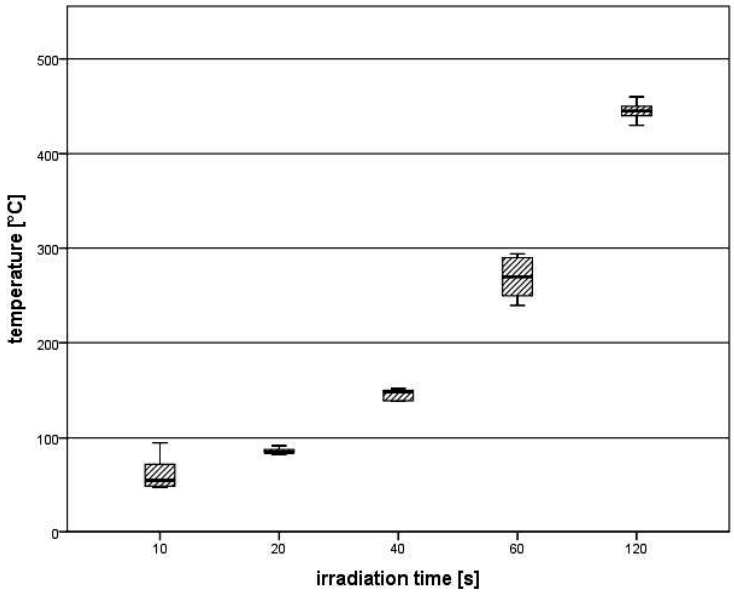

Figure 6-6: Surface-temperature [°C] as function of irradiation time [s] for Weitendorf basalt.

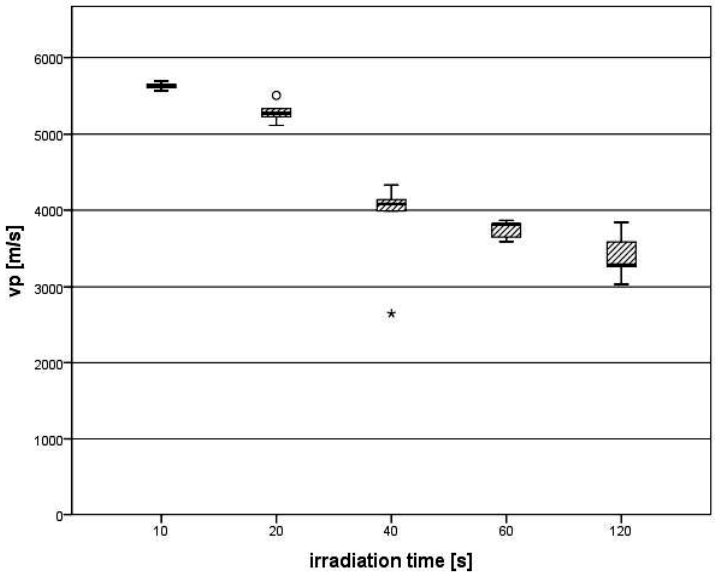

Figure 6-7: Ultrasound velocity (vp) [m/s] as function of irradiation time [s] for Weitendorf basalt.

Figure 6-9 shows a green line from the lower left to the upper right corner of the sample representing the temperature profile shown in Figure 6-10. The Figures show that the temperature in the centre of the sample is significantly higher than the temperature at the rims. Whereas the centre is hotter than 400 °C the rims only heat up to 250 °C in the same time period. The extremely steep decrease towards the outer parts of the Figure 6-10 representing the area near the surface is caused by measuring some contribution from the cooler surroundings during the experiment.

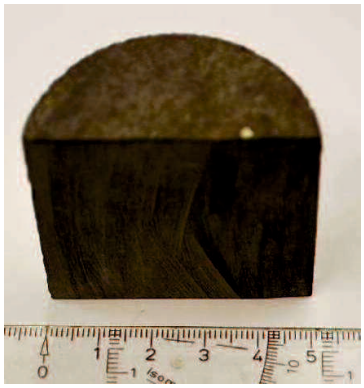

Figure 6-8: Basalt sample cut into two pieces along its axis as used for infrared thermography.

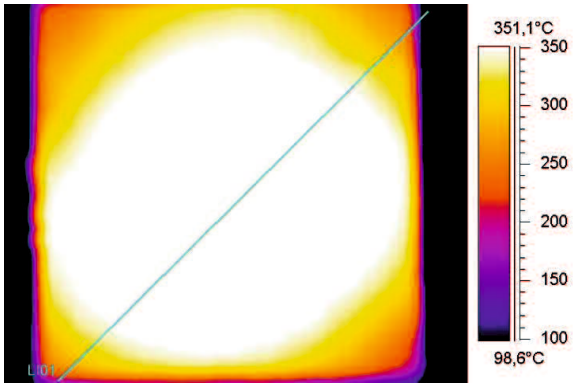

Figure 6-9: Thermographical image of half sample after 60 s of irradiation. The temperature profile along the green line is shown in Figure 6-10.

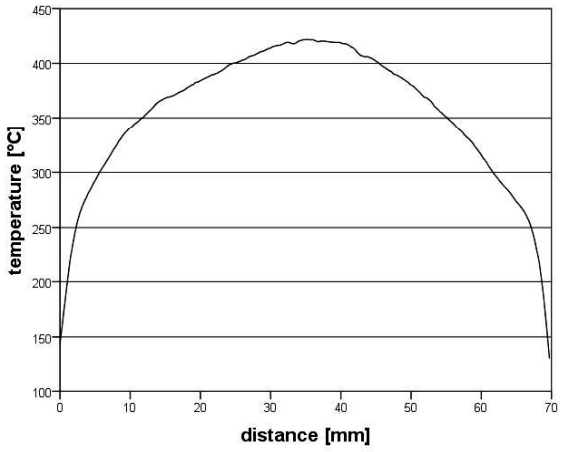

Figure 6-10: Temperature profile through the centre of a basalt sample (along line indicated in Figure 6-9).

6.1.1.3 Optical and microscopical investigations

The strong decrease in p-wave velocity can be correlated with macroscopic observation of cracks within a sample. A comparison of untreated and treated samples is shown in Figure 6-11 and Figure 6-12. The first Figure shows an untreated sample treated with a penetration spray as used in metallographic investigations to display existing cracks. No cracks are visible in this picture. The latter Figure shows the same sample after microwave irradiation for 120 s. One can clearly see the multitude of cracks in different directions. Cracks develop in radial and circumferential direction.

On a microscopic scale these cracks can be made visible with a resin-saturated thin section of the very same sample (Figure 6-13). One can clearly see that cracks cross existing grain boundaries. Small linearly aligned grains as well as larger pyroxenes are

crossed by these cracks in two directions. This thin section is taken from the centre of the sample where a radial crack (x-direction) splits up into an axial branch (z-direction).

Increasing the irradiation time to more than 120 s leads to the formation of even larger cracks and sometimes ablation of small pieces of rock. This extreme behaviour is shown in Figure 6-3 for sample B121.

Figure 6-11: Unirradiated basalt sample treated with a dye-penetrant; no visible cracks.

Figure 6-12: Cracked basalt sample after 120 s of irradiation. Cracks made visible with a dye-penetrant.

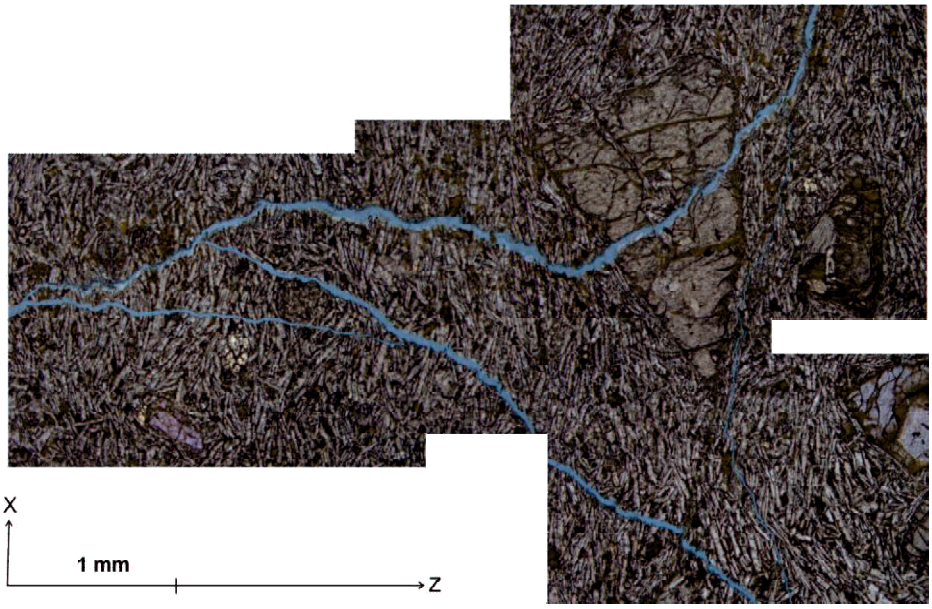

Figure 6-13: Resin saturated thin section of basalt after irradiation with microwaves. Radial crack (x-direction) splits into axial branch (z-direction).

6.1.1.4 Quenching in liquid nitrogen

Basalt samples where heated for 20, 60 and 120 s in the microwave oven and were immersed in a bath of liquid nitrogen immediately afterwards for 15 minutes. The results are compared with those samples that have only been heated for the same amount of time without subsequent cooling in nitrogen. The results of this comparison can be seen in Figure 6-14. The box plot displays that quenched samples have a broader variety of sound velocity than samples that have been conventionally treated. Whereas heated-only samples have a variation in p-wave velocity from 5115 – 5506 m/s after 20 s, 3236 – 3866 m/s after 60 s and 3034 – 3840 m/s after 120 s of irradiation, quenched samples vary from 4237 – 5335 m/s, 3267 – 4132 m/s and 2800 – 3764 m/s respectively. The median values, however, do not change significantly between the two methods of treatment.

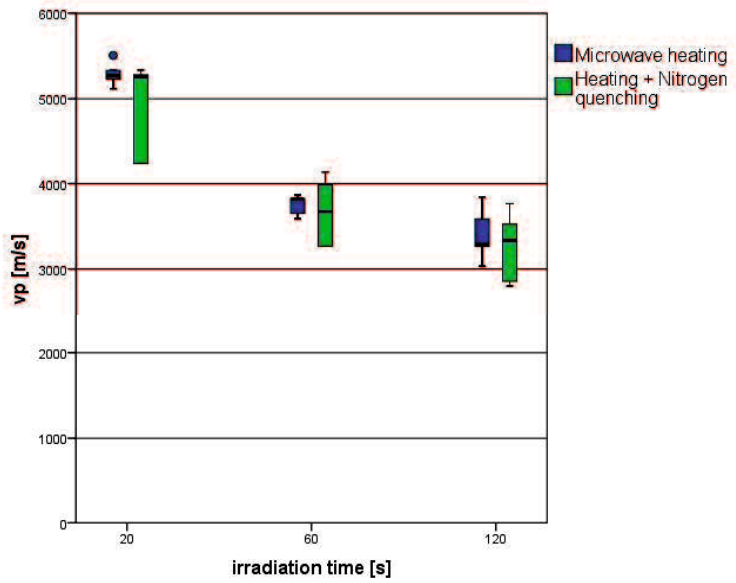

Figure 6-14: Comparison of p-wave velocity as a function of irradiation time of basalt samples heated with microwave energy (blue) and samples quenched in liquid nitrogen after irradiation (green).

6.1.1.5 Second heating cycle

The resulting temperature as function of the irradiation time for these tests is displayed in Figure 6-15 where a comparison of first and second heating cycle is provided. Samples that were irradiated for 20 s reach temperatures between 100 and 128 °C in both irradiation steps. Samples irradiated for 60 s reach temperatures between 295 and 334 °C at both irradiation steps. In contrary to these results, a strong difference in the two heating steps can be observed for samples irradiated for 90 and 120 s. Here the first irradiation reaches much higher temperatures than the second treatment. After 90 s the sample had 393 °C in the first step but only 236 °C after a second irradiation representing a temperature difference of 157 °C. Samples irradiated for 120 s reached temperatures as high as 430 and 466 °C at the first irradiation whereas they only reached temperatures of 330 °C after the second irradiation. This represents exactly the temperature after irradiation for 60 s in the first step.

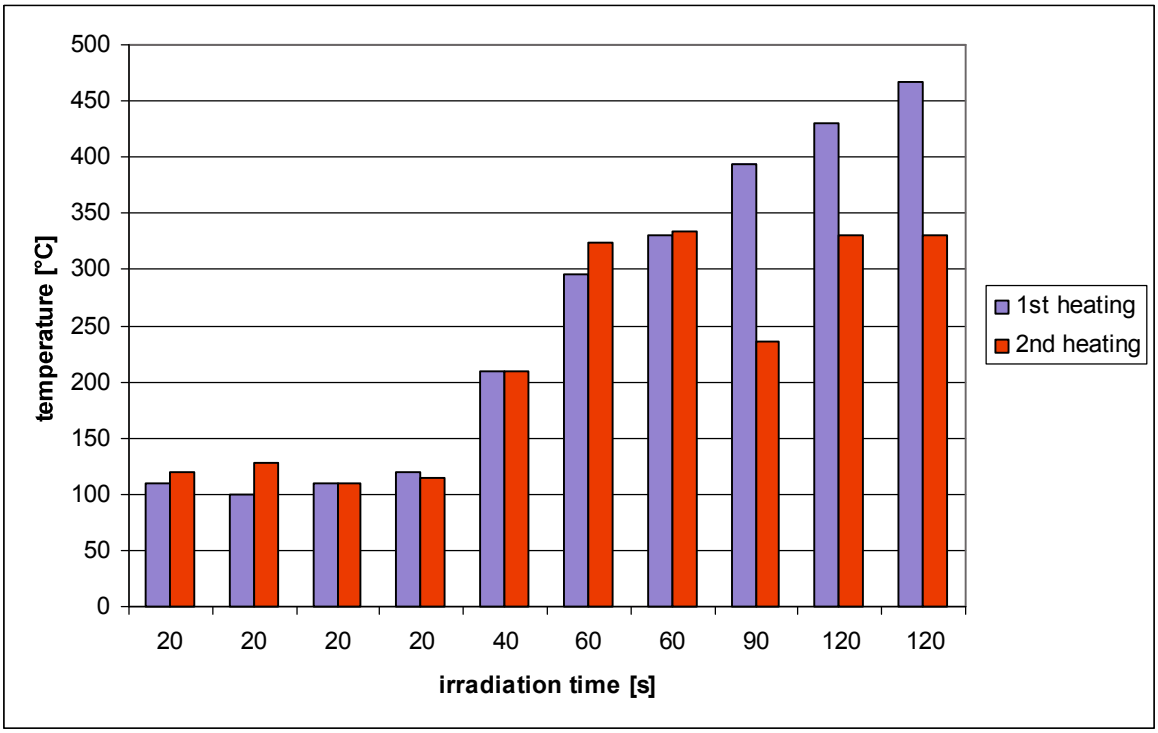

Figure 6-15: Temperature after second heating of selected samples with the same irradiation parameters. Measured temperatures for samples after first heating with 3.2 kW (blue) compared to 2nd heating of same samples with identical parameters (red).

6.1.2 Basalt Klöch

Klöch basalt shows some interesting results that can not be reproduced with other samples. For short irradiation times below 20 s no special behaviour of these samples can be observed. They heat up but no cracks appear. This changes rapidly when samples are irradiated for more than 23 and up to 30 s. Those samples burst and fall apart into small pieces (Figure 6-19). The effect of bursting is accompanied by a change in composition where ilite is replacing water-bearing montmorillonite (6° at 2-Theta scale) as result of the irradiation.

6.1.2.1 Chemistry and Mineralogy

X-ray diffractometric analyses of Klöch basalt are shown in Figure 6-16. The main phases in the untreated sample (displayed in black) are augite, nepheline, montmorillonite, analcime and anorthite. Montmorillonite starts to disappear in favour of illite in the sample irradiated for 30 s (red).

The major element distribution is shown in Table 6-3. Kl0 represents the unirradiated state whereas Kl31 is a sample irradiated for 30 s. SiO_2 is the major oxide with 43.2 and

43.1 wt.%, followed by Al_2O_3 with 14.8 and 14.7 wt.%. A strong change can be observed for LOI and drying with a reduction from 3.36 to 2.86 wt.% and 1.6 to 0.8 wt.%, respectively.

Sample / Oxide	Kl0	Kl31
SiO_2	43.2	43.1
Al_2O_3	14.8	14.7
Fe_2O_3	10.1	10.2
MnO	0.17	0.17
MgO	8.27	8.64
CaO	10.9	11.4
Na_2O	4.86	4.65
K_2O	1.06	1.09
TiO_2	2.28	2.29
P_2O_5	0.78	0.78
LOI	3.36	2.86
Dry	1.6	0.8
SUM	101.38	100.68

Table 6-3: Major elements (wt.%) of Klöch basalt before (Kl0) and after (Kl31) irradiation for 30 s with 3.2 kW.

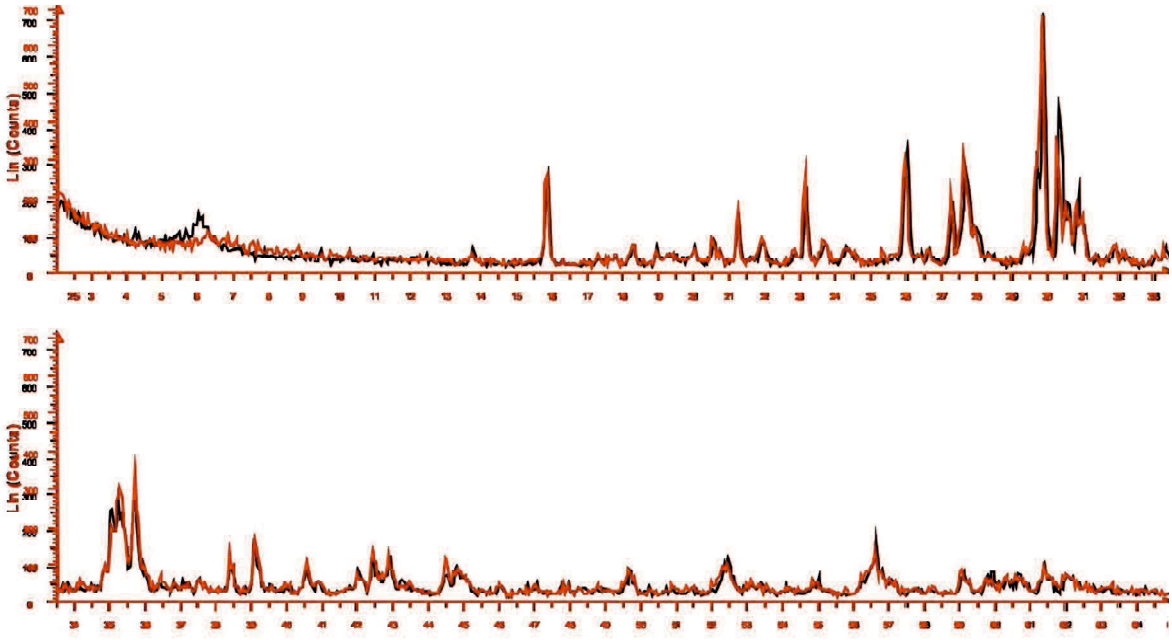

Figure 6-16: XRD analyses of Klöch basalt before (black) and after (red) 30 s of irradiation with microwaves. Montmorillonite peak (at 6°) decreases in the irradiated sample.

6.1.2.2 Temperature and Sound velocity

Due to the fact that basalt from Klöch disintegrates explosively after only 23 s of irradiation with 3.2 kW, only two data points can be displayed. Figure 6-17 and Figure 6-18 show the p-wave velocity and the surface temperature measured after irradiation of Klöch basalt. After 10 s of irradiation a small increase in surface temperature from room temperature to 53 °C can be observed. The samples heat up to an average temperature of 89 °C after 20 s of irradiation. Temperature increases to 150 °C at the surface and up to 350 °C at the centre, represented by broken pieces, of samples irradiated for 30 s.

Average initial sound velocity is as high as 3800 m/s with a broad variation from 1419 to 5159 m/s. After 10 s of irradiation the average velocity is still 3800 m/s with similar variation from 1461 to 4833 m/s and decreases down to 2680 m/s after 20 s of irradiation. However variation is still very broad ranging from 2050 – 4250 m/s.

After 30 s of irradiation no sound velocity could be measured because samples disintegrated explosively after this irradiation time. As shown in Figure 6-19 and Figure 6-20 the samples explode into small pieces. Temperature could be measured at the initial surface of the sample (150 °C) and at faces representing the former centre of the samples (350 °C).

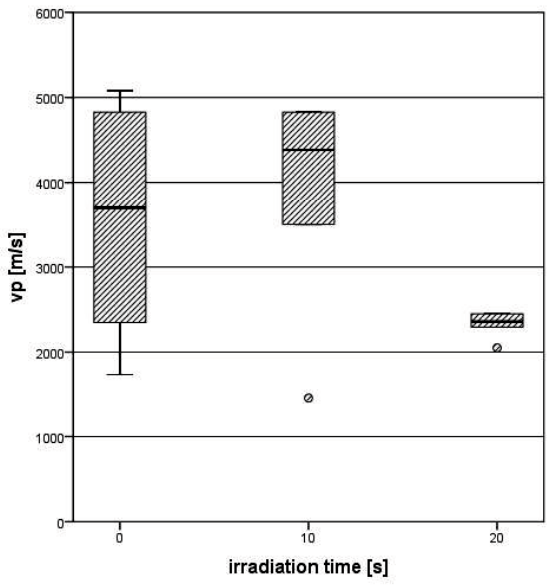

Figure 6-17: P-wave velocity (vp) [m/s] as function of the irradiation time [s] for Klöch basalt.

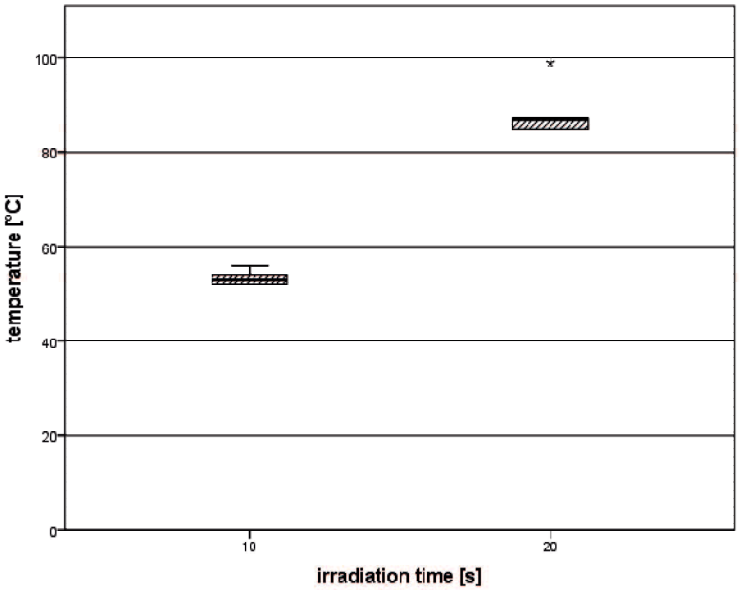

Figure 6-18: Surface-temperature [°C] as function of the irradiation time for Klöch basalt.

Figure 6-19: Fragments of Klöch basalt shattered after 30 s of irradiation.

Figure 6-20: Klöch basalt explodes after 30 s of irradiation in 3.2 kW microwave oven.

6.1.2.3 Optical and microscopical investigations

Figure 6-21 shows a picture of a thin section taken from sample Kl07 after 20 s of irradiation with 3.2 kW. One can clearly see two generations of cracks crossing the matrix minerals from top to bottom. One crack is completely filled with carbonaceous material. Additionally an open crack can be seen. This crack is coated with the same carbonates on both sides. These observations imply that the open crack is more or less a reactivation of the closed crack. The coating on both sides of the open cracks is strongly supporting this theory.

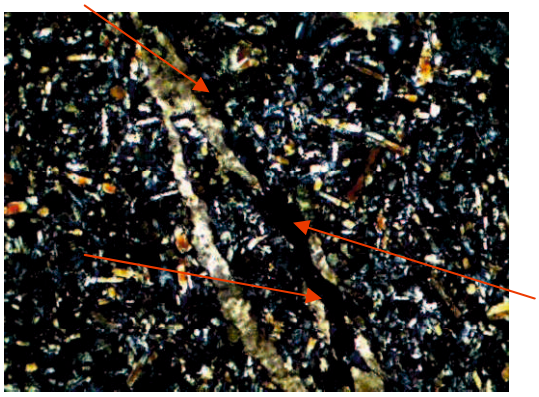

Figure 6-21: Thin section of sample Kl07 (#N) after 20 s of irradiation. Open cracks coated with carbonaceous material on both sides. Image width = 2.6 mm; Crack marked with red arrows.

6.2 Irradiation of Diabase

Diabase has very similar dielectric behaviour to basalt. Several different quarries in Austria are handling these very hard rocks. Thus it was self-evident to test these rocks and compare their behaviour to that of basalt. Furthermore the knowledge of the behaviour of a broad variety of rocks from many different locations helps understanding the mechanisms of microwave-rock interaction and the coinciding effects.

6.2.1 Diabase Oberhaag

Samples from Oberhaag show a similar behaviour to samples from Weitendorf. However it can be reported that they tend to shatter after 160 to 180 s of irradiation. The reduction in p-wave velocity for these samples is significant but shows very broad variation. Minimum values range from as low as 300 m/s up to 3400 m/s.

In a second heating cycle short timed samples show similar behaviour whereas samples irradiated for 180 s in the first cycle break apart after short time in the second step.

6.2.1.1 Chemistry and Mineralogy

XRD-analyses of Oberhaag diabase are shown in Figure 6-22. The untreated sample is displayed in red whereas the sample irradiated for 180 s is displayed in black.

The major mineral phases are albite, quartz, chlorite, calcite, edenite and biotite.

One can see that no major shift in phase can be reported after irradiation. One exception is edenite at 10.5° and 29.5° at the 2-Theta scale. These two peaks show a clear change in intensity from 1600 to 600 counts and from 150 to 400 counts, respectively.

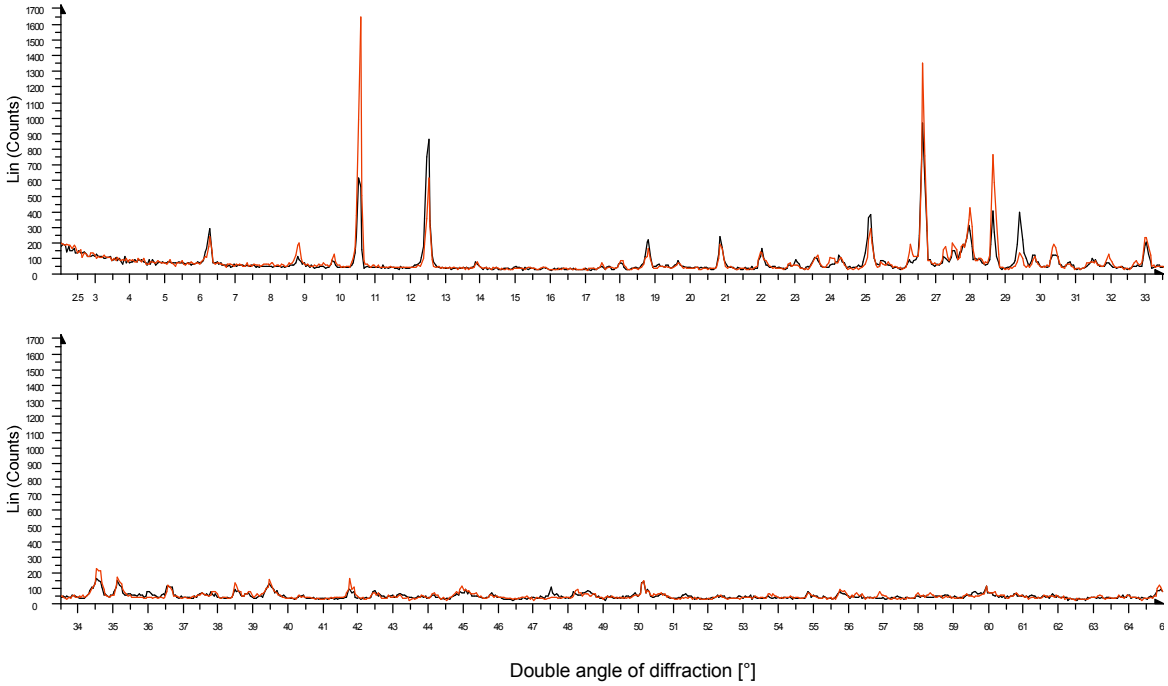

Figure 6-22: XRD analyses of Oberhaag diabase before (red) and after (black) 180 s irradiation with microwaves.

6.2.1.2 Temperature and Sound velocity

Figure 6-23 displays the surface temperature [°C] of Oberhaag diabase as function of the irradiation time. Samples have been irradiated for 60, 120 and 180 s. The surface temperature increases with increasing irradiation time to 168, 328 and 421 °C, respectively.

This increase in temperature coincides with a significant decrease in p-wave velocity. As shown in Figure 6-24 the average initial velocity of 5950 m/s decreases to 5439 m/s varying from 4798 – 6275 m/s after 60 s and 3864 m/s after 120 s with variations from 3326 – 4952 m/s (Figure 6-24). Some samples of Oberhaag diabase shatter after 160 to 180 s of irradiation (e.g. Sample OH12, Figure 6-25). Thus p-wave velocity data for these

samples are rather scarce. However an average velocity of 1764 m/s can be reported varying strongly from 309 – 3430 m/s.

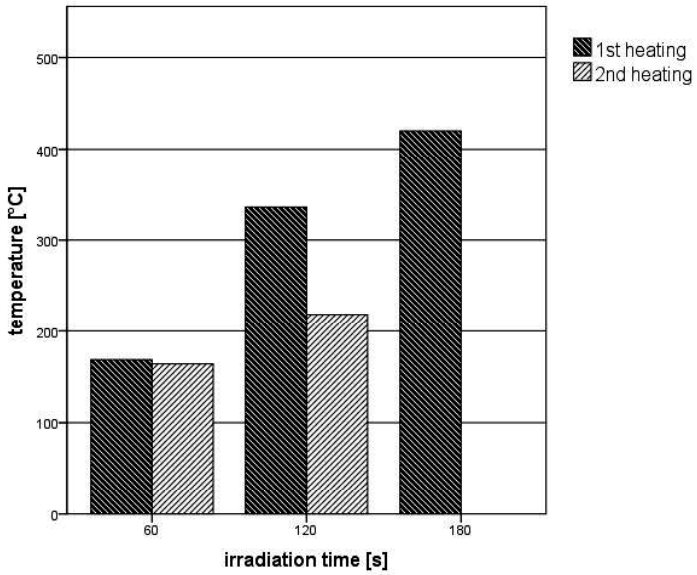

Figure 6-23: Surface temperature [°C] of Oberhaag diabase after 1st and 2nd heating cycle as function of irradiation time [s].

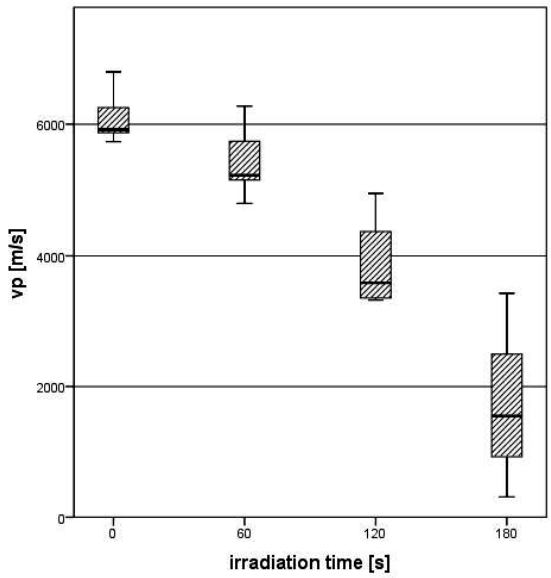

Figure 6-24: P-wave velocity (vp) [m/s] of Oberhaag diabase as function of irradiation time [s].

Figure 6-25: Pieces of sample OH12 of Oberhaag diabase which shatters after irradiation for 160 s.

6.2.1.3 Second heating cycle

Samples remaining intact after the first heating step were heated for a second time with the same parameters. The results are shown in Figure 6-23. After 60 s of irradiation no significant differences in surface temperature can be reported. Here the average temperature moves down to 164 °C, compared to 168 °C in the initial test. After 120 s of a second irradiation average surface temperature is as high as 221 °C, approximately 100 °C colder than 328 °C after the first irradiation. Due to the fact that only 3 samples that had been initially irradiated for 180 s remained intact after the first experiments and that two of those samples shattered after only short secondary irradiation no data for these experiments can be provided.

6.2.2 Diabase Jakomini

The results for samples from Jakomini quarry are relatively inhomogeneous. As will be shown in this chapter some samples break apart easily whereas others remain unaffected. A specifically interesting fact is that surface temperature tends to be higher in the second irradiation step (Figure 6-31). The first small cracks can be observed after 60 s of irradiation. As shown in Figure 6-26 (sample Ja15) some samples show no optical signs of damage after 90 s of irradiation. On the other hand samples that were irradiated for the same amount of time can be severely damaged with the formation of melt and subsequent cracking (Figure 6-27). A similar behaviour can be reported for irradiating Jakomini samples for 120 s. Also after this irradiation time some samples hardly seem to be influenced by the irradiation whereas others shatter after the formation of melt in the centre of the sample (Figure 6-28). A detailed look into the interior where a spot of melt forms is provided in Figure 6-29.

Figure 6-26: Sample Ja15 of Jakomini diabase after 90 s of irradiation. No damage visible.

Figure 6-27: Sample Ja13 of Jakomini diabase after 90 s of irradiation. Sample is melting in the centre and subsequent cracking occurs.

Figure 6-28: Sample Ja12 of Jakomini diabase after 120 s of irradiation. Strong cracking and formation of melt observable.

Figure 6-29: Formation of a small spot of melt in the centre of a diabase sample (highlighted by red arrow) of Jakomini quarry after irradiation with microwaves for 120 s..

6.2.2.1 Chemistry and Mineralogy

XRD-analyses of Jakomini diabase are shown in Figure 6-30. The 120 s irradiated sample is displayed in red whereas the untreated sample is displayed in black. The main phases of this rock are ferriwinchite, quartz, chlorite and albite. As demonstrated in the Figure no significant changes between the two samples can be seen.

The major element distribution for a pair of samples is shown in Table 6-4 Ja0 is an untreated sample whereas Ja22 is a sample of the same origin that was irradiated for 120 s with 3.2 kW. The main oxide is SiO_2 with 48.96 and 48.81 wt.% in the untreated and irradiated sample, respectively. This is followed by Al_2O_3 (14.61 and 14.13 wt.%), Fe_2O_3 (13.39 and 14.46 wt.%) and CaO (8.32 and 8.56 wt.%). The increase in LOI from 2.03 to 2.13 wt.% is remarkable.

6.2.2.2 Temperature and Sound velocity

Figure 6-31 displays the surface temperature [°C] of Jakomini diabase as function of the irradiation time [s]. Samples have been irradiated for 20, 60, 90 and 120 s. The average surface temperature increases with increasing irradiation time to 75 °C (varying from 64 – 90), 166 °C (varying from 160 – 180 °C), 247 °C (varying from 185 – 313 °C) and 354 °C (varying from 302 – 409 °C) after the first heating cycle, respectively.

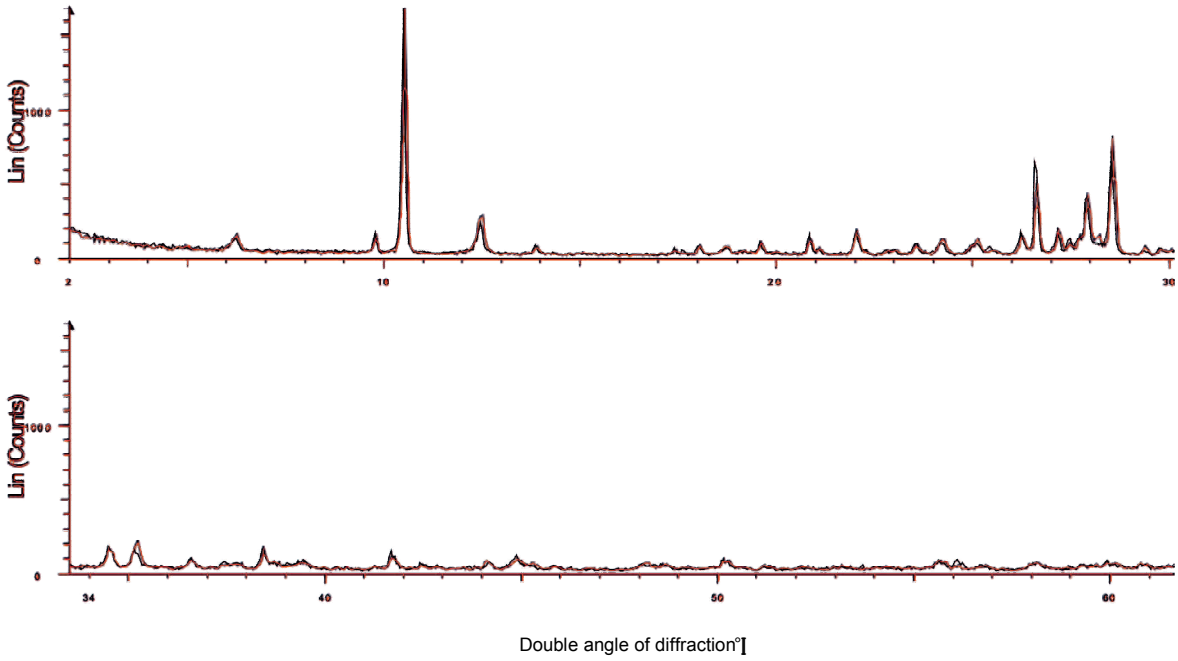

Figure 6-30: Overlapping lines of XRD analyses of Jakomini diabase before (black) and after irradiation for 120 s with 3.2 kW.

Sample / Oxide	Ja0	Ja22
SiO_2	48.96	48.81
Al_2O_3	14.61	14.13
Fe_2O_3	13.39	14.46
MnO	0.20	0.23
MgO	7.99	6.53
CaO	8.32	8.56
Na_2O	3.23	2.71
K_2O	0.31	0.29
TiO_2	0.86	1.88
P_2O_5	0.06	0.19
LOI	2.03	2.13
Dry	n.v.	0.23
SUM	99.96	100.15

Table 6-4: Major elements (wt. %) for an untreated sample (Ja0) and a sample irradiated for 120 s (Ja22) with 3.2 kW.

Sound velocity as function of irradiation time after the first heating cycle is shown in Figure 6-32. Average initial sound velocity is as high as 5270 m/s varying from 4932 – 5851 m/s. This value decreases to 5174 m/s with a variation from 4979 - 5456 m/s after 20 s, 4973 m/s (varying from 4204 to 5851 m/s) after 60 s, 4398 m/s (varying from 3220 to 4817 m/s) after 90 s and 4127 m/s with broad variations from 3170 to 5025 m/s after 120 s of irradiation.

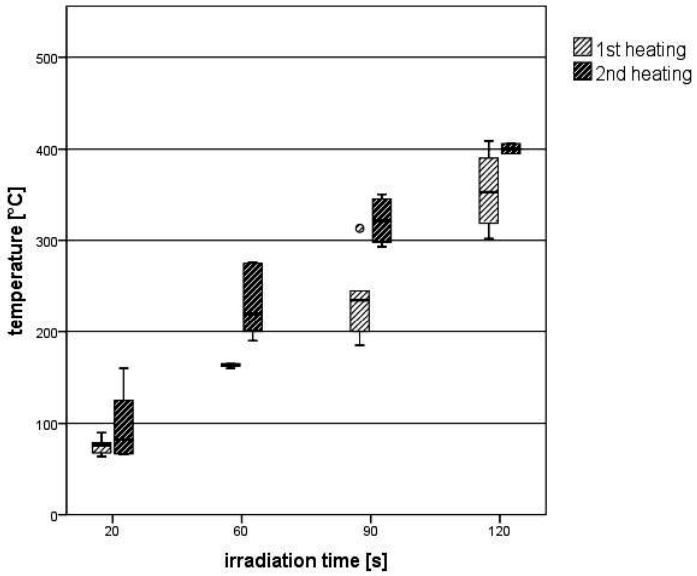

Figure 6-31: Surface Temperature [°C] of Jakomini diabase as function of irradiation time [s] after 1st and 2nd heating cycle.

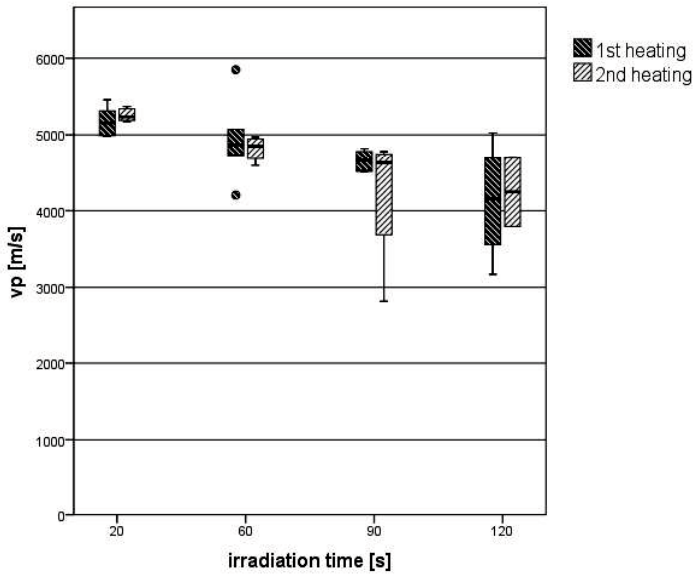

Figure 6-32: P-wave velocity (vp) [m/s] of Jakomini diabase as function of irradiation time [s] after 1st and 2nd heating cycle.

6.2.2.3 Second heating cycle

Samples that remained intact to the greatest extent after the first irradiation have been irradiated for a second time with the same parameters.

Figure 6-33 shows sample Ja8 after a second irradiation for 60 s. Small cracks that existed after the first irradiation step are widened to large cracks and complete destruction of the sample occurs.

Similar to the behaviour after 60 s is the reaction of samples subjected to irradiation for 90 s. Sample Ja25 shows some minor cracks after a first irradiation for 90 s (Figure 6-34). The sample breaks apart after 30 s in the second step. In Figure 6-35 one can see small dark spots in the centre of the sample where the formation of melt had started.

Figure 6-33: Diabase sample Ja8 after a second irradiation with microwaves for 60 s. Sample shatters along a crack.

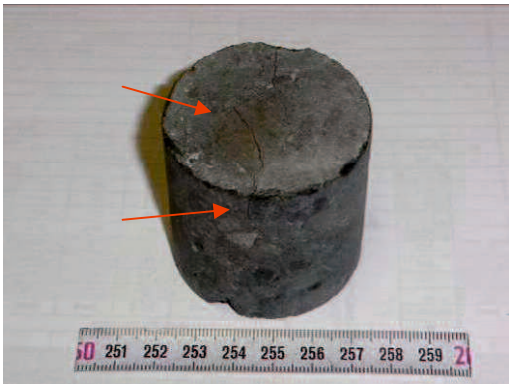

Figure 6-34: Minor cracks in diabase sample Ja25 after the first irradiation with microwaves or 90 s (Cracks marked with red arrows).

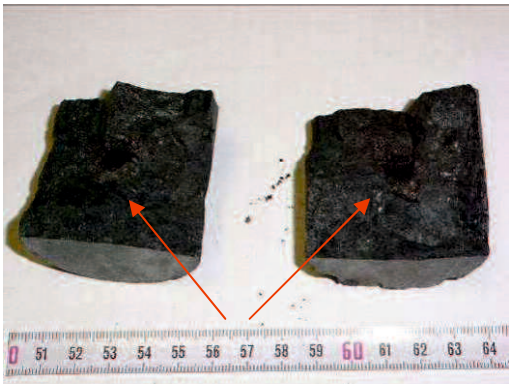

Figure 6-35: Sample Ja25 of Jakomini diabase shatters after 30 s during a second irradiation with microwaves. Molten spots highlighted with red arrows.

The resulting temperatures of these experiments are shown in Figure 6-31. In many cases surface temperature is slightly higher after the second heating compared to the first heating cycle. The average values are as high as 97 °C (varying from 66 – 160 °C), 230 °C (varying from 180 -275 °C), 321 °C (varying from 293 – 350 °C) and 400 °C (only two values with 365 and 406 °C) after 20, 60, 90 and 120 s of irradiation, respectively. It is obvious that the data shows a much broader variation for short irradiation times and lower variation for longer heating times compared to the first heating step.

P-wave velocity shows similar median-values after when compared to only one heating cycle. The scattering towards low-bound outliers is however striking (Figure 6-32).

6.2.3 Diabase Saalfelden

Samples of both quarries have a very similar behaviour when subjected to microwaves. Both types show the occurrence of tiny cracks after 30 s of irradiation. Those cracks widen with increasing irradiation time. Complete destruction can be observed only after a 2nd irradiation for 60 or more seconds.

A general and significant reduction in p-wave velocity with increasing irradiation time can be reported for both sets of samples.

Minor mineralogical changes are observed but are not of significance.

6.2.3.1 Chemistry and Mineralogy

Major element analyses for Saalfelden diabase are shown in Table 6-5 where two pairs of samples are shown. SF-HB-0 and SF-HB-18 are from Hinterburgbruch where SF-HB-18 has been irradiated for 75 s whereas SF-HB-0 has not been treated. Samples SF-T21-03 and SF-T21-21 represent the Tagebau21 and are untreated and irradiated for 90 s, respectively.

In Hinterburgbruch the main oxide is SiO_2 which is as high as 49.95 and 47.61 wt.% in untreated and irradiated state. It is followed by Al_2O_3 (14.44 and 12.80 wt.%), Fe_2O_3 (13.51 and 16.00 wt.%), CaO (7.85 and 7.08 wt.%) and MgO (5.80 and 5.10 wt.%) . Irradiating the sample leads to a significant decrease in LOI from 2.59 to 2.02 wt.% for the Hinterburgbruch. Drying these samples does not lead to such big differences. 0.24 are compared to 0.16 wt.% after irradiation.

The main oxide occurring in the samples of Tagebau21 is SiO_2 with 52.91 and 53.58 wt.% in the untreated and irradiated sample. It is followed by Fe_2O_3 (13.99 and 13.10 wt.%), Al_2O_3 (13.91 and 13.58 wt.%), Cao (4.35 and 5.09 wt.%), Na_2O (4.18 and 4.05 wt.%) and MgO (3.37 and 3.27 wt.%). Microwave irradiation leads to a decrease in LOI. Initial 2.33 are compared to 2.14 wt.% after irradiation. Drying leads to a slight change from 0.27 to 0.21 wt.% for Tagebau21.

X-ray diffractograms of Hinterburgbruch are shown Figure 6-36. The sample irradiated for 75 s is displayed in red whereas the untreated sample is displayed in black. The main phases of this rock are quartz, ferriwinchite, chlorite and albite. In the irradiated sample the occurrence of ferriwinchite ($[(CaNa)(Mg_4Fe^{3+}, Al)Si_8O_{22}(OH)_2]$; 10.5, 28.5 and 33° at 2-Theta scale) decreases significantly.

X-ray diffractograms of Tagebau21 are shown Figure 6-37. The sample irradiated for 90 s is displayed in red whereas the untreated sample is displayed in black. The main phases of this rock are quartz, chlorite, albite and ferriwinchite. For this pair of samples no significant changes in the XRD analyses can be reported.

Sample / Oxide	SF-HB-0	SF-HB-18	SF-T21-03	SF-T21-21
SiO_2	49.95	47.61	52.91	53.58
Al_2O_3	14.44	12.80	13.91	13.58
Fe_2O_3	13.51	16.00	13.99	13.10
MnO	0.21	0.24	0.22	0.22
MgO	5.80	5.10	3.37	3.27
CaO	7.85	7.08	4.35	5.09
Na_2O	3.05	2.97	4.18	4.05
K_2O	0.24	1.26	1.31	1.46
TiO_2	2.19	3.80	2.24	2.30
P_2O_5	0.23	0.44	0.82	0.78
LOI	2.59	2.02	2.33	2.14
Dry	0.24	0.16	0.27	0.21
SUM	100.30	99.48	99.90	99.78

Table 6-5: Major element analyses (wt.%) of sample pairs SF-HB and SF-T21 of Saalfelden diabase before and after irradiation with microwaves.

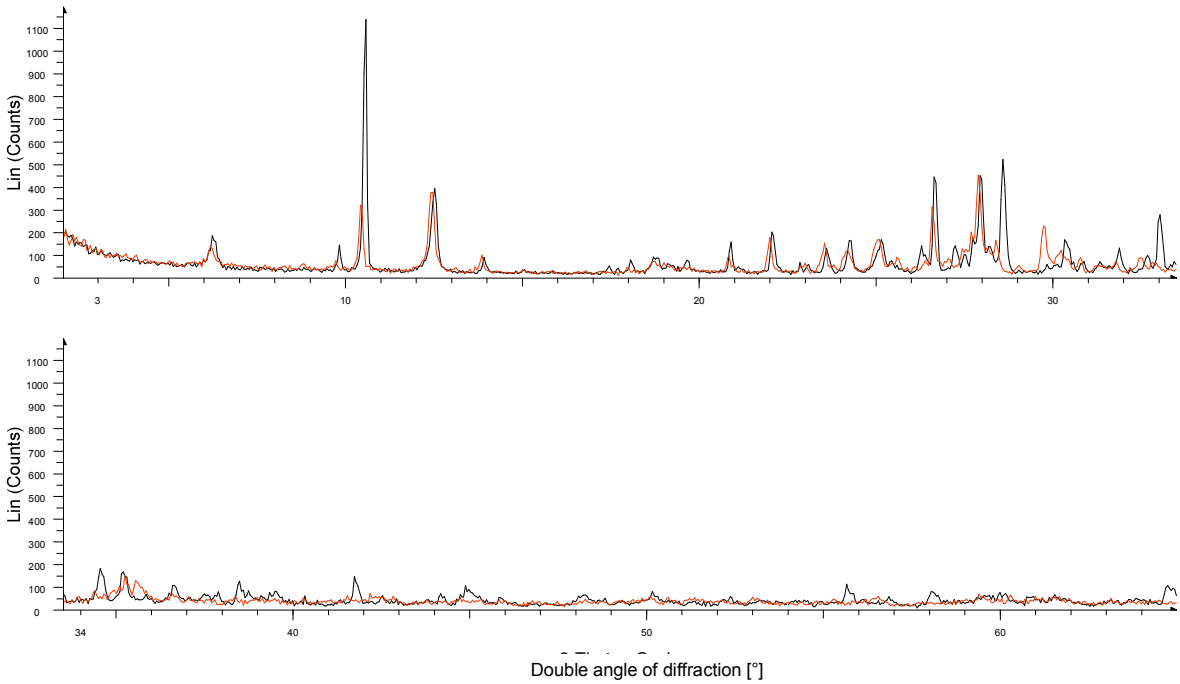

Figure 6-36: XRD analyses of Saalfelden diabase, Hinterburgbruch before (black) and after irradiation for 75 s (red).

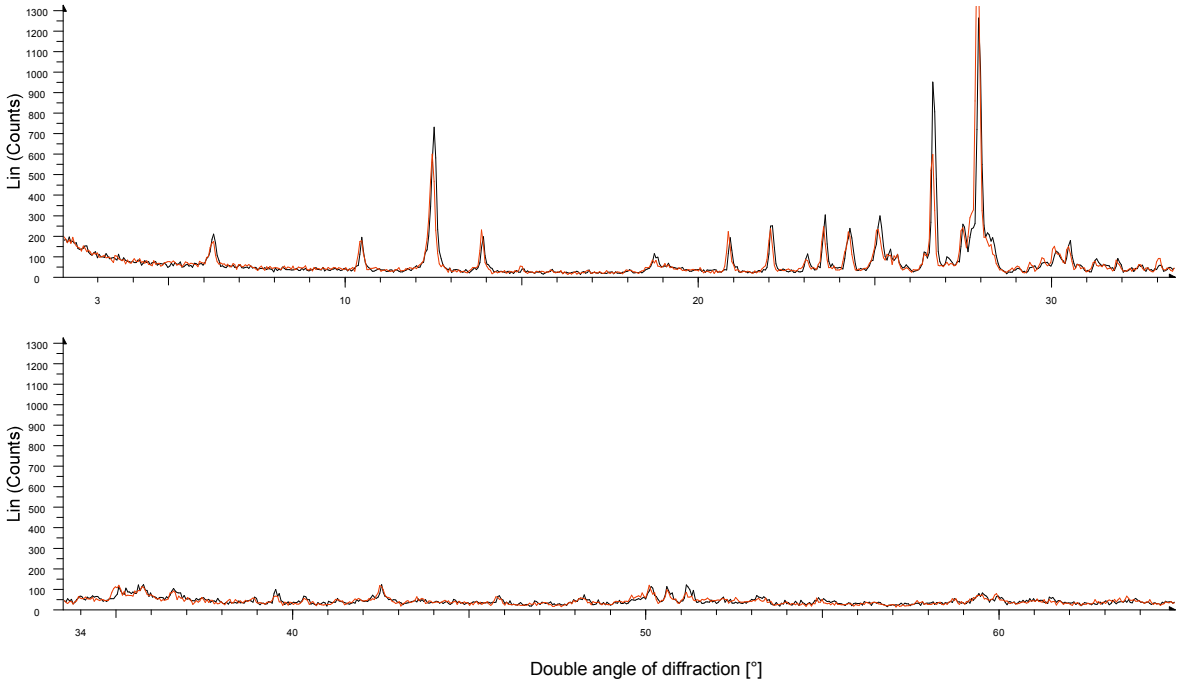

Figure 6-37: XRD analyses of Saalfelden diabase, Tagebau21 before (black) and after irradiation for 90 s (red).

6.2.3.2 Temperature and Sound velocity

Figure 6-38 displays the surface temperature as a function of irradiation time for samples of Saalfelden diabase. Samples from Hinterburgbruch heat up to an average temperature of 190 °C (varying from 175 – 213 °C) after 30 s, 334 °C (variation from 327 – 337 °C) after 60 s, 375 °C (varying from 330 – 433 °C) after 75 s and 451 °C (varying from 395 – 527 °C) after 90 s of irradiation, respectively, in the first heating cycle with 3.2 kW.

Samples from Tagebau21 have a slightly different behaviour than those of Hinterburgbruch. On average they heat up to 145 °C (varying from 138 – 151 °C) after 30 s, 268 °C (varying from 261 – 278 °C) after 60 s, 331 °C (varying from 307 – 369 °C) after 75 s, 372 °C (varying from 333 – 401 °C) after 90 s and 487 °C (varying from 470 – 498 °C) after 120 s of irradiation with 3.2 kW after the first heating cycle.

In Figure 6-39 one can see the adjacent p-wave velocity for Hinterburgbruch. Here the resulting p-wave velocity is displayed as a function of irradiation time. Average initial velocity is as high as 5915 m/s varying from 5516 to 6354 m/s. This value decreases to 5202 m/s (varying from 5122 – 5284 m/s) after 30 s, 4668 m/s (varying from 4365 – 4922 m/s) after 60 s, 4428 m/s (varying from 2988 – 4970 m/s) and 3528 m/s (varying from 3392 – 4606 m/s) after 120 s of irradiation.

The initial sound velocity of samples of Tagebau21 is 4643 m/s (varying from 4031 – 5533 m/s) and significantly slower than that of samples from Hinterburgbruch. This value decreases to 4266 m/s (varying from 4160 – 4522 m/s) after 30 s, 3614 m/s (varying from 3465 – 3741 m/s) after 60 s, 3768 m/s (varying from 3434 – 4166 m/s) after 75 s, 3071 m/s (varying from 2781 – 3270 m/s) after 90 s and 2244 m/s (varying from 2176 – 2353 m/s) after 120 s of irradiation.

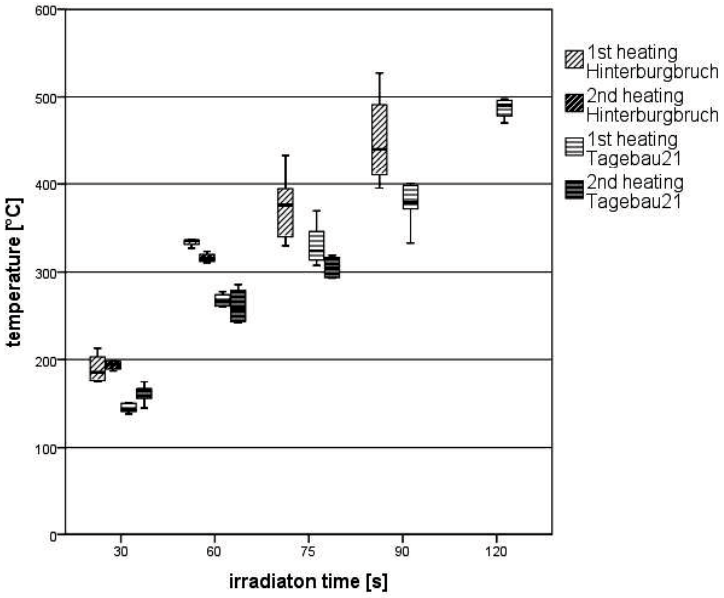

Figure 6-38: Surface temperature [°C] after different irradiation cycles for samples of Saalfelden diabase as function of the irradiation time [s].

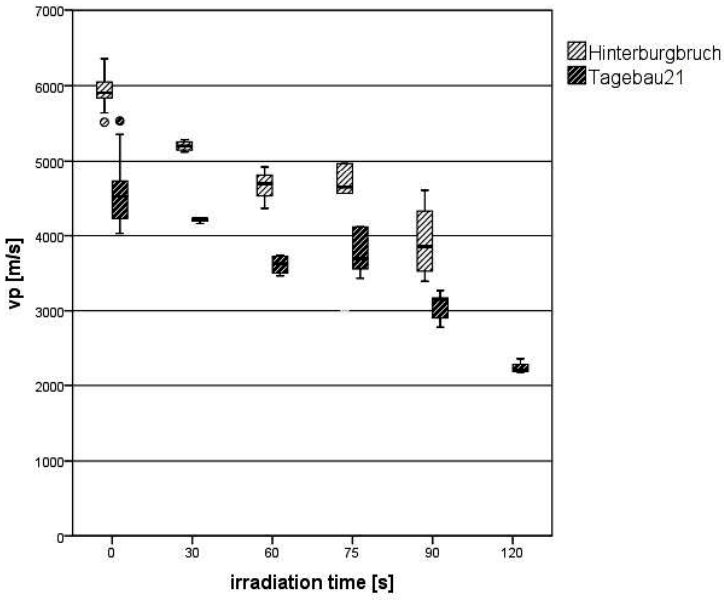

Figure 6-39: P-wave velocity [m/s] after first irradiation for different samples of Saalfelden diabase as function of the irradiation time [s].

6.2.3.3 Second heating cycle

Most samples were irradiated for a second time with the same parameters. Results regarding the surface temperature can be seen in Figure 6-38.

One can see that samples from Hinterbergbruch heat up to an average temperature of 193 °C with variations from 187 to 198 °C after 30 s and 316 °C varying from 311 to 323 °C after 60 s of irradiation.

Samples from Tagebau21 heat up to an average temperature of 156 °C (varying from 156 – 175 °C) after 30 s, 261 °C (varying from 242 – 286 °C) after 60 s and 305 °C with variations from 293 to 319 °C after 75 s of irradiation.

6.3 Irradiation of Gabbro

6.3.1 Nerro Assoluto

The result of microwave irradiation of this kind of rock is the formation of cracks and coinciding significant reduction in p-wave velocity from approximately 6200 m/s down to 4000 m/s after 90 s of irradiation.

6.3.1.1 Chemistry and Mineralogy

X-ray diffractometric-analyses of gabbro samples Ga17 and Ga08 in the untreated and irradiated status, respectively, are shown in Figure 6-40. The major phases are pyroxene, anorthite, clinochlore, biotite and glaucophane. The major phase in the irradiated sample is anorthite followed by pyroxene.

Major element analyses of gabbro are shown in Table 6-6 where an untreated (Ga17) and a sample irradiated for 60 s (Ga08) are shown. The major oxide is SiO_2 with 49.55 and 49.02 wt.% in the untreated and irradiated sample, respectively. It is followed by Al_2O_3 (15.13 and 15.55 wt.%), Fe_2O_3 (11.47 and 11.99 wt.%) and CaO (9.84 and 9.47 wt.%). Drying and LOI lead to no significant changes with 1.64 and 1.63 as well as 0.12 and 0.08 wt.% in the untreated and irradiated samples, respectively.

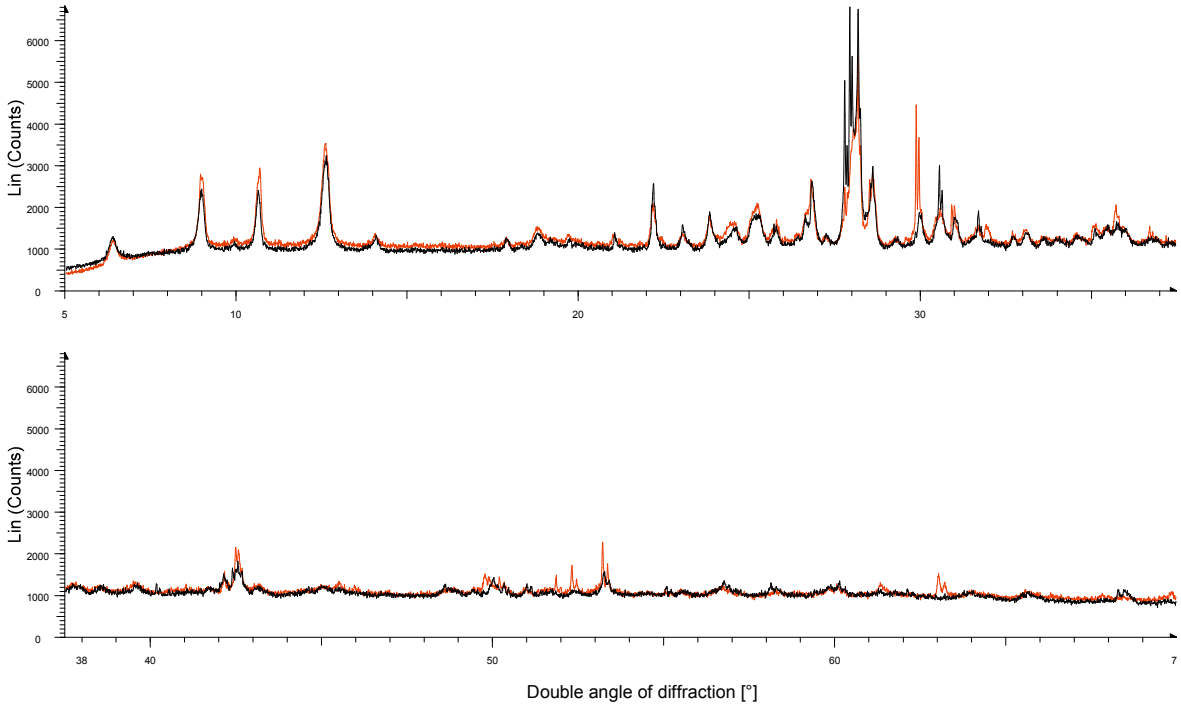

Figure 6-40: XRD-analyses of untreated gabbro (Ga17, red line) and gabbro irradiated for 60 s with 3.2 kW (Ga08, black line).

Sample / Oxide	Ga08	Ga17
SiO_2	49.02	49.55
Al_2O_3	15.55	15.13
Fe_2O_3	11.99	11.47
MnO	0.16	0.16
MgO	6.67	6.88
CaO	9.47	9.84
Na_2O	2.60	2.59
K_2O	0.89	0.90
TiO_2	1.65	1.47
P_2O_5	0.19	0.19
LOI	1.63	1.64
Dry	0.08	0.12
SUM	99.90	99.94

Table 6-6: Major element analyses (wt.%) of gabbro before (Ga17) and after irradiation with microwaves for 60 s (Ga08).

6.3.1.2 Temperature and Sound velocity

Figure 6-41 shows the surface temperature of gabbro as function of the irradiation time. Samples have been irradiated for 30, 45, 60 and 90 s. With increasing irradiation times the average surface temperature rises to 163, 199, 301 and 391 °C, respectively after irradiation with 3.2 kW.

As shown in Figure 6-42 this increase in surface temperature is accompanied by a decrease in p-wave velocity. Initial average p-wave velocity is as high as 6201 m/s with variations from 6045 to 6310 m/s. This value decreases to 5915 m/s (varying from 5769 – 6023 m/s) after 30 s, 5333 m/s (with only 2 values at 5320 and 5347 m/s) after 45 s, 5006 m/s (ranging from 4887 - 5114) after 60 s and 4051 (varying from 3000 - 4658 m/s) after 90 s of irradiation with 3.2 kW. Complete disintegration of a sample is possible after a minimum of 140 s of irradiation leading to the formation of melt and shattering of the sample.

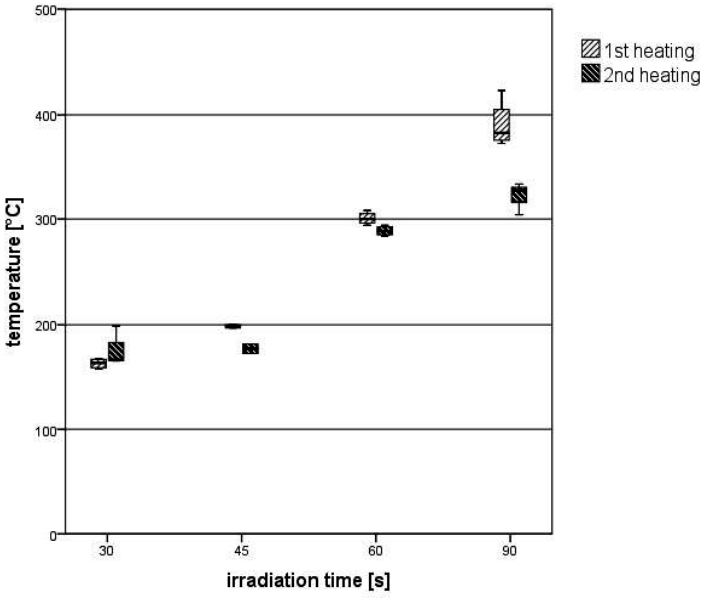

Figure 6-41: Surface temperature [°C] as function of the irradiation time [s] for 1st and 2nd heating cycle of gabbro.

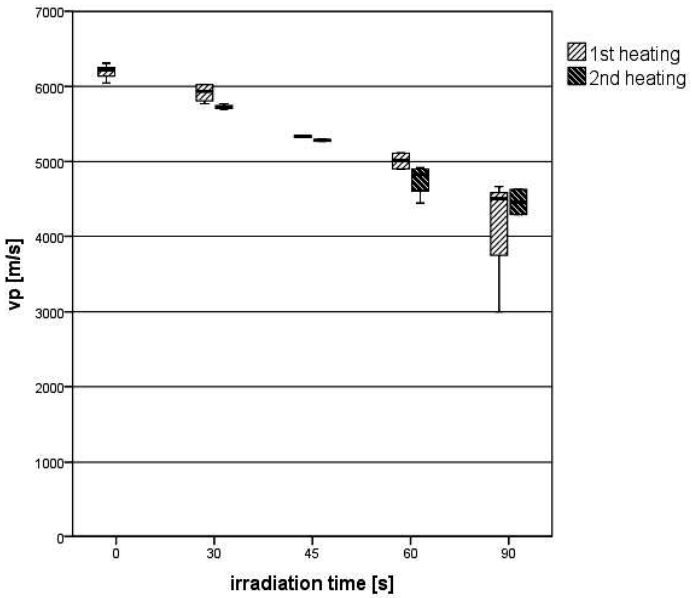

Figure 6-42: P-wave velocity [vp] as function of the irradiation time [s] after 2 cycles of irradiation of gabbro.

The reduction of p-wave velocity can be linked to the formation of optically visible cracks. Figure 6-43 shows a sample of gabbro after 90 s of irradiation. A large circumferential crack is clearly visible.

Figure 6-43: Sample Ga09 (gabbro) after 90 s of irradiation with 3.2 kW. A significant circumferential crack is visible (red arrows).

Figure 6-44: Gabbro sample Ga09 after 2nd irradiation for 90 s resulting in formation of melt and complete disintegration.

6.3.1.3 Second heating cycle

Samples were irradiated for a second time with the same parameters. It can be seen in Figure 6-41 that the surface temperature is very similar to the first irradiation step. However, after 90 s the average temperature remains at only 321 °C compared to 391 °C after the first irradiation. Figure 6-42 shows that also the p-wave velocity is very similar between the two irradiation steps. After the first irradiation the variation of velocity after 90 s is higher with a minimum of 3000 m/s. The reduction of variation in the second step can be explained by the elimination of samples that have been destroyed after only one irradiation leading to these low values after the first test.

Figure 6-44 shows a sample after the generation of melt and complete disintegration after a second irradiation for 90 s.

6.4 Irradiation of sulphidic ores

6.4.1 Neves Corvo copper ore

When irradiating samples of Neves Corvo one can observe discrepancies between the literature and the real time experiments. Samples do not heat up as quickly as expected from the excellent dielectric properties and damage is far less significant compared to other rock types investigated in this study (Figure 6-47 and Figure 6-48).

Irradiating these samples does not lead to the development of cracks as observed with other lithologies. Interesting features observed with these samples are the strong heating at the bottom side of the samples where the internal heat can obviously not be cooled by

air. As shown in Figure 6-45 glowing can occur in these regions. Surface temperature at the side of the cylinder increases slightly with irradiation time. However it takes 4 minutes for a temperature rise to 370 °C coinciding with an only slight reduction of p-wave velocity.

This strong development of heat at the bottom is associated with the breaking off of small pieces. As demonstrated in Figure 6-46 a small wedge breaks off. An interesting additional effect is the development of sulphurous acid. After the breaking off of a wedge a very distinct odour can be smelt leading to the conclusion that sulphurous acid was generated by oxidizing the sulphides of the sample.

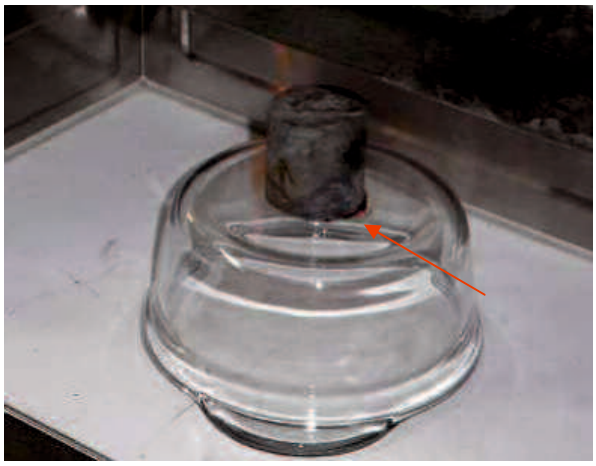

Figure 6-45: Sample of Neves Corvo copper ore after microwave irradiation for 120 s. Glowing may be observed at the bottom (red arrow).

Figure 6-46: Neves Corvo sample after 120 s of irradiation. Ablation of small pieces after microwave irradiation with 3.2 kW.

6.4.1.1 Temperature and Sound velocity

Surface temperature for samples from Neves Corvo as a function of irradiation time is shown in Figure 6-47. After 10 s the temperature rises to an average of 51 °C with variations from 47 to 53 °C. The average temperature increases with increasing irradiation time. After 20 s a temperature of 82 °C (variation from 78 – 89°C) can be achieved. Temperature is as high as 170 °C (varying from 157 – 183°C) after 60 s, 270 °C (varying from 239 – 294°C) after 120 s and 370 °C with variations from 360 to 385 °C after 240 s of irradiation with 3.2 kW.

Along with the increase in temperature is a change in p-wave velocity. This is demonstrated in Figure 6-48. Initial velocity is 6230 m/s with variations from 5328 to 6228 m/s. After 10 s of irradiation a slight increase in p-wave velocity can be observed with values between 6259 and 6668 m/s and an average of 6436 m/s. The average p-wave velocity for samples irradiated for 20, 60, 120 and 240 s are 6189 m/s with variations from 5894 to 6434 m/s, 5732 m/s (varying from 5328 – 6143 m/s), 5384 m/s (varying from 5030 – 5834 m/s) and 5097 m/s in the range of 4645 to 5446 m/s, respectively.

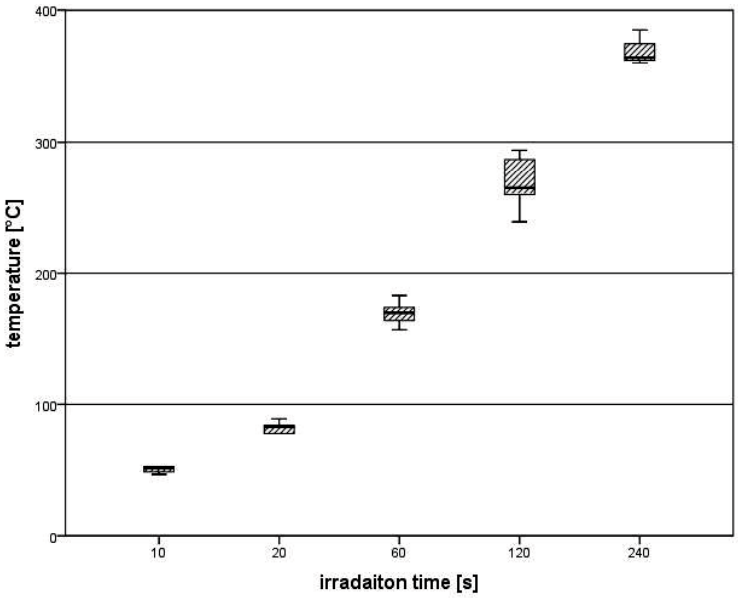

Figure 6-47: Surface temperature [°C] as function of the irradiation time [s] for Neves Corvo copper sulphide ore.

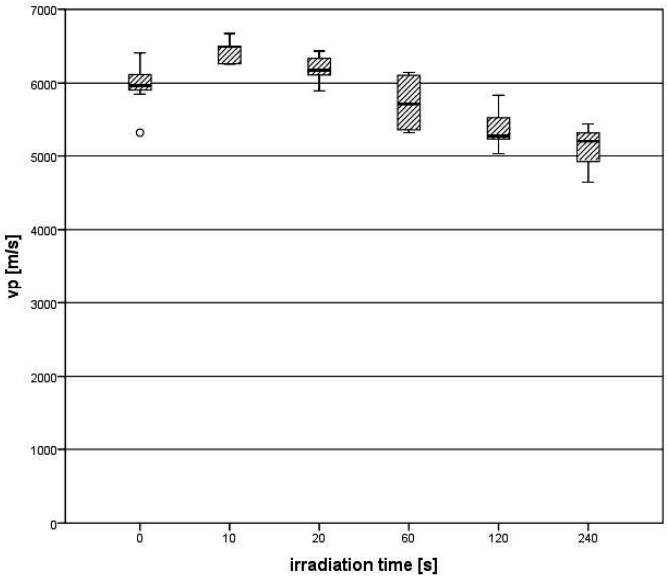

Figure 6-48: P-wave velocity [vp] as function of the irradiation time [s] for Neves Corvo copper sulphide ore.

6.5 Irradiation with the help of a steel cone

In general also rocks with poor dielectric properties can be damaged by this method of treatment. This is not possible with conventional treatment as shown in the previous chapters as well as literature sources. Spots of molten material appear at the contact of the cone and the sample. The size of these spots depends on the applied irradiation time. These spots are the root for further cracks destabilizing the whole sample and leading to clear signs of destruction.

A side effect is the creation of fire balls under certain circumstances which are consuming a vast amount of the provided energy and thus preventing sufficient damage.

6.5.1 Basalt Weitendorf

As already shown in Chapter 6.1.1 basalt of Weitendorf can be heated with microwaves sufficiently to induce a network of cracks leading to a significant decrease in p-wave velocity with increasing irradiation time.

While irradiating samples of Weitendorf with the help of the steel cone first spallation at the contact zone of sample and cone can be observed after only 10 s of irradiation (Figure 6-49). After 60 s a small molten point can be observed in addition (Figure 6-50). This point is the origin for tiny radial cracks of which one is highlighted in red. The same sample shows a large network of cracks under closer observation ina cross section (Figure 6-51).

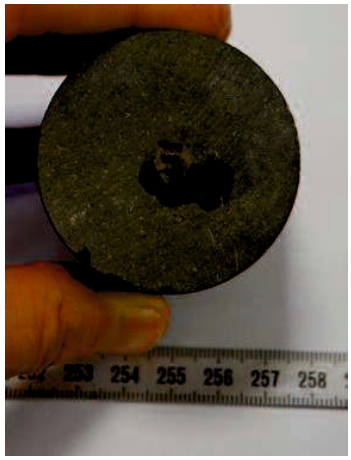

Figure 6-49: Basalt sample Ba33 after 10s irradiation with the help of steel cone. Spallation at contact zone of steel cone and sample.

Figure 6-50: Basalt sample Ba52 after 60 s of irradiation with the help of steel cone. Small molten point and spallation at the contact of cone and sample. Red line highlighting crack.

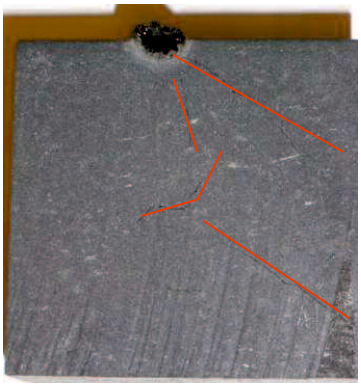

Figure 6-51: Crosscut through basalt sample Ba52 after 60 s of irradiation with help of steel cone. Crack network visible throughout the whole sample (cracks highlighted by red lines).

After 120 s of irradiation the molten point gets even bigger and additional damage can be observed several millimetres below the surface of the sample (Figure 6-52).

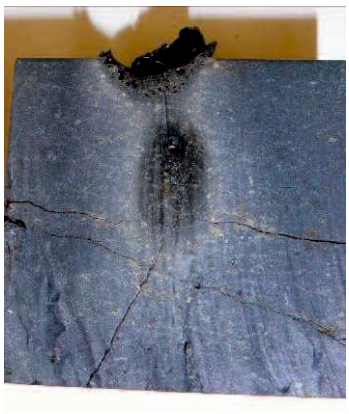

Figure 6-52: Crosscut through basalt sample Ba60 after 120s of irradiation with the help of a steel cone. Molten spot at surface and large cracks throughout the entire sample visible.

The results of these measurements are shown in Figure 6-53. Only few samples were treated that way and thus the available data is rather limited. After 10 s of irradiation only a slight decrease in velocity can be observed. No usable data was obtained after 30 s of irradiation. One can see that the median value after 60 s of irradiation is comparable to the results of conventional treatment. However the minimum value measured for this kind of treatment lies approximately 1500 m/s below the value for conventional treatment of this kind of sample.

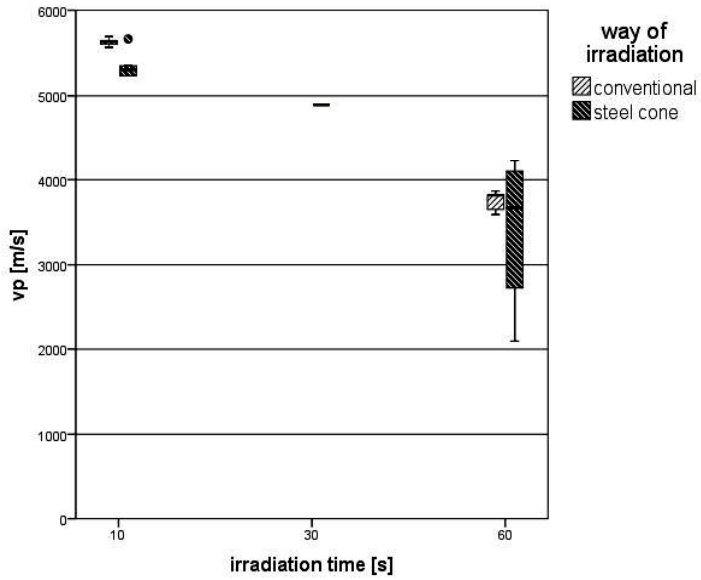

Figure 6-53: Comparison of the p-wave velocity (vp) [m/s] as function of the irradiation time [s] for samples of Weitendorf basalt irradiated with and without the help of an additional steel cone at 3.2 kW in the multimode cavity.

6.5.2 Sandstone

As shown by Peinsitt et al. (2010) sandstone can only be heated and destroyed under certain circumstances. This includes the presence of water as good absorber for microwave energy.

With the help of the steel cone these prerequisites can be avoided and energy is brought into the system directly at the contact of sample and cone. As shown in Figure 6-54 spallation occurs in the vicinity of the contact zone. The brownish circle represents the placing of the glass cylinder used for the stabilization of the cone.

After 120 s the irradiation leads to a picture as shown in Figure 6-55. The first step of damage is spallation as described for the shorter irradiation time as well. When irradiation lasts longer the sample starts to melt at the contact zone and underneath the surface. This leads to the formation of a rather big molten bubble and of large radial cracks. The cross-cut through this sample (Figure 6-56) reveals another crack which is more or less aligned parallel to the surface in a depth of some millimetres. This crack dips towards the rim where it occurs in a depth of 15 mm.

Due to a limited availability of samples no measurement of p-wave velocity was conducted with the sandstone samples treated in this way.

Figure 6-54: Sandstone sample SS3 after 60 s of irradiation with additional steel cone. Significant spallation visible at the surface.

Figure 6-55: Sample SS55 after 120 s of irradiation with additional steel cone. Spallation and melting of material at the surface leading to the development of cracks.

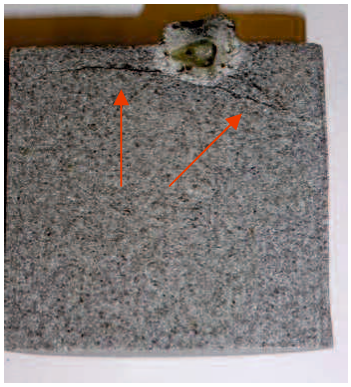

Figure 6-56: Cross-cut through sample SS55 after 120 s of irradiation with application of additional steel cone (cracks indicated by red arrows).

6.5.3 Granite

Peinsitt et al. (2010) have shown that granite behaves in a similar manner to sandstone. It is very hard to damage with the help of microwaves. These problems can be overcome by the application of the steel cone which focuses the microwave field at its tip.

Figure 6-57 shows sample Ne6 after 10 s of irradiation with the help of the additional steel cone. One can see that spallation has already started at the contact of the steel cone and the sample. Increasing the irradiation time results in the sample beginning to melt at the contact point (Figure 6-58). The molten spot is the source and initial point of several cracks in radial direction. In the cross-cut of the very same sample (Figure 6-59) a crack that goes from the centre of the melt towards the right-end rim where it ends in about 20 mm of depth. No p-wave velocity data is available for this kind of treatment on granite samples.

Figure 6-57: Granite sample Ne6 after 10 s of irradiation with additional steel cone. Slight spallation visible at surface (inside red circle).

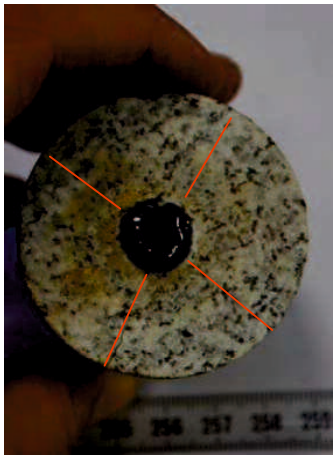

Figure 6-58: Granite sample Ne13 after 120 s of irradiation with steel cone. Melting at contact of cone and sample as origin of radial cracks (highlighted in red).

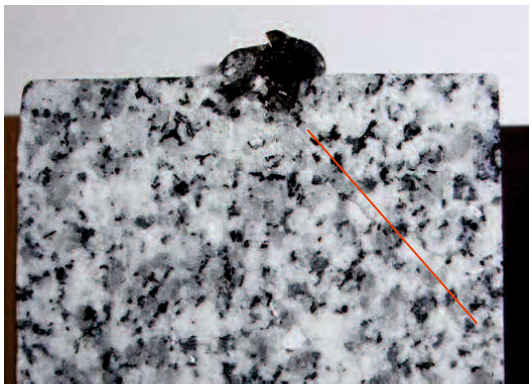

Figure 6-59: Cross-cut of granite sample Ne13 after 120s of irradiation with additional steel cone. Crack emanating from molten spot at surface (highlighted in red).

6.5.4 Neves Corvo copper ore

In chapter 6.4 the problems of irradiating the metallic ore of Neves Corvo have been explained in detail. With the help of the additional steel cone at least little damage can be inferred in this very hard and only minimally absorbing rock. Figure 6-60 shows that a hole with a depth of approximately 2 mm can be created after 120 s of treatment. No further damage or the formation of cracks can be reported for this kind of treatment. The described treatment method of these samples leads to similar behaviour as described in chapter 6.4 with the production of sulphurous acid. Additionally a considerably large amount of a black condensate was produced which precipitates on the steel cone (Figure 6-61).

Figure 6-60: Sample So63 of Neves Corvo copper ore after 120 s of irradiation with the help of additional steel cone. Dark area and small depression at contact zone of steel cone and sample.

Figure 6-61: After the treatment of Neves Corvo copper ore an unspecified black powder precipitates at the tip of the steel cone.

6.5.5 Additional observations – formation of fireballs

Applying the described technique when irradiating samples leads to a very interesting phenomenon, the creation of fireballs. Under certain circumstances the energy at the tip is high enough to ionize a limited amount of air and a fireball is created. These fireballs disappear as soon as the microwave field is turned off.

As long as the glass cylinder supporting the steel cone remains intact some sparks can be observed within this confined space. However the vast amount of energy goes into the heating and destructing of the rock mass. When a rock is irradiated long enough the glass cylinder can partially melt due to the high temperature at the surface (Figure 6-62). This creates a free passage for flashes leading to the ionization of the surrounding air and leads to the creation of fireballs. Figure 6-63a demonstrates how lightning remains within the boarders of the intact glass cylinder whereas it goes into the larger volume when the cylinder is damaged by the influence of heat (Figure 6-63b).

A similar effect was already described by Dikhtyar and Jerby (2006). Here a fireball is generated at the contact of the microwave drill bit with the underlying substrate.

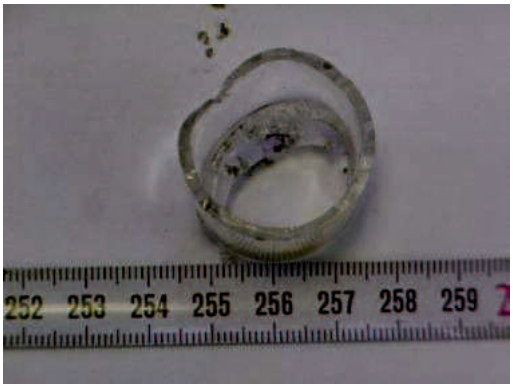

Figure 6-62: Partially molten glass cylinder after irradiation with the help of a steel cone.

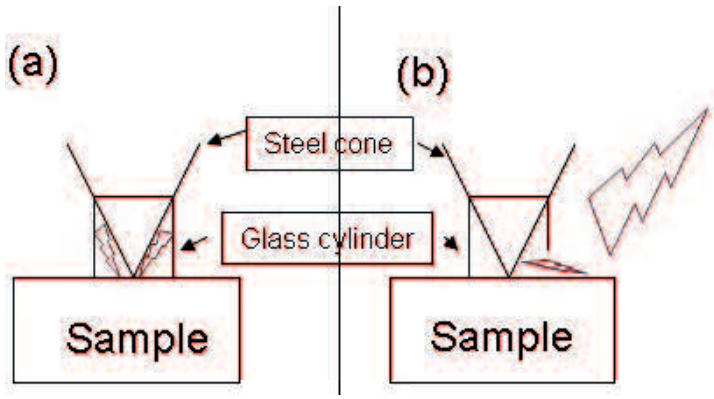

Figure 6-63: Sketch of the development of ball lightning. a) Intact glass cylinder, lightning within the cylinder. b) Damaged glass cylinder, larger amount of air volume leads to the creation of fire balls.

7 Large-scale microwave irradiation tests

Investigated samples include Weitendorf Basalt, Sandstone with moisture as well as dried, granite and gabbro. An overview of tested rock types and test procedures as well as results can be seen in Table 7-1.

Overview of large-scale laboratory tests and results

Sample Location	Treatment	Parameters	min Time (s)	max Time (s)	T max (°C)	Effect	Remarks	Tests
Basalt Weitendorf	on spot / cont.	80%	6	60	500	Spallation after 6s, melting and arc after 60s, generation of cracks and deep holes (6mm)	good absorption	cores / pen spray / thin sections
	on spot / pulse	2s - 20% / 1s - 100%		15	240	Spallation 55*35*5mm		cores / pen spray / thin sections
	on spot /cont.	80%		15	370	spallation, cracks		
	precut / cont. / movement	80% - 3.5 mm/s		90	370	spallation of small spots		linear cutting testrig
	precut / pulse / movement	2s - 20% / 1s - 100%		60				
	precut / cont / movement	80% - 3 mm/s		90	450	spallation / cracking		linear cutting testrig
	precut / cont / movement	80% - 3.5 mm/s			320	Arcs	Several arcs, instead of "checkboard pattern" whole lines irrdiated	linear cutting testrig
Sandstone with moisture	precut / cont / movement	80% - 3 mm/s		90	290	spallation of large parts, Arcss	good absorption of water leads to increase steam pressure inside sample and bursting	
	precut / cont / movement	80% - 6 mm/s			200	spallation, Arcs	faster speed leads to slower heating	linear cutting testrig
	on spot / cont	80%	10	20	270	spallation after 8s, deep holes (24mm), corner breaks apart	good absorption of water leads to increased vapour pressure inside sample and bursting	cores / pen spray / thin sections
	on spot / pulse	2s - 20% / 1s - 100%	9	21 (7 Pulses)	220	spallation and holes/craters (28mm), several spallation events during 1 irradiation		cores / pen spray / thin sections
Sandstone dry dried for 48h at 110°C	on spot / cont	80%	10	13	300	No special events, formation of radial cracks	Arc after 13s, no longer time possible	cores / pen spray / thin sections
	on spot / pulse	2s - 20% / 1s - 100%	9 (3 Pulses)	21 (7 Pulses)	240	No special events, cracks after 15 and 21s		cores / pen spray / thin sections
	precut / cont / movement	80% - 5 mm/s		25	210	Arcss after 20-25s	"Checkboard pattern"	linear cutting testrig
Granite	on spot / cont	80%		72	270	radial cracks at surface, arc after 72		cores / pen spray / thin sections
	on spot / pulse	2s - 20% / 1s - 100%		90 (30 Pulses)	330	radial cracks after 60 and 90s		cores / pen spray / thin sections
	precut / cont / movement	80% - 4 mm/s			190		"Checkboard pattern"; arcs after 16-25s, tests continued at same spot	linear cutting testrig
Gabbro	on spot	80%	10	30	455	radial cracks at surface	Possible arc after 24s, extreme hardness (290 MPa)	cores / pen spray / thin sections

Table 7-1: Overview of large scale laboratory experiments performed during the project. Four different kinds of rocks have been irradiated at one single spot with continuous irradiation (on spot / cont), at one single spot with pulsed irradiation (on spot / pulse) and with moving waveguide and continuous irradiation (precut / cont / movement). The basic irradiation parameters are listed along with the major effects and a listing of further investigations performed on the samples.

7.1 Basalt Weitendorf

Due to its relatively good heating characteristics which have also been described in chapter 6 samples of Weitendorf basalt can be damaged rapidly by means of high-power microwave irradiation. Effects range from spallation at the surface after only 6 s of irradiation with 25 kW via cracking beneath the surface to the formation of melt beneath the surface after longer irradiation times. The results will be described in detail in the following chapters.

7.1.1 Continuous wave positioned at one spot

Tests at single spots of basaltic samples were performed with irradiation times between 6 and 52 seconds with an applied power of 25 kW.

After only 6 seconds of irradiation first small pieces of rock start breaking out of the samples surface (Figure 7-1). The pieces reach temperatures as high as 270 °C and the effected area is 44 x 32 mm² with a maximum depth of 3.5 mm. Additional cracks can be observed in a radius of approximately 15 mm.

A drillcore of the spot reveals that one crack is going deeper beneath the surface of the sample (Figure 7-2). No further damage can be detected on this scale. The crosscut through this sample reveals another interesting feature. Directly below the centre of the irradiation cracks are aligned parallel to the surface and the feature of spallation (Figure 7-3).

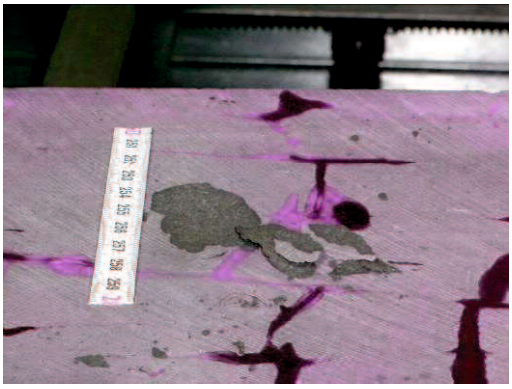

Figure 7-1: Basalt sample after 6 seconds of irradiation with 25 kW. Spallation at surface visible.

Figure 7-2: Drillcore of basalt sample irradiated for 6 s with 25 kW. One crack developed in axial direction for a depth of approximately 50 mm (highlighted by red arrow).

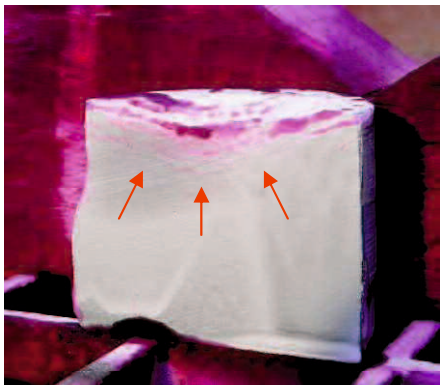

Figure 7-3: Cut through the centre of irradiation after irradiation for 6 s with 25 kW. Cracks in alignment to the surface in depth of 10 mm (red arrows).

Figure 7-4: Two neighbouring spots of basalt, each irradiated for 15 s with 25 kW. Spallation visible at both places.

After 15 seconds a maximum temperature of 370°C can be reached leading to even larger effects of damage. Two such spots can be seen in Figure 7-4 where craters of approximately 70 mm of length are formed.

While irradiating samples for this comparably short period of time persistent ablation / spallation can be observed. After 10 to 15 seconds this effect stops and all the applied energy obviously solely goes into generation of heat of the irradiated area and the underlying volume. After 50 seconds heating of the sample results in the generation of melt below the surface. The result is a crater of 65 x 50 mm² with a depth of approximately 6 mm. Measurable surface temperature is approximately 500 °C although it is assumed that the effective temperature below the surface is much higher but can not be measured. A network of circumferential cracks in a radius of about 20 mm to the crater is an additional observation.

The depth of damage can be inferred from a drill core taken from this spot (Figure 7-6). Only one large crack is visible with an axial length of approximately 10 cm. A larger network of cracks can be detected directly under the spot which is shown in Figure 7-7. Beneath the glass bubble of molten material fine cracks are visible to a depth of 45 mm below the surface.

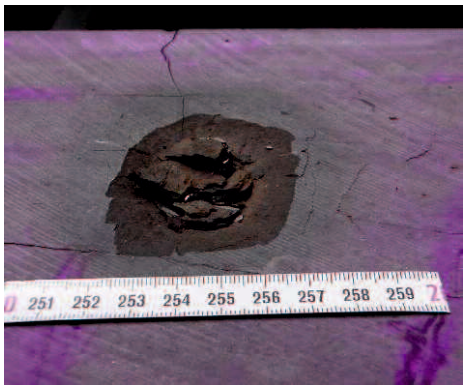

Figure 7-5: Basalt sample after 50 s of irradiation. Deep crater with glass as a result of melting process in the centre. Generation of cracks at the circumference.

Figure 7-6: Drill core taken from basalt sample after 50 s of irradiation with 25 kW treated with dye-penetrant. One axial crack has a length of approximately 10 cm.

Figure 7-7: Crosscut through a drill core taken from large block of basalt sample irradiated for 50 s with 25 kW. Depth of crack network approximately 45 mm.

In all described situations cracks are aligned in a semicircle below the irradiated spot. In Figure 7-3 one can see that this semicircle has the same shape as the crater generated by the spallation effects. Figure 7-7 reveals a very similar impression for the longer lasting irradiation time of 50 s.

It is also demonstrated in thin sections of the very same samples (Figure 7-8 and Figure 7-9) that these cracks are orientated parallel to the surface of the spallation are. Furthermore it can be seen that cracks are not bound to grain boundaries. In Figure 7-9 it is obvious that the direction and form of cracks is not governed and influenced by the fine grained matrix.

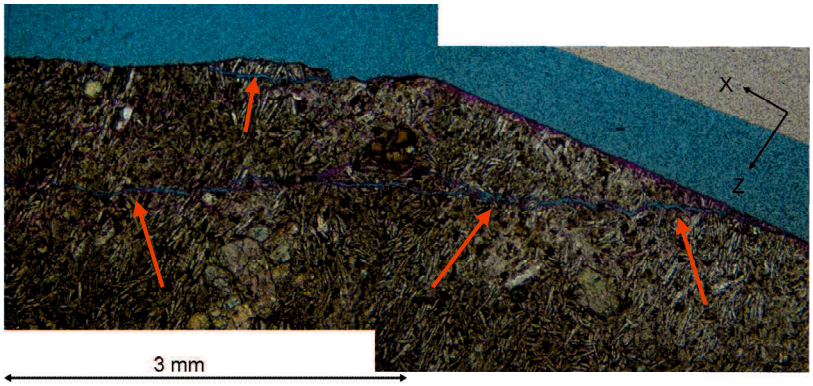

Figure 7-8: Resin saturated thin section of basalt sample after irradiation for 6 s with 25 kW. Transition of plain surface (right side) to spallation area (left side). Cracks indicated with red arrows.

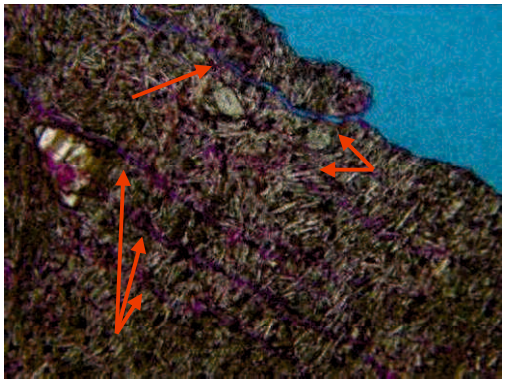

Figure 7-9: Resin saturated thin section of basalt sample after irradiation for 6 s with 25 kW. Fine network of cracks below the surface of spallation area. Cracks indicated with red arrows. Width of picture = 2.9 mm.

7.1.2 Pulsed wave positioned at one spot

Only few tests with (pseudo-)pulsed waves have been performed. The first observation of these tests shows that surface temperature is lower under the given circumstances for comparable irradiation times of continuous irradiation. Only 240 °C are reached after 15 s - representing 5 pulses - compared to 370 °C after 15 s with continuous wave. Although the temperature is much lower the optically visible effect can be compared to the effects described in Chapter 7.1.1. Figure 7-10 shows one spot of a basalt sample after 15 s of irradiation in pulsed mode. First events of spallation can be observed after 5, 8 and 10 s during the irradiation process. The result is a crater with an area of 55 x 35 mm² and a maximum depth of 5 mm. Several circumferential cracks can be observed in a distance between 10 and 20 mm to the crater. A thin section of the same sample (Figure 7-11)

shows that cracks are aligned parallel to the surface of damage. They cross cut all grains inside the matrix and no link of the crack-propagation to the mineralogy can be observed.

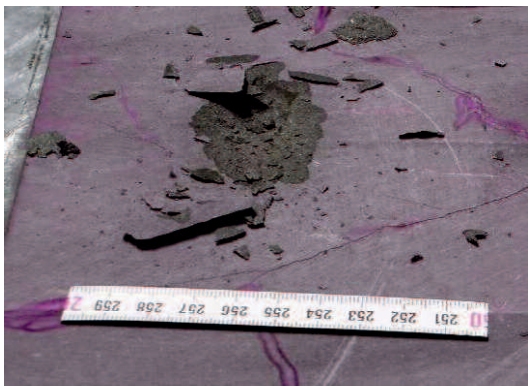

Figure 7-10: Basalt sample after 5 pulses (2s – 20% of 30 kW and 1s – 100% ➔ totally 15 s).

Figure 7-11: Resin saturated thin section of the area beneath the spot shown in Figure 7-10. Cracks (blue and indicated by red arrows) are aligned parallel to main damage patterns and show no affiliation to mineralogical boundaries. Height of picture = 2.9 mm.

7.1.3 Continuous wave with moving sample

Samples dedicated for this kind of investigation were preconditioned in a linear cutting test-rig in order to provide a rough surface. The irradiation time and moving speed were chosen in a way to guarantee an average energy input per area which can be compared to the results and parameters described in the previous chapter. For basalt an average moving velocity of 3.5 mm/s was chosen in this way. The observed effects are in many cases similar to the effects of single spot irradiation. Spallation of the surface is common as well as the formation of cracks. Figure 7-12 shows a basalt sample after the irradiation of four parallel stripes. Spallation is visible in the upper left corner and at the right side. A further feature is the generation of very large cracks going throughout the whole sample.

The maximum temperature at the surface is about 370 °C. An unfortunate effect coinciding with this method of irradiation was the generation of electric arcs preventing the energy to go into the rock mass and automatically stopping the microwave source. This effect could not be overcome and limited the possible irradiation time of rough surfaces.

Figure 7-12: Basalt sample after irradiation with moving sample. Irradiated areas changed to darker colour. Large cracks develop throughout the whole sample.

Because of natural variations the homogeneity of basalt samples treated and investigated in these tests could not be ensured. Small joints and healed cracks could not be excluded due to limited sample material. It became obvious during the tests performed that rocks tend to break along these zones of weakness either during the irradiation process or during subsequent cutting tests. A sample that broke apart during microwave irradiation is shown in Figure 7-13.

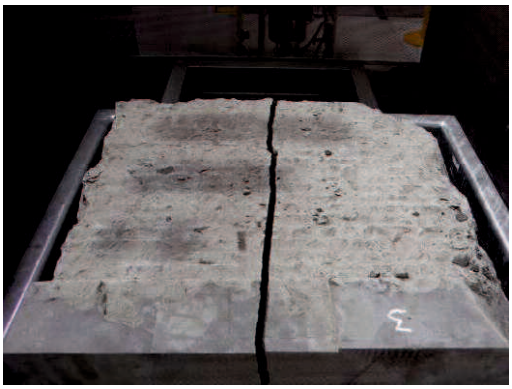

Figure 7-13: Basalt sample breaks into to halves during irradiation in large-scale microwave irradiation test-rig.

7.2 Sandstone Imberg

This kind of rock was investigated by (Peinsitt et al. 2010) on a small-scale basis. The authors could demonstrate that microwave absorption of dried sandstone is rather poor in

a 3.2 KW multimode cavity. Temperature only rises as high as 250 °C after 360 s of irradiation and only little damage coincdes with this rise in temperature. On the other hand it could be demonstrated that sandstone can be destroyed after only short irradiation time when samples are saturated with water. After 30 s of irradiation the surface temperature of irradiated samples is only slightly above 100 °C but vapour pressure from the included water is believed to cause the described damage.

The following chapters will describe the behaviour of both, dried and moist sandstone under the influence of high-power large-scale microwave irradiation. One series of samples has been dried for 48 h at 110 °C to avoid the influence of moisture whereas the other series of samples was investigated in a naturally wet condition. It will be shown that moisture plays a major roll also at this scale but that the high energy provided can lead to damage of a sample even without the influence of water.

7.2.1 Continuous wave positioned at one spot

Experiments for this chapter have been performed with irradiation times between 6 and 20 s with an applied power of 25 kW.

Dried sandstone

Dried sandstone reaches temperatures of 180 and 300 °C after 10 and 13 s, respectively. Due to the generation of arcing after only 13 s longer irradiation times could not be realized. As demonstrated in Figure 7-14 a network of cracks develops at the irradiated spots. For continuous wave irradiation treatment times of 10, 13 and 13 s (left to right) have been realised. No effects are visible after 10 s but to a multitude of radial cracks are obvious after 13 s of irradiation. These radial cracks have their centre directly beneath the position of the waveguide during the irradiation process and can reach as far as 20 cm in the undisturbed rock mass or to the nearest surface. No axial cracks can be observed.

A core taken from the centre of one irradiated area reveals only one deeper going crack with a depth of about 50 mm (Figure 7-15). The resin saturated thin section of the surface near areas of that sample is displayed in Figure 7-16-a. One can see that the volatile dye-penetrant (pink) penetrates the open pores but that the blue resin, having a higher viscosity, does not penetrate so deep beneath the surface. The surface of the sample is rough and its structure is obviously bound to grain boundaries. No cracks below or parallel to the surface can be seen. The sample shattered at a crack during the subsequent preparation process. It had to be agglutinated, can be seen in the central part of the Figure and prolongs deeper into the rock mass. Also this crack is mostly aligned on grain

boundaries. Only in very rare situations this crack crosses through grains (Figure 7-16-b, showing the deeper lying parts of the sample).

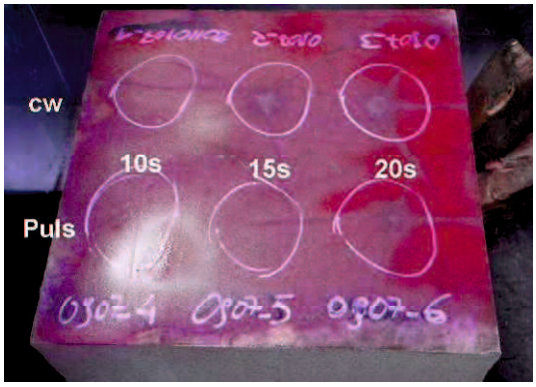

Figure 7-14: Dried sandstone after irradiation with 25 kW for 10, 13 and 13 s in cw (upper row from left to right) and for 10, 15 and 20 s in pulsed mode (lower row from left to right). Surface treated with a dye-penetrant.

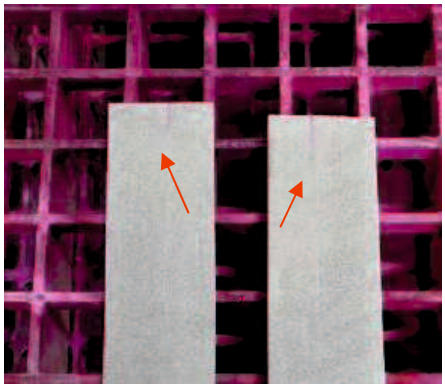

Figure 7-15: Drill core taken of the irradiated spot of dried sandstone sample after 10 s of irradiation with 25 kW. Sample diameter = 50 mm. Cracks marked with red arrows.

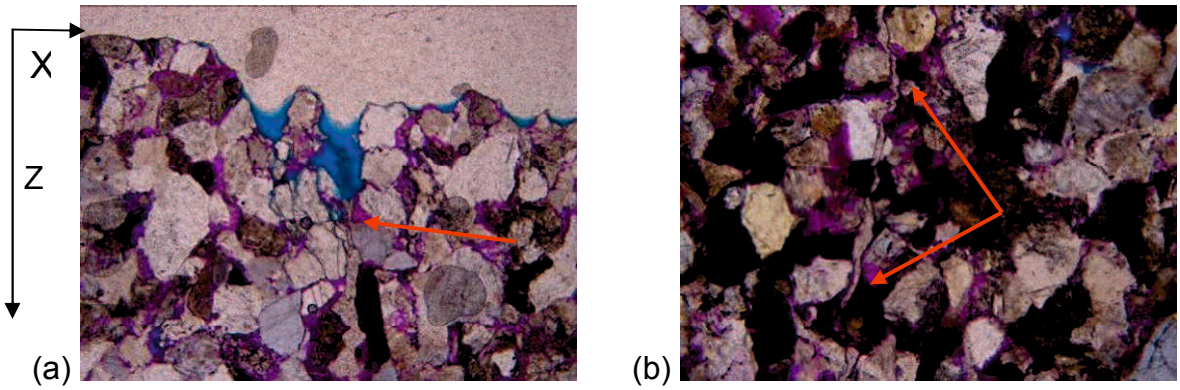

Figure 7-16: Resin saturated thin sections of dried sandstone after 10 s of irradiation with 25 kW. (a) near the surface, with deeper going crack; (b) deeper going crack along grain boundaries as well as crossinggrains. Width of pictures = 3 mm.

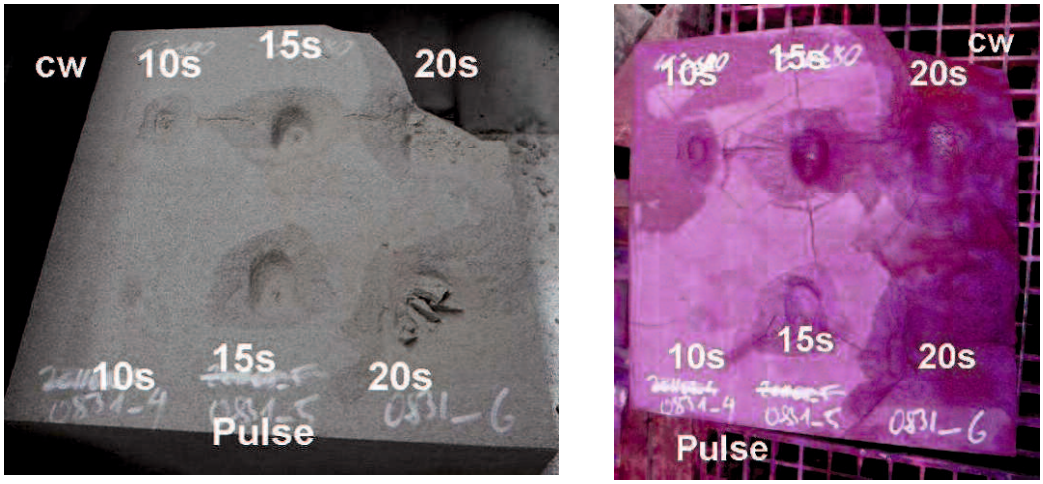

(a) (b)

Figure 7-17: (a) Moist sandstone after irradiation with continuous and pulsed waves after 10, 15 and 20 s. (b) same sample after treatment with penetration spray.

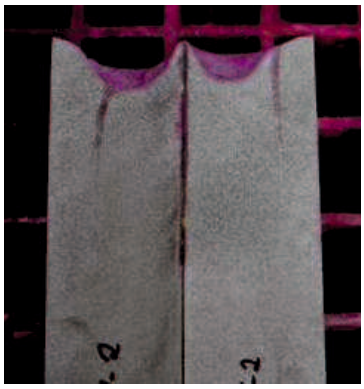

Figure 7-18: Cross-cut through drill core taken from centre of spot of moist sandstone irradiated for 15 s with 25 kW.

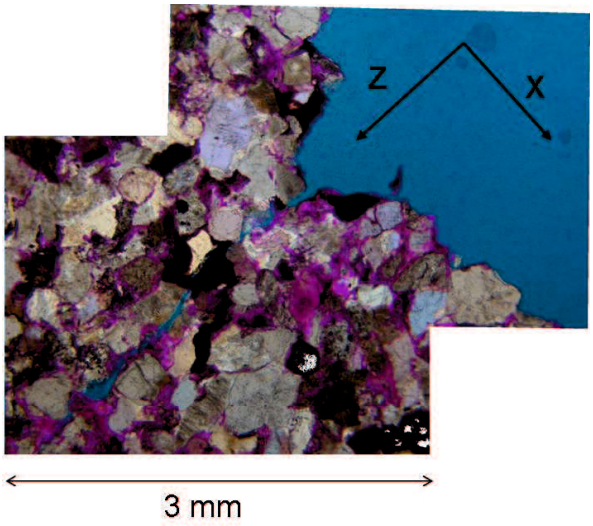

Figure 7-19: Resin saturated thin section of spot of moist sandstone irradiated for 15 s with 25 kW.

Moist sandstone

On the contrary to dried sandstone the specimen investigated in this series of tests was not dried at 110 °C. They were tested as received and with their natural moisture content. A detailed measurement of the actual moisture could not be performed.

Tested irradiation times were 10, 15 and 20 s and maximum temperatures of 270 °C could be measured for all three irradiation times. Figure 7-17 a-b demonstrates that continuous wave irradiation leads to breaking off of large craters after 10 and 15 s and that a large corner breaks out after 20 s of irradiation. The depth of the crater is 10 and 24 mm, respectively. One can see in Figure 7-17-b that radial as well as circumferential cracks are a further feature of the irradiation with 25 kW. The size of the shattered corner is approximately 20*20*10 cm³ (w*l*h).

Drill cores taken from the centres of the irradiated spots show the crater with a maximum depth of 24 mm and reveal that cracks can proceed for several centimetres in vertical direction but that no other obvious signs of damage can be seen (Figure 7-18). It is eye-catching that the crack is not centred below the crater but that its origin is slightly shifted to one side. Resin saturated thin sections of the surface near areas show very similar images for all three irradiation times. Figure 7-19 shows the surface near area and the beginning of the deeper going crack for the spot irradiated for 15 s. The formation of the newly generated surface is obviously bound to grain boundaries. The blue resin adapts to the forms of the grains. On the picture one can also see remnants of the pink dye-penetrant which infiltrates the pores of the rock. However, the blue resin only penetrates the large vertical crack which is displayed in z-direction. It can be seen that the crack is partly aligned to grain boundaries but that it also cross cuts single grains.

7.2.2 Pulsed wave positioned at one spot

Experiments explained in this chapter were performed for 9, 15 and 21 seconds representing 3, 5 and 7 pulses of alternately irradiating for 2 s with 6.4 and for 1 s with 30 kW.

Dried sandstone

The surface temperature after irradiation increased to 80, 160 and 240 °C respectively and is thus significantly lower than with continuous waves for dried samples.

The lower part of Figure 7-14 shows the three irradiated spots after treatment with a dye-penetrant. In direct comparison to continuous-wave irradiation only after 7 pulses (spot 0907_6) a comparable network of cracks can be seen. Shorter irradiation times do not lead to the formation of any cracks. It is shown in the thin section of sample with shorter irradiation time that the dye-penetrant used to investigate the surface infiltrates the pore volume but that no additional damage is observed (Figure 7-20).

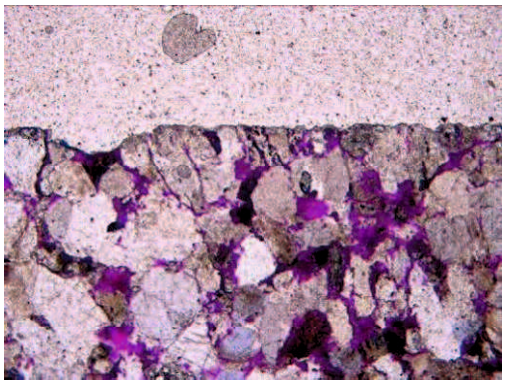

Figure 7-20: Thin section of sample of dried sandstone irradiated with 5 pulses of alternating 6.4 and 30 kW.

Moist sandstone

Similar to results described in chapter 7.2.2 also effects of pulsed wave irradiation differ significantly between dried and moist sandstone samples. Surface temperature is lower than for comparable experiments with continuous wave (190 °C after 5 pulses compared to 265 °C after 15 s). It is shown in Figure 7-17 that no crater develops after irradiation with only 3 pulses (9 s), a 20 mm crater breaks out after irradiation with 5 pulses and that a deep crater of 28 mm develops after 7 pulses (21 s). One single crack can be observed after the shortest irradiation time and several larger radial cracks are visible after 7 pulses. In the contrary to continuous wave experiments no circumferential cracks can be observed.

7.2.3 Continuous wave with moving sample

Dried sandstone

Due to its dielectric properties the coupling of microwaves to sandstone is relatively difficult. It was already described in the previous chapters that arcing may be observed when irradiating dry sandstone. The precut, rough surface which is subjected to tests in this chapter enhances the effect of arcing and therefore complicates the handling of the microwave. Several tests have been performed with an average moving speed of 5 mm/s. A slower movement would be preferable to bringing more energy into the rock and to making the energy input of the tests completely comparable to chapter 7.2.1. However, extensive arcing after very short irradiation time with slower moving velocity lead to the decision to increase the velocity and thus decrease the residence time at single spots. This measure could not completely avoid the negative effects but reduce them significantly to an average time without arcs of about 20 to 25 s or 100 mm of movement. For the irradiation of longer stripes subsequent irradiation steps had to be performed. The additional irradiation steps started at the position where first arcing forced the microwave source to turn off. Unfortunately a time period of approximately 3 minutes passed by between the single steps due to technical limitations. This leads to an uncontrollable heat flow to adjacent parts of the sample. The maximum surface temperature achieved in this way was 270 °C which is very similar to the temperature measured in single-spot experiments. In contrary to those experiments no cracks or any signs of damage could be observed after irradiation.

Moist sandstone

Differing to dried sandstone samples moist sandstone provides better coupling of the microwave and different effects compared to dried samples. Two different moving velocities were tested. At slow speed (3 mm/s) the average residence time of a spot beneath the waveguide is long enough to generate extensive spallation and the breaking off of large corners as also described above. Figure 7-21 shows a moist sandstone sample of which two corners were broken off explosively after short of microwave irradiation time. The maximum temperature was 290 °C. The negative feature of arcing which has already been described can not be prohibited.

Faster moving speed (6 mm/s) still leads to spectacular effects. Spallation is very common and happens at several spots (Figure 7-22). The maximum surface temperature is as high as 200 °C. The generation of arcs is still a problem that can not be excluded.

Figure 7-21: Sample of moist sandstone after 2 tests of irradiation with a sample moving speed of 3 mm/s at 25 kW. Direction of movement parallel to the rims. Two large corners were breaking off.

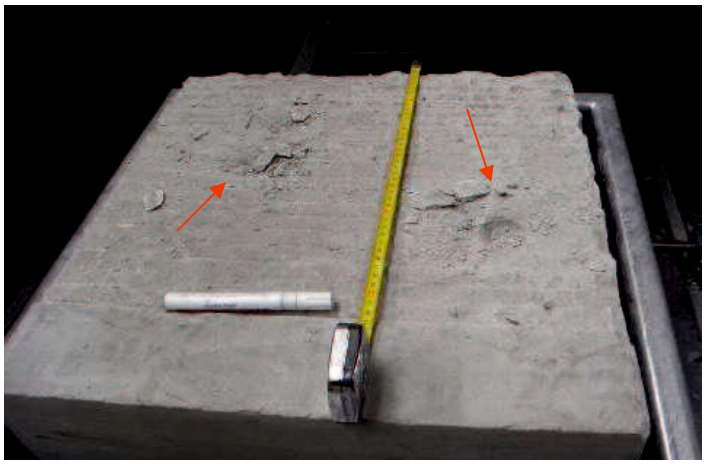

Figure 7-22: Moist sandstone after irradiation of several stripes with a moving speed of 6 mm/s at 25 kW. Small spallation effects at surface are visible (indicated with red arrows).

7.3 Granite Neuhaus

As with the sandstone this rock type was intensively investigated by other authors on a laboratory scale (e.g. Peinsitt 2009, Peinsitt et al. 2010). They showed that this type of granite heats up very slowly to 230 °C after 300 s of irradiation in a 3.2 kW multi-mode cavity. This generation of heat goes along with an only slight decrease in p-wave velocity from 4300 to 3500 m/s after 300 s of irradiation. It is believed that the comparably bad dielectric properties of the components of granite (mainly quartz, feldspars and micas) are the main cause for this behaviour.

It will be shown in the subsequent chapters how the increase in applied power to 25 kW influences the heating and damage of samples. A network of cracks can be initiated in predominantly radial direction.

7.3.1 Continuous wave positioned at one spot

Experiments described in this chapter have been performed for 30, 60 and 72 s with 25 kW. Surface temperature climbed to 240, 370 and 374 °C, respectively. Due to arcing longer irradiation times than 72 s could not be realized. Radial cracks have their origin in a larger spot directly beneath the waveguide (Figure 7-23). It can be seen from this image that the extension of the central spot increases with increasing irradiation time. A tendency to form thicker cracks can be observed after irradiation for 60 and 72 s compared to 30 s of irradiation. The spacing of irradiated spots was relatively close on this sample and an interference of cracks could not be avoided. It is assumed that this effect does not influence the behaviour directly at the irradiated spots.

The vertical reach of the described cracks is several cm. It can also be seen from Figure 7-24 that circumferential cracks can develop in about 3 cm of depth. Here a sample irradiated for 72 s is shown.

The formation of cracks is strongly related to grain boundaries. Figure 7-25 shows the upper most millimetres of a sample irradiated for 72 s with 25 kW. It is clearly visible how the blue resin penetrates open spaces around grain boundaries especially at the surface of the sample (left part). It can be observed in the deeper lying parts of the sample that the crack is not solely oriented along grain boundaries. Here it cross-cuts quartz as well as feldspar grains. However, in many cases the alignment of intragranular cracks is governed by the cleavage of the grains. This effect can be observed for feldspar and biotite. Figure 7-26 shows a biotite grain which is crossed by a crack along its cleavage.

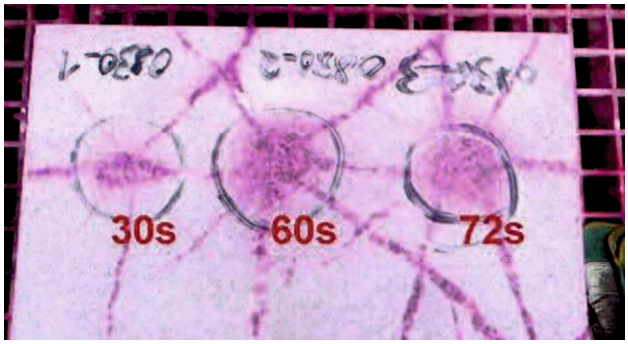

Figure 7-23: Surface of granite after the irradiaton with 25 kW for 30, 60 and 72 s (left to right spot). Cracks originated in the second (60 s) and third (72 s) irradiation, respectively, cross those generated previously. Cracks made visible by dye-penetrant. Width of sample = 50 cm).

Figure 7-24: Drill core taken from granite spot irradiated for 72 s with 25 kW continuous wave. Circumferential cracks align in about 30 mm of depth.

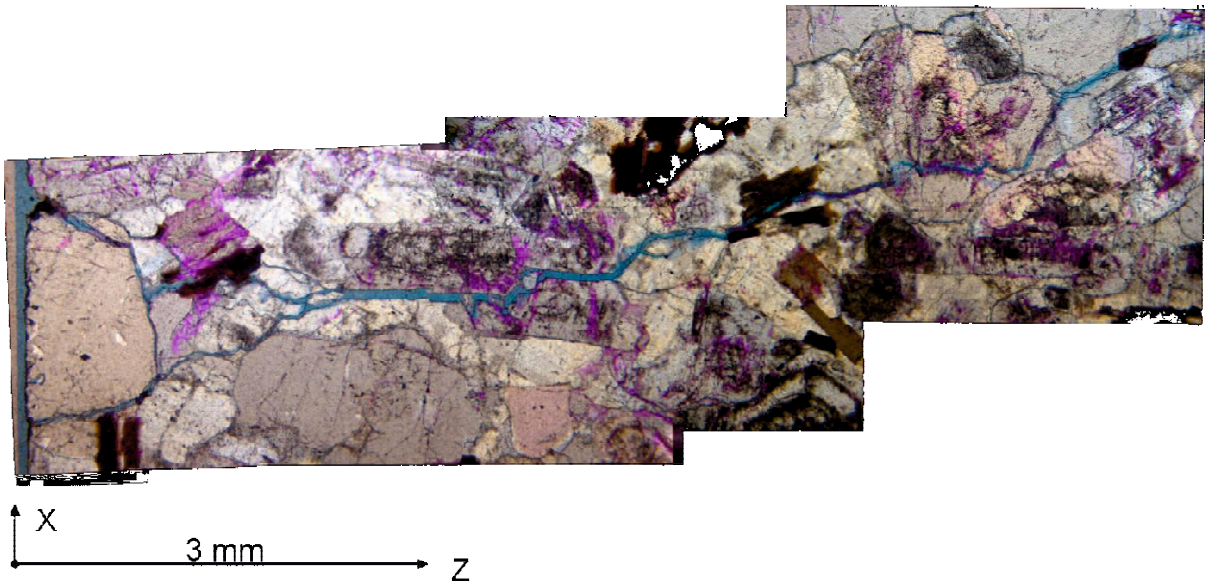

Figure 7-25: Thin section of deeper going crack in granite after irradiation with 25 kW for 72 s. Crack aligned to grain boundaries and natural cleavage of minerals. Surface in x-direction.

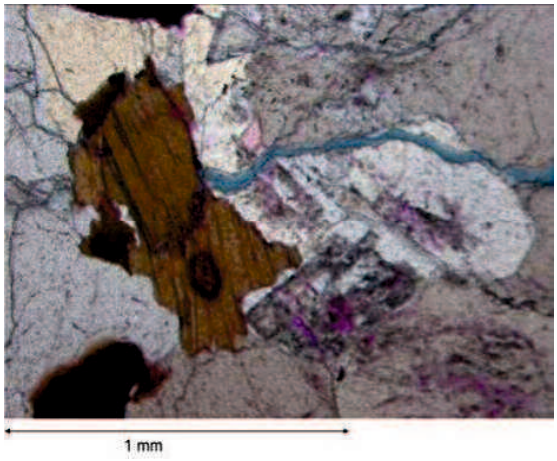

Figure 7-26: Biotite between feldspar and quartz of granite sample after microwave irradiation. Crack (blue) partly aligned to cleavage of biotite.

7.3.2 Pulsed wave positioned at one spot

Pulsed experiments have been performed with irradiation of 2 s with 6.4 kW alternating with pulses of 1 s with 30 kW. The number of pulses was chosen in a way to guarantee the same irradiation time as with continuous wave irradiation. Experiments with 10, 20 and 30 pulses (30, 60 and 90 s) have been performed. Maximum surface temperatures reached 140, 240 and 330 °C, respectively. Comparable experiments with continuous waves lead to significantly higher temperatures (see chapter 7.3.1). The lower temperatures also lead to different patterns of damage. Whereas for the shortest irradiation time only one single crack can be observed longer irradiation times lead to a similar crack network as described earlier for continuous wave irradiation (Figure 7-27). Especially for the longest irradiation of 30 pulses visible damage can be compared to those experiments performed for 90 s. Based in a large spot in the centre of the irradiation a set of 7 radial cracks spreads out after this irradiation time.

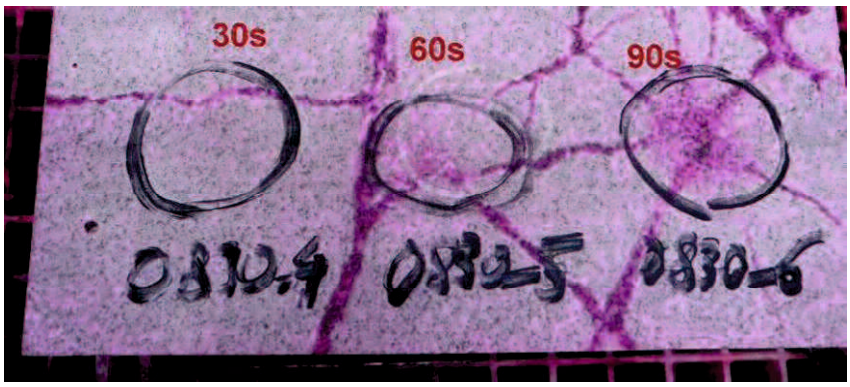

Figure 7-27: Surface of granite after irradiation in pulses for 30, 60 and 90 s (10, 20 and 30 pulses of 2 s at 6.4 kW and 1 s at 30 kW).

7.3.3 Continuous wave with moving sample

In strong similarity to previously described experiments of that method applied at other rock types arcing effects are a major problem when irradiating rough surfaces of weakly absorbing rocks. Experiments on rough granite surfaces have been performed with 25 kW and an average moving speed of the sample of 4 mm/s equalling an average exposure time of single spots of 15 s. Arcing occurs after 16 to 25 s of irradiation. The maximum surface temperature after irradiation was 190 °C. No obvious signs of damage are visible at the surface of irradiated samples.

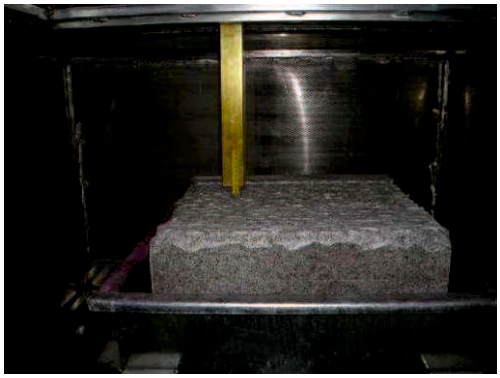

Figure 7-28: Granite sample with preconditioned, rough surface prior to irradiation with the 25 kW microwave.

7.4 Gabbro

As shown in chapter 6.3 gabbro has similar dielectric properties as many other greenstone rocks. It could be demonstrated that small samples heat up reasonably fast to 390 °C after 90 s of irradiation with 3.2 kW. This increase in temperature coincides with a decrease in rock strength represented by a reduction in p-wave velocity from 6200 to 4000 m/s.

Large-scale experiments with the 25 kW microwave source show that no visible damage can be seen after 10 s of irradiation, some cracks can be initiated after only 20 s of irradiation an that a network of cracks can be observed after 30 s of irradiation.

7.4.1 Continuous wave positioned at one spot

Experiments on gabbro were performed for 10, 20 and 30 s with 25 kW microwave power. The sample surface reaches temperatures of 160, 325 and 455 °C, respectively. Longer irradiation times could not be performed because of arcing after approximately 30 s of irradiation or sometimes less. In Figure 7-29 three irradiated spots are displayed showing different patterns of damage according to the time they have been exposed to irradiation. No crack can be observed after 10 s of irradiation (circle at the left side). After 20 s of

irradiation four branches of cracks reach out 15 – 20 cm from the central spot. The impression of some circumferential cracks arises by taking a closer look on the picture. More cracks are visible at the spot being irradiated for 30 s with 25 kW. In the centre a network of tiny cracks can be seen as well as some circumferential cracking.

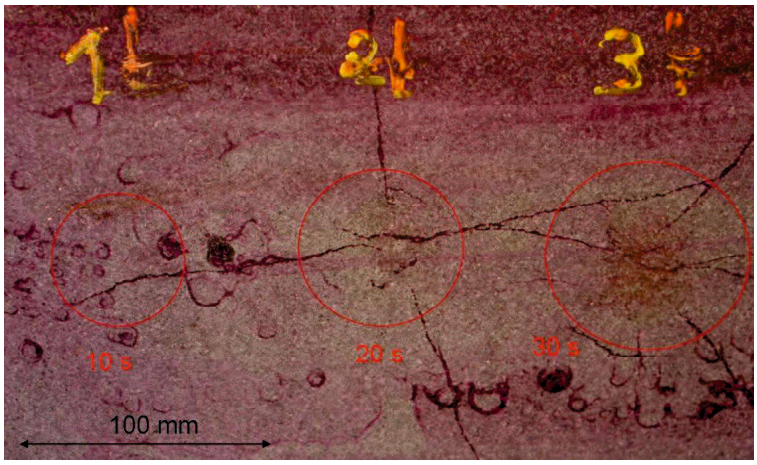

Figure 7-29: Surface of gabbro treated with dye-penetrant after irradiation with 25 kW for 10, 20 and 30 s (left to right). No cracking after short irradiation time and crack network after longer time (spot 2 and 3).

These cracks have a maximum vertical extension of 50 mm. Figure 7-30 shows a drill core taken from the spot irradiated for 30 s. One can see the radial crack at the surface as well as its vertical extension of about 30 mm and another set of cracks aligned parallel to the surface in a depth of approximately 20 mm. These circumferential cracks can also be observed in thin sections taken from the uppermost part of the core (Figure 7-31). A fine network of cracks is aligned in a semicircle beneath the surface. The picture shows the left semicircle of that rim. The fine cracks show no alignment to any grain boundaries and cross all grains. An image taken from a radial crack is shown in Figure 7-32. It is obvious that the opening of the radial crack is wider than that of the cracks described above. An interesting feature of this crack is its behaviour at grain boundaries. Whereas it follows a general direction perpendicular to the surface on a macroscopical scale the orientation along predamaged zones like grain boundaries or cleavage is obvious on the microscopical scale. In Figure 7-32 such a situation is displayed. The crack searches its way through the grains by forming corners and abrupt turns where cleavage is appropriate.

Figure 7-30: Drill core of gabbro sample under spot irradiated for 30 s with 25 kW. Circumferential cracks below the surface (red arrow) and radial crack at surface clearly visible.

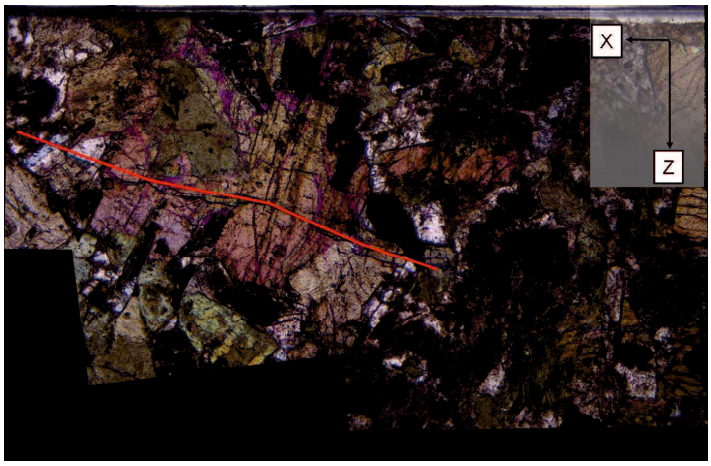

Figure 7-31: Thin section of gabbro irradiated for 30 s. Fine cracks aligned in a semicircle around the centre of irradiation cross-cut mineral boundaries. Cracks made visible by blue resin and electronically highlighted in red.

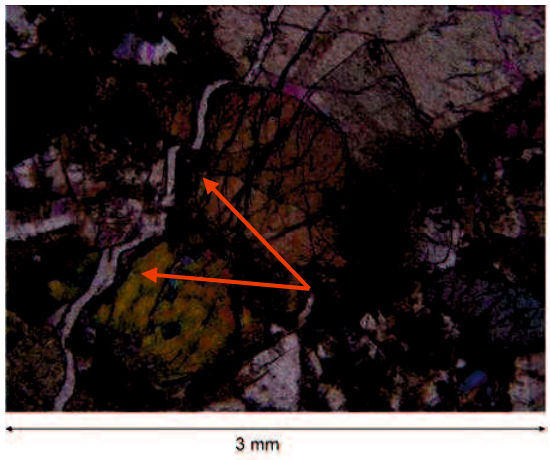

Figure 7-32: Interaction of crack and different grains in gabbro after irradiation with microwaves.Position of crack indicated by red arrows.

8 Mechanical cutting tests

This chapter is dedicated to describing the results obtained while cutting several different kinds of rocks after microwave irradiation. As described earlier (chapter 5.2.8) investigated rock types had to be pre-treated in order to provide comparable results between single experiments. A rough surface was produced by this pre-treatment. The irradiation of rough surfaces is accompanied by some technical constraints like enhancement of microwaves at sharp edges leading to the ionization of air and arcing effects. Coinciding is a reduced irradiation time leading to significant decrease in surface temperature compared to experiments performed at plain surfaces. No macroscopic signs of damage were visible for any of the investigated rock samples.

The following chapters provide an overview of the performed tests and results. For more detailed results please refer to the Appendix where single testing procedures and results are provided.

8.1 Cutting tests of basalt

The description of irradiation of basalt samples can be found in chapter 7.1.3. Irradiation was performed with 25 kW and the sample was moved with 3.5 mm/s beneath the waveguide. Obvious signs of damage were spallation at the surface and the opening of large cracks in some cases. After irradiation the irradiated areas had a darker colour than the untreated parts (Figure 7-12). Cutting tests were performed with a Diamond pick, a cutting speed of 1.5 m/s, spacing of 16 mm and a penetration depth of 8 mm.

Figure 8-1 and Figure 8-2 show the principal set-up and results of one test. A total number of 15 cutting lines were tested of which line 1-9 have been irradiated and lines 10 - 15 remained untreated. The average value of every single cut was taken and a profile across the area was generated in this way (Figure 8-3). Due to safety measures the last few centimetres in x-direction of a block could not be irradiated. These parts were not excluded from averaging due to technical reasons but it is assumed that they have only little influence on the average value of the entire cutting line because of the small area covered by them. It can be seen from Table 8-1 that most average values for the applied forces are lower when cutting irradiated areas. However, both irradiated and untreated areas show large standard deviations of all measured forces that compensate for the differences in average values. Cutting force in the uppermost layer is 3.41 kN in irradiated areas compared to 4.49 kN in untreated sectors of the sample. Side forces on the contrary

are smaller in the untreated area with 3.69 compared to 4.05 kN in the irradiated part of the sample. Going deeper into the rock mass the average cutting force decreases in irradiated areas as well as in untreated parts in the second layer and increases slightly in both areas in the third layer. Standard deviation is high for all measurements. The average values of these measurements are also displayed in Figure 8-2.

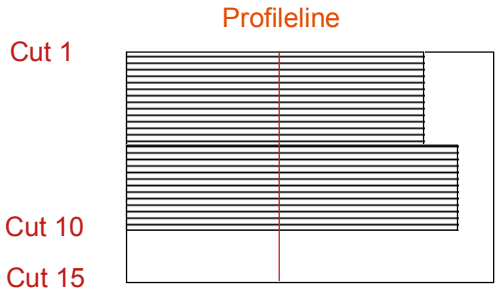

Figure 8-1: Sketch of irradiation pattern for continuous irradiation with moving sample of basalt. Cutting direction left to right. Red line and annotation indicates profile line of Figure 8-3. Indication of position and numbering of 15 cutting lines.

Layer		Irradiated Area				Untreated Area			
		Cutting Force [kN]	Side Force [kN]	Normal Force [kN]	Normal / Cutting Force	Cutting Force [kN]	Side Force [kN]	Normal Force [kN]	Normal / Cutting Force
8 mm	Average	3,41	4,05	6,98	2,05	4,49	3,69	7,40	1,52
	Stdv	0,58	0,64	1,35	0,19	1,05	1,36	3,38	0,68
16 mm	Average	2,67	4,19	5,82	1,90	3,79	3,89	6,82	1,59
	Stdv	1,69	2,08	3,36	1,43	1,75	2,31	3,34	0,62
24 mm	Average	3,35	3,77	5,89	1,35	3,95	3,73	5,86	1,22
	Stdv	1,48	1,79	2,90	1,18	1,84	2,91	4,01	0,73

Table 8-1: Comparison of average forces and standard deviation for cutting different consecutive layers of irradiated and untreated basalt.

Figure 8-3 provides a more detailed look into the results of layer 1. Average forces for every single cut are calculated and arranged in a profile across the sample as indicated by the red line in Figure 8-1. One can see that all three measured forces have a trend towards higher values towards the right end side of the diagram representing the areas not subject to irradiation. One might also interpret that a slight jump / increase is visible between cut 8 and 9. A positive shift of approximately 1 and 0.4 kN may be observed for cutting and side forces whereas the normal force goes down by 0.4 kN. Taking into account the standard deviation of 0.6, 0.6 and 1.4, respectively, the change in measured forces is compensated by the high variations. The outermost cuts (cut 1, 14 and 15) show a clear trend towards very low values for all measured forces. It is evident that the influence of the geometry of the sample plays a major role in this case. The strong

reduction in measured forces for these cuts is caused by the conditions at the rim of the samples where the exact positioning of the pick is not possible.

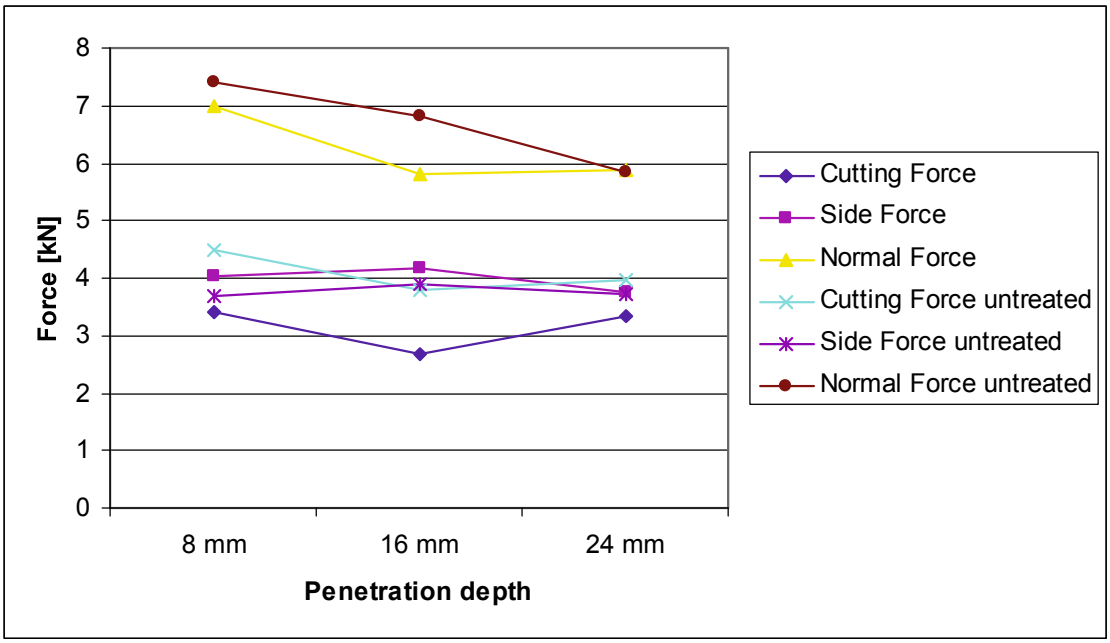

Figure 8-2: Comparison of measured forces [kN] as function of the penetration depth (Layer 8 – 24 mm) for basalt irradiated with 25 kW and a moving speed of 3.5 mm/s.

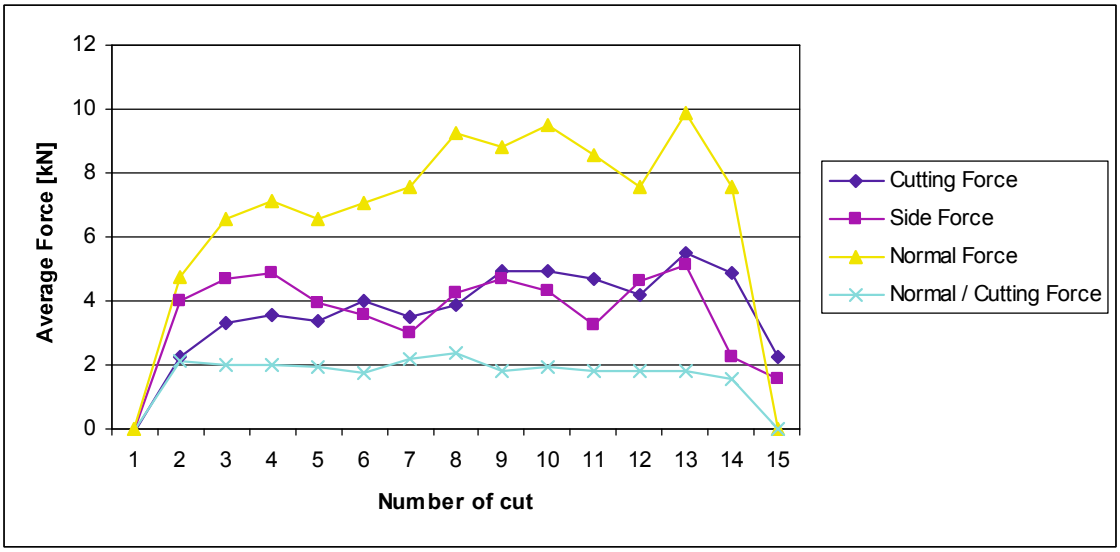

Figure 8-3: Profile of applied forces for cutting the uppermost layer (8 mm) of a basalt sample. Cut 1-9 performed in irradiated area. Cut 10-15 performed in untreated area.

As a result of the breaking apart of some samples during the irradiation process (described in chapter 7.1.3) due to pre-existing cracks only limited samples could be tested and data are only available for those samples that remained largely intact after

irradiation as well as cutting. Nonetheless the breaking apart of rocks as a result of microwave irradiation may be considered as 100 % damage and complete reduction of applied forces.

8.2 Cutting tests of sandstone

A detailed description of the irradiation process of large and rough sandstone samples is provided in chapter 7.2.3. The difference between the irradiation of dry and moist samples is highlighted. It is shown that coupling of microwaves and rock is complicated and irradiation times are limited because of enhancement of the microwave field on sharp edges and subsequent arcing effects. Although irradiation times for these experiments have been significantly shorter in comparison to experiments performed at plain surfaces and no macroscopic signs of damage could be observed a detailed investigation of the influence of microwave irradiation on the cutability is provided in the following paragraphs. Cutting tests were performed with a Diamond pick, a moving speed of 1.5 m/s, spacing of 20 mm and a penetration depth of 10 mm.

Dried sandstone

The schematic set-up of one irradiation pattern of dried sandstone is provided in Figure 8-4. Dashed areas of approximately 250 x 200 mm² were irradiated with 25 kW and a moving speed of the sample beneath the waveguide of 5 mm/s. A total number of 21 cuts could be performed in the uppermost of 5 layers. Table 8-2 shows the average forces acting on a pick when cutting irradiated and untreated areas of dried sandstone and Figure 8-5 provides a graphical analysis of these values as function of the depth inside the sample. One can see that all applied forces have their highest values in the uppermost segment of the tested rock in both treated and untreated areas. Values for cutting-, side- and normal forces are decreasing in the second layer representing 10 mm of depth. Whereas cutting and side forces remain steady in the underlying layers normal forces in irradiated as well as in untreated areas rise again till they reach a plateau in 40 mm of depth (layer 4). Standard deviation for all measured data is rather high being up to 1/3 of the average values. Slight changes and differences between different treatment methods are thus not significant. For example the difference between irradiated and untreated are in cutting force in the first layer is about 0.3 kN whereas standard deviation is as high as 1.9 and 1.8 for irradiated and untreated part, respectively.

A profile along the red line indicated on Figure 8-4 is provided in Figure 8-6. Cutting lines 1 – 10 represent average values of untreated areas of layer 1 and lines 11 – 21 represent the irradiated parts of that sample. As one can see no difference is visible between

irradiated and untreated part of this sample. All three measured forces show rather broad variation between single cutting lines. The trend towards lower values for cutting line 1 and higher values for cutting line 21 is caused by side effects due to the geometry of the sample and the test facility.

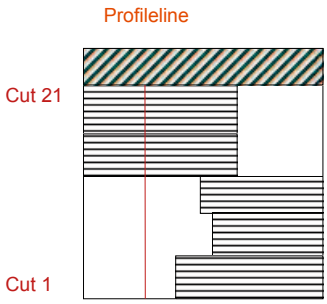

Figure 8-4: Arrangement of irradiated areas (dashed) on dry sandstone. White areas were not irradiated, green dashed areas neither irradiated nor tested. Indication of number and position of 21 cutting lines (Cut 1 – Cut 21). Red line indicates position of profile in Figure 8-6.

Layer		Irradiated Area				Untreated Area			
		Cutting Force [kN]	Side Force [kN]	Normal Force [kN]	Normal / Cutting Force	Cutting Force [kN]	Side Force [kN]	Normal Force [kN]	Normal / Cutting Force
10 mm	Average	7,01	7,39	8,96	1,07	6,69	6,88	8,30	0,81
	Stdv	1,90	3,04	3,77	0,93	1,79	2,70	3,72	1,89
20 mm	Average	5,97	5,37	7,10	0,77	6,02	5,41	7,69	1,17
	Stdv	1,83	2,17	3,37	1,73	1,68	2,04	3,02	0,60
30 mm	Average	5,64	4,89	8,85	1,57	5,42	5,27	8,35	1,56
	Stdv	1,70	1,80	2,84	0,15	1,87	2,40	2,86	0,23
40 mm	Average	5,78	5,75	9,98	1,58	5,41	4,37	9,48	1,72
	Stdv	1,62	1,76	3,29	0,62	1,33	1,21	3,18	0,29
50 mm	Average	5,60	5,04	9,90	1,64	5,68	4,91	9,74	1,59
	Stdv	1,68	1,93	3,30	0,51	1,67	1,51	3,26	0,57

Table 8-2: Comparison of average forces and standard deviation for cutting five consecutive layers of irradiated and untreated dried sandstone.

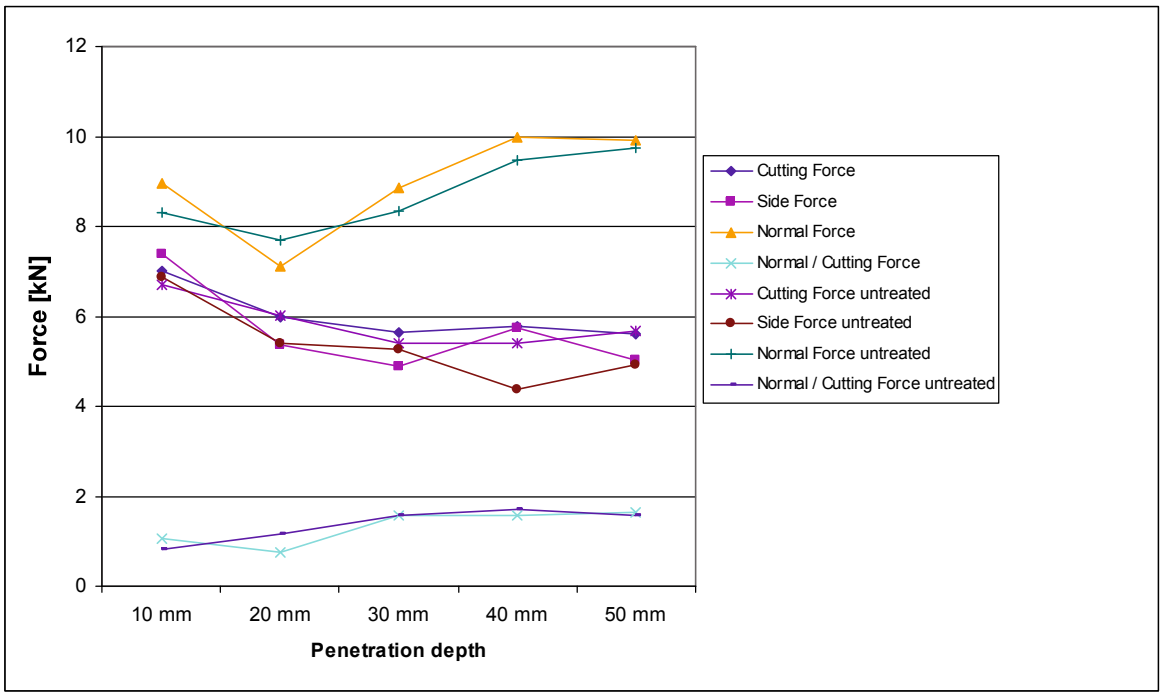

Figure 8-5: Comparison of measured forces [kN] as function of the penetration depth [layer 1-5] for dried sandstone irradiated with 25 kW and a moving speed of 5 mm/s.

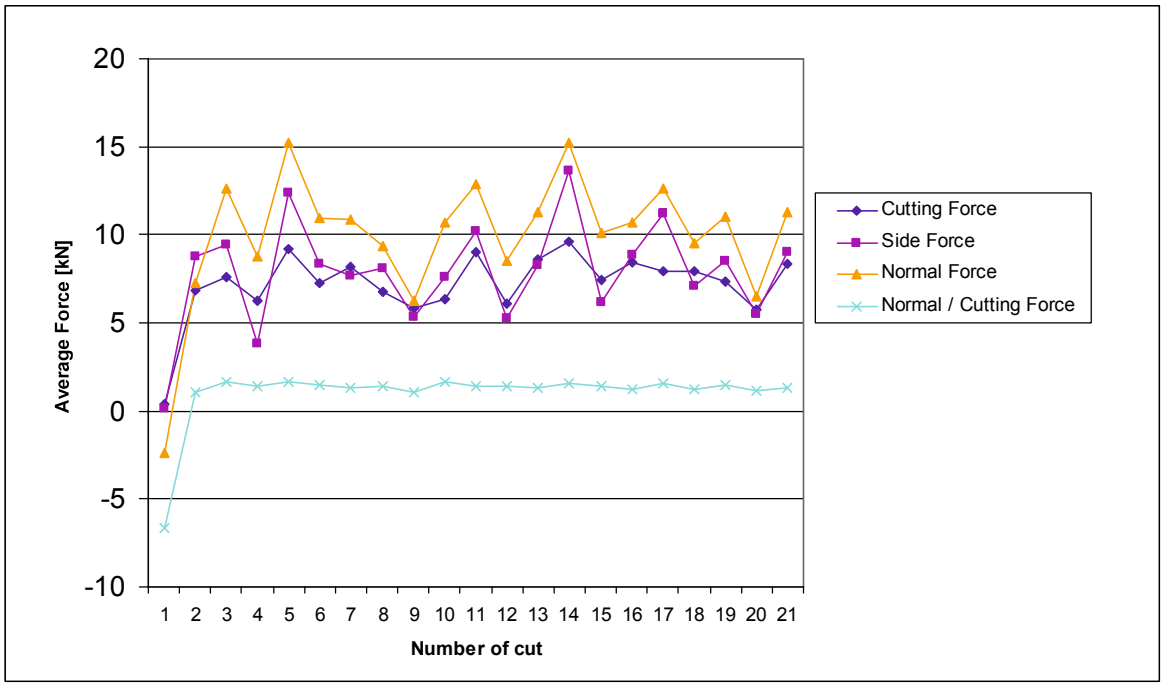

Figure 8-6: Profile along line from Figure 8-4 of applied forces for cutting the uppermost layer of dried sandstone irradiated. Cut 1-11 performed in irradiated area. Cut 10 – 15 performed in untreated area.

Moist Sandstone

A large field of approximately 370 x 200 mm² was irradiated with 25 kW and a moving speed of 6 mm/s (Figure 8-7). A total number of 20 cuts could be performed for the first of four measured layers. A comparison between irradiated and untreated areas is provided in Table 8-3 and graphically shown in Figure 8-8 as function of the penetration depth. It is shown that cutting forces are lower in untreated areas compared to irradiated areas in layers 1, 3 and 4 representing a total penetration depth of 10, 30 and 40 mm.

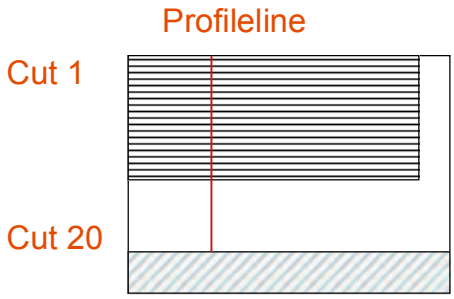

Figure 8-7: Arrangement of irradiated areas (dashed) on moist sandstone. White areas were not irradiated, green dashed areas neither irradiated nor tested.

Layer		Irradiated Area				Untreated Area			
		Cutting Force [kN]	Side Force [kN]	Normal Force [kN]	Normal / Cutting Force	Cutting Force [kN]	Side Force [kN]	Normal Force [kN]	Normal / Cutting Force
10 mm	Average	5,36	2,03	12,51	2,34	4,75	1,84	10,07	2,12
	Stdv	0,33	0,61	0,98	0,13	0,26	0,37	0,52	0,11
20 mm	Average	7,18	8,05	15,34	2,14	7,35	8,57	14,83	2,02
	Stdv	0,65	1,13	1,42	0,09	0,70	1,64	1,30	0,08
30 mm	Average	6,53	6,38	13,49	2,07	5,84	6,23	11,43	1,96
	Stdv	0,50	0,91	1,31	0,19	0,56	1,16	1,38	0,09
40 mm	Average	6,32	6,59	13,36	2,11	6,01	5,80	11,55	1,92
	Stdv	0,44	1,27	1,20	0,12	0,45	0,76	1,10	0,08

Table 8-3: Comparison of average forces and standard deviation for cutting four consecutive layers of irradiated and untreated moist sandstone.

Side- and normal forces show a very similar behaviour throughout all measurements. In most cases the difference in measured forces lies within the standard deviation for the measurements. A slight increase in all three forces in irradiated and untreated areas is observed for layer 2 decreasing to a static level in layers 3 and 4.

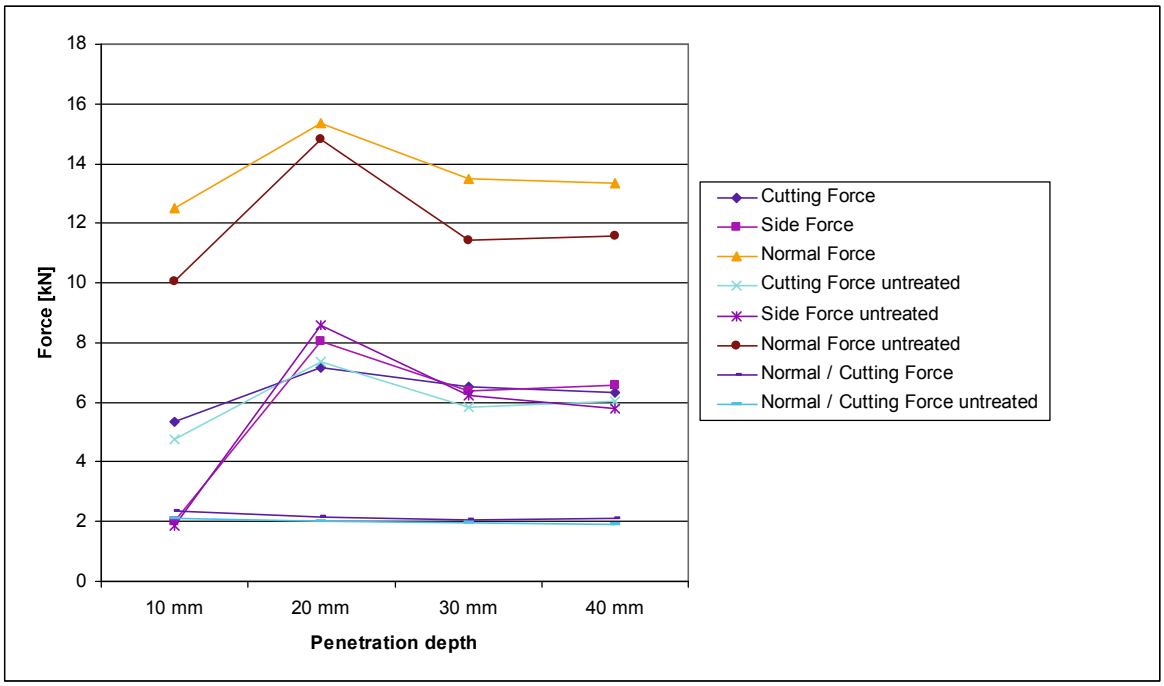

Figure 8-8: Comparison of measured forces [kN] as function of the penetration depth (Layer 10 -50 mm) for moist sandstone irradiated with 25 kW and a moving speed of 6 mm/s.

8.3 Cutting tests of granite

A description of the irradiation of large granite samples with rough surfaces is provided in 7.3.3. Also for these samples the arcing effects caused a major problem. The sample was moved underneath the waveguide with a speed of 4 mm/s. Maximum temperature reached 190 °C. The basic irradiation pattern is displayed in Figure 8-9. Cutting tests were performed with a Diamond pick, a moving speed of 1.5 m/s, spacing of 20 mm and a penetration depth of 10 mm. A total of 25 cutting lines could be tested in the uppermost layer and 24 in the 2nd layer equalling a penetration depth of 20 mm.

The average values of measured forces are shown in Table 8-4. It is shown that average cutting force in irradiated areas is 6.10 kN in the first layer compared to 6.59 in the 2nd layer. In both layers the forces in untreated areas are in the same level with 6.18 and 6.32 kN in first and second layer, respectively. Other forces show a similar behaviour of only little change between the layers and from irradiated to untreated areas. Side force changes from 6.4 to 6.6 kN in depth and to 6.63 and 6.49 in untreated areas and normal force changes from 13.17 to 14.73 in depth and from 13.31 to 14.23 in untreated areas. Standard deviation for all values lies in the range of 0.47 to 2.09 compensating for all described changes and variations.

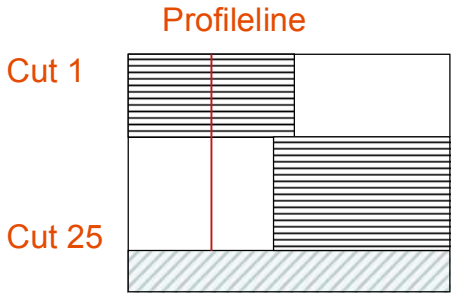

Figure 8-9: Arrangement of irradiated areas (dashed) on granite. White areas were not irradiated, green dashed areas neither irradiated nor tested.

Layer		Irradiated Area				Untreated Area			
		Cutting Force [kN]	Side Force [kN]	Normal Force [kN]	Normal / Cutting Force	Cutting Force [kN]	Side Force [kN]	Normal Force [kN]	Normal / Cutting Force
10 mm	Average	6,10	6,40	13,17	2,16	6,18	6,63	13,31	2,20
	Stdv	0,82	1,35	1,83	0,11	1,17	1,32	2,09	0,43
20 mm	Average	6,59	6,60	14,73	2,24	6,32	6,49	14,23	2,25
	Stdv	0,47	1,07	1,09	0,13	0,49	1,10	1,58	0,20

Table 8-4: Comparison of average forces and standard deviation for cutting two levels of irradiated and untreated granite.

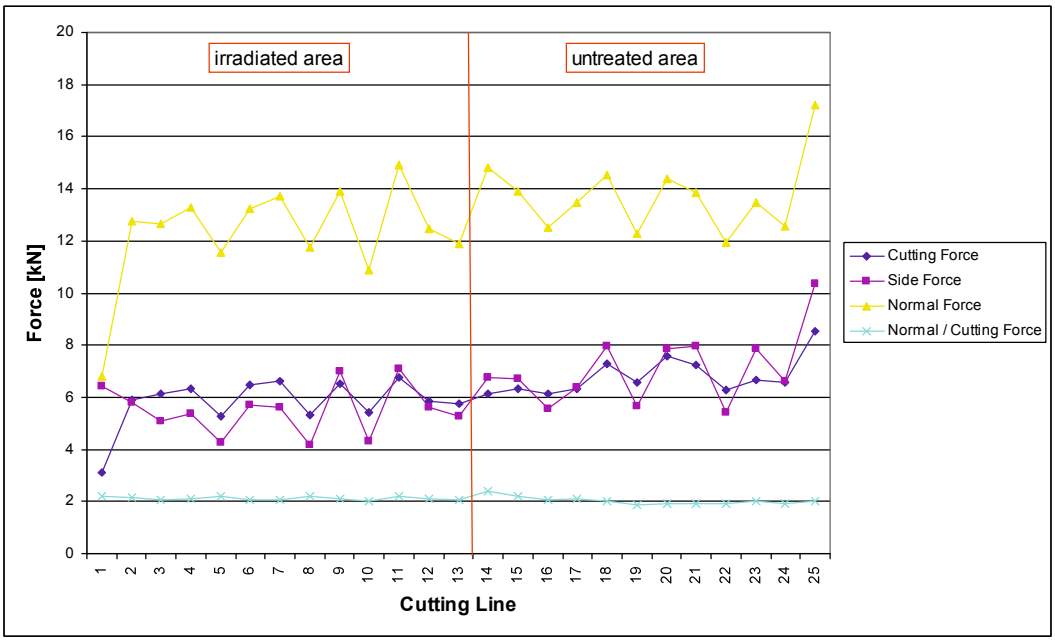

Figure 8-10: Profile along line from Figure 8-9. Average values of all three measured forces are plotted for each cutting line. Left of red line - Irradiated area; right of red line – untreated area.

9 Summary of testwork

The previous chapters deal with experimental investigations on the irradiation of different rock types with microwave energy. Two basic experimental setups were investigated.

Small-scale experiments were performed with a standard 3.2 kW microwave oven operating at 2.45 GHz as also used in households or gastronomy (chapter 5). Here more than 300 rock samples of 11 sample locations and different rock types ranging from basalt to diabase and gabbro were tested. Samples of 50 mm in length and diameter have been irradiated under different conditions and an assessment of the inferred damage and consequences for the texture of the investigated rock types was performed. As will be shown in the following chapter basic conclusions on the influence of the sample geometry and the mineralogy on the heating behavior of different rock types can be drawn from these experiments.

Chapter 7 deals with *large-scale* experiments with a 30 kW microwave source. An apparatus was designed and built fulfilling the needs of handling large samples, decreasing irradiation time by applying large amounts of power, increasing intergranular stresses by this high amount of applied power, providing the possibility of pulsed irradiation and providing a setup that closely resembles a realistic mining environment in terms of sample size, sample conditioning and geometry of the application. It is demonstrated how the 10-fold increased power and increased specific power due to changed geometrical conditions of the irradiation apparatus influence the irradiation characteristics and induced modifications of all investigated rock types in comparison to small-scale experiments.

A key task of the underlying project was the evaluation of the influence of microwave irradiation of selected rock types on the cutting performance of mechanical excavation tools. This evaluation was performed with a cutting test-rig where the forces acting on a cutting pick were measured and a comparison could be made between cutting a beforehand irradiated and cutting an untreated part of rock (see also chapter 8).

This chapter will provide an overview of the experimental results described in course of this thesis.

9.1 Basalt

Irradiation of basalt from the quarry of Weitendorf was best investigated in course of this study. Detailed results of the irradiation of Weitendorf basalt can be found in chapters

6.1.1 and 7.1. The rock heats reasonably fast in both test setups. With an applied power of 3.2 kW temperatures of up to 450 °C of surface temperature could be achieved after 120 s of irradiation. This strong increase in surface temperature is coinciding with a significant decrease in p-wave velocity being the major indicator of damage used in this study. After 120 s of irradiation a remaining p-wave velocity of 60 % of the initial velocity can be reported. It is shown in Figure 9-1 how cracks develop (a) at the surface and (b) in the interior of a basalt sample as result of microwave irradiation. Cracks are strongly governed by the geometrical conditions of the sample. This conclusion is supported by their direction in the sample and backed-up by observation on the thin sections where mineralogical boundaries do not influence the crack growth which is therefore not aligned on grain boundaries.

The irradiation of Weitendorf basalt on a large scale and with 25 kW leads to comparably rapid heating of the surface up to 500 °C after 50 s of irradiation. First spallation effects at the irradiated surface can be observed after only 6 s of irradiation with surface temperatures as high as 270 °C. Although some cracks are formed at the surface of the sample the majority of cracks is aligned in a semicircle beneath the centre of irradiation and spallation. Figure 9-2 shows the development of (a) spallation at the surface and (b) coinciding semi-circled cracks beneath the surface which obviously follow the main surface structures and direction of spallation and are not governed by or aligned to grain boundaries.

It is known from small-scale tests that a strong temperature difference develops between centre and rim of irradiated basalt samples. It was shown in chapter 2 that this difference can be as high as 200 °C after 60 s of irradiation. Considering the fact that power of 25 kW is applied to an area of only 43*86 mm², resulting in a very high power density, in the large-scale experiments leads to the conclusion that temperature gradients beneath the surface may be much larger than in the small-scale case. The observation of spallation after 6 s of irradiation with 25 kW is a further evidence for extremely large temperature gradients in the first 20 mm below the surface of the basalt sample, resulting in the described effect. For both energy levels (3.2 kW and 25 kW) very high gradients develop across the entire sample, or distances exceeding the grain size significantly. Small-scaled temperature gradients leading to the development of cracks along grain boundaries could not be observed for any basalt sample and testing procedure.

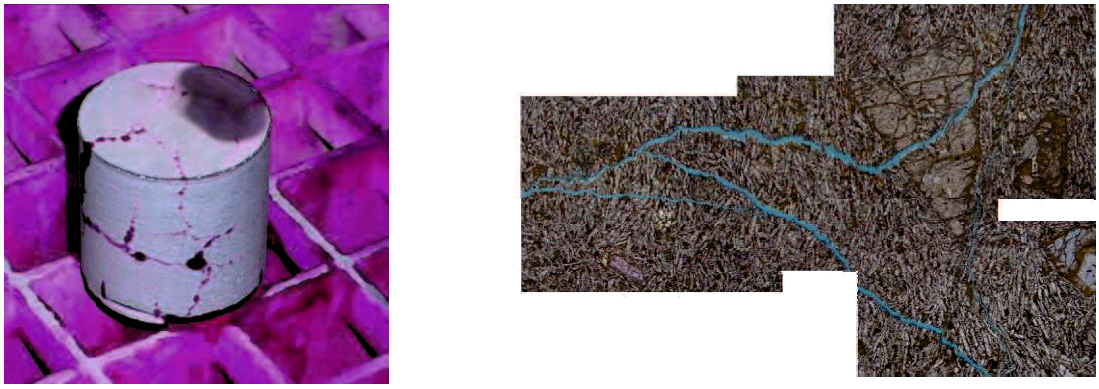

(a) (b)

Figure 9-1: Crack network at surface (left) and thin section of basalt sample (right) after 60 s of microwave irradiation with 3.2 kW.

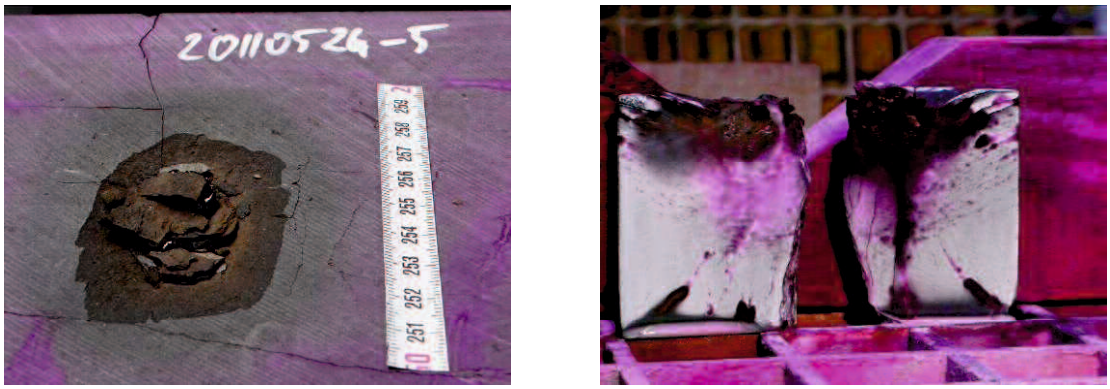

(a) (b)

Figure 9-2: Spallation at the surface of Weitendorf basalt after irradiation for 50 s with 25 kW (left) and cut through centre of the irradiated area (right) revealing a network of cracks aligned in a semicircle below the irradiated area.

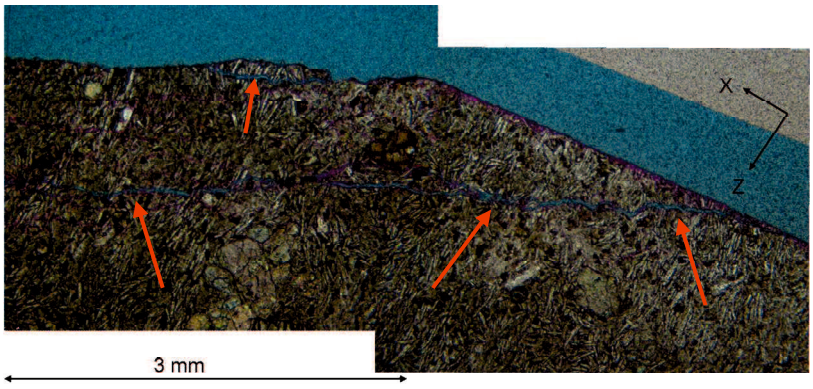

Figure 9-3: Thin section of basalt sample after 6 s of irradiation with 25 kW. Cracks beneath the surface are aligned parallel to major structures (surface and area of spallation) and cross cut grains and grain boundaries.

9.2 Sandstone

Small-scale laboratory tests of Imberg sandstone have been performed by Peinsitt (2009 and 2010). These studies demonstrated that dried sandstone is hardly affected by microwave irradiation with 3.2 kW. The maximum temperature was as high as 205 °C after 300 s of irradiation coinciding with an only minimal reduction in p-wave velocity of 300 m/s representing a reduction of 7 %. This only limited reduction in p-wave velocity indicates that microwave irradiation of dried sandstone leads to only limited cracking and destruction. In addition no macroscopical signs of damage are reported in these studies.

In contrary to small-scale tests the high amount of energy provided in large-scale tests performed in course of this study leads to stronger heating and the formation of cracks in dried sandstone samples. Surface temperature reached 300 °C after 13 s of irradiation. It is shown in Figure 9-4-a how radial cracks develop at the surface of a dried sandstone sample after irradiation for 10 and 13 s with 25 kW. Figure 9-4-b shows the thin section of a spot of this same sample demonstrating that cracks are aligned to grain boundaries indicating the presence of strong temperature gradients as well as stresses at the interfaces of the constituents of the rock.

Water saturated sandstone samples heated much faster during the tests described in literature (Peinsitt 2009; Peinsitt et al. 2010). This lead to explosive disintegration after 28 – 31 s of irradiation. A maximum temperature of approximately 130 °C was reported after 30 s of irradiation of saturated sandstone samples.

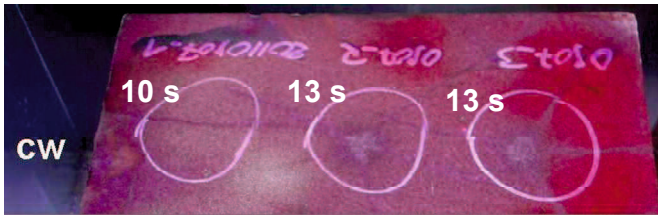

(a)

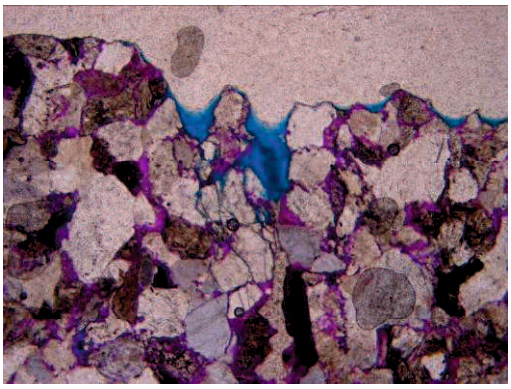

(b)

Figure 9-4: (a) Dried sandstone sample after irradiation with continuous microwaves with 25 kW for 10, 13 and 13 s – left to right field. Formation of radial cracks after irradiation times longer than 10 s of cw. (b) Resin saturated thin section of dried sandstone after 10 s of irradiation with 25 kW – beginning of deeper going crack, aligned to grain boundaries. Width of picture = 3 mm.

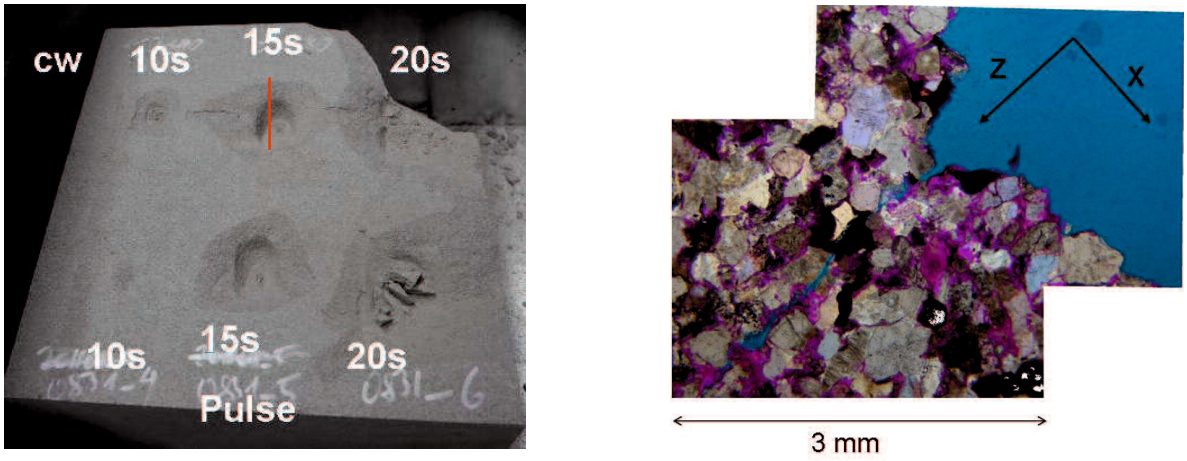

(a) (b)

Figure 9-5: (a) Moist sandstone after irradiation with continuous and pulsed waves for 10, 15 and 20 s with 25 kW. Red line indicating position of the thin section perpendicular to surface. (b) Thin section perpendicular to axis of crater after 15 s of irradiation with 25 kW with deeper going crack.

Explosive behaviour of saturated sandstone samples can also be observed in large-scale tests with an applied power of 25 kW. In strong analogy to the results described by Peinsitt (2009) and Peinsitt et al. (2010) craters of 24 mm burst out after short irradiation time of 10 – 20 s of naturally moist sandstone samples. After 20 s a corner of approximately 20*20*10 cm³ is breaking off (Figure 9-5-a; upper right part). The formation of cracks and the newly formed surface is governed by the boundaries of existing grains. It is shown in Figure 9-5-b how the blue resin aligns itself along these grain boundaries. One deeper going crack is oriented perpendicular to the initial surface originating in the centre of the spalled area.

The orientation of cracks along grain boundaries in moist sandstone samples stands in strong analogy their dried counterparts. In both small- and large-scale tests moist sandstone samples disintegrate explosively whereas the dry counterparts behave far less spectacular. No information about cracking is available for small-scale tests on sandstone. However, in large-scale tests cracks are always aligned to grain boundaries irrespective of the moisture content and nature of disintegration.

9.3 Granite

Small-scale laboratory test of Neuhaus granite have been performed by Peinsitt (2009 and 2010). A maximum temperature of 230 °C after 300 s of microwave irradiation with 3.2 kW is reported. This increase in temperature coincides with a decrease in p-wave velocity of approximately 1000 m/s after 300 s of irradiation. Advanced damage is

reported for water saturated granite samples with a p-wave velocity reduced by 1300 m/s after 300 s of microwave irradiation.

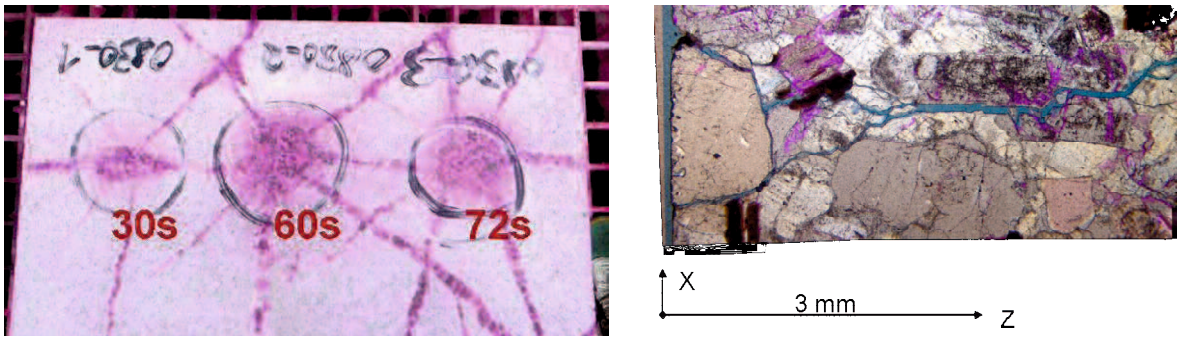

(a) (b)

Figure 9-6: (a) Granite sample after 30, 60 and 72 s of microwave irradiation with 25 kW (left to right). Intense cracking originating in a hot spot beneath the waveguide. Cracks originated in the second (60 s) and third (72 s) irradiation, respectively, cross those generated previously. (b) Vertical crack (blue) aligned to grain boundaries.

High-power irradiation of this rock types (chapter 7.3) leads to fast heating and a maximum temperature of 374 °C after 72 s of irradiation. First radial cracks develop after 30 s of irradiation with an increase in crack density and width of fractures after longer irradiation times (Figure 9-6). The cracks have a clear geometric alignment with an angle of approximately 45° to each other which could be regarded as sign of the influence of the general setup and geometry of the application. On the other hand cracks follow grain boundaries and also mineralogical cleavage planes. This fact can be interpreted as an indication of the existence of either sufficient temperature gradients or at least tension between the single grains of the investigated samples.

Concluding it can be said that damage qualitatively increases with increasing input power and increasing irradiation time. Large signs of obvious damage could not be initiated and observed in small-scale tests but are an eye-catching result of large-scale microwave irradiation and investigations.

9.4 Gabbro

Small-scale irradiation of gabbro leads to similar results as also described for basalt. Heating is relatively good with surface temperatures reaching 390 °C after 90 s of microwave irradiation with 3.2 kW reducing the initial sound velocity of 6200 m/s by 35 % to 4000 m/s. In similarity to Weitendorf basalt melting and subsequent complete

disintegration and shattering of specimen may occur after longer irradiation times. Cracks are aligned in circumferential and radial direction.

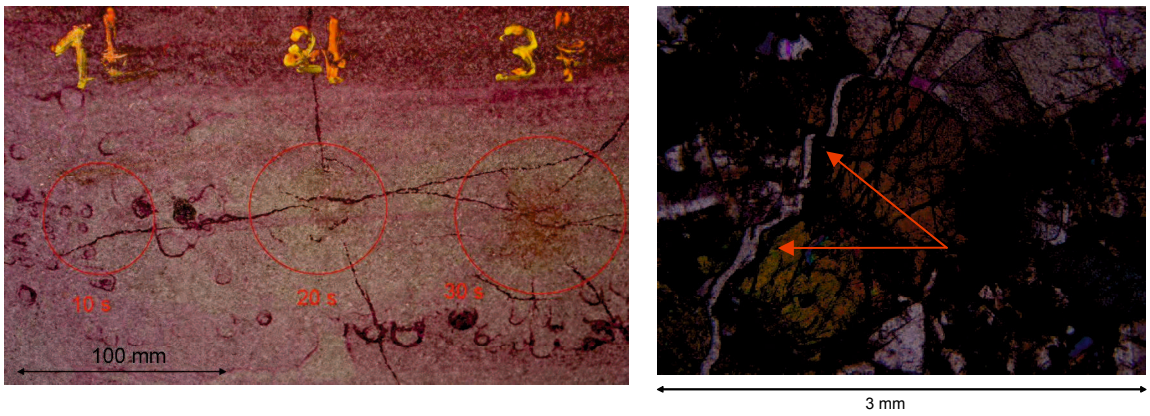

(a) (b)

Figure 9-7: (a) surface of gabbro sample after irradiation for 10, 20 and 30 s left to right and (b) thin section of spot 3 after 30 s of irradiation. Position of crack along grain boundaries are indicated by red arrows.

With high-power microwave irradiation of 25 kW large gabbro samples heat rapidly to 455 °C after 30 s of irradiation. Surface cracks develop after 20 or more seconds of irradiation. No network of cracks can be observed after only 10 s with a maximum surface temperature of 160 °C. Figure 9-7-a shows how cracks develop at the surface of an irradiated sample after 10, 20 and 30 s of irradiation (spot 1-3) and Figure 9-7-b shows one crack in more detail. It is shown that this specific crack is aligned along grain boundaries. Although such an orientation to grains can be reported the general crack network follows a structure that is seemingly aligned to the confining surfaces. Similar to the irradiation of basalt also the irradiation of gabbro results in a semi-circled structure of tiny cracks beneath the surface indicating strong temperature gradients at some millimetres in depth acting perpendicular to the surface (Figure 7-30).

The small-scale tests indicate excellent heating and prospective cracking of the investigated gabbro specimen. Large-scaled experiments yielded results in qualitative similarity to the irradiation of dried sandstone and granite. Small-scaled tests show analogies to the irradiation of basalt, especially with the formation of circumferential cracks and melting after longer irradiation times.

9.5 Mechanical cutting tests

A prerequisite for proper comparison of the results between single experiments is the generation of a rough “pre-cut” surface prior to the first stage of irradiation. Unfortunately this pretreatment generates sharp edges where the microwave field is enhanced and arcing or ball lightning may occur. This effect could hardly be circumvented with the given laboratory equipment and thus irradiation parameters had to be adapted to preventing these side effects. Shorter irradiation times equaling faster moving speed of the samples beneath the waveguide could minimize the likelihood of these side effects but, however, also decreased the applied amount of energy brought into the sample. Although microwave irradiation of single spots on smooth surfaces showed that cracking can be initiated in all investigated rock types no obvious signs of damage, especially no large cracks, could be monitored after tests on the rough surface and after comparably shorter irradiation time.

None of the investigated samples showed a distinctive reduction of measured forces as result of microwave irradiation. It is shown in chapter 8 that a change in measured forces can be observed between irradiated and untreated areas. Scattering and standard deviation of measured forces are rather high, being in the order of measured changes, and compensating for most observed differences between irradiated and untreated areas. Only some single measurements indicate significant reduction in forces acting on the tool after microwave irradiation of the rock whereas others show no reaction to microwave treatment.

An example is provided in Figure 9-8. Lines 13 and 14 show two neighbouring cutting lines in the uppermost layer of dried sandstone. The general pattern for both lines are completely different. Whereas in line 13 a trend towards lower forces in the irradiated area (red hatching) is obvious this observation is not supported by line 14 where such a trend is not shown. In contrary to Line 13 the forces rather seem to increase in the irradiated area. Thus a statistically backed up statement of the influence of microwave irradiation on the cutting process cannot be made. However, it has to be pointed out that both, the existence of large cracks dividing large samples in two halves after irradiation or during the cutting process (Figure 7-13) and single cutting lines with significantly decreased forces are major indicators for the possibility of sustainable damage induced by microwave irradiation in all investigated rock types.

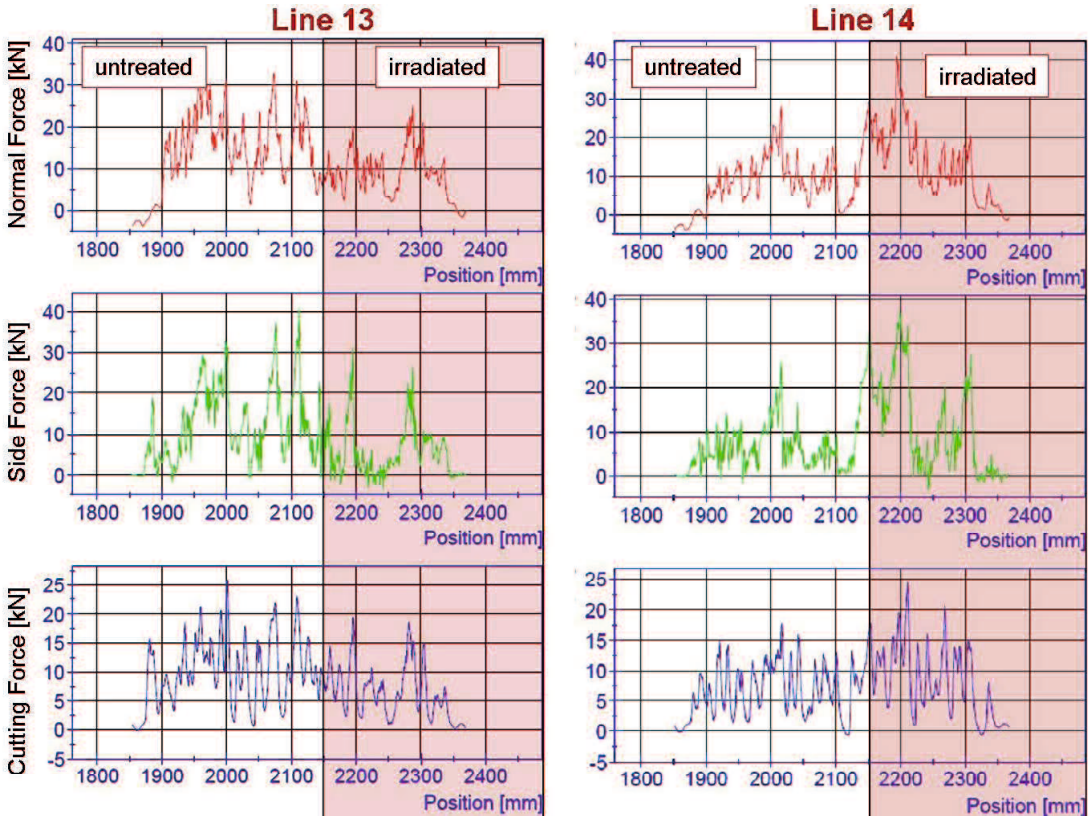

Figure 9-8: Comparison of two neighbouring cutting lines in dry sandstone, layer 1, and the allocation of irradiated (red hatching) and untreated (white) areas. Although both lines are from the same area cutting lines show completely different features.

9.6 Experimental side effects

It could be shown in small-scale experiments that the electromagnetic field enhances at sharp edges represented by a steel cone. Damage and melting of samples was observed in the vicinity of the contact of the steel cone to the rock samples. However, under certain circumstances the enhanced microwave field lead to ionization of the surrounding air and the formation of fire balls or ball-lightning. A similar behaviour was observed during high-power microwave irradiation. Especially when rough surfaces were irradiated the microwave field was strongest at sharp edges and corners formed by the preparational cuts of the surface itself leading to the described arcing effects. It is shown in the end of chapter 6 how the enhancement of the electromagnetic field and ball-lightning was controlled and utilized in small-scale tests. This kind of beneficiation was not maintainable in large-scale tests. The possible focuses in form of irregularities of the surface were randomly distributed and arcing effects could therefore not be concentrated at certain spots. The resulting lightning arcs follow the strong microwave field inside the waveguide towards the magnetron leading to an automatic shut-down of the system

.

10 Analysis of results and discussion

10.1 Experimental results and qualitative assessment of microwave rock interaction

The primary effect of interest was the reduction of a rocks' strength as response to microwave irradiation. In **small-scale experiments** this effect was measured by the travelling time of sound waves through small cylindrical samples. Figure 10-1 shows the relative p-wave velocity of various rock types as function of the irradiation time with a 3.2 kW multimode microwave. The relative p-wave velocity v_r is calculated as the relation between initial p-wave velocity before irradiation (v_o) and the measured velocity after irradiation (v_t) and can be expressed as follows.

$$v_r = \frac{v_t}{v_0} \text{ [\%]} \qquad \textbf{10-1}$$

A value of 100 % represents no change in p-wave velocity as function of microwave irradiation whereas values of 50 and 30 represent 50 % and 30 % remaining p-wave velocity, respectively. For reasons of simplification the remaining p-wave velocity will also be called remaining strength, representing indirectly the strength of a rock after microwave irradiation. Three large groups of rocks with different response to microwave irradiation can be identified in this figure: Group (I) is not affected by microwave irradiation, shows no decrease in relative strength; group (II) is only slightly affected by microwave irradiation and group (III) is strongly affected by microwave irradiation, represented by a strong decrease in relative p-wave velocity.

Group (I) is represented by granite and (dry) sandstone. These two rock types are mainly composed of minerals like quartz and feldspar being comparably transparent to microwave irradiation. This is also represented by very slow heating to only approximately 250 °C after 300 s of irradiation for both kinds of rock (Peinsitt et al. 2010). As shown in Figure 10-1 this slow increase in temperature leads to nearly no reduction in p-wave velocity and a remaining strength of above 95 % for both kinds of rock even after 300 s of irradiation.

Group (II) is represented by a sulphidic copper ore from Somincor. Heating to 370 °C after 240 s of irradiation coincides with a slight decrease in p-wave velocity from 6000 to 5100 m/s. This decrease in velocity represents a remaining strength of 82 % after 240 s of irradiation.

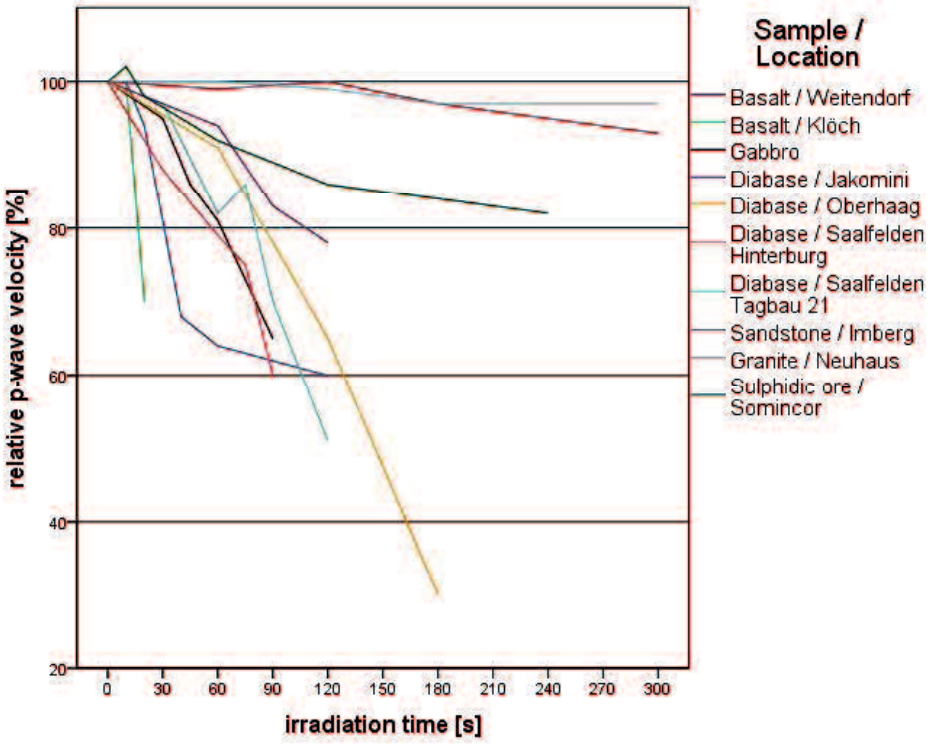

Figure 10-1: P-wave velocity relative to initial value as function of irradiation time [s] after irradiation with 3.2 kW in a multimode cavity. Data for sandstone and granite taken from Peinsitt (2009).

Group (III) is represented by the wide spectrum of rocks subsumed as greenstones (basalt, diabase and gabbro). In Figure 10-1 it is represented by a group of 8 lines with significant and steep decrease in v_r as function of the irradiation time. However, it is also obvious from this graph that different greenstones respond differently to the applied radiation. Klöch basalt (green) shows a very steep decrease of v_r after short irradiation time and explodes after 23 s of irradiation. Weitendorf basalt (blue) shows a steep decrease in the beginning with a flattening curve after 60 s of irradiation. Melting and coinciding shattering are observed after 240 s and would lead to a remaining strength of 0 % but this cannot be displayed in this graph. Investigated diabases (violet, yellow, red) show nearly linear decrease towards a total loss of remaining strength as result of microwave irradiation.

Rocks of groups (I) and (III) were also investigated during **large-scale experiments**. Although no quantification of the inferred damage can be provided the qualitative trend is similar. Large-grained rocks with relatively weak microwave absorption properties (sandstone and granite) heat comparably slowly as a result of microwave irradiation with 25 kW resulting in radial cracking whereas fine-grained good absorbers in basalt heat rapidly resulting in spallation at the surface.

The presence of water plays a major role in microwave heating of hard rocks. Mineralogical and chemical investigations of the rocks subsumed under group (III) show significant differences in mineralogically bound as well as free water compared to untreated samples as a result of microwave irradiation. Even small amounts of water in the untreated sample act as focus for microwave energy, heating up strongly when power is applied. The resulting vapour pressure in the porous volume of the rock can exceed the strength of the irradiated rock and lead to the shattering of the irradiated sample. It is shown for Klöch basalt that samples explode after only 23 s of irradiation. The microwave irradiation coincides with a reduction of Loss On Ignition (LOI) and loss on drying from 3.36 to 2.86 wt.% and 1.6 to 0.8 wt.%, respectively, as well as a change in mineralogical composition from the clay mineral montmorillonite which is a major phase in the untreated samples to illite, another clay mineral, which is abundant in irradiated samples. Although no explosive behaviour can be reported for Weitendorf basalt a very similar chemical behaviour can be reported. Irradiation with microwaves leads to a significant reduction of both LOI and loss on drying (1.59 to 0.84 wt.% and 1.22 to 0.28 wt.%; Table 6-2). A clear reduction in the amount of montmorillonite in favour of illite can also be reported after 120 s of irradiation for samples from Weitendorf. A second heating of the same samples shows that the temperature does not rise above a certain limit in this second experiment (Figure 6-15). The temperature reached in the subsequent heating cycle equals the temperature reached after 60 s of irradiation in the first heating cycle. A similar behaviour is also observed for other rock types. Oberhaag diabase reaches this limit after 120 s of irradiation, Saalfelden diabase after 75 s and gabbro after 60 s of irradiation. It is concluded that the water content acting as focus of microwave irradiation and strong heating in the initial experiments is missing in the subsequent experiments leading to the described observations. With the absence of water the heating of the samples is solely controlled by the mineralogical composition of the rock and is obviously not comparably strong.

Also sandstone, which falls into group (I) is significantly influenced by the presence of water in its porous volume. Water saturated sandstone samples heated much faster than dried ones during tests described in literature (Peinsitt et al. 2010). This leads to explosive disintegration after 28 – 31 s of irradiation with 3.2 kW. Explosive behaviour of saturated sandstone samples can also be observed in large-scale experiments with an applied power of 25 kW. Craters of up to 24 mm in depth burst out after short irradiation time of 10 – 20 s.

In both cases the phase transformation of water at a temperature of 100 °C is believed to play a major role in the process. The volume ratio of liquid and gaseous water is about 1:1000. Vaporization leads to a vapour with increased pressure in the pores. If the stress

generated in the surrounding material exceeds the rock strength it leads to the failure of the rock.

It is obvious from the described experimental results that a different behaviour exists between large- and small-scaled irradiation. The geometry of the sample and the way of irradiation (multimode from all sides vs. beneath the waveguide) as well as the mineralogy play a major role in the response of the investigated rock types to microwave irradiation. The basic characteristics of the investigated rock types are summarized in Table 10-1. It is shown how the rocks react to different irradiation parameters. Basic conclusions are drawn from experimental results trying to explain the effects of microwave-rock interaction for each rock type.

Rock Type	Characteristics	Small-Scale	Large-Scale	Conclusions
Basalt and Diabase (Greenstones)	Fine – medium grained matrix, good absorbers	Cracking & Complete destruction (melting)	Spallation Breaking at preexisting cracks	Strong temperature gradients in sample mass, no influence of grain boundaries
Granite	Medium – coarse grained plutonite, mostly weak absorbers	No influence of irradiation observable	Radial cracking at irradiation spot	Slow heating, cracks at grain boundaries
Sandstone	Medium grained sediment, weak absorbers, except with water content	Explosive with water	Explosive with water	Incorporated water favourable for damage
		No effect observable when dry	Radial cracking without water	Slow heating when dry, cracks mostly at grain boundaries
Gabbro	Medium - coarse grained plutonic rock	Cracking & Complete destruction (melting)	Radial cracking at irradiation spot	Rapid heating, cracks at grain boundaries

Table 10-1: Characteristics of investigated rock types. Basic results of microwave irradiation on small-scale and large-scale and conclusions about the cracking mechanisms. Colours indicate a strong (green) and weak (red) response in terms of heating and damage.

Amongst the investigated rock types basalt, diabase and gabbro have the highest imaginary part of the permittivity guaranteeing for excellent coupling of microwave and rock. Typical κ”-values provided in literature (e.g. Santamarina 1989) for basalt range from 0.08 to 0.8 being equivalent to a penetration depth between 74 and 5 cm. It is shown in all investigations that these rocks heat comparably well and that damage occurs in all investigated samples after a certain irradiation time. In our small-scale experiments after short irradiation times a first set of circumferential and radial cracks develops in fully irradiated cylindrical samples. Similar behavior is also reported in literature sources for the irradiation of different rock types with similar dielectric and mineralogical properties but with different sample geometries (ø:h varying between 0.5 and 2; Hassani et al. 2012).

After much longer irradiation times samples break apart at the described major axial cracks (Figure 10-2).

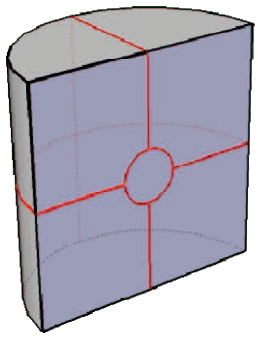

Figure 10-2: Schematic crack pattern of small-scale experiments. Hot spot in the centre of the sample resulting in radial and axial cracking. Cracks and hot spot displayed in red.

It is demonstrated in simulations performed at the Institute of Mechanics of the University of Leoben (Antretter, Leindl 2011, Hartlieb et al. 2012, chapter 5.2.7) how heating of cylindrical basalt samples leads to the formation of temperature gradients and stresses inside the samples. They postulate that the heat conduction and radiation off the surface lead to the cooling of the rims whereas thermal conduction in the interior cannot compensate for this loss. The result is a higher temperature in the centre which can even result in a run-away effect due to enhanced imaginary part of the permittivity (κ") as result of the increased temperature and subsequently increased temperature gradients as function of the heating time. Figure 10-3 shows the stress fields after 60 s of heating for such an arrangement. The tensile stress exceeds the given tensile strength of 6 MPa at several points which is assumed to lead to the crack pattern observed in the experiments.

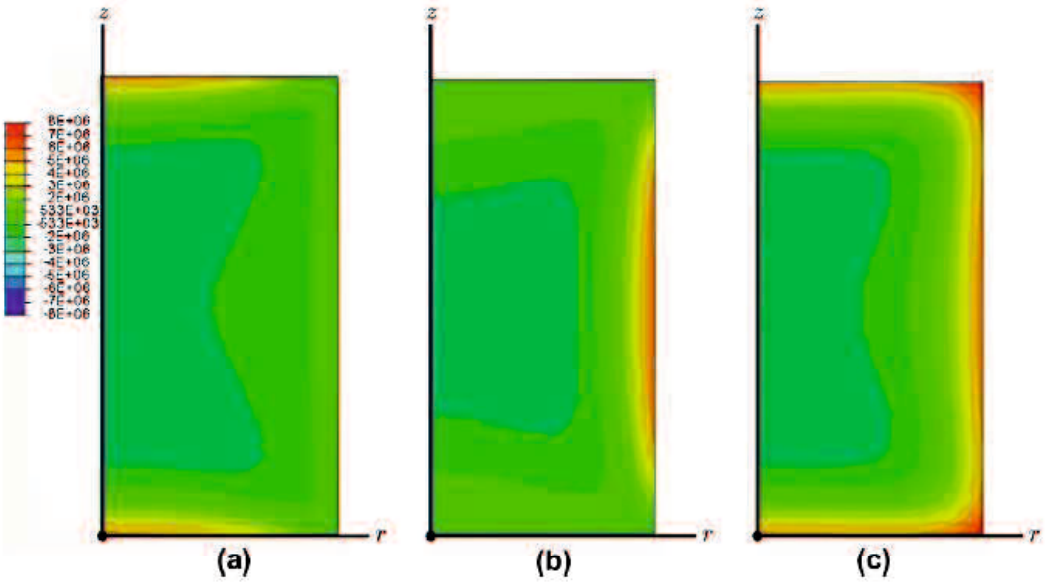

Figure 10-3: Simulation of the components of the stress tensor in Pa after 60 s of homogeneous heat input with 3.2 kW of cylindrical basalt samples. R = 25 mm, h = 50 mm. (a) radial stress σ_r, (b) axial stress σ_z and (c) circumferential stress σ_φ. Positive sign = tensile stress; negative sign = compressive stress. From Hartlieb et al. (2012). In the red regions the tensile strength of basalt (6 MPa) is exceeded.

Combining the effects of heating of abundant water and increased microwave absorption properties of pre-heated rocks leads to a possible damage mechanism for this kind of rock: The initial rise of temperature is governed by heating and simultaneous removal of occurring water. Similar effects are also reported by Marcos and Rodriguez (2011) who demonstrated the removal of water and coinciding expansion when irradiating vermiculites with microwave energy. Heat conduction leads to a homogeneous distribution of temperature in the entire sample. As demonstrated by Pickles (2004) the removal of water of limonitic ores leads to an increase of both κ' and κ" as result of the de-hydroxylation of goethite. The same effect is assumed to lead to strong initial heating of the investigated basalt. Subsequently the permittivity which is increased due to the high temperature causes fast heating of the water free rock constituents. The surface is cooled by air but thermal conduction in the centre is not fast enough to remove all the heat leading to increased temperature in the centre and again an increase of the permittivity there. Heating and subsequently the formation of melt most likely causes an increase of volume in the center and subsequent shattering of the cylindrical samples. Heating causes an increase in thermal expansion coefficient (α) from approximately 7 to 16 [10^{-6}/K] when heating basalt from 25 to 200 °C (Pohl 1982) possibly leading to volumetric expansion of the centre and thus initiation of cracking as function of microwave irradiation.

In the absence of water the described initial temperature rise as result of the heating of water does not take place and thus the permittivity does not increase to a threshold necessary for efficient heating of the remaining rock constituents.

Vorster et al. (2001) describe how microwave processing of Neves Corvo copper ore results in a reduction of work index by 70 % after microwave exposure for 90 s. The very same ore was also investigated during this study. Results fall into group (II) with only limited reduction of p-wave velocity as function of microwave irradiation. The difference in sample size is obvious. Whereas Vorster et al. treated bulk powder samples with a particle size of 80 % < 6.5 µm results in this study where obtained by irradiating cylinders of 50 mm. Although microwave absorption properties of the sulphidic components of the ore are rather good absorbers the penetration depth of microwaves is limited to a thin layer beneath the surface. Fine grained lumps will therefore provide more irradiable surface and result in better absorption whereas large samples can only provide limited specific surface resulting in weaker absorption and no significant heating and damage.

Large-scaled samples have been irradiated at one specific spot of the surface. In contrast to small-scale experiments only parts of the rock could be treated with this setup leaving large areas untreated and thus cool. Figure 10-4 shows that large areas of the sample surface and interior remain unaffected by irradiation. It is shown by numerical simulations how the electric field of the electromagnetic wave propagates through a rock sample. The maximum of the intensity is observed directly at the front of the waveguide at about -1 cm. The highest intensity inside the simulated basaltic rock mass can be observed between the surface and about 8 cm in the rock itself. The lateral extension is in about 5 cm around the centre of irradiation and decreasing towards depth.

Figure 10-5-a,b,c show two principal failure modes and an intermediate structure achieved with this experimental setup. The range of possible damage spreads from explosive spallation at the surface after only short irradiation time with no further cracking of the rock mass to radial cracking originating in a hot spot at the centre of irradiation and a combination of the two types.

Spallation can be observed after only 6 s when the strong temperature gradients in a depth of 2-3 cm beneath the surface develop in very short time. It is only possible due to heating being faster than the thermal conduction equalling out the strong initial temperature gradients.

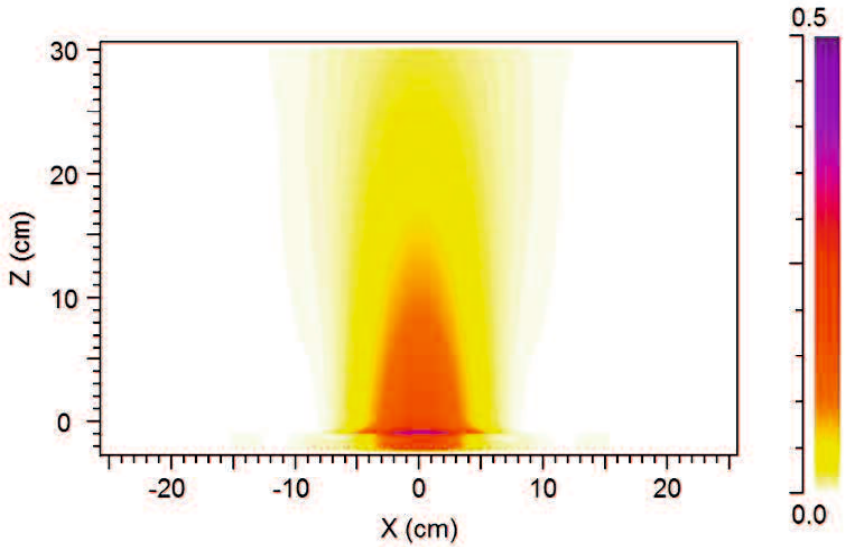

Figure 10-4: 2-dimensional model of wave propagation shown as distribution of E_y^2 , proportional to the intensity, in the block and in front of it. κ_r = 7.4 , κ_i = 0.3 (average values for basalt at 2.45 GHz). The microwave source is at Z= -1 cm and radiates in positive Z direction only. Intensity reflected from the rock can penetrate the source in negative Z direction. The thickness of the rock in the direction of propagation is from Z= 0 cm to 30 cm, the width in X direction is 50 cm. The computational domain is 32 cm x 50 cm. Total-absorption conditions are applied at its boundaries. (Meisels 2012).

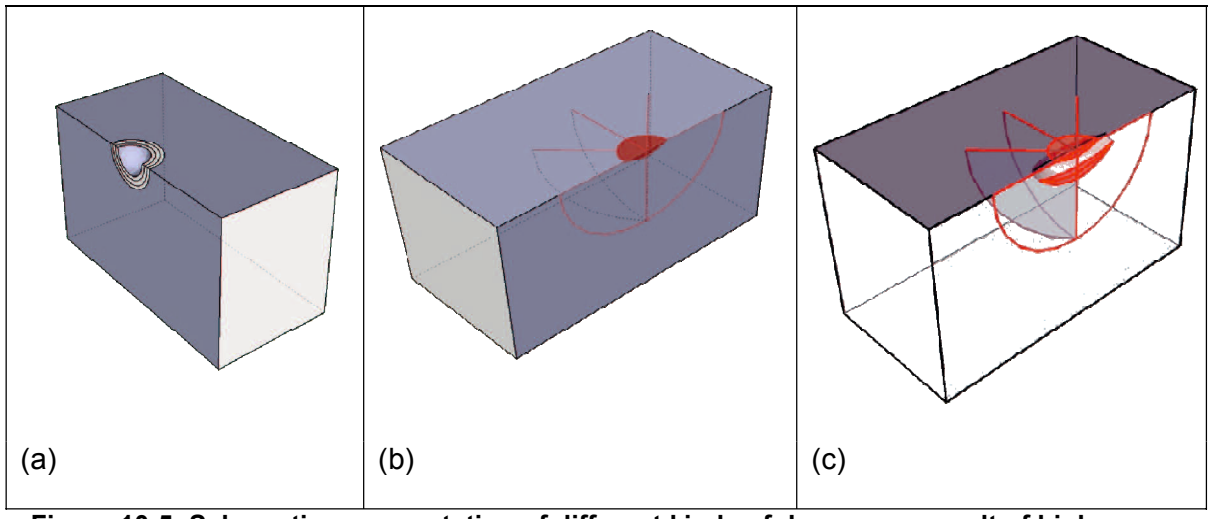

Figure 10-5: Schematic representation of different kinds of damage as result of high-power microwave irradiation experiments. (a) Spallation and hemispherical cracks as result of very fast heating; (b) Radial racking after relatively slow heating; (c) Mixture of radial cracking and beginning spallation. Cracks and hot spots highlighted in red.

Rauenzahn and Tester (1989) and the therein cited literature demonstrate that thermal spalling generally depends on two major factors: (a) the samples dimension and (b) the confining conditions. The heated area must be a small portion of the entire surface of an

unconfined specimen and the heating rate must be high enough to guarantee for a high surface temperature before a larger volume of the sample is affected by heating. This would allow for a reduction of thermal stresses in the direction of least resistance. As shown in Figure 10-6 stresses are acting on a flaw beneath the surface leading to buckling and spallation of the surface (Preston 1934 in Rauenzahn and Tester 1989). Especially fine grained basalt provides several microscopic cracks and flaws which could be activated by this mechanism.

Rauenzahn and Tester (1989) furthermore provide a spalling temperature (ΔT_s) for several rock types. This temperature depends on the compressive strength, Poissons's ratio, Young's Modulus and the linear thermal expansion coefficient of the selected rock types. According to the authors spalling can only occur at a temperature difference of at least 560, 320 and 550 °C for basalt, granite and sandstone (Table 10-2). Especially the value for basalt lies significantly above the actually measured value of 250 °C after 6 s of irradiation. The measured value would therefore not allow for a successful spallation as observed in the present experiments. However, this temperature was measured at the surface. It could already be shown in course of this thesis that the temperature at the surface does not resemble the maximum temperature which occurs at some cm in depth. It is therefore assumed, but unfortunately not measured, that the temperature beneath the surface of irradiated basalt samples lies in the range named as prerequisite for spallation. This stands in analogy to the runaway effect described earlier. Strongest heating takes place at the point of highest microwave intensity near the surface where the permittivity subsequently increases as function of the increased temperature presumably resulting in runaway effect.

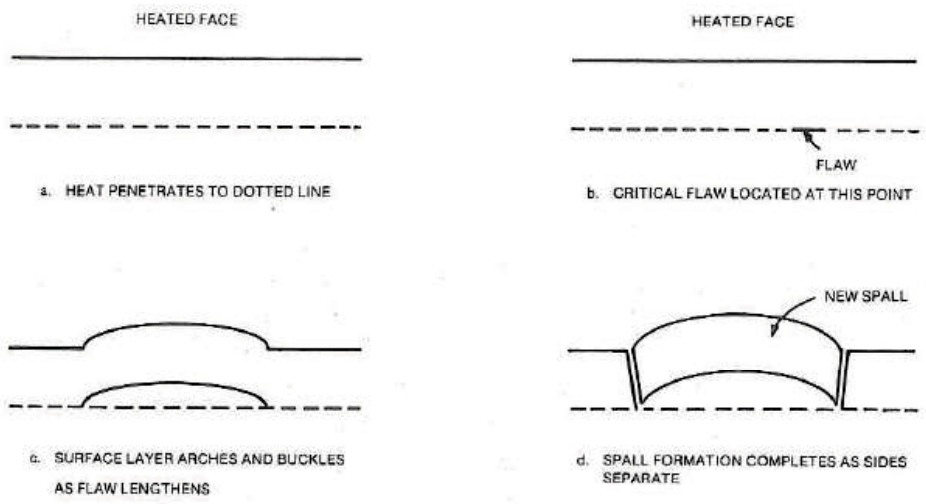

Figure 10-6: Simplyfied chain of events leading to spallation on surface (from Rauenzahn and Tester 1989).

Also granite and sandstone do not reach the desired temperature necessary for successful spallation. Secondly it takes much longer to heat these rocks to comparable temperatures (Granite: 30 s ΔT = 220 °C, Sandstone: 13 s ΔT = 280 °C). Thus both factors named as prerequisites for spallation are not met for these rock types. (a) Heating takes too long and therefore thermal stresses are allowed to smooth out and (b) the maximum temperature is too low.

Rock Type	ΔTs
Basalt	560
Granite	320
Sandstone	550

Table 10-2: Rock spall temperature (ΔT_s) after Rauenzahn and Tester (1989) for selected rock types.

Instead of spallation a hot spot is created in the area beneath the waveguide. This spot is located in the area of highest intensity of electric field (Figure 10-4) and is the centre of 8 radial cracks growing for several tens of centimetres (Figure 10-5-b). This crack pattern shows strong analogies to Hertzian contact cracks as described by Lawn (1993), Latella et al. (1997) as well as Lawn et al. (1998).

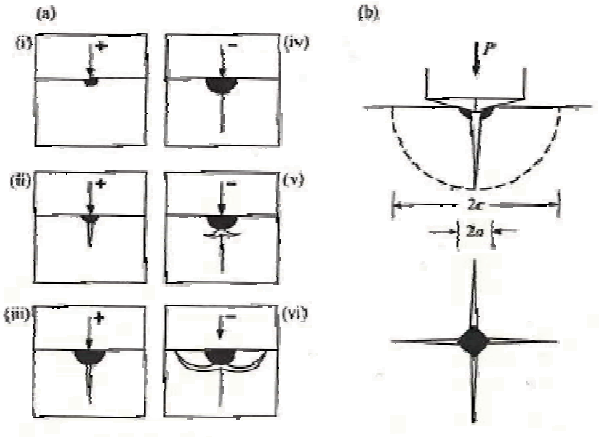

Figure 10-7: Radial-median and lateral crack systems from Lawn (1993). (a) Evolution of cracks during loading (+) and unloading (-). (b) Geometrical parameters of the system.

At the beginning of loading inelastic, irreversible damage is induced (i). At a critical load radial cracks develop at tensile median planes (ii – iv). On unloading median cracks below the surface close up and open at the surface in the residual tensile field (v). After the removal of the load both crack systems ultimately tend to form a half-pennies at the load point (Figure 10-7, Lawn 1993).

In the investigated case of microwave irradiation the heating of a distinct volume beneath the waveguide could be considered as the load case leading to the formation of the first vertical crack planes. Depending on both, thermal and dielectric properties of rocks as well as the geometry of the application, in a further step tensile stresses occur at the surface leading to the formation of the described crack pattern (see also Figure 10-5).

Similar investigations have been performed by Wagner and Schümann (1971). They investigated the influence of the pressure of an elastic stamp applied to the surface of a rock. It is also shown in Figure 10-8 that all three principal stresses are compressive directly beneath the stamp. The greatest tensile stresses occur at about a distance of one stamp diameter and decrease with depth. For this model the failure of rock would start with a tensile ring crack near the edge of the stamp. With increased stress the rock would start failing along the contour of a spherical region beneath the stamp. This failure would partly be tensile and partly compressive.

This concept gives a good explanation of the development of half-circled hemispherical cracks beneath the centre of irradiation. Nevertheless this concept does not explain the formation of so-called hot spots beneath the waveguide. Furthermore a central vertical crack, as observed in several experiments, cannot be explained.

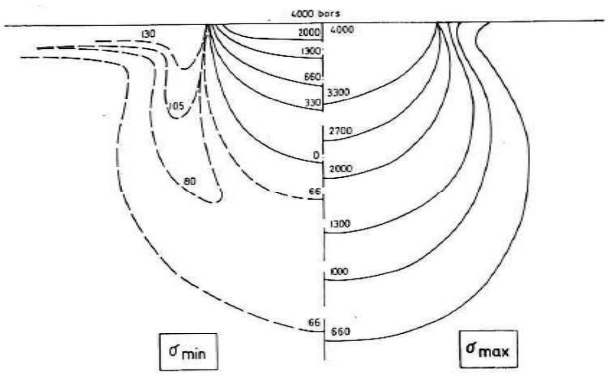

Figure 10-8: Elastic Stamp - Distribution of maximum and minimum principal stresses. ------ tension; ——— compression. From Wagner and Schümann (1971).

One of the key theories of microwave irradiation of different rock-types is the beneficiation of the different absorption characteristics of the rocks' constituents. It is highly stressed by several authors of simulations that microwave irradiation of a two-phase system of a strong absorber in a relatively fine-grained matrix leads to the generation of cracks along these the grain boundaries because of differential heating and resulting thermal stresses between the phases (e.g: Whittles 2003; Jones et al. 2005, 2007; Ali and Bradshaw 2010). Results of this study demonstrate that the occurrence of cracks is only in some

cases governed by the mineralogy and that the geometry of the application plays a greater role than the small-scaled differences in absorption properties. It is demonstrated in case of gabbro that both kinds of damage can occur (chapter 7.4, Figure 7-30, Figure 7-31 and Figure 7-32). Strong gradients directly beneath the surface, leading to spallation-like patterns, result in cracks that are crossing all grain boundaries. Additional radial cracks have a regular pattern of 8 branches originating in the centre of irradiation but are microscopically aligned along irregular grain boundaries.

A speculative answer to this problem is the strength of the occurring temperature gradient. Where the thermal stresses are strong they are even sufficient to break single grains. Where these thermal stresses are lower the presumably weakest parts of the rock (the grain boundaries) get damaged. Quite obviously the justification of these cracks in granite and sandstone as the result of selective heating is not valid because of (a) the general geometrical alignment in 8 cracks without any link to specific grains and (b) the long irradiation times of several tens of seconds which allow for thermal conduction and smoothing of temperature differences without the generation of strong gradients between single grains.

10.2 Quantification of microwave-induced rock-heating and damage

As mentioned in the previous chapters cutting tests on various rock types have been performed in order to quantify the damage induced by high-power microwave irradiation. They indicate the possibility of a reduction of mechanical cutting forces caused by microwave pre-conditioning of the investigated rock types. However the obtained results do not specifically proof the advantage of the applied technology for the rock cutting process. Scattering of the measured forces is rather large hiding for all indicated changes of the applied forces as result of microwave irradiation. It is strongly assumed that the observed cracks resulting from microwave irradiation do contribute to the damage of the rock mass but this could not be sufficiently quantified by studying the forces from mechanically cutting the damaged rock.

Besides the damage studies, the total energy consumption is one of the most important factors for the future utilization of the microwave technology for rock breakage. It was already stressed that only a tiny portion of the totally applied energy results in effective breakage of a rock when applying conventional methods. Microwave technique can hopefully contribute to a reduction of breakage energy in the entire mining process from

mine to mill. This chapter is therefore dedicated to estimate the benefits of microwave irradiation on the breakage energy of the various rock types under consideration.

As also shown in chapter 1 the crack density and the status of inter-granular joints within a rock mass influence the cutting rates as well as the specific pick consumption of roadheaders significantly (Bieniawski 1989; Vasek and Dlouhy 1978; Sandbak 1985, Restner and Gehring 2002). As shown earlier the application of microwaves leads to cracking inside the rock mass and may further on lead to a reduction of cutting forces. Several tests on different rock types have been performed in course of this study in order to investigate the differences between cutting intact rock and cutting microwave-preconditioned rocks. The results are summarized in chapter 9.5. Unfortunately the testing procedure was not suitable for measuring the small differences of applied forces which lead to results that can not be reliably interpreted. This stands in contrast to the observation of a vast amount of cracks in all rock types which should theoretically be beneficial in the cutting process. Even more interesting is the depth of the effects caused by microwave irradiation. It is of vital interest to precondition a volume that represents at least the penetration depth of the cutting tool which is of the order of a few centimetres depending on the rock type.

The described cutting tests are very elaborate. Thus this chapter tries to provide a simpler approach for the quantification of damage and the exploitation of the applied microwave energy.

Microwave energy is applied to a small volume of the entire rock mass. It was already shown in chapter 10.1 (e.g. Figure 10-4) how the power of the electromagnetic wave decreases as function of the penetration depth and furthermore how different kinds of damage occur in different rock types depending on mineralogy and heating rate. In addition this chapter discusses how different heating performance leads to extended cracking at the surface and in depth. On the surface a distinction between a small densely cracked centre and a poorly cracked outer ring around the centre of irradiation may be made. It is for example shown in Figure 7-23 how this crack pattern may look like. The damage into depth is partly made up of closely spaced half-circled cracks beneath the surface (Figure 7-7) or of one single vertical crack (Figure 7-15) depending on the reaction of the rock mass to microwave irradiation.

The major question therefore is: How do you define the damaged volume? Is it (a) the entire rock mass because one assumes that one crack can damage the whole block if the conditions are good or is it (b) just the inner, densely cracked centre directly beneath the waveguide because this is the volume where damage is obviously happening? Similar to

known rock mass ratings (e.g. Bienawski 1989) a difference will therefore be made between the strength of joints and the strength of the entire rock mass. We call it direct and indirect damage. **Direct damage** is defined as macro- and microscopical cracking within a defined volume directly in the sphere of influence of the microwaves whereas **indirect damage** is defined as the region of damage influence around a directly damaged core but can contribute to a possible strength reduction of the rock mass and profit from microwave irradiation of the centre.

From the observations reported in this study direct damage can be limited to a maximum depth of 50 mm in all of the investigated rock types but is depending on the actual irradiation time. This is justified by the observation that cracks are limited to this depth in all investigated rock types (see chapter 7) The lateral extent is per definition limited to the cross section of the waveguide (86 * 43 mm). A general assessment of the performance of the technology has to consider all effects influenced by preconditioning of the rock mass (energy, pick consumption, breakage characteristics and chip size). Table 10-3, however, provides an overview of the heating efficiency and specific energy when only the directly damaged volume is taken under consideration. The energy utilized is calculated by

$$dQ = C_p \; dT \; m \qquad \textbf{10-2}$$

where dQ is the change in heat energy, C_p is the specific heat capacity of the irradiated rock, dT the measured increase in temperature and m the mass of the affected volume. The surface temperature is well known from experimental investigations whereas the higher temperature in the interior of samples (see small-scale experiments, chapter 6) could not be measured during large-scale irradiation and is thus not considered in these calculations.

Underlying the calculation of the efficiency and specific energy consumption are several major assumption of which the most important are:

- Heating only of damaged volume
- Entire heated volume has same temperature
- Damage limited to this volume (direct damage)
- All available energy used (no reflection or other loss)
- Reduction of strength of entire rock mass not considered (indirect damage)

This Table 10-3 shows how the described definition of the influenced area influences every consideration of the efficiency of the technique. For basalt 3 different values for large-scale irradiation are provided in this table. The most obvious sign of damage are the described craters (see also Figure 7-4 and Figure 7-5). Only considering those craters as the influenced volume would lead to a heating efficiency of only 2 % or a specific energy for the destruction of this volume of 7398 kWh/m³ which is unacceptably high for an economic application. The surface temperature was measured in the experiments. No considerations are made in respect to the presumably higher temperature beneath the surface as also reported for small-scale experiments. Considering the fact that approximately 50 mm of depth have been obviously heated to the given temperature a heating efficiency (applied energy vs. the energy necessary for heating the described volume) of 78 % is calculated. The theoretical heating efficiency of 100 % would be reached at a heated volume of 83*43*64 mm³ representing a specific energy of 175 kWh/m³ for the destruction of this volume.

rock type	time	Cp	l	w	h	V	ρ	m	dT	W_u	W_p	Eff	specific energy	considered volume
	[s]	[J/gK]	[cm]	[cm]	[cm]	[cm³]	[g/cm³]	[g]	[°C]	[kWs]	[kWs]	[%]	[kWh/m³]	
basalt	6	0.9	4.4	3.2	0.4	5,6	2.8	16	250	4	150	2	7398	resulting crater
	6	0.9	8.6	4.3	5,0	184,9	2.8	518	250	116	150	78	225	area of waveguide + actual crack depth
	6	0.9	8.6	4.3	6,4	238,1	2.8	667	250	150	150	100	175	area of waveguide + calculated depth
dried sandstone	13	0.96	8.6	4.3	5,0	184,9	2.5	462	280	124	325	38	488	area of waveguide + actual crack depth
	13	0.96	8.6	4.3	13,1	483,6	2.5	1209	280	325	325	100	187	area of waveguide + calculated depth
gabbro	20	0.84	8.6	4.3	5,0	184,9	3.0	555	305	142	500	28	751	area of waveguide + actual crack depth
	20	0.84	8.6	4.3	17,6	650,5	3.0	1952	305	500	500	100	214	area of waveguide + calculated depth
granite	30	0.85	8.6	4.3	5,0	184,9	2.8	518	220	97	750	13	1127	area of waveguide + actual crack depth
	30	0.85	8.6	4.3	38,7	1432,4	2.8	4011	220	750	750	100	145	area of waveguide + calculated depth

Table 10-3: Calculation of direct efficiency of microwave irradiation of several rock types. Different penetration depths and affected volumes demonstrate the sensitivity of the calculation to major assumptions. Time = irradiation time; dT = change in temperature; Cp = specific heat capacity (from Cermak and Rybach 1982); l,w,h = length, width and depth of affected volume; W_u = energy utilized = energy necessary for heating the given volume by measured dT; W_p = energy provided = energy provided with 25 kW irradiation for investigated irradiation time; Eff = efficiency of heating; specific energy = total provided energy : affected volume.

Similar calculations are provided for dried sandstone, gabbro and granite. Longer irradiation times are necessary to result in damage comparable to basalt. In the calculation this leads to significantly decreased heating efficiency of 38, 28 and 13 % for dried sandstone, gabbro and granite, respectively. For 100 % efficiency, in these weak

absorbers the depth of the affected volume would therefore have to be significantly larger being 13, 18 and 39 cm for the three rock types, respectively. The specific heating energies for this volume would reach 488, 751 and 1127 kWh/m³ respectively, in the realistic calculation (low efficiency) and 187, 214 and 145 kWh/m³ in the idealized calculation (100 % efficiency) for dried sandstone, gabbro and granite, respectively.

These values, however, do not represent what was called indirect damage earlier in this chapter. It is shown in investigations of granite, gabbro and sandstone that cracks are stretching out of the centre for longer distances than the extensions of the waveguide. The length of these cracks is varying according to side effects and geometrical conditions. The depth of damage, however, remains constant for the irradiation times specified in Table 10-3. The influenced cracking volume is aligned hemispherically a salso demonstrated in Figure 10-5. The volume of such a spherical segment with average horizontal crack length of r = 10 cm and depth of h = 5 cm is 654 cm³. In case of granite the consideration of this volume would lead to a significant reduction of calculated specific energy use from 1127 to 310 kWh/m³ for heating and cracking of this volume.

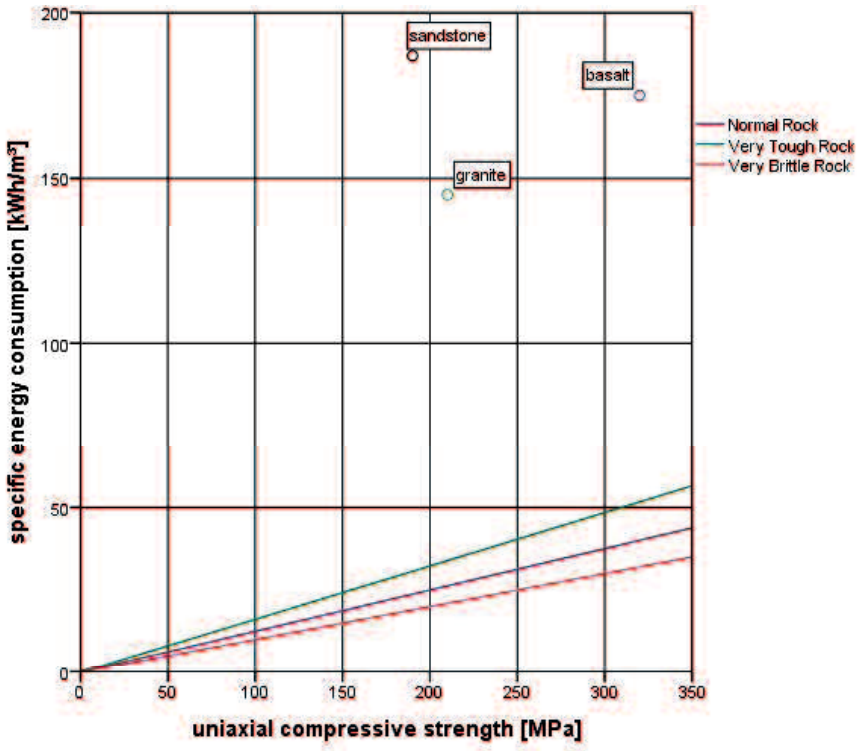

Figure 10-9: Specific cutting energy for Sandvik MR/MT720 (300 KW cutter power / 555 kW total power) equipped with cutter head R400-TC60 and 22 mm TC Diameter Picks as function of uniaxial compressive strength for intact to moderately fractured rock mass (after Restner 2008) compared to specific energy as result of microwave irradiation for selected rock types (100 % efficiency for basalt, sandstone and granite from Table 10-3).

Comparing these values to specific energy required for cutting 1 m³ with a standard roadheader reveals that heating efficiency with microwaves alone does not allow for a competitive technique. For comparison the specific energy necessary for cutting rock types with different uniaxial compressive strength and toughness (data from Restner 2008) as well as the optimum efficiency calculated in Table 10-3 for basalt, sandstone and granite are shown in Figure 10-9.

It demonstrates that very tough rocks with a UCS of up to 300 MPa require approximately 50 kWh/m³ of specific cutting energy. Even in the most ideal situation the specific values for destruction of the rock mass with microwaves only are, by a minimum factor of approximately 5, much higher. The lowest value lies at 145 kWh/m³ for 100 % heating efficiency in case of granite (Table 10-3) compared to approximately 35 kWh/m³ for cutting with a roadheader. It has to be highlighted that the values for the microwave efficiency are strongly depending on the consideration of the affected volume which was already explained earlier on.

No values can be provided for cutting rocks after microwave irradiation. It is however assumed that the initiation of cracks as result of microwave irradiation has a positive influence on the cutting process. Such a positive influence is also reported by Thuro and Plinninger (2002) who demonstrate that the joint spacing of the rock mass has a significant influence on the advance rate of a roadheader. The implementation of artificial joints (joints or cracks produced by microwave heating) could lead to a beneficial behaviour of the irradiated rock mass in the cutting process because of the generation of free surfaces on which the stresses formed by the cutting tool can act.

Calculating heating efficiency of a comparably small volume only is therefore partly misleading in terms of efficiency of microwave irradiation as complementary technique in hard rock cutting. It only provides a number representing the heating rate and the conversion of provided energy into heat. For consideration of the efficiency of a combined process of microwave irradiation and cutting more investigations are necessary on the nature, form and extension of the induced cracks and their interaction with the cutting tool.

11 Conclusions and outlook

The experimental investigations of the interaction of microwaves and rocks performed during this study demonstrate the feasibility of applying the microwave technology in combination with roadheaders in the future mining operation. Different kinds of damage and effects were identified for the investigated rock types which contribute to cracking, spallation or shattering of the samples. A short description of the major effects is listed below:

- Different effects with different mineralogy and texture: Coarse grained rocks show cracks along grain boundaries, fine grained rocks not.
- Different effects with different sample size: Axial and circumferential cracks aligned to geometry in small samples with irradiation in a cavity. Orientation to planar surface in large samples with single-sided irradiation.
- Different effects with different power levels:
    - With low-power irradiation slow heating and melting of good absorbers; no significant influence on weak absorbers; shattering of water saturated samples.
    - With high-power irradiation fast heating and spallation of good absorbers; In weak absorbers slow heating and development of radial cracks as well as orientation along grain boundaries; explosive behaviour of water saturated samples.
- High-power application leading to cracking in all investigated rock types in contrary to low-power application.
- Water acting as the driving force of destruction in porous rocks: Vapour pressure leading to stresses exceeding tensile strength of rocks even at low temperatures slightly above 100 °C.
- Water acting as major force in rocks with inherited clay minerals.
- Water in other rocks: rocks with inherited OH-groups (Pickles 2004)
- Fast generation of high gradients only possible with high power and strong absorption: Rocks that simply melt during small-scale experiments (greenstones, gabbro) react explosively with spallation under high-power irradiation. Weak

absorbers (granite, sandstone) heat slowly during high-power irradiation and show radial cracking around the irradiated spot.

- Coupling of high-power microwaves into rock volume depends on the roughness of the surface: Smooth surfaces prevent enhancing of the microwave field and arcing effects, leading to improved energy input in the sample, whereas rough surfaces lead to limited energy input due to arcing and the formation of fire balls.
- Performed cutting tests reveal large scattering of results: Available data is not sufficient for statistical confirmation of influence of microwave irradiation on the mechanical cutting process.
- Only limited efficiency of application: Depending on the rock type and application efficiency. Irradiation of basalt leads to highest efficiency, whereas irradiation of sandstone, gabbro and gabbro leads to lower respective efficiencies in decreasing order. Efficiency is also strongly depending on the kind of damage (direct or indirect) that is considered for the calculations. Only integral approaches (mine to mill) can provide profound statements on this topic.

Only an integral approach which is able of measuring the energy inserted by microwave irradiation and the reduction of strength of the entire rock mass or at least the depth for a single cut with a mechanical tool will lead to a firm statement on the possible beneficiation of this technology in the cutting process. For a proper projection of the provided results to a possible large-scale application the effective damage of a certain volume of rock has to be known or at least properly estimated. Due to a lack of this data a reasonable estimation can not be provided at this point.

Nevertheless, one has to bear in mind that not only the applied forces are an important factor but that also the breakage characteristic of the exposed rock type is of importance for the energy balance of the entire process from mine to mill. The resulting sample surface after cutting, chip size and breakage geometry could be a topic for future investigations dealing with the beneficiation of the described technology

The described results only provide a basic classification of the interaction of microwaves and different rock types. Several variables of the process, listed below, are still not known with sufficient precision yet and have to be clarified in future projects and investigations.

- No precise knowledge of dielectric properties of the investigated rock types and their behaviour with increasing temperature: Permittivities are individual for each rock type and vary within a type. They also change with increasing temperature. More data necessary for proper numerical investigations.
- No precise knowledge of thermal properties of the investigated rock types: Thermal properties like thermal conduction, heat capacity and thermal expansion have to be determined, also as function of temperature, for respective rock types in order to perform precise calculations of heating and formation of stresses.
- Determination of the strength at grain boundaries and of single grains: With the knowledge of precise material data improved forecasting can be made on the cracking behaviour. Identification of the driving parameters of damaging coarse grained rocks (grain boundaries vs. bulk composition).
- Lacking of definition of damage and damaged volume: How is sufficient damage defined? Which volume can be considered as sufficiently damaged as result of microwave irradiation? What kind of damage (cracking, disintegration, deformation) is necessary to achieve a beneficiation of the cutting process? How does one single crack influence the breakage behaviour of the entire volume? Does the directly damaged volume stand in any correlation to the breakage effects in the entire rock mass?
- More precise data of the cutting process needed: For proper evaluation of the influence of microwave irradiation on the mechanical cutting process more laboratory tests have to be performed. Only with an increased data-set of the behaviour of various rock types in the cutting test-rig reliable statements on the process can be made.

12 Bibliography

Ali, A.Y., Bradshaw, S.M., 2009. Quantifying damage around grain boundaries in microwave treated ores. Chemical Engineering and Processing: Process Intensification 48 (11-12), 1566–1573.

Ali, A.Y., Bradshaw, S.M., 2010. Bonded-particle modelling of microwave-induced damage in ore particles. Minerals Engineering 23 (10), 780–790.

Ali, A.Y., Bradshaw, S.M., 2011. Confined particle bed breakage of microwave treated and untreated ores. Minerals Engineering 24 (14), 1625–1630.

Amankwah, R.K., Khan, A.U., Pickles, C.A., Yen, W.T., 2005. Improved grindability and gold liberation by microwave pretreatment of a free-milling gold ore. Mineral Processing and Extractive Metallurgy 114 (1), 30–36.

Amankwah, R.K., Ofori-Sarpong, G., 2011. Microwave heating of gold ores for enhanced grindability and cyanide amenability: Special issue: Processing of Precious Metal Ores & Concentrates. Minerals Engineering 24 (6), 541–544.

Amankwah, R.K., Pickles, C.A., 2009. Microwave roasting of a carbonaceous sulphidic gold concentrate. Minerals Engineering 22 (13), 1095–1101.

Angenheister, G. (Ed.), 1982. The Landolt-Börnstein Database. Springer-Verlag, Berlin/Heidelberg.

Antretter, T., 2011. Stresses in heated rock samples. Personal Communication.

Bergqvist, U., Jammet, H.P., Court, L.A., Bernhardt, J.H., Szabo, L.D., Ahlbom, A., Stolwok, J.A., Taki, M., Matthes, R., Repacholi, M.H., Swicord, M.L., Cesarini, J.P., Tenforde, T.S., Grandofo, M., Hietanen, M., Sliney, D.H., McKinlay, A.F., 1998. Guidelines for limiting exposure to time-varying electric, magnetic, and electromagnetic fields (up to 300 GHz). Health Physics 74 (4), 494–522.

Bieniawski, Z.T., 1989. Engineering rock mass classifications: A complete manual for engineers and geologists in mining, civil, and petroleum engineering. Wiley, New York [u.a.], XII, 251.

Brown, W., Green, S., Hakala, W., Hustrulid, W., Maurer, W. (Eds.), 1976. Rock Fragmentation: A report of a special seminar sponsored by excavation technology program of national science foundation / research applied to national needs, Salt Lake City, Utah.

Cartz, L., 1995. Nondestructive testing: Radiography, ultrasonics, liquid penetrant, magnetic particle, eddy current. ASM International, Materials Park, OH, x, 229.

Cermak, V., Rybach, L., 1982. Table 7 (igneous - metamorphic rocks), in: Angenheister, G. (Ed.), The Landolt-Börnstein Database. Springer-Verlag, Berlin/Heidelberg.

Ciccu, R., Grosso, B., 2010. Improvement of the Excavation Performance of PCD Drag Tools by Water Jet Assistance. Rock Mechanics and Rock Engineering 43 (4), 465–474.

Cohen, J., Deskins, W., Rogers, J., 2005. High-Pressure Jet Kerf Drilling Shows Significant Potential To Increase ROP, in: SPE Annual Technical Conference and Exhibition. Society of Petroleum Engineers, Dallas, TX.

Didenko, A., Kozlov, E., Sharkeev, Y., Sulakshin, A., Filipenko, N., Girsova, N., Fortuna, S.M.Y.V., 1997. Formation of the defective structure in copper under the effect of powerful pulsed microwave radiation. Physics and Chemistry of Materials Treatment 31 (5), 441–446.

Didenko, A., Zverev, B., Prokopenko, A., 2005. Microwave fracturing and grinding of solid rocks by example of kimberlite. Doklady Physics 50, 349–350.

Dikhtyar, V., Jerby, E., 2006. Fireball ejection from a molten hot spot to air by localized microwaves. Physical Review Letters 96 (4).

Fischer, T., 1978. Der Diabasbruch Saalfelden. Lapis 3, 15–17.

Gupta, M., Wong, W.L., 2007. Microwaves and metals. John Wiley & Sons, Singapore; Hoboken, NJ, viii, 228.

Hagan, P., 1992. The cuttability of rock using high pressure water jet, in: Proceeedings of Western Australia Conference on Mining Geomechanics, 399–412.

Haque, K.E., 1999. Microwave energy for mineral treatment processes - a brief review. International Journal of Mineral Processing 57 (1), 1–24.

Hartlieb, P., Leindl, M., Kuchar, F., Antretter, T., Moser, P., 2012. Damage of basalt induced by microwave irradiation: Special Issue - Physical Separation. Minerals Engineering 31, 82–89.

Hassani, F., Nekoovaght, P.M., Radziszewski, P., Waters, K.E., 2012. Microwave assisted mechanical rock breaking, in: Harmonising Rock Engineering and the Environment - Proceedings of the 12th ISRM International Congress on Rock Mechanics, Beijing, 2075–2080.

Heritsch, H., 1963. Exkursion zum Basaltbruch Weitendorf. Mitteilungen des des Naturwissenschaftlichen Vereines für Steiermark 96, 199–205.

Heritsch, H., 1976. Über Nephelinbasalte und ein basaltisches Glas des Vulkangebietes von Klöch, Oststeiermark. Mitteilungen des des Naturwissenschaftlichen Vereines für Steiermark 106, 21–29.

Hutcheon, R., Jong, M. de, Adams, F., Wood, G., McGregor, J., Smith, B., 1992a. A System for Rapid Measurements of RF and Microwave Properties up to 1400°C – Part 1: Theoretical Development of the Cavity Frequency-Shift Data Analysis Equations. Journal of Microwave Power and Electromagnetic Energy 27 (2), 87–92.

Hutcheon, R., Jong, M. de, Adams, F., Wood, G., McGregor, J., Smith, B., 1992b. A System for Rapid Measurements of RF and Microwave Properties up to 1400°C – Part 2: Description of Apparatus, Data Collection Techniques and Measurements on Selected Materials. Journal of Microwave Power and Electromagnetic Energy 27 (2), 93–102.

Jerby, E., Dikhtyar, V., 2001. Drilling into hard non-conductive materials by localized microwave radiation, in: Proceedings of the Eigth Ampere International Conference on Microwave and High Frequency Heating, Bayreuth.

Jerby, E., Dikhtyar, V., Aktushev, O., Grosglick, U., 2002. The Microwave Drill. Science 298 (5593), 587–589.

Jones, D.A., Kingman, S.W., Whittles, D.N., Lowndes, I.S., 2005. Understanding microwave assisted breakage. Minerals Engineering 18 (7), 659–669.

Jones, D.A., Kingman, S.W., Whittles, D.N., Lowndes, I.S., 2007. The influence of microwave energy delivery method on strength reduction in ore samples. Chemical Engineering and Processing 46 (4), 291–299.

Jordan, E.W., Holben, T., Kim, J., Restner, U., Hallett, G., 2011. Roadheader excavations in hard rock - A case history from midtown manhattan, in: Proceedings - Rapid Excavation and Tunneling Conference, San Francisco, CA, 765–795.

Kasap, S.O., 2000. Principles of electrical engineering materials and devices, Rev. ed. McGraw Hill, Boston, xii, 690.

Kingman, S.W., Corfield, G.M., Rowson, N.A., 1999. Effects of Microwave Radiation Upon the Mineralogy and Magnetic Processing of a Massive Norwegian Ilmenite Ore. Magnetic and Electrical Separation 9 (3), 131–148.

Kingman, S.W., Jackson, K., Bradshaw, S.M., Rowson, N.A., Greenwood, R., 2004a. An investigation into the influence of microwave treatment on mineral ore comminution. Powder Technology 146 (3), 176–184.

Kingman, S.W., Jackson, K., Cumbane, A., Bradshaw, S.M., Rowson, N.A., Greenwood, R., 2004b. Recent developments in microwave-assisted comminution. International Journal of Mineral Processing 74 (1-4), 71–83.

Kingman, S.W., Vorster, W., Rowson, N.A., 2000. Influence of mineralogy on microwave assisted grinding. Minerals Engineering 13 (3), 313–327.

Kumar, H., Lester, E., Kingman, S., Bourne, R., Avila, C., Jones, A., Robinson, J., Halleck, P.M., Mathews, J.P., 2011. Inducing fractures and increasing cleat apertures in a bituminous coal under isotropic stress via application of microwave energy. International Journal of Coal Geology 88 (1), 75–82.

Latella, B.A., O'Connor, B.H., Padture, N.P., Lawn, B.R., 1997. Hertzian contact damage in porous alumina ceramics. Journal of the American Ceramic Society 80 (4), 1027–1031.

Lawn, B.R., 1993. Fracture of brittle solids, 2nd ed. Cambridge University Press, Cambridge / New York, xix, 378.

Lawn, B.R., Lee, S.K., Peterson, I.M., Wuttiphan, S., 1998. Model of strength degradation from hertzian contact damage in tough ceramics. Journal of the American Ceramic Society 81 (6), 1509–1520.

Leindl, M., 2011. Stresses in heated rock samples. Personal Communication.

Lester, E., Kingman, S., Dodds, C., 2005. Increased coal grindability as a result of microwave pretreatment at economic energy inputs. Fuel 84 (4), 423–427.

Liu, Y., 2008. Box plots: use and interpretation. Transfusion 48 (11), 2279–2280.

Lovás, M., Kováčová, M., Dimitrakis, G., Čuvanová, S., Znamenáčková, I., Jakabský, Š., 2010. Modeling of microwave heating of andesite and minerals. International Journal of Heat and Mass Transfer 53 (17–18), 3387–3393.

Mali, H., 2007. Petrographische Untersuchung von Granit und Metasandstein nach Brennen bei 573 und 850 °C. Chair of geology and mineral exploration, University of Leoben, Leoben. 2007.

Marcos, C., Rodríguez, I., 2011. Expansibility of vermiculites irradiated with microwaves. Applied Clay Science 51 (1-2), 33–37.

Maurer, W., 1976. Novel rock disintegration techniques, in: Rock Fragmentation. A report of a special seminar sponsored by excavation technology program of national science foundation / research applied to national needs, Snowbird, Utah, Salt Lake City, Utah.

McGill, S.L., Walkiewicz, J.W., Smyres, G.A., 1988. The Effects of Power Level on the Microwave Heating of Selected Chemicals and Minerals. MRS Proceedings 124.

Meisels, R., 2012. Microwave propagation in rock samples. Personal communication.

Mosteller, F., Tukey, J.W., 1977. Data analysis and regression: A second course in statistics. Addison-Wesley, Reading, Mass, xvii, 588.

Murová Ingrid, Lovás Michal, Jakabský Štefan, 2000. The influence of microwave radiation on the failure of rocks. Acta Montanistica Slovaca 5 (3), 283–285.

Nelson, S.O., Lindroth, D.P., Blake, R.L., 1989. Dielectric properties of selected minerals at 1 to 22 GHz. Geophysics 54 (10), 1344–1349.

Okrusch, M., Matthes, S., 2005. Mineralogie: Eine Einführung in die spezielle Mineralogie, Petrologie und Lagerstättenkunde, 7th ed. Springer, Berlin [etc.], XVII, 526.

Österreichischer Verband für Elektrotechnik Fachausschuss Elektromagnetische Verträglichkeit, 2006. Elektrische, magnetische und elektromagnetische Felder im Frequenzbereich von 0 Hz bis 300 GHz - Beschränkung der Exposition von Personen E 8850. Österr. Verb. für Elektrotechn. [etc.], Wien.

Peinsitt, T., 2009. Demonstration of the Feasibility of weakening rocks with Microwave Techniques. Master Thesis, Graz University of Technology.

Peinsitt, T., Kuchar, F., Hartlieb, P., Moser, P., Kargl, H., Restner, U., Sifferlinger, N., Sifferlinger, N.A., 2010. Microwave heating of dry and water saturated basalt, granite and sandstone. International Journal of Mining and Mineral Engineering 2 (1), 18–29.

Pickles, C.A., 2004. Microwave heating behaviour of nickeliferous limonitic laterite ores. Minerals Engineering 17 (6), 775–784.

Pickles, C.A., 2009a. Microwaves in extractive metallurgy: Part 1 – Review of fundamentals. Minerals Engineering 22 (13), 1102–1111.

Pickles, C.A., 2009b. Microwaves in extractive metallurgy: Part 2 – A review of applications. Minerals Engineering 22 (13), 1112–1118.

Plinninger, R., 2011. Teilschnittmaschinen als alternatives Vortriebsverfahren in innerstädtischen Tunnel- und Stollenbau - Chancen und Risiken, in: Veröffentlichungen zur 18. Tagung für Ingenieurgeologie und zum Forum für Junge Ingenieurgeologen. Univ.-Verl. der Techn. Univ, Berlin, 139–145.

Pohl, J., 1982. 9.4 Thermal properties of lunar rocks, in: Angenheister, G. (Ed.), The Landolt-Börnstein Database. Springer-Verlag, Berlin/Heidelberg.

Pohl, W., Petrascheck, W., Petrascheck, W.E., 1992. W. & W.E. Petrascheck's Lagerstättenlehre: Eine Einführung in die Wissenschaft von den mineralischen Bodenschätzen, 4th ed. Schweizerbart, Stuttgart, VIII, 504.

Preston, F., White, H., 1934. Observations on Spalling. Journal of the American Ceramic Society 17 (1-12), 137–144.

Prokopenko, A., 2011. Microwave Heating for Emolliating and Fracture of Rocks, in: Grundas, S. (Ed.), Advances in Induction and Microwave heating of Mineral and Organic Materials, 313–338.

Rankin, D.W.H., 2009. CRC handbook of chemistry and physics, 89th edition, edited by David R. Lide: Crystallography Reviews. Crystallography Reviews 15 (3), 223–224.

Rauenzahn, R.M., Tester, J.W., 1989. Rock failure mechanisms of flame-jet thermal spallation drilling-theory and experimental testing. International Journal of Rock Mechanics and Mining Sciences and 26 (5), 381–399.

Restner, U., 2008. Specific Cutting and Total Energy Consumption for Sandvik MR/MT720. Personal Communication.

Restner, U., Gehring, K., 2002. Quantification of rock mass influence on cuttability with roadheaders, in: Proceedings TUR 2002. 2nd International Conference on Mining Techniques, Krakow - Krynica, 53–68.

Restner, U., Reumueller, B., 2004. "Metro Montreal" - Successful operation of a state-of-the-art roadheader - ATTM 105-ICUTROC - competing with drill & balst operation in urban tunneling, in: Proceedings of the ISRM regional symposium EUROCK 2004 & 53rd Geomechanics colloquy. Rock engineering, theory and practice, October 7-9, 2004, Salzburg, Austria. Verlag Gluckauf, Essen, Germany.

Rizmanoski, V., 2011. The effect of microwave pretreatment on impact breakage of copper ore. Minerals Engineering 24 (14), 1609–1618.

Sahoo, B.K., De, S., Meikap, B.C., 2011. Improvement of grinding characteristics of Indian coal by microwave pre-treatment. Fuel Processing Technology 92 (10), 1920–1928.

Sahyoun, C., Rowson, N.A., Kingman, S.W., Groves, L., Bradshaw, S.M., 2005. The influence of microwave pretreatment on copper flotation. Journal of The South African Institute of Mining and Metallurgy 105 (1), 7–13.

Saint-Amant, M., Strangway, D.W., 1970. Dielectric properties of dry, geologic materials. Geophysics 35, 624–645.

Salsman, J.B., Williamson, R.L., Tolley, W.K., Rice, D.A., 1996. Short-pulse microwave treatment of disseminated sulfide ores. Minerals Engineering 9 (1), 43–54.

Samanli, S., 2011. A comparison of the results obtained from grinding in a stirred media mill lignite coal samples treated with microwave and untreated samples. Fuel 90 (2), 659–664.

Sandbak, L.A., 1985. Roadheader drift excavation and geomechanical rock classification at San Manuel, Arizona, in: Proceedings of the Rapid Excavation and Tunneling Conference. Soc of Mining Engineers of AIME, New York, NY, USA, 902–916.

Santamarina, J.C. (Ed.), 1989. Rock excavation with microwaves: a literature review. Foundation Engineering: Current Principles and Practices. Publ by ASCE, Evanston, IL, USA, 459-473.

Satish, H., Ouellet, J., Raghavan, V., Radziszewski, P., 2006. Investigating microwave assisted rock breakage for possible space mining applications. Transactions of the Institutions of Mining and Metallurgy, Section A: Mining Technology 115 (1), 34–40.

Schiffmann, R., 1997. Principles of Industrial Microwave Heating, in: Clark, D., Sutton, W., Lewis, D. (Eds.), Microwaves: Theory and Applications in Materials Processing IV. Ceramic Transactions, 80, Westerville, Ohio, 41–60.

Scott, G.B.S.E.J., 2008. The effect of microwave pretreatment on the liberation of a copper carbonatite ore after milling. International Journal of Mineral Processing 85 (4), 121–128.

Sharkeev, Y.P., Kozlov, E.V., Didenko, A.N., 1997. Defect structures in metals exposed to irradiation of different nature. Surface and Coatings Technology 96 (1), 95–102.

Sikong, L., Bunsin, T., 2009. Mechanical property and cutting rate of microwave treated granite rock. Songklanakarin Journal of Science and Technology 31 (4), 447–452.

Stein, D., Edgar, R., Iskander M.F., Johnson, D., Johnson, S., Lob, C., Shaw, J., Sutton, W., Tieng, P., 1994. Microwave processing of materials. National Academy Press, Washington, D.C.

Thostenson, E.T., Chou, T.W., 1999. Microwave processing: fundamentals and applications. Composites Part A: Applied Science and Manufacturing 30 (9), 1055–1071.

Thuro, K., Plinninger, R., 2002. Klassifizierung und Prognose von Leistungs- und Verschleißparametern im Tunnelbau, Taschenbuch für den Tunnelbau 2002, 27. Deutsche Gesellschaft für Geotechnik e.V., Essen, 62–126.

Tukey, J.W., 1977. Exploratory data analysis. Addison-Wesley Pub. Co., Reading, Mass, xvi, 688.

Vasek, J., Dlouhy, J., 1978. Efficiency Evaluation of Tunneling Header AM-50. Glueckauf Forschungshefte 39 (2), 45–51.

Vorster, W., 2001. The effect of microwave radiation on mineral processing. PhD Thesis, University of Birmingham.

Vorster, W., Rowson, N.A., Kingman, S.W., 2001. The effect of microwave radiation upon the processing of Neves Corvo copper ore. International Journal of Mineral Processing 63 (1), 29–44.

Wagner, H., Schümann, E.H.R., 1971. The stamp-load bearing strength of rock an experimental and theoretical investigation. Rock Mechanics Felsmechanik Mécanique des Roches 3 (4), 185–207.

Walkiewicz, J.W., Kazonich, G., McGill, S.L., 1988. Microwave heating characteristics of selected minerals and compounds. Minerals and Metallurgical Processing 5 (1), 39–42.

Wang, G., Radziszewski, P., Ouellet, J., 2008. Particle modeling simulation of thermal effects on ore breakage. Computational Materials Science 43 (4), 892–901.

Wang, X., Guo, H., Wang, C., Chen, P., Shi, Y., 1999. Relative dielectric constant from dry rocks. Chinese Science Bulletin 44 (24), 2286–2293.

Whittles, D.N., Kingman, S.W., Reddish, D.J., 2003. Application of numerical modelling for prediction of the influence of power density on microwave-assisted breakage. International Journal of Mineral Processing 68 (1-4), 71–91.

Young, K.F., Frederikse, H.P.R., 1973. Compilation of the Static Dielectric Constant of Inorganic Solids. Journal of Physical and Chemical Reference Data 2 (2), 313–410.

Appendix A: Small-scale experiments. Detailed overview of rock types treatment methods and results

Irradiation of Weitendorf basalt with 3.2 kW microwave - results after 1st irradiation

				before irradiation				after 1st irradiation			
Sample	irrdaition time [s]	length [mm]	diameter [mm]	mass [g]	density [g/cm³]	us-time [µs]	usv [m/s]	mass [g]	us-time [µs]	usv [m/s]	T [°C]
Ba1	0	49.88	50.75	273.0	2.71	8.9	5604	n.v.	n.v.	n.v.	n.v.
Ba2	0	49.91	50.80	272.5	2.70	8.8	5672	n.v.	n.v.	n.v.	n.v.
Ba3	0	49.89	50.79	273.0	2.70	8.7	5734	n.v.	n.v.	n.v.	n.v.
Ba4	0	50.26	50.86	273.0	2.67	8.4	5983	n.v.	n.v.	n.v.	n.v.
Ba5	0	50.07	50.70	273.0	2.70	8.6	5822	n.v.	n.v.	n.v.	n.v.
B11	10	50.77	51.69	287.5	2.70	8.9	5704	287.0	9.0	5641	85
B81	10	50.87	51.60	288.0	2.71	8.8	5757	286.0	9.1	5567	95
B82	10	50.90	51.72	287.5	2.69	9.0	5649	284.5	9.1	5587	60
B41	10	50.66	51.58	286.5	2.71	8.9	5690	286.0	9.0	5627	56
B12	10	50.65	51.64	286.5	2.70	8.9	5716	287.5	9.0	5652	55
B52	10	50.74	51.93	286.0	2.66	8.9	5706	286.5	9.0	5642	48
B72	10	50.64	51.62	286.0	2.70	8.9	5692	286.0	9.0	5629	49
B61	10	50.65	51.75	285.5	2.68	8.9	5693	286.0	8.9	5693	50
B53	20	50.61	51.55	286.5	2.71	8.9	5687	285.5	9.6	5272	92
B43	20	50.66	51.72	286.5	2.69	8.9	5692	286.5	9.5	5333	83
B112	20	50.72	51.56	286.0	2.70	8.8	5764	286.0	9.7	5229	85
B51	20	50.64	51.60	286.0	2.70	8.9	5690	286.0	9.9	5115	85
B22	20	50.66	51.58	286.5	2.71	8.9	5692	286.5	9.2	5507	88
B31	30	50.65	51.64	286.5	2.70	8.9	5691	n.v.	n.v.	n.v.	120
B04	30	27.69	50.95	153.5	2.72	5.1	5429	152.0	6.9	4013	160
B10	30	65.06	51.72	360.0	2.63	12.2	5333	359.0	26.4	2464	140
B13	30	50.50	51.29	280.0	2.68	9.1	5549	279.5	23.3	2167	106
B07	30	52.63	51.20	290.0	2.68	9.5	5540	289.0	13.5	3899	113
B21	40	50.90	51.72	287.5	2.69	8.9	5719	286.5	12.3	4138	139
B83	40	50.40	51.54	282.0	2.68	9.0	5600	280.5	19.0	2653	152
B91	40	50.60	51.59	285.5	2.70	9.0	5622	284.0	12.4	4081	148
B132	40	50.65	51.51	285.5	2.70	9.0	5628	284.0	11.7	4329	150
B133	40	50.68	51.71	285.0	2.68	9.1	5569	284.0	12.7	3991	139
B71	60	50.62	51.57	285.5	2.70	9.0	5624	284.0	14.1	3590	240
B32	60	50.74	51.93	286.0	2.66	8.9	5701	283.5	13.9	3650	250
B42	60	50.65	51.75	285.5	2.68	9.0	5628	283.5	13.1	3866	270
B92	60	50.81	51.55	286.5	2.70	9.0	5646	284.0	13.3	3820	294
B102	60	50.76	51.56	286.0	2.70	9.0	5640	284.0	13.3	3817	290
Ba6	60	49.84	50.68	274.0	2.73	9.2	5417	271.5	15.4	3236	260
Ba7	60	49.90	50.72	272.5	2.70	8.6	5802	270.0	14.9	3349	250
Ba17	60	49.84	50.82	274.0	2.71	8.8	5664	271.0	14.2	3510	350
B122	120	50.48	51.61	284.5	2.69	8.8	5736	n.v. - broken			450
B123	120	50.68	51.56	286.5	2.71	8.8	5759	282.0	16.7	3035	450
B131	120	50.74	51.67	285.5	2.68	9.1	5576	281.5	15.6	3253	445
B121	120	50.93	51.91	283.0	2.63	9.1	5597	n.v. - broken			438
B111	120	50.81	51.61	286.0	2.69	9.1	5584	282.0	15.1	3365	430
B113	120	50.70	51.86	285.5	2.67	8.8	5761	n.v.	13.2	3841	460
B101	120	50.73	51.64	285.5	2.69	9.1	5575	n.v.	15.5	3273	440
B63	120	50.63	51.54	286.0	2.71	9.0	5626	n.v.	13.3	3807	440
B62	120	50.64	51.58	286.0	2.70	9.0	5627	n.v.	15.4	3288	445

2nd heating cycle of selected samples of Weitendorf basalt - same irradiation paramters as 1st heating

sample	irradiation time 1 [s]	temperature 1 [°C]	irradiation time 2 [s]	temperature 2 [°C]	usv untreated m/s]	usv after 1st irradiation [m/s]	usv after 2nd irradiation [m/s]
B22	20	110	20	120	5805	5426	4894
B25	20	100	20	128	5673	5486	4497
B26	20	110	20	110	5687	5596	n.v.
Ba8	20	120	20	115	n.v.	4237	4717
B20	40	210	40	210	5948	3469	2414
Ba19	60	295	60	324	5643	3466	3595
Ba9	60	330	60	334	n.v.	3268	2976
Ba26	90	393	90	236	5508	n.v.	2483
Ba18	120	430	120	330	5514	3393	3542
Ba25	120	466	120	330	5653	n.v.	2481

Quenching in water and liquid nitrogen after irradiation of Weitendorf basalt

Sample	irradiation time [s]	quenching in	usv untreated [m/s]	usv after MW + quenching [m/s]	temperature [°C]
B25	20	water	5673	5486	100
B26	20	water	5859	5596	110
B22	20	water	5805	5426	119
B20	40	water	5948	3469	210
B21	40	water	6014	3753	217
B23	60	water	5800	2834	280
B24	60	water	5865	2583	280
Ba8	20	nitrogen (15 min)	n.v.	4237	120
Ba11	20	nitrogen (15 min)	5665.91	5248	135
Ba9	60	nitrogen (15 min)	n.v.	3268	330
Ba12	60	nitrogen (15 min)	5598.88	3637	350
Ba10	120	nitrogen (15 min)	5034.34	2800	460
Ba13	120	nitrogen (15 min)	5737.93	3467	470

Irradiation of Klöch basalt with 3.2 kW microwave - overview over samples, treatment and results

				before irradiation				after 1st irradiation				after 2nd irradiation			
sample	irradiation time [s]	length [mm]	diameter [mm]	mass [g]	density [g/cm³]	us-time [µs]	usv [m/s]	mass [g]	us-time [µs]	usv [m/s]	T [°C]	mass [g]	us-time [µs]	usv [m/s]	T [°C]
KL01	20	50	50.86	280.5	2.76	13	5385	280.0	20.4	3431	85	2800	11.1	6306	105
KL02	20	49.63	50.57	269.0	2.70	28.6	1735	268.5	24.2	2051	85	2685	33.5	1481	106
KL04	20	49.78	50.84	276.5	2.74	21.2	2348	275.5	21.7	2294	87	2760	23.1	2155	114
KL05	20	49.52	50.82	272.0	2.71	23.3	2125	272.0	21	2358	99	2715	20.9	2369	115
KL06		49.25	50.83	275.0	2.75	12.6	3909								
KL07	20	49.73	50.61	274.0	2.74	10.3	4828	271.0	11.7	4250	87	2750	11.3	4401	99
KL08	30	48.86	50.56	268.0	2.73	21.8	2241	broken after 30s - n.v.			150				
KL09	10	49.72	50.78	271.0	2.69	14	3551	269.0	10.3	4827	56				
KL10	10	49.78	50.49	273.5	2.74	9.8	5080	271.5	10.3	4833	52				
KL11	10	48.66	50.54	273.5	2.80	10	4866	272.0	11.1	4384	53				
KL12	10	49.7	50.5	266.0	2.67	14.4	3451	265.5	34	1462	54				
KL13	10	49.7	50.55	271.0	2.72	11.7	4248	270.5	14.2	3500	52				
KL14		49.6	50.65	267.0	2.67	23.7	2093								
KL15		49.8	50.93	275.0	2.71	9.8	5082								
KL16		49.1	50.75	267.0	2.69	34.6	1419								
KL17		49.94	51.05	275.0	2.69	9.9	5044								
KL18		49.7	50.88	275.0	2.72	19.1	2602								
KL19		49.66	50.95	273.5	2.70	10	4966								
KL20		49.87	50.92	270.0	2.66	10.6	4705								
KL21		49.27	50.45	269.0	2.73	23.4	2106								
KL22		49.69	50.95	272.5	2.69	15.8	3145								
KL23		49.76	50.5	271.0	2.72	10.1	4927								
KL24		49.73	50.61	272.5	2.72	9.8	5074								
KL25		49.67	50.61	275.0	2.75	9.7	5121								
KL26		49.53	50.9	275.0	2.73	9.6	5159								
KL27		49.45	50.57	267.0	2.69	21.5	2300								
KL28		49.49	50.5	269.5	2.72	13	3807								
KL29		49.67	50.41	271.0	2.73	10.2	4870								
KL30	35	48.46	50.86	268.5	2.73	10.1	4798	broken after 35s - n.v.			195				
KL31	35	49.76	50.91	275.0	2.71	13.4	3713	broken after 30s - n.v.			150				
KL32		49.73	50.82	272.0	2.70	10.5	4736								

Irradiation of gabbro with 3.2 kW microwave - overview over samples, treatment and results

Sample	irradiation time [s]	length [mm]	diameter [mm]	before irradiation				after 1st irradiation				after 2nd irradiation			
				mass [g]	density [g/cm³]	us-time [µs]	usv [m/s]	mass [g]	us-time [µs]	usv [m/s]	T [°C]	mass [g]	us-time [µs]	usv [m/s]	T [°C]
GA01	30	53.0	51.5	327	2.96	8.4	6310	327	8.8	6023	167	327	9.3	5699	166
GA02	30	53.8	51.3	327	2.94	8.9	6045	326	9.2	5848	166	326	9.4	5723	166
GA03	30	52.5	51.4	321	2.95	8.4	6250	321	9.1	5769	157	321	9.1	5769	165
GA04	30	56.0	51.2	345	2.99	9.0	6222	345	9.3	6022	160	345	9.8	5714	199
GA05	60	53.7	51.2	330	2.98	8.6	6244	330	10.5	5114	308	330	11.0	4882	286
GA06	60	54.6	51.4	334	2.95	8.9	6135	334	11.1	4919	302	334	12.3	4439	284
GA07	60	54.1	51.2	332	2.98	8.7	6218	332	10.6	5104	294	332	11.0	4918	291
GA08	60	51.8	51.2	317	2.97	8.4	6167	317	10.6	4887	298	317	10.9	4752	294
GA09	90	47.1	51.4	286	2.93	7.7	6117	285	15.7	3000	423	broken - no value			333
GA10	90	55.3	51.3	340	2.97	8.9	6213	340	12.3	4496	373	340	12.9	4287	327
GA13	90	54.5	51.3	336	2.98	8.7	6264	336	11.7	4658	387	336	11.8	4619	304
GA14	45	54.0	51.2	332	2.99	8.6	6279	333	10.1	5347	197	333	10.2	5294	181
GA15	45	54.8	51.2	337	2.99	8.8	6227	337	10.3	5320	200	337	10.4	5269	172

Irradiation of Oberhaag diabase with 3.2 kW microwave - overview over samples, treatment and results

				before irradiation				after 1st irradiation				after 2nd irradiation			
Sample	irradiation time [s]	length [mm]	diameter [mm]	mass [g]	density [g/cm³]	us-time [µs]	usv [m/s]	mass [g]	us-time [µs]	usv [m/s]	T [°C]	mass [g]	us-time [µs]	usv [m/s]	T [°C]
OH1	60	57.11	50.71	303.0	2.63	8.4	6799	303.0	9.1	6276	174	303.0	9.2	6208	150
OH2	60	47.03	50.63	287.0	3.03	7.7	6108	287.0	9.0	5226	149	287.5	11.3	4162	184
OH3	60	49.90	50.71	290.0	2.88	8.7	5736	290.0	10.4	4798	183	290.0	10.5	4752	170
OH4	60	49.99	50.61	294.5	2.93	8.5	5881	293.5	9.7	5154	130	294.0	10.0	4999	142
OH5	60	49.95	50.57	305.5	3.05	7.9	6323	306.0	8.7	5741	207	306.5	8.7	5741	174
OH6	120	49.90	50.64	298.5	2.97	8.5	5871	298.0	15.0	3327	327	298.5	16.4	3043	220
OH7	120	50.03	50.60	298.5	2.97	8.4	5956	broken			410				
OH8	120	49.86	50.88	292.5	2.89	8.5	5866	292.5	14.7	3392	280	292.5	16.4	3040	228
OH9	120	49.98	50.76	297.5	2.94	8.5	5880	297.5	13.2	3786	257	297.5	13.4	3730	228
OH10	120	50.02	50.68	302.0	2.99	8.0	6253	301.5	10.1	4952	367	301.0	10.1	4952	208
OH11	180	49.96	50.67	296.0	2.94	8.7	5743	295.5	32.2	1552	404				
OH13	180	49.55	50.64	286.5	2.87	11.2	4424	296.0	160.0	310	416	broken - n.v.			
OH15	180	50.08	50.78	298.5	2.94	8.4	5962	broken			440				
OH16	180	50.09	50.65	297.5	2.95	8.5	5893	297.0	14.6	3431	427	297.0	15.2	0.00	323
OH18	120	50.10	50.81	294.5	2.90	8.6	5826	broken			376				

Irradiation of Jakomini diabase with 3.2 kW microwave - overview over samples, treatment and results

				before irradiation				after 1st irradiation				afer 2nd irradiation			
Sample	irradiation time [s]	length [mm]	diameter [mm]	mass [g]	density [g/cm³]	us-time [µs]	usv [m/s]	mass [g]	us-time [µs]	usv [m/s]	T [°C]	mass [g]	us-time [µs]	usv [m/s]	T [°C]
Ja1	20	49.30	51.30	298.0	2.92	9.3	5301	298.0	9.9	4980	76	298	9.5	5189	125
Ja2	20	50.25	51.25	305.0	2.94	9.5	5289	305.0	9.5	5289	77	305	9.6	5234	66
Ja3	20	49.95	51.05	298.0	2.91	9.5	5258	298.0	9.4	5314	64	299.5	9.3	5371	67
Ja4	20	50.20	51.00	306.0	2.98	9.7	5175	306.0	10.0	5020	79	306	9.7	5175	73
Ja6	20	50.20	51.20	305.0	2.91	9.2	5457	305.0	9.2	5457	90	306	9.4	5340	92
Ja7	60	50.20	51.25	305.0	2.95	9.6	5229	305.0	9.8	5122	170	305	10.1	4970	275
Ja8	60	50.45	51.10	302.0	2.95	9.6	5255	302.0	12.0	4204	165	302.5		broken	190
Ja9	60	50.15	51.20	304.0	2.92	9.6	5224	304.0	10.3	4869	164	304.5	10.5	4776	230
Ja10	60	50.20	51.00	305.0	2.94	9.3	5398	306.0	9.9	5071	160	305.5	10.2	4922	210
Ja11	60	49.15	51.10	298.0	2.97	9.7	5067	297.0	10.4	4726	180	298	10.7	4593	276
Ja12	80	50.10	51.15	305.0	2.96	9.7	5165	broken with melting			305				
Ja13	90	50.25	50.95	303.0	2.96	9.1	5522	303.0		broken	280				
Ja15	90	50.10	51.15	307.0	2.96	9.8	5112	306.5	10.4	4817	185	306.5	11.0	4555	303
Ja16	90	50.20	51.10	301.0	2.96	9.4	5340	301.5	10.5	4781	200	301.5	10.5	4781	293
Ja17	90	49.90	51.15	301.0	2.98	9.3	5366	broken			275				
Ja18	90	49.60	51.00	299.0	2.92	9.9	5010	300.5	15.4	3221	245	300.5	17.6	2818	340
Ja19	90	48.95	51.05	296.0	2.94	9.2	5321	296.5	10.5	4662	235	297	10.4	4707	350
Ja20	120	50.10	51.10	301.0	2.95	9.9	5061	300.5	12.7	3945	302	301	13.2	3795	406
Ja21	120	49.80	51.10	302.0	2.95	9.4	5298	303.0	11.4	4368	335	302.5	10.6	4698	395
Ja22	120	50.25	51.10	304.0	2.93	9.1	5522	305.5	10.0	5025	370				
Ja23	20	48.90	51.10	295.0	2.96	9.5	5147	297.0	9.7	5041	68	297	9.8	4990	64
Ja24	60	49.15	51.15	300.0	2.95	8.4	5851	300.5	8.6	5715	162	300.5	8.4	5851	170
Ja25	90	50.10	51.15	308.0	2.94	9.2	5446	307.5	11.1	4514	313	307.5	11.1	4514	n.v.
Ja26	120	50.10	51.00	301.0	2.97	9.8	5112	300.5	15.8	3171	409	300.5	15.8	3171	n.v.

Irradiation of diabase Saalfelden Hinterburgbruch with 3.2 kW microwave - overview over samples, treatment and results

				before irradiation				after 1st irradiation				after 2nd irradiation			
sample	irradiation time [s]	length [mm]	diameter [mm]	mass [g]	density [g/cm³]	us-time [µs]	usv [m/s]	mass [g]	us-time [µs]	usv [m/s]	T [°C]	mass [g]	us-time [µs]	usv [m/s]	T [°C]
SF-HB-01	30	51.50	49.60	290.2	2.92	9.1	5516	290.4	9.6	5229	177	n.v.	9.7	5175	187
SF-HB-02	30	52.00	49.20	286.6	2.90	8.6	5837	286.6	9.8	5122	213	n.v.	9.7	5175	191
SF-HB-03	30	51.40	49.60	289.6	2.92	8.6	5837	289.8	9.7	5175	175	n.v.	9.5	5284	197
SF-HB-04	60	51.60	49.20	285.5	2.91	8.9	5640	285	11.5	4365	337	n.v.	11.2	4482	311
SF-HB-05	60	52.10	49.60	291.5	2.90	8.6	5837	291.3	10.7	4692	327	n.v.	10.8	4648	314
SF-HB-06	30	49.20	51.40	300.1	2.94	8.4	5976	300.1	9.5	5284	193	n.v.	9.5	5284	198
SF-HB-07	60	50.20	51.30	303.5	2.93	8.3	6048	303.4	10.2	4922	336	n.v.	10	5020	317
SF-HB-08	60	49.70	51.30	305.4	2.97	8	6275	305.4	10.7	4692	336	n.v.	10.2	4922	323
SF-HB-09	75	49.70	51.20	295.6	2.89	8.4	5976	294.9	10.1	4970	330				
SF-HB-10	75	50.10	51.20	278.3	2.70	8.3	6048	278.2	10.8	4648	376				
SF-HB-11	90	50.20	51.10	298.4	2.90	8.4	5976	297.7	10.9	4606	426				
SF-HB-12	90	49.80	51.40	305.1	2.95	8.2	6122	304.3	12.4	4048	455				
SF-HB-13		50.20	51.30	306.9	2.96	8.5	5906								
SF-HB-14	75	49.50	51.30	302.1	2.95	8.5	5906	302	11.0	4564	340				
SF-HB-15	75	49.90	51.20	291.1	2.83	8.8	5705	290.6	16.8	2988	433				
SF-HB-16		49.30	51.10	294.4	2.91	8.9	5640								
SF-HB-17		50.00	51.20	275.7	2.68	8.2	6122								
SF-HB-18	75	49.20	51.10	291.6	2.89	7.9	6354	n.v.	10.1	4970	395				
SF-HB-19	82	49.90	51.40	306.1	2.96	8.5	5906	305.3	broken		433				
SF-HB-20	90	50.10	51.20	298.9	2.90	8.6	5837	297.2	13.7	3664	527				
SF-HB-21	90	49.70	51.30	301.2	2.93	8.7	5770	299.7	14.8	3392	395				
SF-HB-22		49.50	51.50	279.7	2.71	8.5	5906								

Irradiation of diabase Saalfelden Tagbau21 with 3.2 kW microwave - overview over samples, treatment and results

				before irradiation				after 1st irradiation				after 2nd irradiation			
sample	irradiation time [s]	length [mm]	diameter [mm]	mass [g]	density [g/cm³]	us-time [µs]	usv [m/s]	mass [g]	us-time [µs]	usv [m/s]	T [°C]	mass [g]	us-time [µs]	usv [m/s]	T [°C]
SF-T 1-01	30	52.40	49.60	283.9	2.80	11.3	4602	284.0	12.4	4194	151	n.v.	13.1	3881	167
SF-T21-02	30	51.70	49.60	281.0	2.81	11.9	4370	281.2	12.3	4228	138	n.v.	12.9	4031	175
SF-T21-04	30	52.10	49.60	282.0	2.80	12.3	4228	282.2	11.5	4522	141	n.v.	12.4	4194	156
SF-T21-05	143	52.80	49.60	285.4	2.80	11.0	4727	283.6	29.9	1739	422				
SF-T21-06	30	51.80	49.60	283.4	2.83	12.8	4063	283.6	12.5	4160	150	n.v.	13.1	3969	166
SF-T21-07	60	52.40	49.60	284.1	2.81	12.5	4160	284.1	13.9	3741	261	n.v.	14.9	3490	246
SF-T21-08	60	51.00	49.60	279.7	2.84	12.3	4228	279.6	14.7	3537	262	n.v.	16.4	3171	272
SF-T21-09	60	52.70	49.60	281.8	2.77	11.5	4522	281.7	14.0	3714	278	n.v.	14.8	3514	242
SF-T21-10	60	52.30	49.60	284.1	2.81	12.9	4031	284.0	15.0	3465	271	n.v.	16.5	3152	286
SF-T21-11	90	51.80	49.60	279.5	2.79	11.4	4561	279.2	15.9	3270	401	n.v.	16.7	3114	729
SF-T21-12	90	52.40	49.70	283.0	2.78	10.9	4771	282.6	17.9	2905	382	n.v.	21.6	2407	268
SF-T21-13	90	52.10	49.50	277.9	2.77	11.4	4561	277.6	16.6	3133	333	n.v.	broken		535
SF-T21-14	90	51.80	49.60	279.3	2.79	11.0	4727	278.8	18.7	2781	376	n.v.	14.1	3688	155
SF-T21-15	90	51.70	49.60	282.2	2.82	12.4	4194	281.8	16.4	3171	398	n.v.	19.1	2723	171
SF-T21-16	118	51.90	49.60	283.6	2.83	11.0	4727	282.4	23.6	2203	495				
SF-T21-17	104	51.30	49.50	281.4	2.85	12.0	4333	280.1	22.1	2353	470				
SF-T21-18	120	51.60	49.60	281.3	2.82	12.1	4298	279.7	23.9	2176	487				
SF-T21-19	120	51.80	49.60	283.5	2.83	11.5	4522	281.9	broken		498				
SF-T21-20	30	51.90	49.70	284.5	2.83	12.8	4063	284.6	12.3	4228	143	n.v.	12.9	4031	145
SF-T21-21	90	52.40	49.60	284.2	2.81	11.5	4522	n.v.	16.4	3171	372				
SF-T21-22	75	51.90	49.60	281.7	2.81	11.7	4094	n.v.	14.5	3586	328	n.v.	16.1	3230	319
SF-T21-23		49.70	51.10	287.6	2.82	9.2	5413								
SF-T21-24		49.70	51.10	286.8	2.81	9.7	5134								
SF-T21-25	75	49.70	51.10	286.8	2.81	9.0	5533	n.v.	12.1	4116	314	n.v.	12.5	3984	294
SF-T21-26	75	49.80	51.20	289.2	2.82	9.3	5355	n.v.	14.0	3557	369	n.v.	14.2	3507	325
SF-T21-27	75	49.70	51.10	285.9	2.80	9.4	5298	n.v.	12.1	4116	308	n.v.	13.2	3773	315
SF-T21-28	75	49.70	51.20	288.9	2.82	9.5	5242	n.v.	14.5	3434	321	n.v.	13.1	3802	293
SF-T21-29		50.10	51.10	288.0	2.80	9.8	5082								
SF-T21-30	75	49.80	51.10	288.9	2.83	9.4	5298	n.v.	13.1	3802	346	broken - n.v.			199

Irradiation of Somincor sulphidic ore with 3.2 kW microwave - overview over samples, treatment and results

				before irradiation				after 1st irradiation			
sample	length [mm]	irradiation time [s]	diameter [mm]	mass [g]	density [g/cm³]	us-time [µs]	usv [m/s]	mass [g]	us-time [µs]	usv [m/s]	T [°C]
So11	50.96	240	51.7	451.0	4.22	8.3	6140	n.v.	9.8	5200	385
So12	50.7	20	51.53	459.5	4.35	8.1	6259	459.5	8.3	6108	78
So13	50.73		51.62	465.5	4.39	7.8	6504				
So21	50.99	60	51.5	456.5	4.30	7.9	6454	456.0	8.3	6143	164
So22	50.72		51.94	433.0	4.03	8.5	5967				
So23	50.72	10	51.49	453.0	4.29	8	6340	453.0	8.1	6262	53
So31	50.63	240	51.62	433.0	4.09	7.9	6409	n.v.	10.9	4645	40
So32	50.83	20	51.66	462.5	4.34	7.7	6601	463.0	7.9	6434	78
So33	50.64		51.97	462.0	4.30	7.9	6410				
So41	50.68	10	51.96	452.5	4.21	7.7	6582	452.5	7.8	6497	47
So42	50.71	120	51.73	438.5	4.12	8.4	6037	438.0	9.6	5282	297
So43	50.7	10	51.58	466.5	4.41	8	6338	466.0	8.1	6259	51
So51	50.77	90	51.55	466.0	4.40	7.7	6594	465.5	8.1	6268	n.v.
So52	50.69	20	51.93	442.5	4.12	8.4	6035	442.5	8.6	5894	83
So53	50.65	240	51.5	460.0	4.36	8.1	6253	0.0	9.3	5446	360
So61	50.89		51.67	456.0	4.28	8.7	5849				
So62	50.62	60	51.64	449.0	4.24	8.7	5818	449.0	9.5	5328	174
So63	50.59		51.49	458.0	4.35	7.6	6657				
So71	50.88	60	51.79	457.0	4.27	8.4	6057	457.0	8.9	5717	183
So72	50.66		51.62	452.5	4.27	8.5	5960				
So73	50.68	10	51.62	464.5	4.38	7.6	6668	465.0	7.6	6668	53
So81	50.84	120	51.97	460.5	4.27	7.9	6435	460.5	9.7	5241	239
So82	50.45	60	51.58	454.5	4.31	9	5606	454.5	9.4	5367	157
So83	50.64	40	51.85	463.5	4.34	8.2	6176	463.5	8.3	6101	n.v.
So91	50.81	120	51.68	453.5	4.26	8.7	5840	453.0	10.1	5031	294
So92	50.68	60	51.61	463.5	4.37	7.9	6415	463.0	8.3	6106	170
So93	50.76	120	51.86	456.0	4.26	7.9	6425	456.0	8.7	5834	265
So101	50.66	20	51.85	469.0	4.39	8	6333	469.0	8	6333	84
So102	50.88	120	51.89	467.0	4.34	8	6360	466.5	9.2	5530	260
So103	50.64	20	51.65	460.0	4.34	8.1	6252	461.0	8.2	6176	89
So111	50.64	10	51.84	478.5	4.48	7.8	6492	479.0	7.8	6492	49
So112	50.82		51.98	454.5	4.22	8.2	6198				
So113	50.68		51.66	458.5	4.32	8.4	6033				
So123	50.08		51.63	441.0	4.21	9.4	5328				
So131	49.75	240	51.72	454.5	4.35			n.v.	n.v.	n.v.	n.v.
So132	50.47		51.84	459.0	4.31						
So133	50.78	300	51.71	464.0	4.35			n.v.	n.v.	n.v.	430

Appendix B: Large-scale experiments. Overview of testing parameters and results of cutting tests

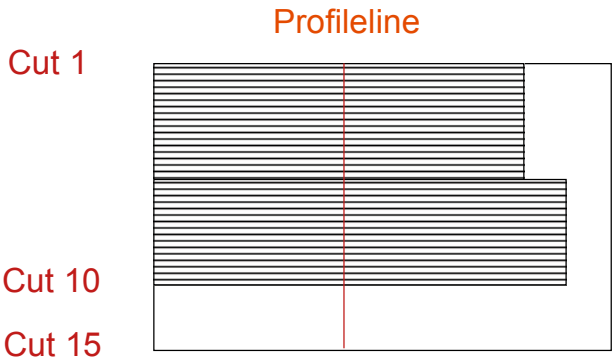

Figure A: Sketch of irradiation parameters and cutting lines on basalt sample of Weitendorf. P = 25 kW, moving speed = 3.5 mm/s, penetration depth = 8 mm, line spacing = 16 mm, cutting velocity = 1.5 m/s.

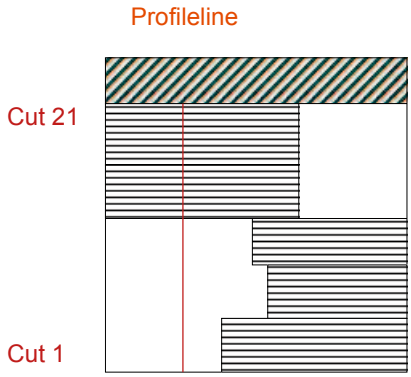

Figure B: Sketch of irradiation parameters and cutting lines on dried sandstone. P = 25 kW, moving speed = 5 mm/s, penetration depth = 10 mm, line spacing = 20 mm, cutting velocity = 1.5 m/s.

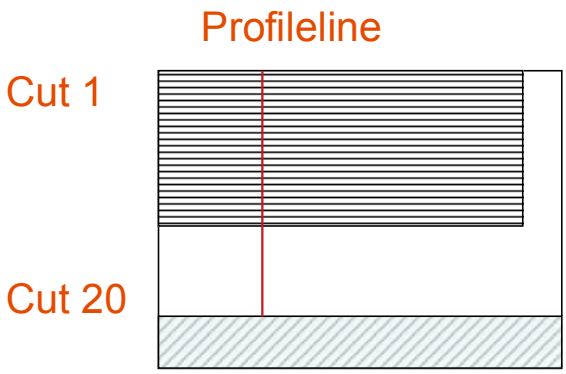

Figure C: Sketch of irradiation parameters and cutting lines on moist sandstone. P = 25 kW, moving speed = 6 mm/s, penetration depth = 10 mm, line spacing = 20 mm, cutting velocity = 1.5 m/s.

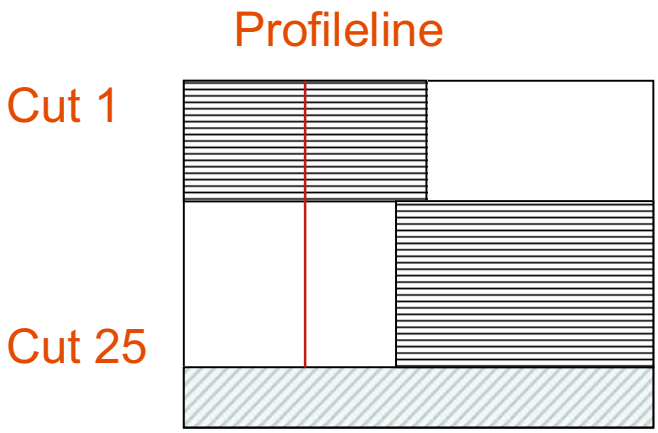

Figure D: Sketch of irradiation parameters and cutting lines on granite. P = 25 kW, moving speed = 4 mm/s, penetration depth = 10 mm, line spacing = 20 mm, cutting velocity = 1.5 m/s.

Irradiation of Basalt with 25 kW, sample moving with 3.5 mm/s spacing = 16 mm, penetration depth = 8 mm, cutting speed = 1.5 m/s

Layer 1 / Cutting Line	Data File	Cutting Force [kN]	Side Force [kN]	Normal Force[kN]	Normal / Cutting Force	
1	20111124_6	-0.12	-0.08	0.01	-0.08	irradiated area
2	20111124_7	2.22	4.02	4.75	2.14	
3	20111124_9	3.34	4.66	6.59	1.97	
4	20111124_10	3.59	4.89	7.12	1.98	
5	20111124_11	3.35	3.91	6.54	1.95	
6	20111124_12	3.97	3.58	7.05	1.78	
7	20111124_13	3.5	3.01	7.59	2.17	
8	20111124_14	3.89	4.28	9.25	2.38	
9	20111124_16	4.94	4.69	8.82	1.79	untreated area
10	20111124_17	4.96	4.29	9.48	1.91	
11	20111124_18	4.7	3.25	8.54	1.82	
12	20111124_19	4.21	4.65	7.55	1.79	
13	20111124_20	5.47	5.13	9.86	1.80	
14	20111124_21	4.87	2.22	7.55	1.55	
15	20111124_22	2.26	1.58	0	0.00	

Layer 2 / Cutting Line						
1	20111124_25	-0.13	-0.11	0.17	-1.31	irradiated area
2	20111124_26	0.49	4.69	1.84	3.76	
3	20111124_27	2.71	3.69	4.87	1.80	
4	20111124_28	2.37	3.33	5.37	2.27	
5	20111124_29	4.27	6.15	8.49	1.99	
6	20111124_30	4.37	5.02	8.88	2.03	
7	20111124_31	3.77	6.62	8.32	2.21	
8	20111124_32	3.53	4.09	8.58	2.43	
9	20111124_33	3.81	5.3	7.91	2.08	untreated area
10	20111124_34	4.97	5.8	9	1.81	
11	20111124_35	3.78	3.54	6.92	1.83	
12	20111124_36	4.66	5.01	8.56	1.84	
13	20111124_37	5.11	4.22	8.39	1.64	
14	20111124_38	0.41	-0.52	0.15	0.37	

Layer 3 / Cutting Line						
1	20111129_6	0.14	0.25	-0.22	-1.57	irradiated area
2	20111129_7	2.91	5.45	5.1	1.75	
3	20111129_8	3.22	3.6	5.05	1.57	
4	20111129_9	3.02	3.04	5.44	1.80	
5	20111129_10	4.11	4.72	6.89	1.68	
6	20111129_11	3.93	2.62	7.26	1.85	
7	20111129_12	4.87	4.85	9.18	1.89	
8	20111129_13	4.58	5.6	8.43	1.84	
9	20111129_14	5.2	6.88	9.34	1.80	untreated area
10	20111129_15	4.71	5.09	7.78	1.65	
11	20111129_16	5.9	6.08	9.24	1.57	
12	20111129_17	4.45	3.91	7.08	1.59	
13	20111129_18	2.29	0.4	1.81	0.79	
14	20111129_19	1.14	0.01	-0.09	-0.08	

Irradiation of dried Sandstone with 25 KW, sample moving at 5 mm/s
Data of layer 1 in cutting test-rig, spacing = 20 mm, penetration depth = 10 mm, cutting speed = 1.5 m/s

		average values overall				average values irradiated area				average values untreated area			
Layer 1 / Cutting Line	Data File	Cutting Force [kN]	Side Force [kN]	Normal Force [kN]	Normal / Cutting Force	Cutting Force [kN]	Side Force [kN]	Normal Force [kN]	Normal / Cutting Force	Cutting Force [kN]	Side Force [kN]	Normal Force [kN]	Normal / Cutting Force
1	20111108_2	2.60	3.45	-0.72	-0.28	0.81	0.87	-2.10	-2.59	0.35	0.15	-2.34	-6.69
2	20111108_4	6.48	8.84	7.29	1.13	6.01	8.77	6.81	1.13	6.81	8.76	7.27	1.07
3	20111108_5	8.18	8.26	12.50	1.53	6.59	4.24	7.45	1.13	7.61	9.40	12.59	1.65
4	20111108_6	6.60	6.39	9.88	1.50	7.04	9.04	10.10	1.43	6.23	3.86	8.80	1.41
5	20111108_7	9.29	10.64	14.65	1.58	7.29	4.89	8.27	1.13	9.19	12.37	15.19	1.65
6	20111108_8	7.78	8.05	10.54	1.35	7.14	4.94	9.59	1.34	7.26	8.32	10.97	1.51
7	20111108_9	7.75	8.03	11.14	1.44	7.25	7.98	9.84	1.36	8.17	7.69	10.86	1.33
8	20111108_10	6.40	7.12	8.02	1.25	6.19	5.93	6.10	0.99	6.74	8.14	9.33	1.38
9	20111108_11	5.68	5.05	5.58	0.98	5.76	5.06	5.34	0.93	5.85	5.37	6.22	1.06
10	20111108_13	6.99	8.63	10.37	1.48	9.27	11.37	12.91	1.39	6.37	7.56	10.69	1.68
11	20111108_14	7.14	7.38	9.69	1.36	n.v.	n.v.	n.v.	n.v.	n.v.	n.v.	n.v.	n.v.
12	20111108_15	6.18	6.33	8.31	1.34	n.v.	n.v.	n.v.	n.v.	n.v.	n.v.	n.v.	n.v.
13	20111108_16	8.27	9.11	11.36	1.37	n.v.	n.v.	n.v.	n.v.	n.v.	n.v.	n.v.	n.v.
14	20111108_17	7.32	8.45	10.14	1.39	9.59	13.60	15.23	1.59	7.01	6.83	8.40	1.20
15	20111108_18	7.32	6.66	8.35	1.14	7.44	6.15	10.08	1.35	7.51	7.48	6.97	0.93
16	20111108_19	7.13	6.96	9.06	1.27	8.47	8.84	10.72	1.27	6.12	5.20	6.73	1.10
17	20111108_20	7.19	8.31	9.75	1.36	7.96	11.17	12.60	1.58	6.84	5.58	7.34	1.07
18	20111108_22	7.41	6.48	8.40	1.13	7.93	7.07	9.50	1.20	7.67	8.13	8.58	1.12
19	20111108_23	7.33	7.89	9.83	1.34	7.36	8.50	11.01	1.50	5.99	3.25	3.87	0.65
20	20111108_24	5.82	6.54	7.47	1.28	5.76	5.51	6.48	1.13	6.88	8.65	10.41	1.51
21	20111108_25	7.72	7.99	9.54	1.24	8.36	9.05	11.30	1.35	7.75	7.08	7.58	0.98
	Average	6.98	7.46	9.10	1.25	7.01	7.39	8.96	1.07	6.69	6.88	8.30	0.81
	Stdv	1.31	1.53	2.97	0.38	1.90	3.04	3.77	0.93	1.79	2.70	3.72	1.89

Irradiation of dried Sandstone with 25 KW, sample moving at 5 mm/s
Data of layer 2 in cutting test-rig, spacing = 20 mm, penetration depth = 10 mm, cutting speed = 1.5 m/s

		average values overall				average values irradiated area				average values untreated area			
Layer 2 / Cutting Line	Data File	Cutting Force [kN]	Side Force [kN]	Normal Force [kN]	Normal / Cutting Force	Cutting Force [kN]	Side Force [kN]	Normal Force [kN]	Normal / Cutting Force	Cutting Force [kN]	Side Force [kN]	Normal Force [kN]	Normal / Cutting Force
1	20111108_29	1.01	2.28	-0.80	-0.79	0.40	0.45	-2.27	-5.68	1.04	2.23	-0.93	-0.89
2	20111108_30	5.78	7.58	6.54	1.13	5.02	6.96	4.85	0.97	5.56	6.61	7.17	1.29
3	20111108_31	7.86	6.65	12.24	1.56	7.62	6.48	11.40	1.50	7.02	5.68	10.77	1.53
4	20111108_32	7.10	6.31	10.85	1.53	7.17	6.36	10.65	1.49	6.39	6.53	10.37	1.62
5	20111108_33	6.77	3.99	8.77	1.30	7.37	5.61	8.01	1.09	5.45	1.99	7.53	1.38
6	20111108_34	6.71	6.53	9.38	1.40	7.66	8.72	10.01	1.31	5.35	4.27	7.69	1.44
7	20111108_35	5.80	4.78	7.53	1.30	4.26	3.37	3.74	0.88	6.87	5.66	10.47	1.52
8	20111108_36	5.31	3.57	6.99	1.32	5.17	3.95	5.68	1.10	4.59	2.86	6.56	1.43
9	20111108_37	6.29	6.10	8.91	1.42	6.16	6.25	7.63	1.24	6.35	5.92	9.91	1.56
10	20111108_38	6.91	7.07	10.09	1.46	7.46	7.70	9.66	1.29	6.59	6.65	9.86	1.50
11	20111108_39	6.93	6.62	10.15	1.46	n.v.	n.v.	n.v.	n.v.	n.v.	n.v.	n.v.	n.v.
12	20111108_40	5.94	5.64	7.86	1.32	n.v.	n.v.	n.v.	n.v.	n.v.	n.v.	n.v.	n.v.
13	20111108_41	6.70	5.98	8.25	1.23	n.v.	n.v.	n.v.	n.v.	n.v.	n.v.	n.v.	n.v.
14	20111108_42	5.31	4.75	6.73	1.27	5.79	5.78	8.26	1.43	5.24	3.89	5.80	1.11
15	0	0.00	0.00	0.00	0.00	0.00	0.00	0.00	0.00	0.00	0.00	0.00	0.00
16	20111108_44	6.19	5.51	7.19	1.16	5.88	4.05	7.00	1.19	7.96	8.55	9.44	1.19
17	20111108_45	6.92	6.83	7.73	1.12	7.59	8.14	9.42	1.24	7.31	6.80	7.30	1.00
18	20111108_46	6.42	4.76	6.61	1.03	6.02	3.48	5.69	0.95	7.82	7.08	8.81	1.13
19	20111108_47	5.01	3.14	4.00	0 80	5.39	3.15	4.92	0.91	5.14	3.67	3.51	0.68
20	20111108_48	6.79	6.60	8.44	1.24	6.56	5.54	8.89	1.36	7.57	8.24	8.78	1.16
	Average	6.37	5.69	8.24	1.29	5.97	5.37	7.10	0.77	6.02	5.41	7.69	1.17
	Stdv	0.74	1.27	1.90	2.58	1.83	2.17	3.37	1.73	1.68	2.04	3.02	0.60

Irradiation of dried Sandstone with 25 KW, sample moving at 5 mm/s
Data of layer 3 in cutting test-rig, spacing = 20 mm, penetration depth = 10 mm, cutting speed = 1.5 m/s

		average values overall				average values irradiated area				average values untreated area			
Layer 3/ Cutting Line	Data File	Cutting Force [kN]	Side Force [kN]	Normal Force [kN]	Normal / Cutting Force	Cutting Force [kN]	Side Force [kN]	Normal Force [kN]	Normal / Cutting Force	Cutting Force [kN]	Side Force [kN]	Normal Force [kN]	Normal / Cutting Force
1	20111114_6	1.27	2.00	0.68	0.54	0.00	0.00	0.00	0.00	0.00	0.00	0.00	0.00
2	20111114_7	5.46	6.85	7.45	1.36	5.41	6.91	7.45	1.38	5.74	7.13	7.95	1.39
3	20111114_8	6.21	5.02	10.03	1.62	5.73	4.56	9.36	1.63	6.34	5.06	9.99	1.58
4	20111114_9	6.17	5.07	10.15	1.65	5.84	4.11	9.94	1.70	7.05	6.88	11.32	1.61
5	20111114_12	5.30	4.44	9.06	1.71	7.23	7.00	11.44	1.58	4.46	3.13	8.23	1.85
6	20111114_13	5.51	4.70	10.19	1.85	6.03	3.75	9.94	1.65	5.63	5.69	11.04	1.96
7	20111114_14	5.50	4.54	9.21	1.67	5.32	3.97	7.68	1.44	6.33	5.51	11.31	1.79
8	20111114_15	5.01	3.55	8.07	1.61	4.93	4.63	8.32	1.69	4.83	2.70	7.49	1.55
9	20111114_16	4.84	3.97	7.63	1.58	5.85	4.21	6.88	1.18	3.11	2.79	5.78	1.86
10	20111114_17	4.73	4.40	7.93	1.68	4.76	4.98	7.68	1.61	4.91	4.23	8.45	1.72
11	20111114_18	6.11	4.50	9.81	1.61	n.v.	n.v.	n.v.	n.v.	n.v.	n.v.	n.v.	n.v.
12	20111114_19	5.21	5.70	9.22	1.77	n.v.	n.v.	n.v.	n.v.	n.v.	n.v.	n.v.	n.v.
13	20111114_20	5.89	5.79	9.48	1.61	n.v.	n.v.	n.v.	n.v.	n.v.	n.v.	n.v.	n.v.
14	20111114_21	6.25	6.79	9.33	1.49	6.49	4.29	9.95	1.53	5.41	5.18	7.70	1.42
15	20111114_22	6.95	7.44	11.49	1.65	7.71	8.26	13.02	1.69	5.46	5.99	7.89	1.45
16	20111114_23	6.45	6.05	9.96	1.54	5.84	5.52	9.92	1.70	6.48	6.16	8.45	1.30
17	20111114_24	5.59	4.90	7.55	1.35	6.58	5.51	9.62	1.46	5.54	5.35	6.50	1.17
18	20111114_25	7.07	6.82	10.89	1.54	6.79	5.10	10.72	1.58	8.04	9.95	11.92	1.48
19	20111114_26	6.26	6.49	9.44	1.51	5.80	5.45	9.71	1.67	7.35	8.51	9.51	1.29
	Average	5.81	5.39	9.27	1.60	5.64	4.89	8.85	1.57	5.42	5.27	8.35	1.56
	Stdv	0.68	1.14	1.16	1.71	1.70	1.80	2.84	0.15	1.87	2.40	2.86	0.23

Irradiation of dried Sandstone with 25 KW, sample moving at 5 mm/s
Data of layer 4 in cutting test-rig, spacing = 20 mm, penetration depth = 10 mm, cutting speed = 1.5 m/s

		average values overall				average values irradiated area				average values untreated area			
Layer 4 / Cutting Line	Data File	Cutting Force [kN]	Side Force [kN]	Normal Force [kN]	Normal / Cutting Force	Cutting Force [kN]	Side Force [kN]	Normal Force [kN]	Normal / Cutting Force	Cutting Force [kN]	Side Force [kN]	Normal Force [kN]	Normal / Cutting Force
1	20111201_2	0.94	2.21	1.07	1.14	0.29	0.90	-0.15	-0.52	1.24	2.85	1.89	1.52
2	20111201_3	5.10	6.17	8.24	1.62	5.55	7.41	8.49	1.53	5.10	4.82	8.99	1.76
3	20111201_4	6.72	4.90	12.86	1.91	6.88	5.56	12.67	1.84	5.34	3.31	11.06	2.07
4	20111201_5	6.07	5.09	11.86	1.95	6.20	5.33	12.68	2.05	6.62	5.41	12.07	1.82
5	20111201_6	5.95	4.35	10.94	1.84	5.77	4.81	10.29	1.78	6.57	4.54	12.11	1.84
6	20111201_7	5.60	5.36	11.18	2.00	6.23	7.81	12.05	1.93	5.42	4.00	11.07	2.04
7	20111201_8	6.20	6.11	12.14	1.96	6.36	7.75	11.93	1.88	6.60	5.68	13.18	2.00
8	20111201_9	6.28	5.95	11.35	1.81	5.54	6.03	9.68	1.75	6.74	5.85	12.40	1.84
9	20111201_10	5.53	4.85	9.81	1.77	5.73	7.43	6.26	1.09	5.66	3.53	10.29	1.82
10	20111201_11	5.43	5.17	10.25	1.89	5.35	5.26	9.33	1.74	6.06	5.63	12.18	2.01
11	20111201_12	5.76	4.59	10.60	1.84	n.v.	n.v.	n.v.	n.v.	n.v.	n.v.	n.v.	n.v.
12	20111201_13	5.93	3.90	9.52	1.61	n.v.	n.v.	n.v.	n.v.	n.v.	n.v.	n.v.	n.v.
13	20111201_14	5.57	3.91	10.16	1.82	n.v.	n.v.	n.v.	n.v.	n.v.	n.v.	n.v.	n.v.
14	20111201_15	5.33	3.78	8.28	1.55	6.33	5.03	11.16	1.76	4.58	2.38	4.86	1.06
15	20111201_16	5.78	5.37	10.16	1.76	6.19	5.10	10.82	1.75	5.50	6.15	9.60	1.75
16	20111201_17	5.26	3.83	8.55	1.63	6.09	4.92	10.89	1.79	5.16	2.93	6.90	1.34
17	20111201_18	5.84	4.51	9.36	1.60	6.92	5.47	11.40	1.65	5.39	4.04	8.35	1.55
18	20111201_19	6.53	6.24	10.27	1.57	7.34	7.41	12.14	1.65	5.24	4.38	7.20	1.37
	Average	5.82	4.95	10.33	1.77	5.78	5.75	9.98	1.58	5.41	4.37	9.48	1.72
	Stdv	0.45	0.84	1.32	0.15	1.62	1.76	3.29	0.62	1.33	1.21	3.18	0.29

Irradiation of dried Sandstone with 25 KW, sample moving at 5 mm/s
Data of layer 5 in cutting test-rig, spacing = 20 mm, penetration depth = 10 mm, cutting speed = 1.5 m/s

		average values overall				average values irradiated area				average values untreated area			
Layer 5 / Cutting Line	Data File	Cutting Force [kN]	Side Force [kN]	Normal Force [kN]	Normal / Cutting Force	Cutting Force [kN]	Side Force [kN]	Normal Force [kN]	Normal / Cutting Force	Cutting Force [kN]	Side Force [kN]	Normal Force [kN]	Normal / Cutting Force
1	20111201_22	0.27	0.40	-0.03	-0.11	0.26	0.41	-0.01	-0.04	0.28	0.37	-0.06	-0.21
2	20111201_23	4.91	5.84	7.30	1.49	5.47	7.38	7.76	1.42	5.39	4.92	8.48	1.57
3	20111201_24	5.87	4.85	10.07	1.72	5.78	4.49	9.28	1.61	6.43	5.74	12.02	1.87
4	20111201_25	5.23	3.89	10.39	1.99	5.77	4.54	11.53	2.00	5.07	3.42	9.81	1.93
5	20111201_26	6.15	4.85	11.56	1.88	6.70	4.43	12.66	1.89	5.91	5.12	10.99	1.86
6	20111201_27	6.57	6.33	12.70	1.93	6.75	7.33	13.49	2.00	6.72	6.03	12.68	1.89
7	20111201_28	5.82	5.49	11.42	1.96	6.40	5.89	12.49	1.95	5.74	5.04	11.38	1.98
8	20111201_29	5.78	5.11	10.36	1.79	7.02	6.89	11.56	1.65	5.94	5.04	11.47	1.93
9	20111201_30	5.99	4.93	10.79	1.80	7.09	5.93	11.68	1.65	5.80	4.68	11.38	1.96
10	20111201_31	5.73	4.15	10.43	1.82	5.53	3.54	9.74	1.76	6.75	5.26	12.54	1.86
11	20111201_32	6.29	5.49	11.10	1.76	n.v.	n.v.	n.v.	n.v.	n.v.	n.v.	n.v.	n.v.
12	20111201_33	5.34	4.92	9.12	1.71	n.v.	n.v.	n.v.	n.v.	n.v.	n.v.	n.v.	n.v.
13	20111201_34	6.24	5.21	10.14	1.63	n.v.	n.v.	n.v.	n.v.	n.v.	n.v.	n.v.	n.v.
14	20111201_35	6.22	6.77	10.48	1.68	6.07	7.05	10.75	1.77	6.94	6.70	10.60	1.53
15	20111201_36	5.46	4.47	8.86	1.62	5.13	3.94	9.25	1.80	6.45	5.45	8.97	1.39
16	20111201_38	5.35	3.97	8.13	1.52	5.16	3.33	8.95	1.73	6.87	5.89	8.97	1.31
17	20111201_39	5.26	5.68	8.64	1.64	5.31	5.43	9.44	1.78	5.24	5.11	7.10	1.35
	Average	5.76	5.12	10.09	1.75	5.60	5.04	9.90	1.64	5.68	4.91	9.74	1.59
	Stdv	0.47	0.81	1.39	0.15	1.68	1.93	3.30	0.51	1.67	1.51	3.26	0.57

Irradiation of moist Sandstone with 25 KW, sample moving at 6 mm/s.
Average data of cutting test-rig, spacing = 20 mm, penetration depth = 10 mm, cutting speed = 1.5 m/s

Layer 1 / Cutting Line	Data File	Cutting Force [kN]	Side Force [kN]	Normal Force [kN]	Normal / Cutting Force	
1	20120103_4	2.84	4.33	6.05	0.00	irradiated
2	20120103_5	5.43	2.58	11.60	2.14	
3	20120103_6	5.80	3.05	14.08	2.43	
4	20120103_7	5.71	1.99	12.99	2.27	
5	20120103_8	5.28	1.97	12.11	2.29	
6	20120103_9	5.54	2.44	14.11	2.55	
7	20120103_10	5.18	1.03	12.73	2.46	
8	20120103_11	4.72	1.68	11.65	2.47	
9	20120103_12	5.61	1.43	12.49	2.23	
10	20120103_13	5.13	2.49	11.82	2.30	
11	20120103_14	5.15	1.60	11.48	2.23	
12	20120103_15	4.93	1.60	10.95	2.22	untreated
13	20120103_16	4.50	1.98	10.00	2.22	
14	20120103_17	4.42	1.34	9.29	2.10	
15	20120103_18	4.44	2.28	9.97	2.25	
16	20120103_19	4.70	1.67	9.85	2.10	
17	20120103_20	4.72	2.30	10.14	2.15	
18	20120103_21	5.11	1.69	10.18	1.99	
19	20120103_22	5.00	2.25	10.69	2.14	
20	20120103_23	4.93	1.45	9.53	1.93	

Layer 2 / Cutting Line						
1	20120103_24	5.70	12.14	12.89	0.00	irradiated
2	20120103_25	6.74	7.39	13.40	1.99	
3	20120103_26	7.91	9.91	17.47	2.21	
4	20120103_27	7.66	8.73	15.90	2.08	
5	20120103_28	7.79	8.54	16.95	2.18	
6	20120103_29	7.66	8.40	16.30	2.13	
7	20120103_30	7.78	8.60	15.83	2.03	
8	20120103_31	7.07	8.25	15.13	2.14	
9	20120103_32	6.38	6.56	14.13	2.21	
10	20120103_33	6.51	8.12	14.93	2.29	
11	20120103_34	6.31	6.01	13.31	2.11	
12	20120103_35	7.55	8.64	15.25	2.02	untreated
13	20120103_36	7.05	8.36	14.67	2.08	
14	20120103_37	6.88	6.32	13.91	2.02	
15	20120103_38	6.89	6.97	12.98	1.88	
16	20120103_39	6.45	7.80	13.92	2.16	
17	20120103_40	7.28	8.76	14.66	2.01	
18	20120103_41	8.48	11.01	16.85	1.99	
19	20120103_42	8.25	10.71	16.39	1.99	

Irradiation of moist Sandstone with 25 KW, sample moving at 6 mm/s.
Average data of cutting test-rig, spacing = 20 mm, penetration depth = 10 mm, cutting speed = 1.5 m/s

Layer 3 / Cutting Line	Data File	Cutting Force [kN]	Side Force [kN]	Normal Force [kN]	Normal / Cutting Force	
1		n.v.	n.v.	n.v.	n.v.	irradiated
2	20120103_43	6.84	7.84	10.88	1.59	
3	20120103_44	7.18	6.74	14.70	2.05	
4	20120103_45	6.95	6.36	14.88	2.14	
5	20120103_46	6.68	7.45	13.78	2.06	
6	20120103_47	6.69	5.13	13.02	1.95	
7	20120103_48	6.72	6.52	14.68	2.18	
8	20120103_49	6.52	6.05	13.91	2.13	
9	20120103_50	6.06	6.54	13.64	2.25	
10	20120103_51	6.18	6.28	13.68	2.21	
11	20120103_52	5.45	4.85	11.69	2.14	
12	20120103_53	5.65	4.71	10.51	1.86	untreated
13	20120103_54	6.40	6.94	13.02	2.03	
14	20120103_55	6.79	7.40	13.45	1.98	
15	20120103_56	5.34	6.88	10.80	2.02	
16	20120103_57	5.84	7.24	11.71	2.01	
17	20120103_58	5.34	4.77	9.64	1.81	
18	20120103_61	5.49	5.65	10.88	1.98	

Layer 4 / Cutting Line						
1	20120103_62	1.13	2.58	2.82	0.00	irradiated
2	20120103_64	6.51	8.35	12.83	1.97	
3	20120103_65	6.66	6.81	14.71	2.21	
4	20120103_66	6.59	8.05	14.27	2.17	
5	20120103_67	5.56	5.36	11.54	2.08	
6	20120103_68	6.51	7.48	14.96	2.30	
7	20120103_69	6.23	5.58	13.18	2.12	
8	20120103_70	6.34	5.80	12.68	2.00	
9	20120103_71	7.03	7.27	14.19	2.02	
10	20120103_72	5.82	4.39	11.62	2.00	
11	20120103_73	5.92	6.85	13.57	2.29	
12	20120103_74	5.94	5.13	11.40	1.92	untreated
13	20120103_75	6.42	6.83	13.13	2.05	
14	20120103_76	6.40	5.29	11.70	1.83	
15	20120103_77	5.99	6.39	11.49	1.92	
16	20120103_78	5.31	5.36	10.04	1.89	

Irradiation of Granite with 25 KW, sample moving at 4 mm/s
Data of layer 1 in cutting test-rig, spacing = 20 mm, penetration depth = 10 mm, cutting speed = 1.5 m/s

			average values overall				average values irradiated				average values untreated			
Layer 1 / Cutting Line	Data File	Distance [mm]	Cutting Force [kN]	Side Force [kN]	Normal Force [kN]	Normal / Cutting Force	Cutting Force [kN]	Side Force [kN]	Normal Force [kN]	Normal / Cutting Force	Cutting Force [kN]	Side Force [kN]	Normal Force [kN]	Normal / Cutting Force
1	20111025_1	416	3.05	6.29	6.65	2.18	3.11	6.45	6.82	2.19	2.5	5.08	5.26	2.10
2	20111025_2	481	6.27	6.25	13.7	2.19	5.92	5.82	12.77	2.16	6.64	6.81	14.49	2.18
3	20111025_3	519	5.92	5.19	12.86	2.17	6.15	5.07	12.67	2.06	5.82	5.91	13.42	2.31
4	20111025_4	481	6.42	6.05	14.14	2.20	6.33	5.39	13.27	2.10	5.69	5.72	12.94	2.27
5	20111025_5	480	6.07	5.80	13.06	2.15	5.29	4.26	11.55	2.18	5.96	6.44	12.63	2.12
6	20111025_6	492	6.45	6.63	13.87	2.15	6.46	5.69	13.25	2.05	6.76	8.00	15.10	2.23
7	20111025_7	456	6.71	6.15	14.30	2.13	6.64	5.61	13.74	2.07	6.10	6.12	13.58	2.23
8	20111025_8	480	5.90	5.00	13.07	2.22	5.31	4.18	11.76	2.21	6.58	6.08	14.81	2.25
9	20111025_9	476	6.53	7.23	14.52	2.22	6.54	7.00	13.90	2.13	6.48	7.52	15.02	2.32
10	20111025_10	475	6.02	6.22	12.99	2.16	5.43	4.33	10.89	2.01	3.67	8.22	15.26	4.16
11	20111025_11	473	6.25	6.08	13.83	2.21	6.78	7.11	14.93	2.20	5.29	4.54	11.94	2.26
12	20111025_12	468	5.87	5.72	13.07	2.23	5.84	5.62	12.46	2.13	5.52	5.49	13.02	2.36
13	20111025_13	459	6.00	5.80	12.61	2.10	5.74	5.29	11.89	2.07	5.79	6.03	12.67	2.19
14	20111025_14	489	6.24	5.96	13.73	2.20	6.15	6.76	14.83	2.41	6.07	5.24	12.45	2.05
15	20111025_15	462	6.69	7.02	14.41	2.15	6.17	6.78	13.74	2.23	6.34	6.72	13.92	2.20
16	20111025_16	474	6.28	6.03	13.42	2.14	5.39	5.53	12.31	2.28	6.12	5.56	12.52	2.05
17	20111025_17	489	6.47	6.63	13.55	2.09	6.65	6.95	13.47	2.03	6.32	6.40	13.46	2.13
18	20111025_18	468	7.21	8.52	15.68	2.17	7.12	9.38	16.09	2.26	7.27	7.98	14.54	2.00
19	20111025_19	497	6.30	6.57	13.22	2.10	6.26	7.39	15.12	2.42	6.58	5.64	12.27	1.86
20	20111025_20	485	6.98	7.99	14.01	2.01	5.96	7.69	12.95	2.17	7.60	7.86	14.41	1.90
21	20111025_21	464	7.09	7.43	13.63	1.92	6.85	6.69	13.30	1.94	7.25	7.98	13.85	1.91
22	20111025_22	482	6.60	7.05	13.20	2.00	6.84	8.67	14.34	2.10	6.28	5.44	11.92	1.90
23	20111025_23	486	6.49	7.94	13.70	2.11	6.64	8.39	14.53	2.19	6.67	7.88	13.46	2.02
24	20111025_24	464	6.82	7.16	14.52	2.13	6.93	7.34	15.17	2.19	6.59	6.64	12.55	1.90
25	20111025_25	474	7.14	8.31	14.98	2.10	6.11	6.69	13.51	2.21	8.52	10.35	17.22	2.02
	Average	475.60	6.45	6.61	13.75	2.14	6.10	6.40	13.17	2.16	6.18	6.63	13.31	2.20
	Stdv	18.37	0.40	0.94	0.73	0.08	0.82	1.35	1.83	0.11	1.17	1.32	2.09	0.43

Irradiation of Granite with 25 KW, sample moving at 4 mm/s
Data of layer 2 in cutting test-rig, spacing = 20 mm, penetration depth = 10 mm, cutting speed = 1.5 m/s

			average values overall				average values irradiated				average values untreated			
Layer 2 / Cutting Line	Data File	Distance [mm]	Cutting Force [kN]	Side Force [kN]	Normal Force [kN]	Normal / Cutting Force	Cutting Force [kN]	Side Force [kN]	Normal Force [kN]	Normal / Cutting Force	Cutting Force [kN]	Side Force [kN]	Normal Force [kN]	Normal / Cutting Force
1	20111025_27	489	3.76	6.37	7.57	2.01	3.71	6.44	7.52	2.03	4.68	7.55	9.38	2.00
2	20111025_28	440	6.75	8.27	15.55	2.30	6.73	9.09	15.21	2.26	6.77	6.71	16.04	2.37
3	20111025_29	461	6.97	8.07	16.44	2.36	6.64	6.53	14.50	2.18	6.99	10.08	18.48	2.64
4	20111025_30	447	6.99	8.24	17.16	2.45	7.23	8.85	17.55	2.43	6.49	6.99	16.29	2.51
5	20111025_31	461	6.23	5.87	14.59	2.34	6.89	6.06	15.30	2.22	5.02	5.46	13.15	2.62
6	20111025_32	449	6.93	6.09	15.00	2.16	7.00	5.37	14.51	2.07	6.24	6.61	14.98	2.40
7	20111025_33	487	6.38	6.68	15.24	2.39	6.71	7.15	15.84	2.36	5.44	5.47	13.30	2.44
8	20111025_34	507	6.21	6.85	14.69	2.37	6.78	6.74	15.34	2.26	5.76	7.40	14.59	2.53
9	20111025_35	474	7.00	6.95	15.44	2.21	7.17	7.02	15.69	2.19	6.88	7.13	15.62	2.27
10	20111025_36	473	6.74	7.04	15.33	2.27	6.75	7.18	15.47	2.29	6.19	6.20	13.81	2.23
11	20111025_37	477	6.58	6.40	14.46	2.20	6.82	6.54	14.58	2.14	6.56	6.26	14.92	2.27
12	20111025_38	472	6.40	6.54	14.76	2.31	6.58	6.13	15.23	2.31	6.41	7.14	14.43	2.25
13	20111025_39	468	6.54	5.53	14.08	2.15	6.38	5.13	13.69	2.15	6.17	5.98	13.91	2.25
14	20111025_40	475	6.55	7.15	15.42	2.35	5.99	6.07	14.37	2.40	6.92	7.77	16.37	2.37
15	20111025_41	453	6.94	5.92	14.54	2.10	7.39	7.23	16.03	2.17	6.33	5.05	13.00	2.05
16	20111025_42	463	6.48	7.53	14.45	2.23	5.68	7.40	14.04	2.47	6.92	7.44	14.56	2.10
17	20111025_43	483	5.87	4.86	12.51	2.13	6.05	5.14	14.10	2.33	5.88	4.91	11.93	2.03
18	20111025_44	481	6.52	5.81	13.82	2.12	6.67	5.78	13.81	2.07	6.31	5.77	13.53	2.14
19	20111025_45	477	6.23	6.69	13.46	2.16	6.69	7.62	14.81	2.21	6.16	6.22	12.98	2.11
20	20111025_46	513	6.32	6.11	13.18	2.09	6.19	6.26	13.53	2.19	6.66	6.27	13.48	2.02
21	20111025_47	498	6.20	6.27	13.17	2.12	5.64	6.20	13.03	2.31	6.26	6.03	12.60	2.01
22	20111025_48	501	5.88	5.07	11.94	2.03	6.13	4.98	12.74	2.08	6.03	5.36	11.99	1.99
23	20111025_49	498	6.54	6.80	13.12	2.01	6.96	7.24	13.99	2.01	6.35	6.78	12.71	2.00
24	20111025_50	474	6.79	6.40	15.33	2.26	6.42	6.16	15.48	2.41	6.72	6.24	14.52	2.16
	Average	475.30	6.52	6.57	14.51	2.22	6.59	6.60	14.73	2.24	6.32	6.49	14.23	2.25
	Stdv	19.33	0.33	0.91	1.24	0.12	0.47	1.07	1.09	0.13	0.49	1.10	1.58	0.20

Appendix C: Manual of large-scale microwave irradiation apparatus

Bedienung der Mikrowelleversuchsanlage

Vor dem erstmaligen Betrieb der Mikrowelle ist das Studium der Sicherheitsvorschriften und der *Bedienungsanleitung der Firma Mügge* erforderlich. Eine Einweisung gemäß *Arbeitsanweisung UGSA 7.416* vom 20.6.2011 in der letztgültigen Fassung hat zu erfolgen.

Zweck des Mikrowellenprüfstandes ist die Bestrahlung von Gesteinen mit elektromagnetischen Wellen, um eine Schwächung des Gesteinsgefüges herbeizuführen.

Steuerung und Anlagen

Vor der Inbetriebnahme ist eine optische Überprüfung der Anlage vorzunehmen und sicherzustellen ob keine offensichtlichen Schäden feststellbar sind. Regelmäßige Überprüfungen der Leckstrahlung mit dem bereitgestellten Survey Meter sind bei geringer Leistung durchzuführen.

Im Betrieb müssen folgende Referenzwerte einzuhalten:

- Elektrische Feldstärke (Effektivwert): 137 V/m
- Magnetische Feldstärke (Effektivwert): 0,36 A/m
- Äquivalente Leistungsflussdichte: 50 W/m²

Die gemessenen Leistungsflussdichten bzw,. die quadrierten Feldstärkewerte sind über 6 Minuten zu mitteln. Der zeitliche Spitzenwert der Leistungsflussdichte darf das 100fache des obigen Wertes bzw. die Feldstärken das 32fache der obigen Werte nicht überschreiten.

Die Mikrowellenversuchsanlage besteht aus mehreren einzelnen Komponenten. Vor dem Betrieb ist die Funktionstüchtigkeit aller Einzelteile zu gewährleisten:

- Wasserkreislauf
- Automatischer Tuner
- Analoge Mikrowellensteuerung

- Digitale Steuerung: Die digitale MW-Steuerung ist für die Funktion von zusätzlichen Features, wie Pulsbetrieb und zeitgerechtes Abschalten der Anlage erforderlich. Ein prinzipieller Betrieb ist auch mit der analogen Steuerung alleine möglich.
- Not-Aus-Schalter

Die folgende Anleitung beschreibt die Inbetriebnahme und Funktion der einzelnen Komponenten.

Wasserkreislauf

Wird zur Kühlung der einzelnen Komponenten, sowie zur Aufnahme der reflektierten Leistung benötigt. Um Kondenswassererbildung zu vermeiden sollte sich die Temperatur zwischen 20 und 25°C bewegen. Die Temperatur wird mittels Fühler und automatischen Ventil am Wasserboiler eingestellt und muss im Betrieb von Zeit zu Zeit manuell überprüft werden. Das Magnetron, sowie die Wasserlast haben automatische Durchflusswächter, die den notwendigen Durchfluss gewährleisten und bei Unterschreitung der erforderlichen Mengen ein Fehlersignal an die Steuerung senden. Die benötigten Wassermengen sind im Folgenden dargestellt:

Zirkulator: 5 l/min – ohne Überwachung

Magnetron: 15 l/min

Wasserlast: 10 l/min

Einzuschalten ist der Kühlkreislauf beim Schaltschrank an der Rückwärtigen Wand (Abbildung 1). Die Frischwasserzufuhr muss extra durch ein grünes Rad aufgedreht werden (Abbildung 2). Die einzelnen Leitungen zu Wasserlast, Magnetron und Zirkulator sind durch Handräder gesteuert, an denen man eine Justierung der Durchflussmengen vornehmen kann (Abbildung 3).

Aufgrund der Spezifikationen der Wasserwächter (Abbildung 4) kann es notwendig sein, vor dem Betrieb die Handräder der einzelnen Kreisläufe nachzujustieren um den benötigten Durchfluss sicherzustellen. Im Regelfall reicht es den Kreislauf ganz links (Wasserlast) abzudrehen und nach kurzer Wartezeit wieder auf den eingestellten Wert zurück zu stellen.

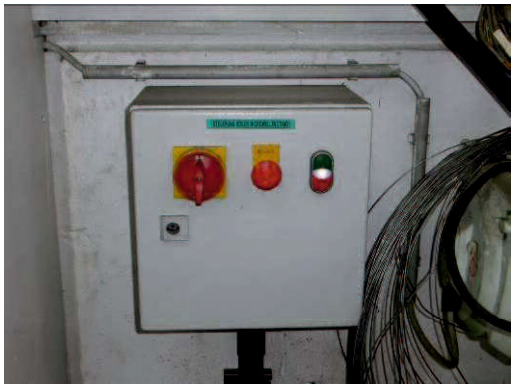

Abbildung 1: Schaltkasten Kühlkreislauf. Hauptschalter und EinAus Schalter (rot/grün).

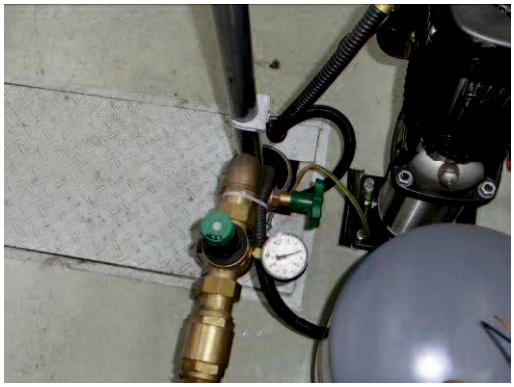

Abbildung 2: Hauptwasserzufuhr. Grünes Rad zu Beginn voll aufdrehen.

Abbildung 3: Rückansicht des Bedienfeldes. Wasserleitunge mit Stellrädern (rot, unten) und Wasserwächtern (Kupfer, rechts oben).

Abbildung 4: Durchflusswächter für Magnetron und Wasserlast.

Automatischer Tuner

Der automatische Tuner regelt die Phase der ausgehenden Mikrowellenstrahlung und somit die Ankopplung ans Gestein und reduziert damit die reflektierte Leistung. Des Weiteren misst er online alle notwendigen Leistungsdaten, um diese später evtl. auswerten zu können. Er wird durch das Programm HomSoft / TurS gesteuert. Der Tuner ist an einem Schalter auf *Automatik* zu schalten. Auf Grund der Unzugänglichkeit der Teile wird der Tuner durch Ziehen des Netzsteckers im Bedienfeld ein- und ausgeschaltet.

Die genaue Anleitung zur Datenaufzeichnung und Bedienung der Software ist dem Handbuch von HomSoft zu entnehmen

Über die Bedienung und die Einstellmöglichkeiten kann man sich im Handbuch von HomSoft informieren.

Analoge Mikrowellensteuerung

Um die analoge Steuerung der Anlage zu betreiben muss zuerst der Netzschalter am „Power Supply“ betätigt werden. Der Not-Aus-Schalter ist durch einen Schlüssel zu entsperren (Abbildung 5). Durch Betätigen des Schalters *Standby ON/OFF* am Bedienpanel (Abbildung 7) wird die Vorheizphase des Magnetrons eingeleitet. Erst wenn diese abgeschlossen ist, kann mit der Bestrahlung begonnen werden. Danach ist die Sollleistung in Prozent der maximalen Leistung (30 kW) mittels *Handrad* einzustellen und die Bestrahlung mit der Taste *Start/Stop* zu beginnen. Aktivität des Magnetrons wird durch ein rotes Blinklicht sowie durch eine Sirene angezeigt (Abbildung 6). Leistung und reflektierte Leistung werden dabei jeweils in Prozent der maximalen Leistung dargestellt. Mehrere Sicherheitsschalter verhindern unsachgemäßen Gebrauch.

Der Betrieb der Mikrowelle kann dabei über den *Start/Stop* Schalter, sowie durch die beiden *Not-Aus*-Schalter am Bedienfeld und am Powersupply gestoppt werden. Durch öffnen der Gehäusetüren (öffnen des Türkontaktes, Abbildung 8) wird auch ein NotStop ausgelöst.

Die Funktionalität der MW ist erste gegeben wenn alle Sicherheitseinrichtungen freigeschaltet sind:

Interlock: Schlusskontakte an den Türen des Gehäuses müssen geschlossen sein. Die beiden Raunschnüffler müssen aktiv sein

Cooling1: Durchflusswächter im Power Supply

Cooling2: Durchflusswächter bei Magnetron und Wasserlast

Diverse weiter Fehlermeldungen können ARCing (Lichtbögen) nd Reflection (zu hohe reflektierte Leistung) beinhalten. Fehlermeldungen müssen durch Betätigung des Schalters *Reset* quittiert werden.

Eine detaillierte Anleitung über den Betrieb und die einzelnen Anlagenzustände findet sich in der Bedienungsanleitung der Firma Mügge.

Abbildung 5: Netzschalter und Not-Aus am Power Supply.

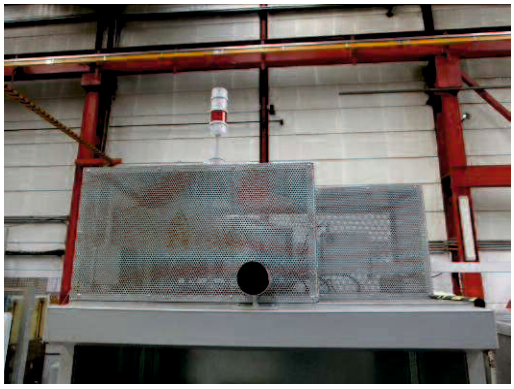

Abbildung 6: Warnlicht und Sirene sind über der Einhausung des Magnetrons angebracht.

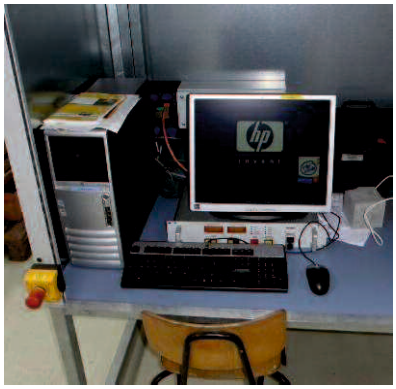

Abbildung 7: Bedienfeld mit analoger Steuerung und PC für digitale Steuerung. Not-Aus-Schalter links unten).

Abbildung 8 Schließkontakt an seitlicher Türe.

Digitale Mikrowellensteuerung

Die Prinzipien der analogen Steuerung sind mit Hilfe einer Schnittstelle auch am PC umgesetzt. Zusätzlich können mit dieser Steuerung auch genaue Zeitabläufe und Pulse programmiert werden.

Die Anwendung wird mit der Verknüpfung *Microwave 0511* am Desktop des MessPCs gestartet. Sie basiert auf einer LabView-Programmierung, ist aber als exe.-file vorhanden und benötigt nur mehr eine LabView Runtime Engine.

Nach der ersten Abfrage *Remote, Ja, Nein* ist auf der analogen Steuerung der Schalter *Remote* aktiv und das Magnetron befindet sich in der Aufwärmphase.

In der *Registerkarte Mikrowelle* sind alle benötigten Anlagenparameter einstellbar (Abbildung 9).

Man kann mehrere Sequenzen (Pulse) unterschiedlicher Energielevels im Sekundentakt einstellen:

1. Erster Schritt ist die Einstellung der Anzahl der unterschiedlichen Sequenzen und die Anzahl der Durchläufe. (Will man zB 20% und 100% 20 mal laufen lassen benötigt man 2 Sequenzen und 20 Durchläufe). Bestätigen durch *OK*.
2. Definition der einzelnen Sequenzen. Welche Sequenz gerade bearbeitet wird wird zuoberst dargestellt. Man kann die Leistung (in % P_{max}) und die Zeit (s) einstellen. Nach betätigen von *OK* springt das Programm auf die nächste Sequenz. Nach Eingabe der letzten Sequenz werden die Einstellungen ganz rechts im Fenster dargestellt.

Sind alle Sicherheitsschalter aktiv ist danach der Button *START* freigegeben und die MW kann in Betrieb genommen werden. Ein Feld links unten zeigt dabei die aktuelle Leistung [% P_{max}] und die verbleibende Zeit in der aktuellen Stufe, sowie die Anzahl der absolvierten Zyklen an.

Der Stop der Anlage erfolgt automatisch nach Ablauf der eingestellten Zeit, manuell durch drücken der Taste *Anlage Stop* in der Steuerung, oder durch betätigen eines Sicherheitsschalters.

Sollte ein Fehler in der Anlage entstehen, der nur durch das Drücken der *Reset*-Taste gelöst werden kann, muss man auf *Programm Ende* klicken. Bei der Abfrage, ob man Remote

wirklich beenden will auf Nein klicken und erneut mit der kurzen Aufwärmphase der MW beginnen.

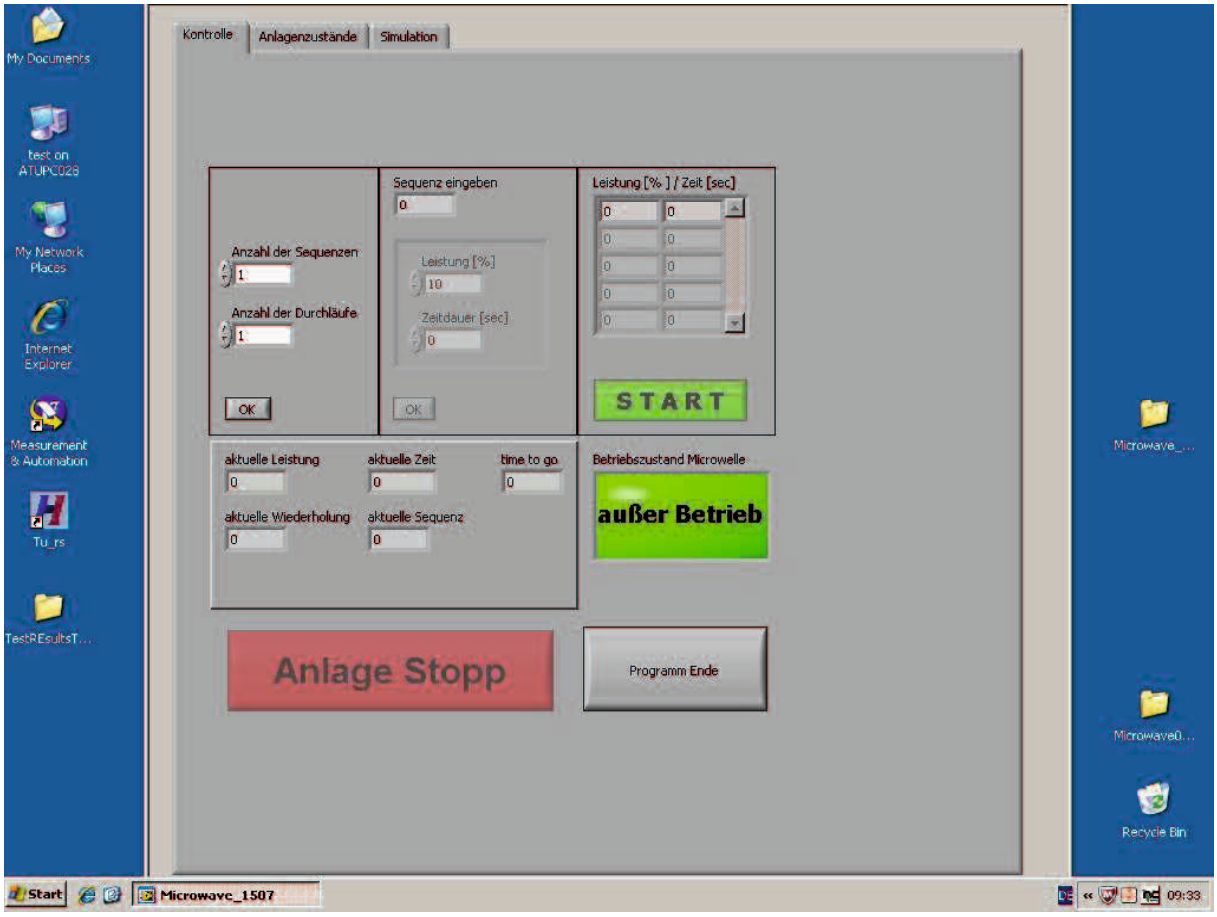

Abbildung 9: Registerkarte Mikrowelle der digitalen Steuerung.

Handbedienräder

Die beiden Handräder am Sicherheitsgehäuse dienen der korrekten Platzierung der Probe unter dem Hohlleiter. Eine digitale Positionsanzeige gewährleistet die korrekte Positionierung. Das Handrad an der Hinterseite kann auch zur Bewegung der Probe während der Bestrahlung verwendet werden. Jenes an der Seite ist auf Grund einer Fehlkonstruktion nicht zu 100% mikrowellendicht. Laut TÜV muss daher ein Sicherheitsabstand von 10 cm eingehalten werden (Abbildung 10).

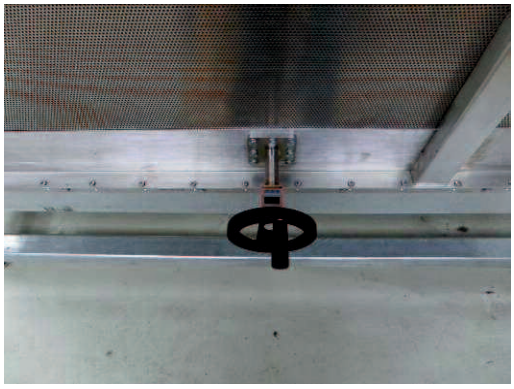

Abbildung 10: Seitliches Bedienrad mit digitaler Positionsanzeige.

Bestrahlung und Probenhandhabung

Die Bestrahlung und Probenbehandlung erfolgt nach den jeweils festgelegten Versuchsparametern. Wichtige Verfahrensschritte und Sicherheitshinweise sind der *Arbeitsanweisung UGSA 7.416* vom 20.6.2011 in der letztgültigen Fassung zu entnehmen.